

REVEALING THE CHAMELEON:  
Young, low-mass stars surrounding  
 $\eta$  and  $\epsilon$  Chamaeleontis

Simon John Murphy

A thesis submitted for the degree of  
Doctor of Philosophy  
of the Australian National University



Research School of Astronomy & Astrophysics

Submitted 8th November 2011  
Accepted 23rd January 2012

## NOTES ON THE DIGITAL COPY

This document makes extensive use of the hyperlinking features of L<sup>A</sup>T<sub>E</sub>X. References to figures, tables, sections, chapters and the literature can be navigated from within the PDF by clicking on the reference. Internet addresses will be displayed in a browser.

Most object names are resolvable in the SIMBAD (<http://simbad.u-strasbg.fr/simbad/>) astronomical database. Click on an object to be taken to its SIMBAD entry.

The bibliography at the end of this thesis has been hyperlinked to the NASA Astrophysics Data Service (<http://www.adsabs.harvard.edu/>). Further information on each of the cited works is available through the link to ADS.

Several of the large catalogues used in this work have been tagged with their Virtual Observatory unique identifier (e.g. ivo://astronet.ru/cas/twomass-psc). As various data centres can have different versions and implementations of the same catalogue, this ensures any analysis is repeatable by denoting the exact catalogue *and* service that was used to obtain the data. Clicking on their identifiers will resolve the service descriptions in the directory hosted by the US Virtual Observatory (<http://www.us-vo.org>).

## Disclaimer

I hereby declare that the work in this thesis is that of the candidate alone, except where indicated below or in the text of the thesis. The work was undertaken between March 2007 and November 2011 at the Australian National University, Canberra. It has not been submitted in whole or in part for any other degree at this or any other university.

**Chapter 2** is an expanded and updated version of the paper '*First detection of a low-mass stellar halo around the young open cluster  $\eta$  Chamaeleontis*'. Murphy, S. J., Lawson, W. A. & Bessell, M. S. 2010, MNRAS, 406, L50.

**Chapter 3** is an expanded and updated version of the paper '*Episodic disc accretion in the halo of the 'old' pre-main-sequence cluster  $\eta$  Chamaeleontis*'. Murphy, S. J., Lawson, W. A., Bessell, M. S. & Bayliss, D. D. R. 2011, MNRAS, 411, L51.

Daniel Bayliss (RSAA / ANU) observed and reduced the *Magellan*/MIKE spectrum of 2MASS J0820–8003 which appears in the second paper and Chapter 3.

The balance of the observations, data reduction and analysis presented in these papers and chapters was performed solely by the candidate, who also wrote the text in its entirety. The co-authors provided valuable discussions and comments on the text.

The thesis was unconditionally accepted by a panel of expert examiners and ratified by the Dean of the College of Science on 23 January 2012. Following the suggestions of the examiners, this copy contains several improvements, additions and minor corrections.



Simon J. Murphy  
16th February 2012



## Acknowledgments

Although it is my name on the cover page, no Ph.D. thesis has ever been written in isolation. This document is the result of a collaborative effort with the dozens of colleagues, friends and loved-ones I have been lucky enough to know and work with over the past four and a half years. As the author Gladys B. Stern once wrote, "*Silent gratitude isn't much use to anyone*", so it is my pleasure to especially thank a few people who made this all possible.

Foremost, I would like to express my sincere gratitude to my supervisors, Professors Mike Bessell and Warrick Lawson, for their continuous support and guidance throughout my candidature. Your enthusiasm for this work, patience and breadth of knowledge have been extraordinary and it has been a privilege to work with and get to know you. I hope that this thesis is just the start of a fruitful collaboration for many years to come.

To my dearest Maggie, thank you for your ever-present love, support, encouragement and interest in what I do, despite the late nights and preoccupied weekends. Although I didn't know you when I started this work, I can't imagine ever completing it without you. You have been, and are as always, truly wonderful.

To my friends here in Canberra and further afield—thank you for the timely distractions and the pleasure of your company these past four and a half years. You are a large part of the reason I am still sane enough to write these words.

I would be amiss if I didn't thank my long-time officemate Wolfgang for the many hours of lively, engrossing discussions over the years, several of which I'm sure were work related! The same goes for the students and staff of Stromlo, current and former—you have made it a pleasure to come to work everyday and for this I thank you all. Thanks also to Geoff, Judy and the team at SSO for ensuring countless observing runs were as pain-free as possible.

Finally, I am perpetually grateful to my parents, who—from the time I first looked up at the dark sky over Arrowtown and started this journey too many years ago—have never wavered in their support and encouragement, even though I'm sure you wished I became an engineer, lawyer or a *real* doctor! This thesis is dedicated to you both.

I would like to gratefully acknowledge the financial support of an *RSAA Joan Duffield Research Scholarship* and an *ANU College of Science Distinguished Research Scholarship*.



## Abstract

The deep southern sky surrounding the Chamaeleon dark clouds is abundant with pre–main sequence stars of various ages. Because of their youth (5–10 Myr) and proximity ( $d \sim 100$  pc), members of two such stellar populations—the open cluster  $\eta$  Chamaeleontis and the nearby  $\epsilon$  Chamaeleontis Association—are ideal laboratories in which to study the formation and evolution of sparse stellar groups and proto-planetary systems. To better understand their role as some of the closest evidence of recent star formation, this thesis explores the birth, dynamical evolution, accretion and disk properties of both groups’ low-mass members.

The notable lack of low-mass stars in the young open cluster  $\eta$  Cha has long been a puzzle. Two possible explanations have been suggested; a top-heavy initial mass function or dynamical evolution, which preferentially ejected the low-mass members. Previous efforts to find these stars several degrees from the cluster core have been unsuccessful. By undertaking a wider (95 deg<sup>2</sup>) photometric and proper motion survey with extensive follow-up spectroscopy, we have identified eight low-mass stars that were ejected from  $\eta$  Cha over the past 5–10 Myr. Comparison with recent  $N$ -body simulations shows our results are consistent with a dynamical origin for the current configuration of the cluster, without the need to invoke an initial mass function deficient in low mass stars.

Two of the dispersed members exhibited strong, variable H $\alpha$  emission during our observations, including a star which had an event suggestive of accretion from a circumstellar disk. New infrared photometry confirms the presence of the disk. This star demonstrates that infrequent, episodic accretion can continue at low levels long after most disks around ‘old’ pre–main sequence stars have dissipated. Furthermore, we show that dynamical evolution is likely to be responsible for the higher-than-expected disk fraction observed in  $\eta$  Cha.

Another two non-members are slightly older than the cluster, but are only 42 arcseconds apart and share similar kinematics and distances. We have shown that they almost certainly form a wide (4000–6000 AU) ~10 Myr-old binary at 100–150 pc. The system is one of the widest pre–main sequence binaries known. Its isolation and dynamical fragility put strong constraints on any birthplace and mode of formation, which we propose was in a turbulent gas filament in the vicinity of the Scorpius-Centaurus OB Association.

In addition to  $\eta$  Cha, we have also examined membership of the unbound  $\epsilon$  Chamaeleontis Association, which lies some 10 degrees to the east and has similar age, distance and kinematics. The two groups were almost certainly born in the outer regions of Sco-Cen only a few million years apart. Many members of  $\epsilon$  Cha have been proposed in the decade since its discovery. After considering the kinematics of candidates from the literature, we have confirmed 11 further stars as likely members. Many of the new members possess infrared spectral energy distributions attributable to circumstellar disks, including four stars with strong H $\alpha$  and forbidden emission which are actively accreting material.

This work on  $\eta$  and  $\epsilon$  Chamaeleontis has identified many interesting targets for follow-up studies of disk evolution, accretion, binarity, and other investigations that require samples of nearby, intermediate-age pre–main sequence stars. Several avenues for future work are discussed in the last chapter of the thesis, including the impact of photometry and astrometry from the forthcoming SkyMapper Southern Sky Survey.



---

# Contents

Notes on the digital copy . . . . .	0
List of Figures . . . . .	ix
List of Tables . . . . .	xiii
<b>1 Introduction</b>	<b>1</b>
1.1 Low-mass star formation . . . . .	1
1.2 Young stars near the Sun . . . . .	2
1.3 The Chamaeleon region . . . . .	14
1.4 Thesis outline . . . . .	19
<b>2 The low-mass stellar halo surrounding <math>\eta</math> Chamaeleontis</b>	<b>21</b>
2.1 Introduction . . . . .	21
2.2 Candidate selection . . . . .	23
2.3 DBS low-resolution spectroscopy . . . . .	29
2.4 WiFeS medium-resolution spectroscopy . . . . .	35
2.5 Other young stars in the region . . . . .	40
2.6 Dynamics . . . . .	41
2.7 Cluster membership . . . . .	45
2.8 Discussion . . . . .	53
<b>3 Episodic disk accretion in the halo of <math>\eta</math> Chamaeleontis</b>	<b>57</b>
3.1 Introduction . . . . .	57
3.2 Multi-epoch spectroscopy . . . . .	58
3.3 Infrared photometry . . . . .	68
3.4 Discussion . . . . .	71
3.5 Conclusion . . . . .	80

<b>4 The young, wide binary system RX J0942.7–7726AB</b>	<b>81</b>
4.1 Introduction . . . . .	81
4.2 Other stars in the region . . . . .	83
4.3 Spectral types and reddening . . . . .	87
4.4 Age of RX J0942.7–7726AB . . . . .	89
4.5 Distance and kinematics . . . . .	94
4.6 Discussion . . . . .	98
4.7 Conclusion . . . . .	103
<b>5 An improved membership of the <math>\epsilon</math> Chamaeleontis Association</b>	<b>105</b>
5.1 Introduction . . . . .	105
5.2 Observations . . . . .	110
5.3 Kinematic membership analysis . . . . .	114
5.4 Discussion . . . . .	121
5.5 Summary . . . . .	134
<b>6 Conclusions</b>	<b>137</b>
6.1 Future prospects . . . . .	140
6.2 Afterword . . . . .	145
<b>Bibliography</b>	<b>147</b>
<b>Appendix A Isochrone colour transformations</b>	<b>165</b>
<b>Appendix B Derivation of the epicyclic approximation</b>	<b>169</b>
<b>Appendix C WiFeS radial velocity precision</b>	<b>173</b>

---

# List of Figures

1.1	Schematic overview of low-mass star formation . . . . .	3
1.2	Members of young local associations on the sky . . . . .	7
1.3	$XYZUVW$ positions of YLA members . . . . .	8
1.4	Disk fraction of young clusters with age . . . . .	10
1.5	Disks in $\eta$ Chamaeleontis . . . . .	12
1.6	The brown-dwarf 2M1207 and its Jupiter-mass companion . . . . .	13
1.7	The Chamaeleon constellation . . . . .	15
1.8	Chamaeleon region as observed by IRAS . . . . .	16
1.9	The $\eta$ Chamaeleontis open cluster . . . . .	18
2.1	DENIS/2MASS colour-magnitude diagram around $\eta$ Cha . . . . .	24
2.2	Distribution of $\eta$ Cha candidates on the sky . . . . .	25
2.3	$\eta$ Cha space motion decomposed into observables . . . . .	27
2.4	Proper motion candidate selection diagram . . . . .	28
2.5	Dwarf and pre-main sequence spectra comparison . . . . .	30
2.6	<i>DBS</i> gravity-temperature diagram . . . . .	32
2.7	<i>DBS</i> spectra of the intermediate-gravity candidates . . . . .	34
2.8	<i>WiFeS</i> integral-field spectrum image format . . . . .	35
2.9	Lithium equivalent widths . . . . .	37
2.10	Comparison of proper motion catalogues . . . . .	44
2.11	Results of candidate dynamical simulations . . . . .	45
2.12	Observed late-type $\eta$ Cha cluster sequence . . . . .	50
2.13	Results of Moraux et al. (2007) $N$ -body simulations . . . . .	54

3.1	H $\alpha$ equivalent width – $v_{10}$ velocity width diagram . . . . .	61
3.2	2MASS J0801–8058 H $\alpha$ profiles during the April 2010 outburst . . . . .	62
3.3	2MASS J0820–8003 H $\alpha$ profiles during the February 2010 outburst . . . . .	63
3.4	Magellan/ <i>MIKE</i> 2MASS J0820–8003 H $\alpha$ profile . . . . .	64
3.5	Multi-epoch H $\alpha$ line profiles: 2MASS J0801–8058 . . . . .	65
3.6	Multi-epoch H $\alpha$ line profiles: 2MASS J0820–8003 . . . . .	66
3.7	2MASS two-colour diagram of $\eta$ Cha members . . . . .	69
3.8	2MASS/WISE spectral energy distributions . . . . .	69
3.9	WISE Atlas colour images . . . . .	70
3.10	2MASS/WISE two-colour diagram . . . . .	71
3.11	IRAS colour image of $\eta$ Cha and surrounds . . . . .	72
3.12	DBS spectra of 2MASS J0801–8058 and 2MASS J0820–8003 . . . . .	73
3.13	The effects of continuum veiling . . . . .	74
3.14	2MASS J0801–8058 periodicity analysis . . . . .	76
4.1	RX J0942.7–7726AB and young groups on the sky . . . . .	82
4.2	RX J0942.7–7726AB finder chart . . . . .	83
4.3	Stars within 10' of RX J0942.7–7726AB . . . . .	84
4.4	Chance alignment comparison sample . . . . .	86
4.5	<i>WiFeS</i> R3000 spectra of RX J0942.7–7726 and 2MASS J0942–7727 . . . . .	88
4.6	Na I indices of RX J0942.7–7726AB and young associations . . . . .	90
4.7	Lithium equivalent widths . . . . .	91
4.8	ASAS3 light curve for RX J0942.7–7726 . . . . .	93
4.9	RX J0942.7–7726AB space motions . . . . .	96
4.10	Dynamical simulations for TW Hydreae and $\beta$ Pic . . . . .	98
4.11	Dynamical simulations for Sco-Cen subgroups LCC and UCL . . . . .	99
4.12	$\beta$ Pictoris colour-magnitude diagram . . . . .	100
5.1	$\epsilon$ Cha members and candidates on the sky . . . . .	109
5.2	POSS2-IR image of the region surrounding $\epsilon$ Cha and HD 104237 . . . . .	109
5.3	Finding charts for RX J1150.9–7411 and RX J1243.1–7458 . . . . .	110
5.4	$\epsilon$ Cha proper motion diagram . . . . .	111
5.5	<i>WiFeS</i> /R3000 spectra of $\epsilon$ Cha candidates . . . . .	115
5.6	Dynamical simulations for $\epsilon$ Cha 12 . . . . .	119
5.7	Northern $\epsilon$ Cha/LCC members . . . . .	122
5.8	$\epsilon$ Cha colour-magnitude diagram . . . . .	125

5.9	Multi-epoch H $\alpha$ velocity profiles . . . . .	127
5.10	WISE photometry of $\epsilon$ Cha candidates . . . . .	129
5.11	2MASS/WISE spectral energy distributions . . . . .	130
5.12	Distribution of $\eta$ and $\epsilon$ Cha members on the sky . . . . .	131
5.13	$\eta$ and $\epsilon$ Cha traceback simulations . . . . .	132
5.14	Ortega et al. (2009) simulations of the formation of $\eta$ and $\epsilon$ Cha . . . . .	133
6.1	Chamaeleon region colour-magnitude diagram . . . . .	141
6.2	Simulated SkyMapper ( $r - i$ ), ( $r - H\alpha$ ) colour plane . . . . .	144
A.1	Linear transformation between $i_{\text{DENIS}}$ and Cousins $I_C$ . . . . .	166
A.2	Transformed and reddened 10 Myr Baraffe et al. (1998) isochrone . . . . .	168
B.1	Schematic of epicyclic motion . . . . .	171
B.2	Orbital motion in the epicyclic approximation . . . . .	171
C.1	Histogram of <i>WiFeS</i> radial velocity differences . . . . .	174
C.2	Results of Kolmogorov-Smirnov tests . . . . .	174
C.3	HAT-South <i>WiFeS</i> radial velocity curve . . . . .	175
C.4	Histogram of HAT-South binary fit RMS values . . . . .	175



---

## List of Tables

1.1	Nearby young associations from Torres et al. (2008) . . . . .	6
1.2	Census of the $\eta$ Chamaeleontis cluster prior to this work . . . . .	18
2.1	Photometric candidates within 5.5 deg of $\eta$ Cha . . . . .	26
2.2	<i>DBS</i> observations of the photometric candidates . . . . .	33
2.3	<i>WiFeS</i> observations of $\eta$ Cha candidates . . . . .	39
2.4	Updated kinematic parameters for $\eta$ Cha . . . . .	43
2.5	Summary of the dynamical simulations . . . . .	51
3.1	<i>WiFeS</i> observations of 2MASS J0801–8058 . . . . .	59
3.2	<i>WiFeS</i> observations of 2MASS J0820–8003 . . . . .	60
4.1	Dynamical simulations against young local associations . . . . .	97
5.1	Late-type $\epsilon$ Cha candidates from the literature . . . . .	108
5.2	Early and solar-type $\epsilon$ Cha candidates from the literature . . . . .	108
5.3	<i>WiFeS</i> observations of $\epsilon$ Cha candidates . . . . .	113
5.4	<i>WiFeS</i> time-series and literature velocities . . . . .	117
5.5	Kinematics of $\epsilon$ Cha members within LCC . . . . .	123



# CHAPTER 1

---

## Introduction

The labour of the astronomer in the present state of his art is much like that of one who should examine, grain by grain, the sands of the sea in the certainty that among them numerous grains must exist of extraordinary value...

– Sir John Herschel<sup>1</sup>

The broad understanding of how stars and planets form was one of the triumphs of 20<sup>th</sup> century observational and theoretical astronomy. Star and planet formation continues to be an extremely active topic of research in astrophysics today, as evidenced by its prominence in the science cases of forthcoming facilities like the *James Webb Space Telescope* (JWST; Gardner et al. 2006), the *Atacama Large Millimetre Array* (ALMA; van Dishoeck & Jørgensen 2008) and the next generation of ground-based colossi (e.g. *E-ELT/GMT/TMT*).

As detailed later in this chapter, the realisation nearly two decades ago that the solar neighbourhood is bestrewn with loose associations of intermediate-age (5–100 Myr) pre-main sequence stars was a watershed moment in the study of young stars and their attendant disks and planets. Like Herschel’s *extraordinary* grains of celestial sand, the youth and proximity of these stars make them ideal laboratories in which to study the formation and evolution of planetary systems. To better understand their role as potential planet hosts and identify promising targets for future studies, this thesis explores the formation, dynamical evolution, accretion and disk properties of two such groups in the deep southern sky; the open cluster  $\eta$  Chamaeleontis and the nearby  $\epsilon$  Chamaeleontis Association.

### 1.1. Low-mass star formation

In contrast to massive stars ( $>8 M_{\odot}$ ), whose formation is still not well constrained (Zinnecker & Yorke 2007), the processes that produce low-mass stars have been generally understood for many years (e.g. Shu et al. 1987; Wilking 1989; McKee & Ostriker 2007). An excellent

<sup>1</sup>*Memoirs of the Royal Astronomical Society*. 1826, Vol. 2, p472

pedagogical review is presented by Stahler & Palla (2004); here we simply summarise the key phases in the journey from a molecular cloud to an isolated low-mass star.

The different stages of low-mass protostellar and pre-main sequence evolution are schematically drawn in Figure 1.1. The formation of a star commences with the growth of condensations in a molecular cloud (*a*). At some point, as the cloud core loses magnetic and turbulent support, the growing central concentration will cause it to be unstable to gravitational collapse. As this “*inside-out*” collapse progresses (*b*), a central hydrostatic core (the protostar) forms and grows as gas and dust continue to fall in. This in-falling envelope is typically thousands of AU in size, a fraction of the parsec-sized clump from which it formed. After a few times  $10^4$  years, a disk begins to form around the deeply-embedded protostar and a strong bipolar outflow develops (*c*). Outflows are intimately associated with the interaction of an accretion disk and the protostellar magnetic fields, and are an essential means of carrying away excess angular momentum from the rapidly accreting protostar. During this phase the protostar is obscured at optical wavelengths by the in-falling envelope and disk but can be observed in the near-infrared. These sources are classified as ‘Type I’ in the infrared spectral energy distribution scheme of Lada (1987). Once the envelope is depleted and dissipated by the strong stellar winds, the young star is surrounded by just its disk (*d*), from which it steadily accretes. This “T Tauri” phase (named after its prototype T Tau) is characterised by the rapid evolution of the circumstellar disk and the formation of planetesimals. Having lost virtually all its envelope, the star is optically visible and its Type II spectrum is dominated by the infrared emission of the disk and the optical/ultraviolet emission associated with accretion. This accretion typically ceases after a few million years with the clearing of gas from the inner disk (*e*), while any remaining material in the outer disk coalesces into planets on the timescale of a few tens of Myr. All the while the young star continues to contract towards its eventual main sequence radius. Once hydrogen is ignited in the star’s interior it has reached the main sequence (*f*). For stars of  $1 M_\odot$ , hydrogen burning starts some  $\sim 30$  Myr after the initial collapse. Lower-mass stars ( $\lesssim 0.2 M_\odot$ ) can take upwards of a Gyr to reach the main sequence.

## 1.2. Young stars near the Sun

Before turning to the Chamaeleon region and the young groups of  $\eta$  and  $\epsilon$  Chamaeleontis, it is instructive to describe the historical context in which they were found. This began two decades ago with the discovery of the first nearby young association around TW Hydrae.

Around the turn of this century, only a handful of pre-main sequence stars had been identified at distances less than 100 pc from the Sun. Nearly all known young stars were located in distant OB associations like Scorpius-Centaurus, or molecular cloud complexes like Taurus, Orion and Chamaeleon. One notable exception was the ‘isolated’ T Tauri star TW Hya (Herbig 1978). At that time the presence of nearby gas and dust was thought to be a ubiquitous sign of recent star formation. Demonstrably young (Rucinski & Krautter 1983), how the star came to be some 13 deg from the nearest dark cloud was a puzzle. This prompted Herbig to posit that TW Hya (and his prototypical example FK Ser) was one of a new class of “Post-T Tauri Stars”, that follow “Classical” and “Weak-lined” T Tauri Stars (see Chapters 3 and 5) in an evolutionary sequence (panel (*e*) of Figure 1.1) and which

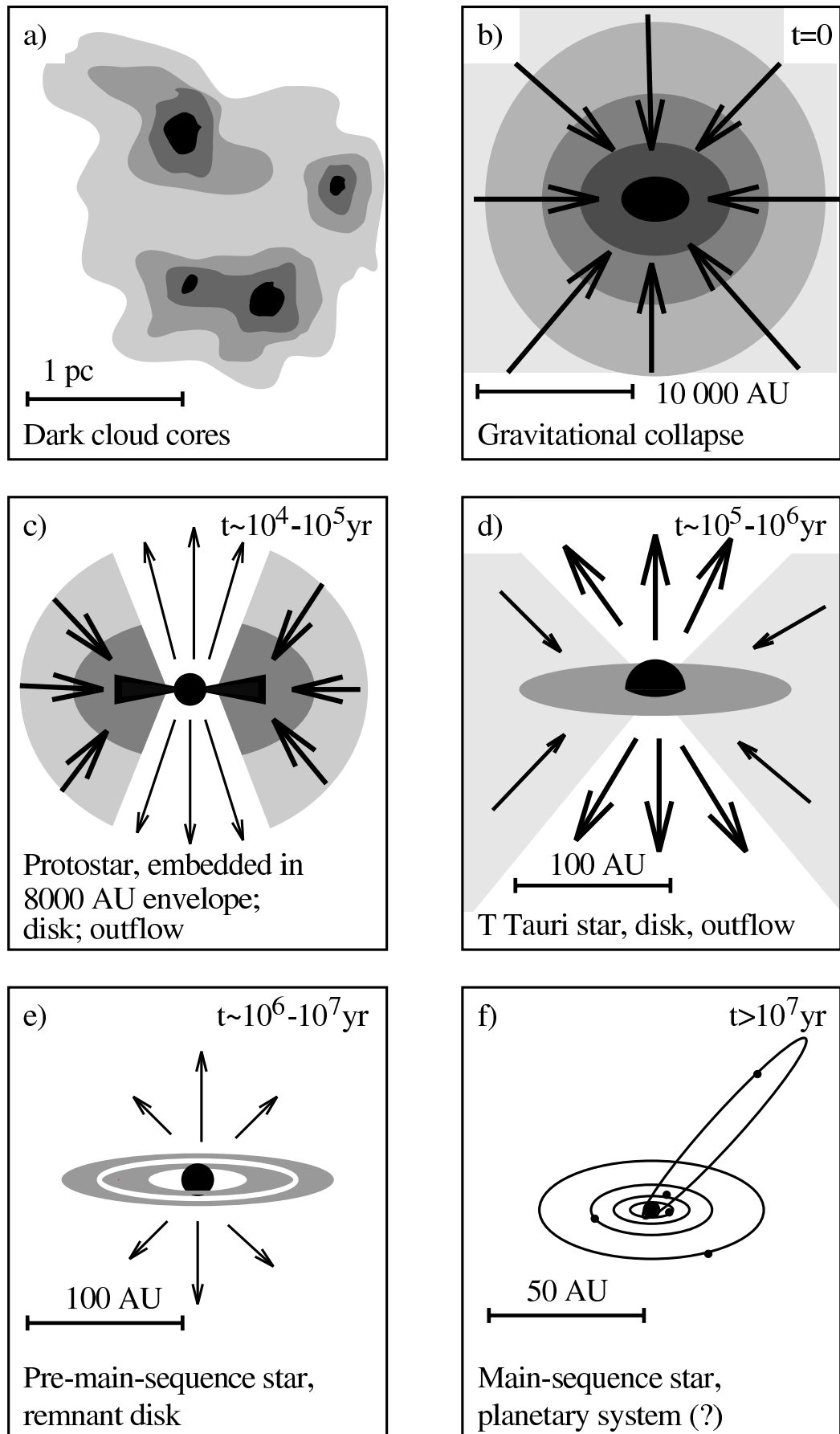


**Figure 1.1** Schematic overview of the key stages in low-mass star formation. Taken from Hogerheijde (1998) after Shu et al. (1987) (used with permission).

should exist in large numbers, mixed in with old field stars following dispersal from their natal molecular clouds (Herbig 1973, 1978). This dispersal was thought to have two main causes; velocity dispersions inherited from turbulent gas flows within the clouds (Feigelson 1996) and to a lesser extent, dynamical ejections following the decay of non-hierarchical “mini-clusters” early in their formation (Sterzik & Durisen 1995).

The mystery deepened when spectroscopy of *Infrared Astronomical Satellite* (IRAS) sources by de la Reza et al. (1989) and Gregorio-Hetem et al. (1992) revealed four additional T Tauri stars within 10 deg of TW Hya. They concluded that this group was a young stellar association close to the Sun, whose molecular remnants had long-since dispersed<sup>2</sup>. From the similarity of their *Röntgensatellit* (ROSAT) X-ray fluxes, spectroscopic characteristics and photometric distances, Kastner et al. (1997) confirmed that these four stars formed a  $20 \pm 10$  Myr-old physical association with TW Hya, at distances of 40–60 pc. They named the group the *TW Hydrea Association* (TWA). Precise trigonometric parallaxes and proper motions from the *Hipparcos* satellite (Perryman & ESA 1997) were of immediate utility. After expanding the search area around the new group, several new members were quickly added (Jensen et al. 1998; Webb et al. 1999; Sterzik et al. 1999). By this time the age of the TWA had begun to converge to its canonical value of 8–10 Myr (Webb et al. 1999; Barrado y Navascués 2006).

Together, these early papers conclusively showed that TW Hya itself is not a high-velocity escapee from some more distant region of star formation as previously thought. Rather, it and the other members of the TWA formed from the same cludlet, in-situ, 8–10 Myr ago, in a region now devoid of molecular material. Since then they have moved through space together, with only their ages and space velocities betraying their common origin. The prototypical young association, TW Hydrea now has at least 29 members at distances of 30–80 pc (Torres et al. 2008;Looper et al. 2010a,b; Shkolnik et al. 2011), including several brown-dwarfs (Lowrance et al. 1999; Gizis 2002; Scholz et al. 2005; Looper et al. 2007).

With this new understanding of star formation and the realisation that there were likely to be many more co-moving groups of stars in the solar neighbourhood, work in the field developed rapidly (see Jayawardhana & Greene 2001). The past decade has seen the discovery of several more young ( $\lesssim 100$  Myr), local ( $d \lesssim 100$  pc) kinematic associations. Progress to that time was summarised by Zuckerman & Song (2004) in their excellent review of nearby young stars. Here we present the major discoveries relevant to our current work.

Soon after the discovery of the TW Hydrea Association, Mamajek et al. (1999) noticed that four *ROSAT* sources were clustered together ten degrees from the Chamaeleon clouds. Their resultant discovery of the 5–8 Myr-old  $\eta$  Chamaeleontis open cluster at a distance of 94 pc is responsible for much of the work upon which this thesis is based. As noted by Mamajek et al. (2000), no younger cluster is closer to the Sun; making  $\eta$  Cha a unique group for the study of pre-main sequence evolution. Soon after and only 10 degrees to the east, a similarly-young association was found around the B9 star  $e$  Cha and the Herbig Ae star HD 104237 (Mamajek et al. 2000; Feigelson et al. 2003). Because of their special relevance to this thesis, these groups and the pre-main sequence stars of the Chamaeleon region are discussed in greater detail in the next section.

---

<sup>2</sup>The only coeval, co-moving groups of stars in the solar neighbourhood known at the time were the Hyades and Ursa Majoris moving groups (e.g. Eggen 1958, 1965). Although nearby (their cores are ~25 and 45 pc away respectively), both are hundreds of millions of years old.

Zuckerman & Webb (2000) searched *Hipparcos* data around 24 stars detected at 60  $\mu\text{m}$  by IRAS for candidates with similar proper motions, radial velocities and distances. Spectroscopy confirmed ten co-moving, 30–40 Myr-old stars in the constellation of Tucana at distances of  $\sim$ 45 pc. They called this group the *Tucana Association*. Independently, Torres et al. (2000) surveyed a 500 deg<sup>2</sup> area around the T Tauri star ER Eri for *ROSAT* sources and discovered the *Horologium Association*. With improved memberships, Zuckerman et al. (2001b) soon recognised that as well as being adjacent on the sky, both groups had the same ages, space motions and distances and merged them into a larger *Tucana-Horologium Association*. The discovery of Tucana by Zuckerman & Webb (2000) was unique at the time as it did not use the characteristic X-ray emission of pre-main sequence stars to select candidates but rather their kinematics. These are a vital criterion for assigning membership of any star to an association, especially for older or nearby groups, whose members can be spread over many hundreds or thousands of square degrees on the sky (e.g. Figure 1.2).

Torres et al. (2001) proposed a large population of young stars in the deep southern sky with kinematical and physical properties similar to Tuc-Hor, which they called GAYA (*Great Austral Young Association*). Further investigation (Torres et al. 2003a,b, 2006, 2008) subdivided GAYA into three distinct, but similar associations: the Tuc-Hor Association of Zuckerman et al. (2001b), the *Columba Association* and the *Carina Association*. All three groups are approximately 30 Myr old but have subtly different space positions and velocities (see Figure 1.3). Torres et al. (2008) noted that they form a structure reminiscent of the Scorpius-Centaurus OB Association, although they are more dispersed due to an older age.

The young A-type star  $\beta$  Pictoris was known to possess a strong infrared excess, betraying the presence of an extended, dusty disk (Smith & Terrile 1984). Like TW Hya however, the isolation and apparent youth of  $\beta$  Pic seemed incongruous. In an attempt to constrain the age of the star, Barrado y Navascués et al. (1999) analysed the kinematics of stars around  $\beta$  Pic, searching for those stars with similar space motions and strong X-ray activity. They found three nearby ( $\sim$ 10 pc) active M-dwarfs (AU Mic and AT Mic AB) and from model isochrones estimated an age for the system of  $20 \pm 10$  Myr. The newly christened  *$\beta$  Pictoris Association* was expanded to 18 systems by Zuckerman et al. (2001a), who searched an extensive list of stars for similar kinematics and various signs of youth. Using isochrones and lithium measurements (see §2.4.1) they estimated the age of  $\beta$  Pictoris to be around 12 Myr; bracketed by TW Hydreae ( $\sim$ 10 Myr) and Tuc-Hor ( $\sim$ 30 Myr). This agrees with the dynamical age estimated by Ortega et al. (2002, 2004), who traced  $\beta$  Pic members back in time to a region of smallest physical size around 11.5 Myr ago. At this epoch  $\beta$  Pic was near the Lower Centaurus Crux subgroup of the Scorpius-Centaurus OB Association (see §1.3.4). A similar technique was applied to TW Hydreae by de la Reza et al. (2006). The 8.3 Myr dynamical age they found agrees with the 8–10 Myr evolutionary age (Barrado y Navascués 2006). Now with over 48 confirmed members in both hemispheres,  $\beta$  Pictoris joins TW Hydreae as one of the youngest groups of stars within 100 pc of the Sun.

Using similar methods to those they used to define  $\beta$  Pictoris, Zuckerman et al. (2004) proposed 40 members of a loose 40–60 Myr-old association around the well-known active system AB Doradus. With a central core of a dozen or so members at 20 pc (including AB Dor itself at 15 pc), the *AB Doradus Association* is the closest young group to the Sun. Torres et al. (2008) confirmed another 49 members but derived an age of  $\sim$ 70 Myr. An older

**Table 1.1** Nearby young associations from Torres et al. (2008)

Association	Age <sup>†</sup> [Myr]	$d$ [pc]	$U$ [km s <sup>-1</sup> ]	$V$ [km s <sup>-1</sup> ]	$W$ [km s <sup>-1</sup> ]	$N_{\text{kin}}^{\ddagger}$
$\epsilon$ Cha	3–7	$108 \pm 9$	$-11.0 \pm 1.2$	$-19.9 \pm 1.2$	$-10.4 \pm 1.6$	20
$\eta$ Cha <sup>#</sup>	5–8	$94 \pm 1$	$-10.2 \pm 0.2$	$-20.7 \pm 0.1$	$-11.2 \pm 0.1$	–
TW Hydrae	8–10	$48 \pm 13$	$-10.5 \pm 0.8$	$-18.0 \pm 1.5$	$-4.9 \pm 0.9$	22
$\beta$ Pictoris	11–12	$31 \pm 21$	$-10.1 \pm 2.1$	$-15.9 \pm 0.8$	$-9.2 \pm 1.0$	48
Octans	~20?	$141 \pm 34$	$-14.5 \pm 0.9$	$-3.6 \pm 1.6$	$-11.2 \pm 1.4$	15
Tuc-Hor <sup>##</sup>	20–40	$48 \pm 7$	$-9.9 \pm 1.5$	$-20.9 \pm 0.8$	$-1.4 \pm 0.9$	44
Columba <sup>##</sup>	20–40	$82 \pm 30$	$-13.2 \pm 1.3$	$-21.8 \pm 0.8$	$-5.9 \pm 1.2$	41
Carina <sup>##</sup>	20–40	$85 \pm 35$	$-10.2 \pm 0.4$	$-23.0 \pm 0.8$	$-4.4 \pm 1.5$	23
Argus <sup>*</sup>	30–50	$106 \pm 51$	$-22.0 \pm 0.3$	$-14.4 \pm 1.3$	$-5.0 \pm 1.3$	64
AB Doradus	50–120	$34 \pm 26$	$-6.8 \pm 1.3$	$-27.2 \pm 1.2$	$-13.3 \pm 1.6$	89

<sup>†</sup> Canonical ages from the literature, in particular the compilation of Fernández et al. (2008).

<sup>‡</sup> Number of members with observed proper motions and radial velocities required for the convergence method. This number should be considered a lower-limit.

<sup>#</sup> Subsumed into  $\epsilon$  Cha by Torres et al. We consider them separate groups (see Chapter 5).

<sup>##</sup> Constituent of the *Great Austral Young Association* (GAYA; Torres et al. 2001)

\* Includes kinematic members of the open cluster IC 2391.

age is consistent with the results of Luhman et al. (2005), who claimed the association is approximately coeval with the Pleiades (100–125 Myr) and is a remnant of the large-scale star-formation event that formed the cluster. Recent dynamical simulations by Ortega et al. (2007) have increased the likelihood of this scenario. They showed the two groups reached a minimum separation of 40 pc around 120 Myr ago. Similar relationships between clusters and loose associations have been proposed for  $\eta$  and  $\epsilon$  Cha, and Argus/IC 2391 (see below).

The state of the field was recently summarised by Torres et al. (2008). As part of their “*Search for Associations Containing Young Stars*” (SACY), they sought to improve the phase-space (heliocentric position and velocity) definitions of the above groups, as well as their ages and kinematic distances. The SACY sample contains stars over 2000 *Hipparcos* and Tycho-2 stars later than G0 that have counterparts in the *ROSAT* Bright Source Catalogue (Voges et al. 1999). After obtaining radial velocities for the sample they applied an iterative algorithm (Torres et al. 2006) that sought to converge the photometric and kinematic distances for a range of model isochrones, whilst maintaining a clustering in six-dimensional XYZUVW phase-space. The results of their analysis are shown in Figures 1.2 and 1.3, and summarised in Table 1.1, with age estimates from the compilation of Fernández et al. (2008). Although these absolute ages may be uncertain by up to a factor of two, the *relative* ages can be trusted, i.e. TWA is younger than  $\beta$  Pic, which is younger than Tuc-Hor, and so on.

As expected of a kinematic group, each association occupies a well-defined region in velocity space, with velocity dispersions of the order 1–2 km s<sup>-1</sup>. Their sizes are generally larger than implied from their velocity dispersions and ages. This suggests that they were not formed by the dissolution of compact clusters, but rather in a more distributed manner, similar to OB associations. Projected onto the plane of the sky (Figure 1.2) the associations

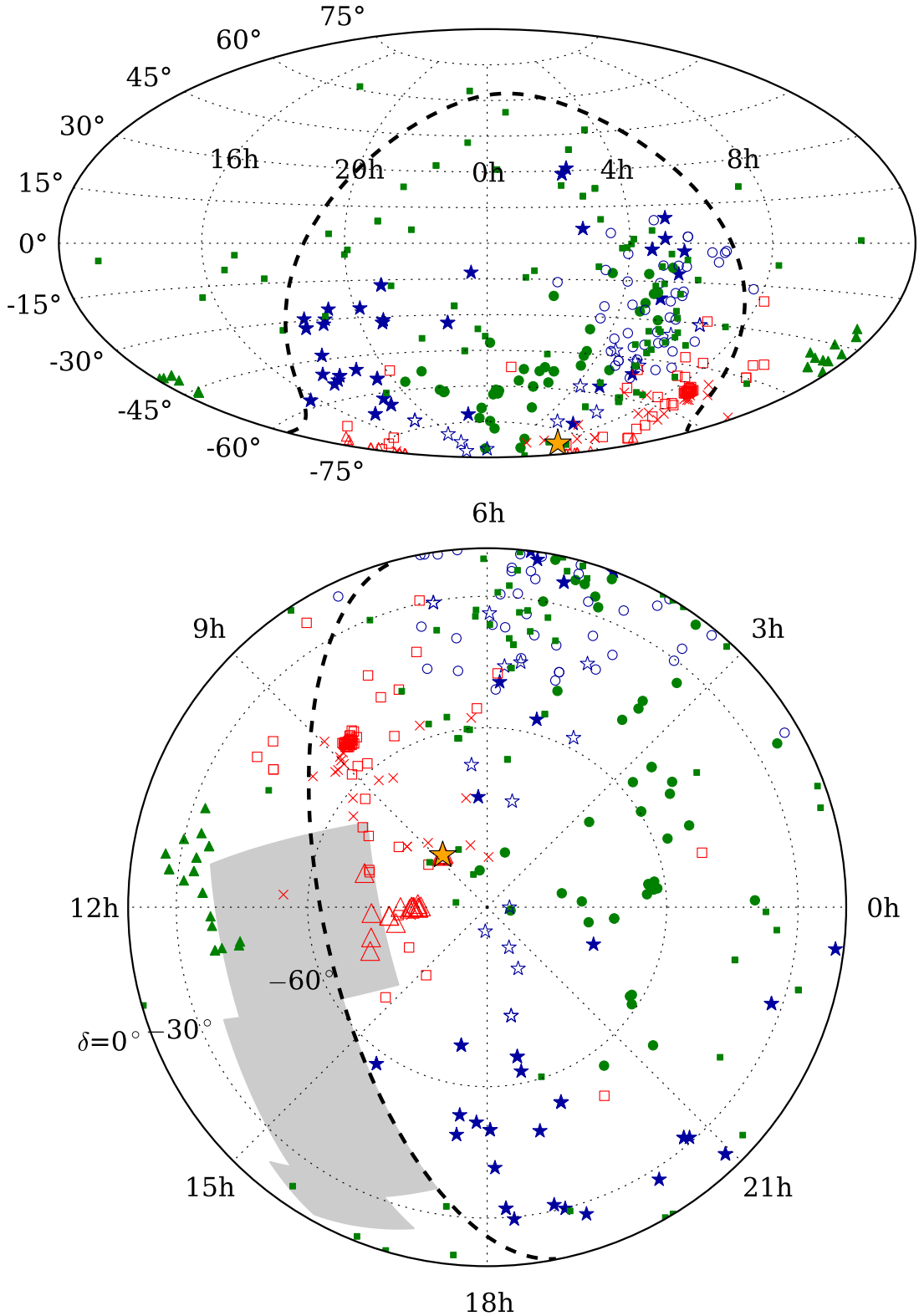


**Figure 1.2** Young local associations as defined by Torres et al. (2008). Plotted are members of  $\beta$  Pictoris (filled blue stars), Tucana-Horologium (filled green circles), Columba (open blue circles), Carina (red crosses), TW Hydrae (filled green triangles),  $\epsilon$  Cha (open red triangles), Octans (open blue stars), Argus (open red squares) and AB Doradus (filled green squares). The gold star denotes the position of  $\eta$  Cha. The dashed line is the Galactic equator. *Top:* Hammer-Aitoff equal-area projection of the entire sky. The distribution of YLA members is strongly biased towards the southern hemisphere and negative Galactic latitudes. The clustering of sources near  $(8^h, -50^\circ)$  is the open cluster IC 2391, which is kinematically linked to Argus. *Bottom:* Polar orthographic projection of the southern celestial hemisphere. The shaded region shows the approximate extent of the Sco-Cen OB Association, whose LCC subgroup lies between TW Hydrae and  $\epsilon$  Cha.

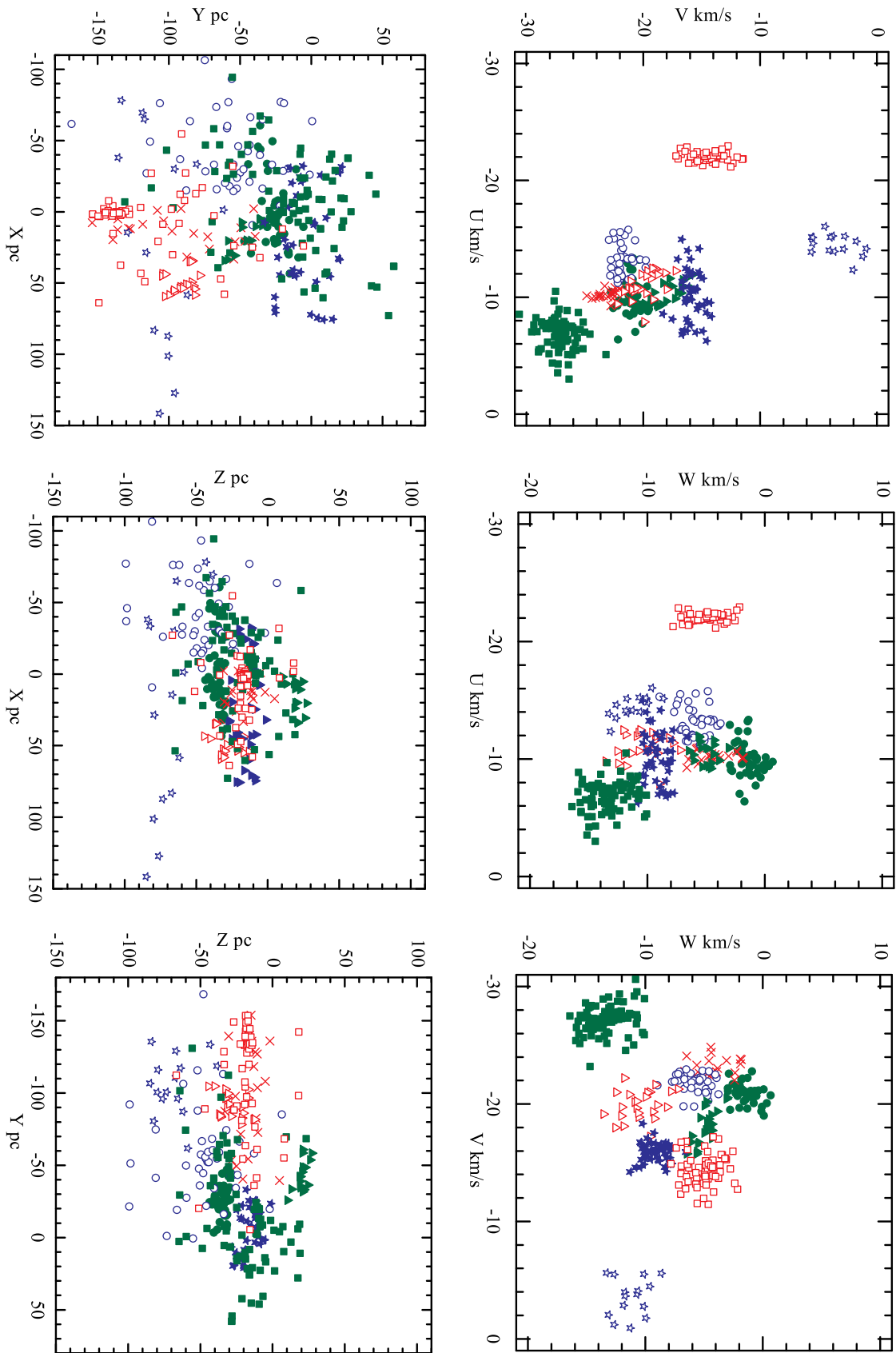


**Figure 1.3** Phase-space locations of young local association members, taken from Torres et al. (2008, used with permission). X is the position from the Sun towards the Galactic centre, Y points in the direction of Galactic rotation and Z towards the north Galactic pole. ( $U, V, W$ ) are the corresponding velocity vectors along these directions. Symbols are as in Figure 1.2. Although spread over the entire sky, YLA members form coherent groups in three-dimensional space and are tightly clustered in velocity space.

are strongly biased towards the southern hemisphere and negative Galactic latitudes. This is likely due to the presence of the Scorpius-Centaurus OB Association (and the greater Gould belt), around which many of the groups likely formed over the past 5–30 Myr (Mamajek & Feigelson 2001; Sartori et al. 2003; Makarov 2007; Fernández et al. 2008; Ortega et al. 2009). Fernández et al. (2008) proposed that Sco-Cen and the young local associations were formed when a spiral density wave collided with a giant molecular cloud in the solar vicinity, while Ortega et al. (2009) found the youngest of the groups ( $\eta$  Cha,  $\epsilon$  Cha, TWA,  $\beta$  Pic) could have been formed in the wake and collision of shells created by supernovae and stellar winds in the subgroups of Sco-Cen. These scenarios are addressed further in later chapters.

In addition to the well-known associations described above, Torres et al. (2008) confirmed two more that were tentatively detected during their previous works (Torres et al. 2003a,b). The *Octans Association* contains only 15 solar-type stars—none with trigonometric parallaxes—and is unusually extended along the X-direction (see Figure 1.3). Despite this, its distinct space motion suggests it is a real kinematic group. Torres et al. (2008) estimated an age of  $\sim$ 20 Myr, but noted that this is very uncertain until the association is better defined.

Finally, the  $\sim$ 40 Myr *Argus Association* was easily identified from its unique  $U$  velocity (Figure 1.3). It may be associated with the 30–50 Myr-old open cluster IC 2391 (see discussion in Riedel et al. 2011; Desidera et al. 2011). As the distance to the cluster (140–160 pc; Platais et al. 2007) was somewhat extreme for their Argus members, Torres et al. (2008) supposed that the association must be larger and that they detected only its nearby members. This was confirmed by Riedel et al. (2011), who announced the discovery of AP Col—the closest young star currently known ( $d = 8.4 \pm 0.1$  pc; trigonometric). The active M4.5e star shares Argus’ distinctive kinematics and has the lithium measurements, gravity and luminosity of a  $\sim$ 40 Myr-old pre-main sequence object.

Because of its dependence on *ROSAT*, the SACY sample is biased against X-ray-faint late-type stars in all but the closest groups (see discussion in §2.5.1). Furthermore, the convergence method used by Torres et al. requires accurate proper motions and radial velocities to calculate kinematic distances. These are not available for all members, especially faint low-mass and substellar candidates. However, with well-defined phase-space locations and ages, future surveys (such as the one undertaken in Chapter 5) can test candidates against these associations and expand their memberships to lower masses.

### 1.2.1. Laboratories for star and planet formation

As most-recently pointed out by Zuckerman et al. (2011), while investigation of these young associations will no doubt reveal new insight into early *stellar* evolution, their most important contribution to astrophysics is likely to be in understanding the formation and evolution of extrasolar planetary systems. Their proximity to Earth make them ideal laboratories for studying circumstellar disks and planetary systems around stars in the crucial age range of 5–50 Myr, when planet formation is well underway and circumstellar disks are rapidly evolving (e.g. Lissauer 1993; Pollack et al. 1996; Raymond et al. 2005).

The next few pages explore two topics easily exploited using members of the above associations; circumstellar disk studies and the direct imaging of extrasolar planets. This is by no means a complete review of ongoing work in these fields, but serves to highlight where young, nearby associations have had a particular impact.

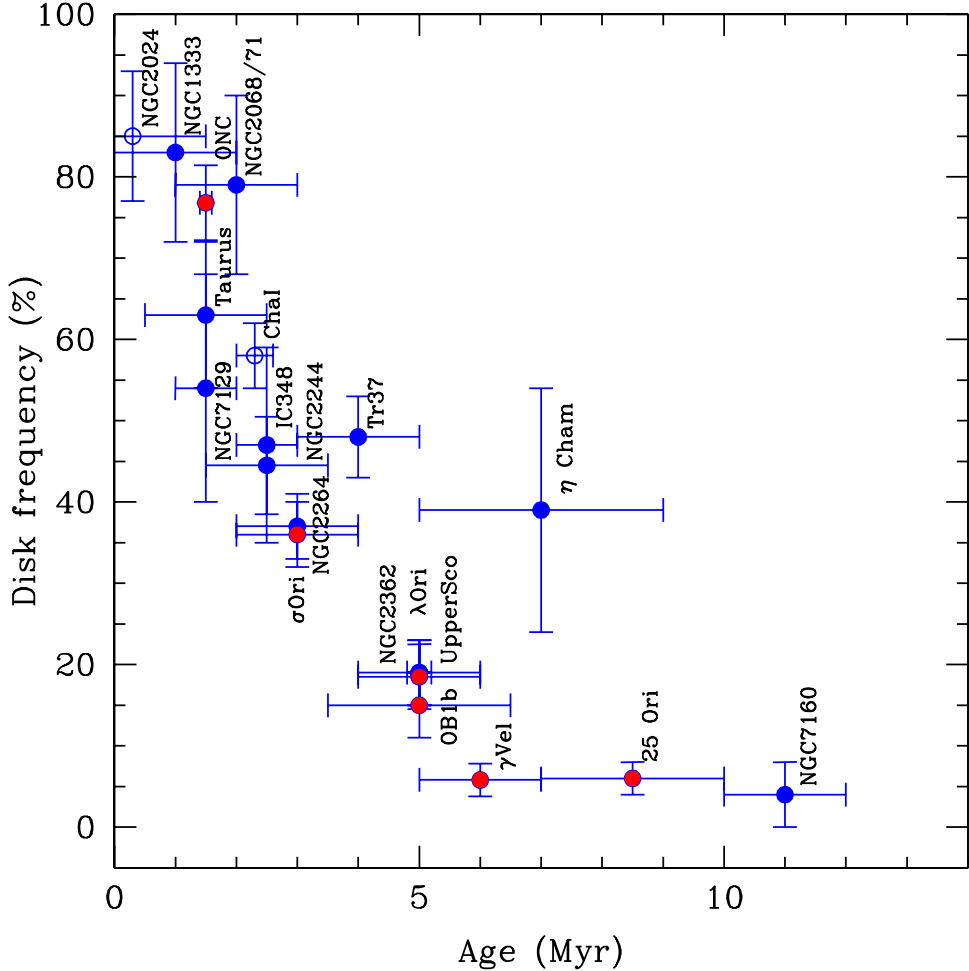


**Figure 1.4** Fraction of stars with near-infrared disk emission as a function of host cluster age, as compiled by J. Hernández (private communication, after Hernández et al. 2008). Solid symbols show the disk frequency in the T Tauri mass range (K5 or later) derived from *Spitzer*/IRAC (3.6–8  $\mu\text{m}$ ) observations. Open points are from JHKL (1.25–3.5  $\mu\text{m}$ ). Red points were observed by the above author, blue clusters were taken from the literature.

### Circumstellar disk studies

The frequency of inner disks around pre–main sequence stars is well-known to decrease with time. Observationally, disks are common at ages of 1–2 Myr in regions like Orion and Taurus, but by  $\sim$ 10 Myr they appear to be very rare. This is illustrated in Figure 1.4, where the near-infrared disk fraction of young clusters is plotted versus their age, as compiled by Hernández et al. (2008) (see similar plots by Haisch et al. 2001; Hillenbrand 2005; Mamajek 2009). As well as the overall decreasing trend, there can be large ( $\lesssim$ 20 percent) cluster-to-cluster differences in the disk fraction at a given age. These can be explained by variations in the disk destruction rate with stellar mass (e.g. Carpenter et al. 2006), environment (Luhman et al. 2008) and dynamical conditions (Armitage & Clarke 1997). Of particular importance, Bouwman et al. (2006) found that binarity is a key factor influencing the retention of disks (at least in  $\eta$  Cha). They showed a strong anti-correlation between binarity and the presence of a disk, and from this implied that the mean disk dissipation timescale in  $\eta$  Cha binaries was half that of the single stars. In addition to physical effects, sensitivity differences between surveys and incomplete cluster memberships (especially for those stars lacking disks, a youth indicator) mean care must be taken when interpreting such a diagram.

These complications aside, the clusters in Figure 1.4 are well-fitted by an exponential, with an  $e$ -folding timescale of 2.5–3 Myr (Mamajek 2009; Fedele et al. 2010). Hence, by an age of 10 Myr we should expect only  $\lesssim 5$  percent of all stars to show signs of inner disks. With estimated ages of 5–12 Myr, the young associations of TW Hydriæ,  $\beta$  Pictoris,  $\eta$  Cha and  $\epsilon$  Cha occupy a region of this diagram where disks are rapidly disappearing around low-mass stars. Despite the small disk fractions expected at such ages, several members of these associations have been observed to still possess optically-thick disks supporting strong active accretion (e.g. Muzerolle et al. 2000; Lawson et al. 2002, 2004; Jayawardhana et al. 2006;Looper et al. 2010a,b). In particular,  $\eta$  Cha appears to have an anomalously high disk fraction for its 5–8 Myr age, though only a handful of stars in the cluster are currently accreting. Pre-empting the discussions of Chapter 3, dynamical evolution of this uniquely sparse, compact cluster may have biased its observed membership towards disk-bearing stars, though sensitivity, completeness and environmental effects are almost certainly complicit (Lyo et al. 2003; Lawson et al. 2004). It is possible other clusters may reside in the region of the diagram occupied by  $\eta$  Cha if their memberships were more complete. This important caveat notwithstanding, the results of the above studies show that, while it seems a small number of stars can continue to accrete from disks for up to  $\sim 10$  Myr, accretion and inner disks beyond this age are increasingly rare. Since the bulk of the disk mass is thought to comprise of gas, the dearth of accretors beyond an age of 10 Myr is an indirect constraint on the timescale of gas dissipation in inner disks (Jayawardhana et al. 2006; Fedele et al. 2010) and, in turn, on giant planet formation.

After the cessation of accretion, most stars in the nearby young associations above show clear signs that their *primordial* disks are rapidly evolving into cold *debris disks* containing a variety of different sized dust grains and larger bodies required for the planetary formation process (Wyatt 2008; Raymond et al. 2005). As expected from the exponential decline in disk frequency, even in a coeval population of stars, disks can take on a variety of morphologies depending on their central star, multiplicity, physical conditions and dynamical history. Grain coagulation and reprocessing, vertical settling and planetesimal formation can all shape the structure and mineralogy of disks (e.g. Sicilia-Aguilar et al. 2008, 2009), and large inner holes can develop as a result of planet formation (Lagrange et al. 2010; Bouwman et al. 2010) or photo-evaporation by the parent star (Alexander et al. 2006).

This is exemplified in Figure 1.5, where we plot the spectral energy distributions of nine members of  $\eta$  Cha observed by Sicilia-Aguilar et al. (2009). As expected of a rapidly evolving ‘transitional’ population of age 5–8 Myr, disks in  $\eta$  Cha show a great variety of morphologies; from a flared, optically-thick Type II (Lada 1987) accretion disk (ECHA J0843.3–7905), to optically-thick but geometrically thin (flat) accretion disks (ECHA J0841.5–7853, ECHA J0844.2–7833) and disks presenting no near-infrared excess due to the formation of inner opacity holes bereft of dust (RECX 5, RECX 9). The prominent ‘bump’ at  $10\ \mu\text{m}$  observed in the spectral energy distribution of RECX 5 is thought to be due to the presence of large amounts of the crystalline silicate forsterite in its disk. Bouwman et al. (2010) have speculated that the clearance of the inner regions of the RECX 5 disk is a consequence of the formation of a Saturn-mass planet, with the planet being responsible for the difference in both the spectral energy distribution and chemical composition of the dust around RECX 5 compared to other disk-bearing members of the cluster.

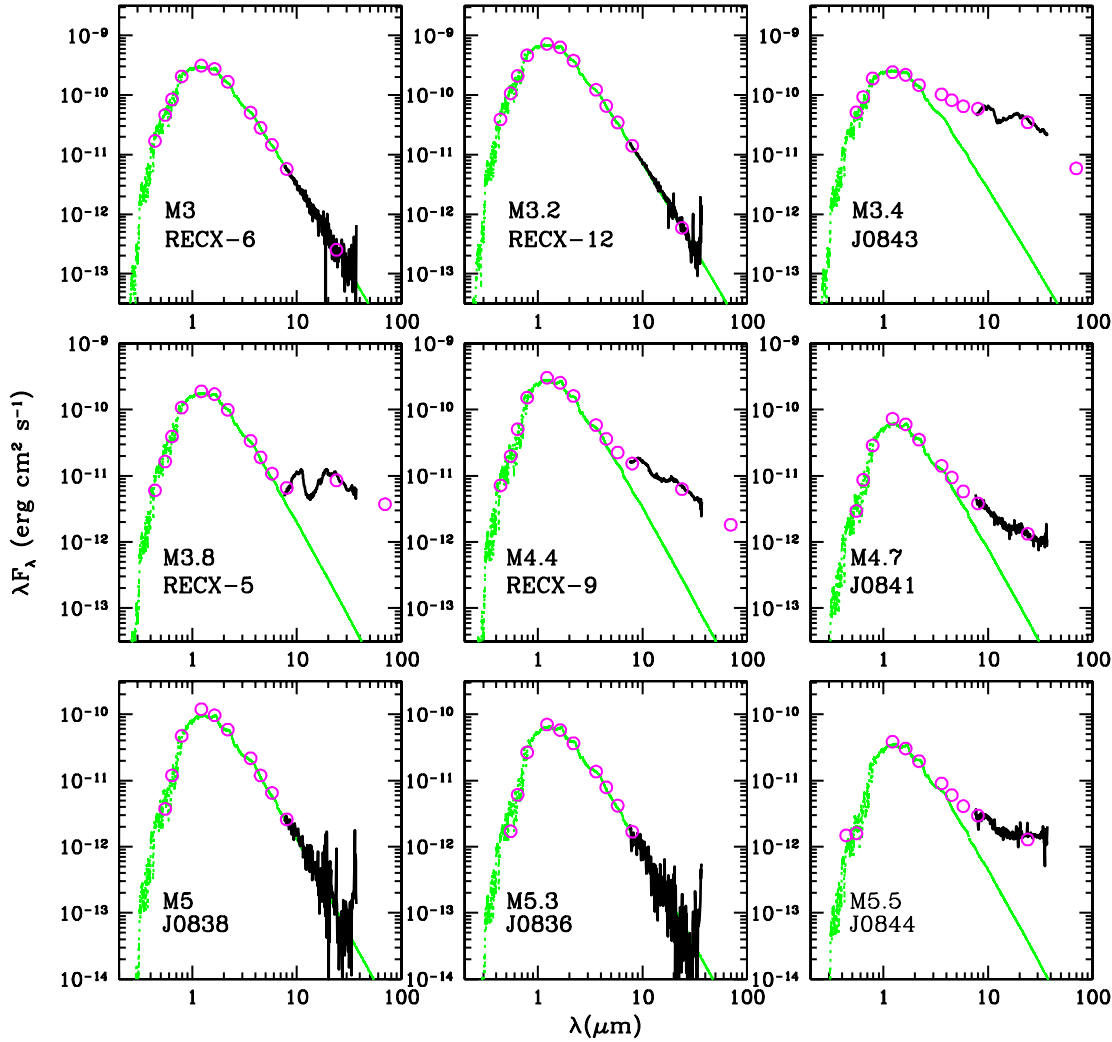


**Figure 1.5** Spectral energy distributions of several  $\eta$  Cha members from Sicilia-Aguilar et al. (2009, reproduced by permission of the AAS), including optical and infrared data (open circles), *Spitzer* IRS spectra (thick black line), and MARCS models (dotted green lines) of the underlying stellar photosphere.

### Direct imaging of extrasolar planets

Another avenue for exploring the formation and architecture of planetary systems is the direct imaging of substellar and planetary-mass companions around young stars. Newly-formed gas giants are hotter, brighter and in-turn easier to detect by direct imaging than planets around more-evolved stars (Burrows et al. 1997; Baraffe et al. 2003). Owing to their youth and proximity, stars in these associations offer themselves as promising targets for extrasolar planet searches by high-resolution and high-contrast imaging.

Exciting early results from such programmes have already been announced. Chauvin et al. (2004, 2005a) imaged the first extrasolar planet around 2MASSW J1207334–393254, an M8 brown-dwarf member of the TW Hydriæ Association (Figure 1.6). A recent trigonometric parallax by Ducourant et al. (2008) limits the mass of 2M1207b to 4–8  $M_{\text{Jup}}$  and places it 41 AU from its primary<sup>3</sup>. This is an orbital and mass regime only now starting to be explored with long-term ( $>10$  year) radial velocity surveys (Udry 2010). Given its age, distance and

<sup>3</sup>Its mass may be as small as  $<1 M_{\text{Jup}}$  if 2M1207b is actually the hot remnant of a protoplanetary collision, as suggested by Mamajek & Meyer (2007).

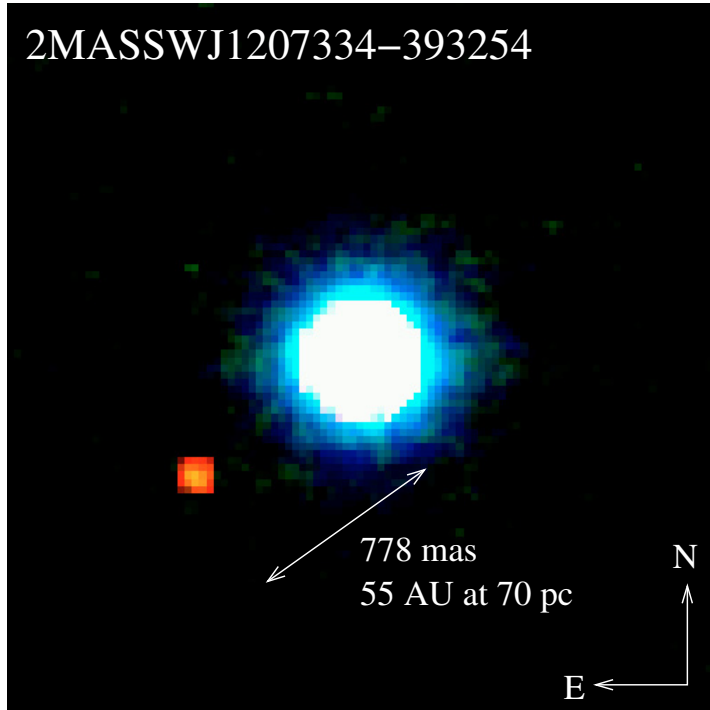


**Figure 1.6** Colour composite  $H/K_s/L'$  image of the brown-dwarf 2MASSW J1207334–393254 and its planetary-mass companion from Chauvin et al. (2004, used with permission). The  $4\text{--}8 M_{\text{Jup}}$  companion is demonstrably cooler than the M8 primary. At the 52 pc trigonometric distance measured by Ducourant et al. (2008) its 778 mas separation would be 41 AU. For comparison, Pluto orbits between 29 AU (perihelion) and 49 AU (aphelion).

spectral type, 2M1207b is under-luminous by a factor of  $\sim 10$  compared to standard models of brown-dwarf/giant-planet evolution (e.g. Baraffe et al. 2003). Various scenarios have been proposed to explain the under-luminosity (Mohanty et al. 2007; Mamajek & Meyer 2007; Patience et al. 2010; Barman et al. 2011; Skemer et al. 2011), but it remains unresolved. Because of its proximity and low mass, 2M1207b will continue to be a benchmark object for the study of atmospheric physics in giant planets.

Soon after the discovery of 2M1207b, a  $13 M_{\text{Jup}}$  object at the planet/brown-dwarf boundary was reported by Chauvin et al. (2005b),  $\sim 260$  AU away from AB Pic, a  $\sim 30$  Myr-old member of the Carina Association (Song et al. 2003). The wide separation of AB Pic b makes formation by core accretion (Pollack et al. 1996) of planetesimals very unlikely because of the long timescale needed for them to form at such distances (Augereau et al. 2001). Gravitational instabilities within the protoplanetary disk (e.g. Boss 1997, 2003) are a much more probable scenario for the origin of wide companions like AB Pic b.

Recently, Lagrange et al. (2010) announced the discovery through adaptive optics imaging of a  $\sim 9 M_{\text{Jup}}$  companion in the disk of  $\beta$  Pictoris, the eponymous member of the 12 Myr-old association. This mass and the 8–15 AU orbital semi-major axis they measured are fully consistent with those predicted by dynamical studies that invoked a planet to reproduce the well-known inner-disk warp of  $\beta$  Pictoris (Mouillet et al. 1997; Augereau et al. 2001).

Multiple planet systems have also been imaged. Most famously, Marois et al. (2008, 2010) discovered four planets of  $5\text{--}7 M_{\text{Jup}}$  orbiting the A5 star HR 8799 at distances of 24–70 AU. Knowledge of the age and luminosity of giant gas planets is critical for deriving their fundamental properties, including mass. In the case of HR 8799, kinematic membership in

the  $\sim$ 30 Myr-old Columba Association was crucial in determining a robust age estimate for the system (Doyon et al. 2010; Zuckerman et al. 2011). This age was recently confirmed from models of dynamical stability and planet cooling by Currie et al. (2011).

Current and as-yet-undiscovered members of associations like  $\beta$  Pictoris, TW Hydrae,  $\epsilon$  Cha and  $\eta$  Cha will be ideal places to continue such work. Upcoming instruments like the *Gemini Planet Imager* (Graham et al. 2007; Kataria & Simon 2010), VLT/SPHERE (Beuzit et al. 2010) and the planned EPIC imager/spectrograph on the E-ELT (Kasper et al. 2010) will be capable of discovering hundreds of giant planets, and dozens of lower-mass planets down to the terrestrial planet regime.

### 1.3. The Chamaeleon region

The constellation of Chamaeleon (Plancius, c1597; Figure 1.7) is abundant with pre–main sequence stars of various ages. Lying near the south celestial pole between Galactic latitudes of  $-25^\circ < b < -10^\circ$ , it is dominated in the east by the Chamaeleon molecular cloud complex and its populations of 2–4 Myr-old stars. In front of the clouds lie members of the  $\epsilon$  Chamaeleontis Association (Figure 1.8, Chapter 5), one of the many young associations discovered in the past decade. Ten degrees to the west is the eponymous open cluster surrounding the bright star  $\eta$  Chamaeleontis. These two groups are the subject of this thesis and are briefly introduced below. Further information can be found in Chapters 2 and 5.

#### 1.3.1. The Chamaeleon molecular cloud complex

Recently reviewed by Luhman (2008) (also see the earlier review by Schwartz 1992), the Chamaeleon complex hosts some of the nearest dark clouds to the Sun. The complex comprises three main clouds (Cha I, II and III) and an assortment of smaller clouds and filaments. Together they dominate 100  $\mu\text{m}$  dust emission maps of the region (Figure 1.8). The accepted distance to the main clouds is 160–180 pc (Whittet et al. 1997; Bertout et al. 1999), although this may be as high as 200–220 pc (Knude 2010). Cha I, II and III each cover several square degrees on the sky (5–10 pc) and their estimated total mass is around 4000–5000  $M_\odot$  (Mizuno et al. 2001). This is small compared to other well-known molecular cloud complexes like Taurus (a few times  $10^4 M_\odot$ ) and Orion ( $10^5$ – $10^6 M_\odot$ ).

Cha I hosts at least  $\sim$ 240 stars with a median age of 2 Myr (Luhman 2004a, 2007). Luhman (2007) determined that star formation began in the clouds 3–6 Myr ago and has continued at a decreasing rate to the present day. The census of Cha II is less complete. Spezzi et al. (2008) have identified  $\sim$ 50 members with mean age of  $4 \pm 2$  Myr and a mode of 3–4 Myr. Cha III has no known stellar or protostellar members (e.g. Persi et al. 2003). It may however be in the very early stages of star formation (Belloche et al. 2011).

#### 1.3.2. The $\eta$ Chamaeleontis open cluster

This nearby ( $\sim$ 94 pc; van Leeuwen 2007) young cluster is the subject of much discussion in Chapters 2 and 3. It was discovered by Mamajek et al. (1999), who noticed that four Weak-lined T Tauri stars detected by ROSAT (Alcalá et al. 1997) southwest of Cha I were clustered

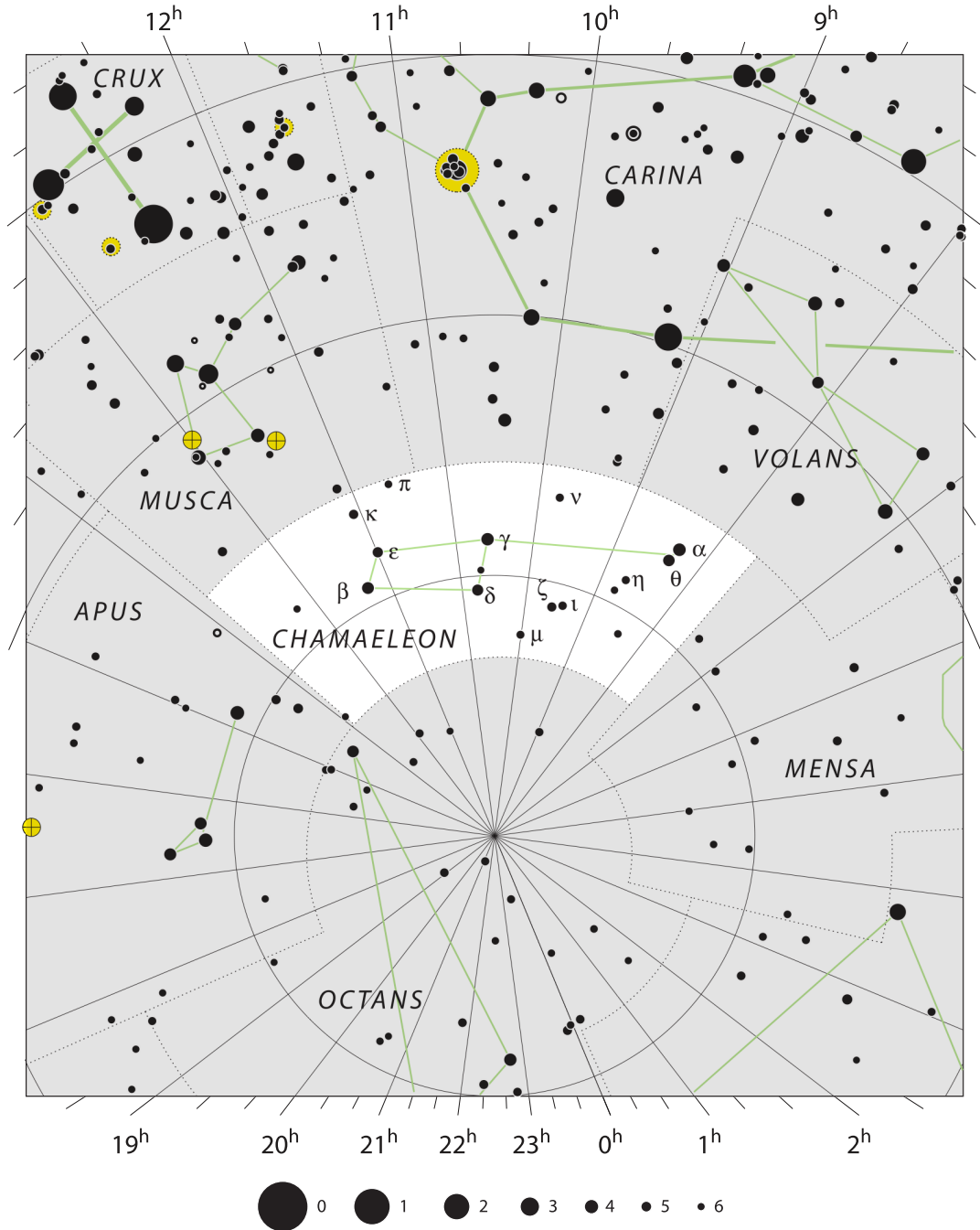


**Figure 1.7** Map of Chamaeleon and the other constellations of the deep southern sky. The size of each star gives its apparent visual magnitude. *Image credit:* IAU/Sky & Telescope Magazine (used with permission).

with the early-type stars  $\eta$  Cha, RS Cha and HD 75505 (the realisation that the WTTs may form a small cluster had been previously noted by Covino et al. 1997). Deep, pointed ROSAT imaging revealed the presence of an additional six X-ray-bright late-type stars. All ten late-type candidates showed Li I  $\lambda$ 6708 equivalent widths greater than those seen in the  $\sim$ 100 Myr-old Pleiades cluster and had luminosities 1–2 mag above the main sequence. From *Hipparcos* astrometry the three early-type stars were found to be co-moving and co-distant at  $\sim$ 97 pc (now 94 pc with updated parallaxes). Mamajek et al. (1999) estimated an age of 2–18 Myr for the cluster, which agrees with the 10–15 Myr dynamical age estimated by Mamajek et al. (2000). More recent determinations have refined the age to 5–8 Myr (Jilinski et al. 2005; Lawson & Feigelson 2001; Luhman & Steeghs 2004).

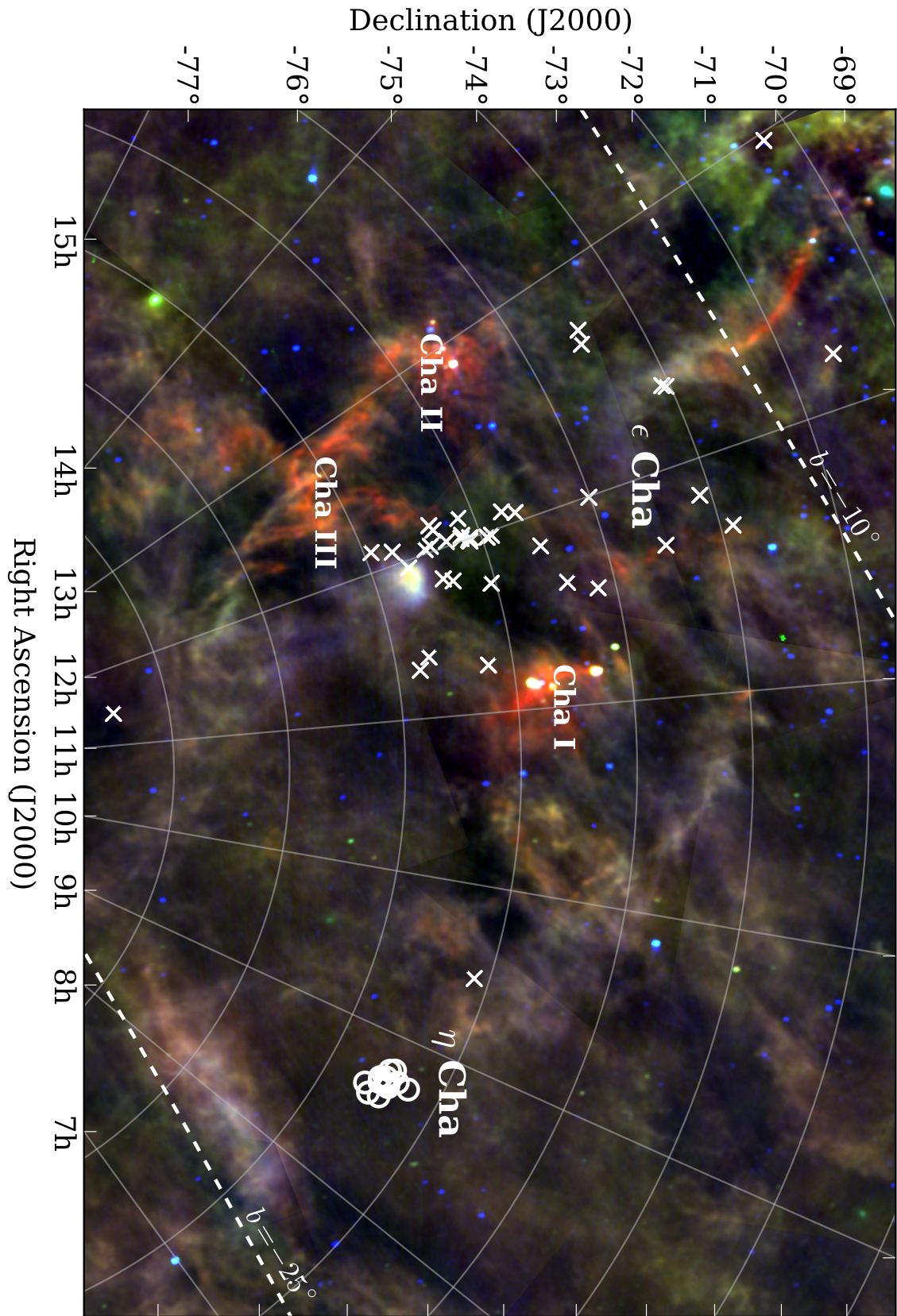


**Figure 1.8** IRAS 25/60/100  $\mu\text{m}$  colour mosaic of the Chamaeleon region. The  $\eta$  Cha open cluster and proposed members of the  $\epsilon$  Cha Association (white crosses) are plotted. Dust emission in the region is dominated by the Chamaeleon I, II and III clouds. The filamentary 100  $\mu\text{m}$  structure around  $b = -10^\circ$  is the Musca clouds. The blue, compact infrared source between Cha I and III is the dark cloud G300.2–16.9 (Nehmé et al. 2008). It has a similar distance and velocity to the  $\epsilon$  Cha member T Cha and is probably associated with it.

Despite Mamajek et al. (2000) predicting the presence of up to 50 further members from existing photometric catalogues, intensive searches have confirmed only five new members out to a radius of 1.5 degrees (Lawson et al. 2002; Lyo et al. 2004b; Song et al. 2004; Luhman & Steeghs 2004). Lyo et al. (2004b) have suggested that another 20–29 low-mass stars and brown-dwarfs remain to be discovered. One of the key contributions of the current work is the detection of a halo of low-mass members beyond 1.5 deg (Chapter 2). Such a population was first suggested by Mamajek et al. (1999) and recently modelled by Moraux et al. (2007).

The 18 member systems of  $\eta$  Cha known prior to this current work are listed in Table 1.2 and shown on the sky in Figure 1.9. With only 22–28 members (including possible unresolved companions) and a total stellar mass of  $<20 M_{\odot}$ , the cluster is incredibly sparse. This fact (and its southern declination) was responsible for its only very recent discovery. Despite its sparcity,  $\eta$  Cha is incredibly compact for a 5–8 Myr cluster. In contrast to the unbound  $\sim 10$  Myr TW Hydrae Association, which extends over 20 pc in space,  $\eta$  Cha is  $<1$  pc in size (Figure 1.9). At this radius the cluster escape velocity is a sedate  $\sim 0.5 \text{ km s}^{-1}$ . In order for  $\eta$  Cha to have remained bound in spite of the 1–2  $\text{km s}^{-1}$  turbulent velocities commonly observed in molecular clouds, it must have had a much larger total mass, both from stars and molecular material. Its compactness today is probably a sign it only recently lost this natal material (Mamajek et al. 2000). Such a notion is borne out by the maximum stellar mass–cluster mass relation proposed by Weidner & Kroupa (2006), which predicts a mass of 30–40  $M_{\odot}$  for the embedded  $\eta$  Cha proto-cluster. This suggests a significant fraction ( $\sim 50$  percent) of its primordial stellar members have indeed already been lost, likely as a result of gas expulsion (Weidner et al. 2007) and dynamical evolution (Moraux et al. 2007).

Because of their age, proximity and lack of appreciable reddening, members of  $\eta$  Cha have already been the subject of many studies of binarity (Köhler & Petr-Gotzens 2002; Bouwman et al. 2006; Brandeker et al. 2006), accretion (Lawson et al. 2004; Jayawardhana et al. 2006; Scholz et al. 2007) and in particular circumstellar disk properties (Lyo et al. 2003; Haisch et al. 2005; Megeath et al. 2005; Ramsay Howat & Greaves 2007; Gautier et al. 2008; Sicilia-Aguilar et al. 2009; Bouwman et al. 2010). The cluster is notable for its apparent excess of circumstellar disks relative to other similarly-aged clusters (Figure 1.4; Hernández et al. 2008; Mamajek 2009). The cause of this excess is currently unknown (if one exists at all, see §1.2.1), but may be related to dynamical evolution over the past 8 Myr (Chapter 3).

### 1.3.3. The $\epsilon$ Chamaeleontis Association

Between the Chamaeleon clouds lies a distinct population of older (3–7 Myr; Fernández et al. 2008), foreground ( $d \sim 100$ –120 pc) objects, co-moving with the early-type stars  $\epsilon$  Cha and HD 104237 (Frink et al. 1998; Terranegra et al. 1999). This grouping, now called the  $\epsilon$  Chamaeleontis Association (Mamajek et al. 2000; Feigelson et al. 2003), shares a similar age, kinematics and distance to  $\eta$  Cha. Their physical similarities and close proximity have led some authors to propose they may be extensions of the same group (Jilinski et al. 2005; Torres et al. 2008). However, recent spectroscopic work by Lyo et al. (2008) (see also discussion in Lawson et al. 2009) suggests  $\eta$  Cha is likely 1–2 Myr older than  $\epsilon$  Cha. The currently proposed membership of  $\epsilon$  Cha is shown on the sky in Figure 1.8. Although most of its members fall in the region between the clouds, there are several outliers across Chamaeleon and north towards the Galactic plane and Scorpius-Centaurus.

**Table 1.2** Census of the  $\eta$  Chamaeleontis cluster prior to this work

Name	Right Ascension (J2000)	Declination (J2000)	Spectral Type <sup>†</sup>	$V^{\ddagger}$ [mag]	Binary? <sup>*</sup>
ECHA J0836.2–7908	08 36 10.6	−79 08 18	M5.3	17.66	suspected
RECX 1	08 36 56.2	−78 56 46	K7.0	10.61	yes
ECHA J0838.9–7916	08 38 51.5	−79 16 14	M5.0	16.82	suspected
$\eta$ Cha (RECX 2)	08 41 19.5	−78 57 48	B8V	5.46	suspected
ECHA J0841.5–7853	08 41 30.6	−78 53 07	M4.7	17.07	
RECX 3	08 41 37.2	−79 03 31	M3.0	14.35	
HD 75505	08 41 44.7	−79 02 53	A6	7.27	
RECX 4	08 42 23.7	−79 04 04	M1.3	12.79	
RECX 5	08 42 27.3	−78 57 49	M3.8	15.20	
RECX 6	08 42 39.0	−78 54 44	M3.0	14.08	
RECX 7	08 43 07.7	−79 04 52	K6.9	10.84	yes
RS Cha (RECX 8)	08 43 12.2	−79 04 12	A8V+A8V	6.28	triple?
ECHA J0843.3–7905	08 43 18.4	−79 05 21	M3.4	13.97	
ECHA J0844.2–7833	08 44 09.1	−78 33 46	M5.5		suspected
RECX 9	08 44 16.6	−78 59 09	M4.4	15.00	yes
RECX 10	08 44 32.2	−78 46 32	M0.3	12.53	
RECX11	08 47 01.8	−78 59 35	K6.5	11.13	
RECX 12	08 47 56.9	−78 54 54	M3.2	13.17	suspected

<sup>†</sup> Lyo et al. (2004a) (K and M members), Mamajek et al. (2000) (early-type members)

<sup>‡</sup> Mamajek et al. (2000), Lawson et al. (2001), Lawson et al. (2002), Lyo et al. (2004b)

<sup>\*</sup> Lyo et al. (2004b), ECHA J0844.2 has an elevated position in the cluster CMD

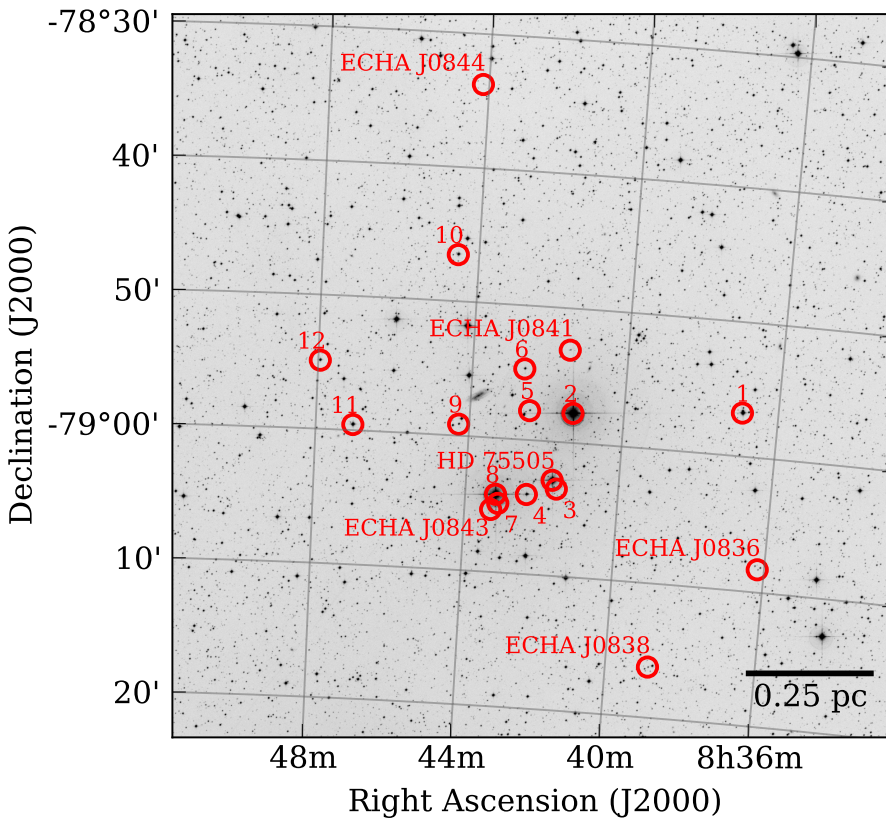


**Figure 1.9**  $0.9 \times 0.9$  deg DSS2-IR image showing the 18 member systems of the  $\eta$  Cha cluster. The bright star at the centre of the image is the eponymous  $\eta$  Cha. The bar shows the linear scale at the 94.3 pc cluster distance.

In contrast to the more-compact  $\eta$  Cha, which has become a benchmark group for the study of intermediate-age pre-main sequence stars,  $\epsilon$  Cha is not as well characterised. Of the several dozen candidates proposed in the literature, many lack the radial velocities and proper motions vital for assessing membership in a kinematic group. Moreover, although they are ideal targets for disk studies, only a handful of confirmed members have been incidentally observed by *Spitzer* (Manoj et al. 2011; Wahhaj et al. 2010). Membership of  $\epsilon$  Cha, and its relationship to nearby  $\eta$  Cha are discussed in depth in Chapter 5.

### 1.3.4. LCC and the Scorpius-Centaurus OB Association

The Scorpius-Centaurus OB Association (Blaauw 1964; de Zeeuw et al. 1999) is the nearest region of recent massive star formation and was recently reviewed by Preibisch & Mamajek (2008). It contains at least  $\sim$ 150 B-type stars divided into three subgroups; Upper Scorpius (5 Myr,  $\sim$ 145 pc), Upper Centaurus Lupus (17 Myr, 140 pc) and Lower Centaurus Crux (LCC; 16 Myr, 120 pc). Although the canonical limits of LCC ( $b = -10^\circ$ ) do not impinge on Chamaeleon, several of its low-mass members have also been proposed as members of the  $\epsilon$  Cha Association (Chapter 5; Mamajek et al. 2002; Torres et al. 2008).

As noted by Preibisch & Mamajek (2008), LCC appears to show a trend in age and distance with Galactic latitude, which is probably due to substructure. The median age of the low-mass stars (Mamajek et al. 2002) south of the Galactic equator is  $12 \pm 2$  Myr, while northern stars have a median age of  $17 \pm 1$  Myr. *Hipparcos* parallaxes show that the mean distance of the southern part of the group is closer ( $\sim$ 110 pc) than the northern part ( $\sim$ 120 pc). Immediately below LCC at a similar distance is the  $\epsilon$  Cha Association (estimated age 3–7 Myr). The formation of  $\epsilon$  Cha may have been the last in a chain of star formation events across the region, perhaps triggered by supernovae explosions in the north of LCC (see §5.4.1).

By tracing their Galactic motions back in time, it appears that all the youngest associations in the solar neighbourhood ( $\epsilon$  Cha,  $\eta$  Cha, TW Hydriæ,  $\beta$  Pic) formed in the vicinity of Sco-Cen at various times in the past 5–15 Myr (Mamajek & Feigelson 2001; Sartori et al. 2003; Fernández et al. 2008; Ortega et al. 2009). Although the exact mechanism(s) responsible for their (and Sco-Cen’s) formation remain uncertain (spiral density wave, molecular cloud collisions, nearby supernovae?), it is clear that the large number of young, low-mass stars in the southern hemisphere is intimately tied to Sco-Cen.

## 1.4. Thesis outline

The remainder of this thesis details our<sup>4</sup> study of low-mass ( $\lesssim 0.5 M_\odot$ ), intermediate-age (5–10 Myr) pre-main sequence stars around the open cluster  $\eta$  Chamaeleontis and the  $\epsilon$  Chamaeleontis Association. It is divided into the following five chapters:

Chapter 2 presents the discovery of a halo of low-mass stars surrounding  $\eta$  Cha, first predicted by Mamajek et al. (1999) as a result of the dynamical evolution of the cluster. After describing our photometric, proper motion and spectroscopic survey for new members, we

---

<sup>4</sup>For stylistic reasons I use the plural form throughout this thesis to refer to work led by myself but naturally done in collaboration with my supervisor and advisory panel. The text however is solely my own.

discuss the dynamics of several promising candidates and model their ejection from  $\eta$  Cha. We then compare our findings to recent  $N$ -body simulations by Moraux et al. (2007).

Two of the newly-confirmed cluster members show strong, variable H $\alpha$  emission across our multi-epoch spectra, including one star which may be sporadically accreting from a circumstellar disk. The chromospheric, accretion and disk properties of these two remarkable objects are the subject of Chapter 3.

Chapter 4 presents evidence that another two  $\eta$  Cha candidates form a wide (4000–6000 AU) pre-main sequence binary unrelated to the cluster. The system is one of the widest young binaries known. Its isolation and dynamical fragility put strong constraints on any birthplace and mode of formation, which we discuss in detail.

Chapter 5 examines membership of the  $\epsilon$  Cha Association, 10 degrees to the east of  $\eta$  Cha. After considering the kinematics of 20 low-mass candidates proposed in the literature, we confirm 11 new members and examine their disk and accretion properties. We finish by commenting on the relationship between the Association and nearby  $\eta$  Cha.

Concluding remarks and prospects for future work are discussed in Chapter 6, followed by a full bibliography and three appendices.

Chapters 2 and 3 have been published in the *Monthly Notices of the Royal Astronomical Society, Letters* (Murphy et al. 2010, 2011, respectively). Full bibliographic information is provided at the start of each chapter. They are presented here in updated and expanded form.

Chapters 4 and 5 are being prepared for submission to the *Monthly Notices of the Royal Astronomical Society*. A full author list is provided at the start of each chapter.

## CHAPTER 2

---

# The low-mass stellar halo surrounding $\eta$ Chamaeleontis

*Parts of this chapter have been previously published as ‘First detection of a low-mass stellar halo around the young open cluster  $\eta$  Chamaeleontis’, Murphy, S. J., Lawson, W. A., Bessell, M. S., 2010, MNRAS, 406, L50. The work is presented here in expanded and updated form.*

### 2.1. Introduction

The open cluster  $\eta$  Chamaeleontis ( $\eta$  Cha) is one of the closest ( $d \simeq 94$  pc) and youngest (age  $\sim 8$  Myr) stellar aggregates in the solar neighbourhood. As outlined in Chapter 1, its youth and proximity make it ideally suited for many studies related to the evolution of intermediate-age pre-main sequence stars and clusters. This includes determining what role dynamical processes play over time in the construction of observed mass functions in compact, moderately relaxed stellar systems like  $\eta$  Cha.

A census of cluster members currently stands at 18 systems (with 22–28 members, including suspected companions), covering spectral types B8–M5.5 (see Table 1.2). Lyo et al. (2004b) found no statistical difference between the mass function of  $\eta$  Cha and those of the richly populated Orion Trapezium cluster, other sparse young clusters or the field. Extrapolating to lower masses, they predicted an additional 20–29 stars and brown dwarfs in the mass range  $0.025 < M/M_{\odot} < 0.15$  remained to be discovered, a number comparable to the currently known stellar population. This was disputed by Luhman et al. (2009a) and Luhman & Steeghs (2004), who claimed there is no paucity of low-mass members and that the observed mass function of  $\eta$  Cha is not statistically different from those seen in other nearby star-forming regions like IC 348 and Cha I<sup>1</sup>.

In either case, the detection of additional members of  $\eta$  Cha, particularly at lower masses, is of vital importance. However, efforts to observe this missing population of low-mass stars

<sup>1</sup>Due to the small number of stars involved in any such comparison, the applicability of a mass function and indeed the classification of  $\eta$  Cha as an open cluster may be suspect. It may be more realistic to describe  $\eta$  Cha as simply a *clustering* of pre-main sequence stars and not a classical open cluster. However, since it is the densest stellar group within 100 pc (with a core density larger than well-accepted clusters like the Hyades), appears bound and has clearly persisted for several dynamical crossing times, we treat it as the latter.

have so far been unsuccessful. The largest survey to-date was that of Luhman (2004b). Using a combination of DENIS  $i$  and 2MASS  $JHK_s$  near-infrared photometry, Luhman undertook a 1.5 deg radius search around  $\eta$  Cha for new members, four times the radius of known membership. From  $H$  versus  $(i - K_s)$  and  $H$  versus  $(H - K_s)$  colour-magnitude diagrams he identified five promising photometric candidates which were observed spectroscopically. None of the stars were confirmed as young. This survey was a follow-up to a previous search by Luhman & Steeghs (2004), who co-discovered<sup>2</sup> three new  $\eta$  Cha members in a region up to 0.5 deg away from the cluster using similar techniques. Both surveys were estimated photometrically complete down to masses of  $\sim 0.015 M_\odot$ , yet failed to find any new members below a mass of  $\sim 0.08 M_\odot$ , straddling the hydrogen-burning limit.

As well as searching for new members at large angular distances from the cluster core, several studies have tried deep searches for low-mass stars and brown dwarfs that may have been missed by earlier efforts. Lyo et al. (2006) reported the results of their deep  $IJH$  observations over a  $33' \times 33'$  field at the core of the cluster. By forming  $I$  versus  $(I - J)$  and  $J$  versus  $(J - H)$  colour-magnitude diagrams they were able to survey the core region to  $\sim 2$  mag fainter than the 2MASS or DENIS all-sky surveys. However, they reported no new members down to the completeness limit of their photometry, which from DUSTY99 models (Chabrier et al. 2000) they estimated to be  $\sim 0.013 M_\odot$ . More recently, in a deep *XMM-Newton* study of the core of  $\eta$  Cha, López-Santiago et al. (2010) searched for X-ray-bright late-F and G-type members that could have been missed by previous surveys for lower-mass stars. They detected five objects with cross-identifications in 2MASS, but discarded them all as unrelated field stars after considering their photometry and past identifications.

Small number statistics and the definition of an open cluster aside, the failure of past studies to find these low-mass members raises an interesting question—has the cluster’s evolution been driven by dynamical interactions which dispersed the missing stars into a diffuse halo at large radii, or did  $\eta$  Cha possess an abnormally top-heavy Initial Mass Function (IMF), deficient in low-mass objects? The latter result would seemingly be at odds with the growing body of evidence that strongly suggests the IMF is universal and independent of initial star-forming conditions (for a detailed review see Bastian et al. 2010). Conversely, the deficit of wide binaries ( $a > 20$  AU) in the cluster (Köhler & Petr-Gotzens 2002; Brandeker et al. 2006) compared to similarly aged groups like TW Hydreae and a moderate amount of mass segregation (Lyo et al. 2004b) are perhaps hints to a more dynamically active past.

Moraux et al. (2007) have attempted to reconcile  $N$ -body dynamical evolution simulations with the current configuration of the cluster. They were able to replicate the mass function and spatial distribution of the cluster members—including the absence of members at radii between 0.5–1.5 deg found by Luhman (2004b)—assuming a standard log-normal IMF and 30–70 initial members. Their simulations predicted that half of these stars would be lost from the cluster and ejected into the field at distances greater than 1.5 deg from the core (see Figure 2.13 for the results of such simulations)<sup>3</sup>.

---

<sup>2</sup>As noted by Luhman & Steeghs, their three stars were discovered first in the same year by Lyo et al. (2004b, two stars) and Song et al. (2004, three stars). A busy year for  $\eta$  Cha research!

<sup>3</sup>In contrast to observational searches, which in the absence of known distances use *projected* angular separations, the Moraux et al. (2007) simulations predict radii in *physical* degrees. Moreover, the simulations used only single stars with realistic *system* masses. Preliminary results with an initial binary population and individual IMF are described in §2.8.1

Although the Moraux et al. (2007) simulations explicitly take place *after* all the natal gas was removed from the newborn  $\eta$  Cha, their results are broadly consistent with recent work by Weidner et al. (2011), who found sparse ( $N = 100$ ) embedded proto-clusters will lose up to 20 percent of their members in the first 5 Myr *before* gas removal. Ejected stars can be expected to travel distances of 3–6 pc during this time (1.8–3.6 deg at the distance of  $\eta$  Cha), with a 1–12 km s<sup>-1</sup> typical range of ejection velocities. In both studies the lower-mass members were preferentially ejected, such that the mass function of escapees closely resembled the input IMF. Following gas expulsion, these clusters may be expected to further lose up to half their remaining stellar population (Kroupa & Boily 2002; Weidner et al. 2007) and expand to form unbound associations (for example TW Hydriæ or  $\beta$  Pictoris). The fact that the compact core of  $\eta$  Cha persists in an apparently bound state implies that gas removal may have only recently (and perhaps violently) occurred, possibly due to the passage of a shockwave from the nearby Sco-Cen OB Association (Mamajek et al. 2000).

The results of these  $N$ -body simulations indicate that if a deficit of low-mass cluster members exists, it may not be due to a peculiar IMF but to dynamical evolution. The missing stars should be found in a diffuse halo at radii greater than 1.5 deg from the cluster, with similar proper motions and distances as the cluster proper. In this chapter we describe the first detection of the hitherto unseen halo of young stars around  $\eta$  Cha and present dynamical evidence of their ejection early in the cluster’s evolution.

## 2.2. Candidate selection

### 2.2.1. Photometry

As demonstrated by the surveys in the previous section, near-infrared ( $iJHK$ ) photometry is useful in characterising populations of low-mass, pre-main sequence stars. Using the TOPCAT<sup>4</sup> Virtual Observatory tool, we cross-matched DENIS<sup>5</sup> (Epchtein et al. 1999) and 2MASS<sup>6</sup> (Skrutskie et al. 2006) survey photometry within a 5.5 deg radius surrounding  $\eta$  Cha (08<sup>h</sup>42<sup>m</sup>06<sup>s</sup>, -79°01'38'', J2000). Objects were cross-matched with a 3'' search radius and we required a detection in DENIS  $i$  and all three 2MASS bands. Unfortunately, the DENIS catalogue yields multiple detections for each 2MASS source, corresponding to observations from overlapping adjacent 12'  $\times$  30° image strips (Epchtein et al. 1999). These multiple detections have photometry differences at the 0.01–0.05 mag level but are sometimes as high as 0.1 mag in the  $i$ -band. In assigning a single DENIS  $i$ -band magnitude to the cross-matched sources, we chose the catalogue source that minimised the statistic  $(J_{\text{2MASS}} - J_{\text{DENIS}})^2 / \sigma_{J_{\text{DENIS}}}^2$ . For DENIS sources without any  $J$  photometry (~20 percent of all sources) we chose the closest source to the 2MASS coordinates.

Photometric candidates were selected by forming the  $i_{\text{DENIS}}$  versus  $(i - J_{\text{2MASS}})$  colour-magnitude diagram for the 700,000 cross-matched sources in the field. As seen in Figure 2.1, the empirical cluster isochrone is well defined in this diagram through the K and M spectral types. Due to its youth, proximity to Earth and lack of substantial reddening, the cluster

<sup>4</sup>Tool for OPeration on Catalogues And Tables, <http://www.star.bris.ac.uk/~mbt/topcat/>

<sup>5</sup>Third DENIS Release (September 2005), [ivo://astronet.ru/cas/denis](http://astronet.ru/cas/denis)

<sup>6</sup>2MASS All Sky Point Source Catalogue, [ivo://astronet.ru/cas/twomass-psc](http://astronet.ru/cas/twomass-psc)

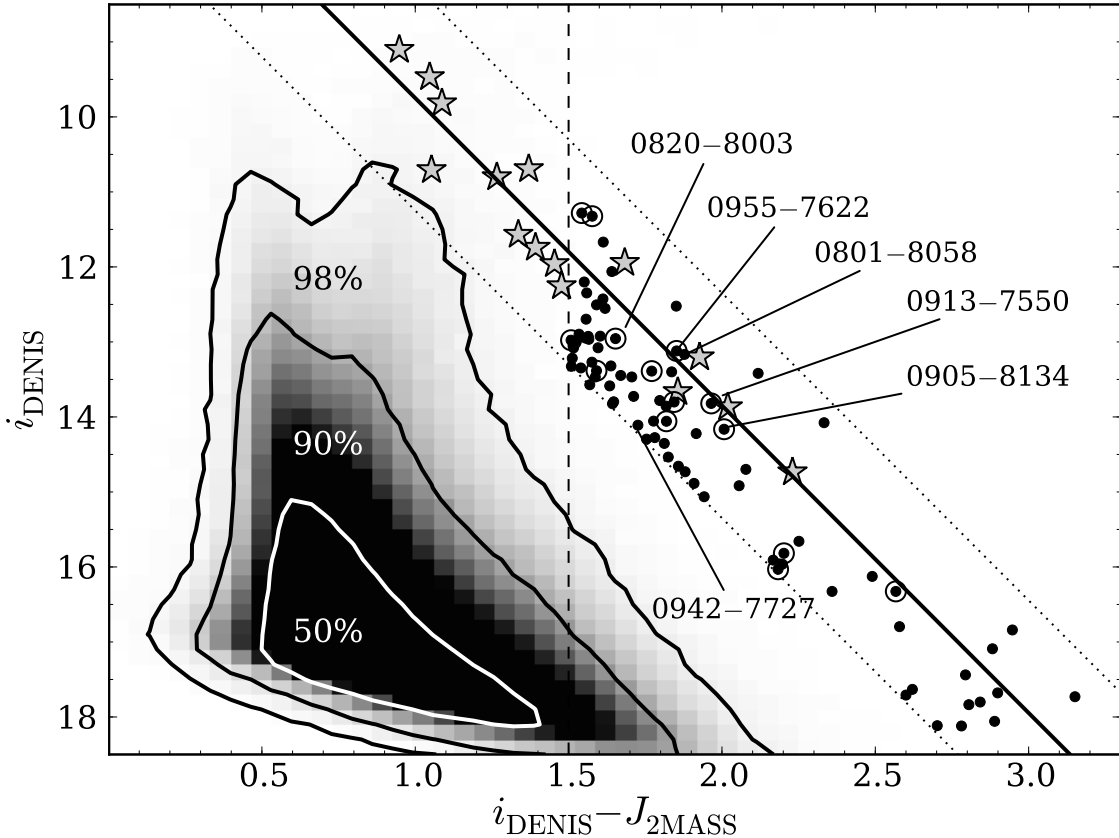


**Figure 2.1** DENIS/2MASS colour-magnitude diagram for the 5.5 deg radius region around  $\eta$  Cha. Contours show the cumulative totals of stars enclosed. Because of their youth and proximity,  $\eta$  Cha members (filled stars) are well separated from the majority of objects in the field. We selected candidates (filled circles) up to 1.5 mag from the empirical cluster isochrone (solid line) also having  $(i - J) > 1.5$  (dashed line). Proper motion candidates are denoted by open circles. The intermediate-gravity stars described in §2.3.2 are labelled.

sequence sits well above the majority of stars in the field. A weak giant branch can be seen overlapping the sequence at mid-K spectral types around  $(i - J) \approx 1$ . To account for unresolved binarity, reddening and distance variations and any non-linearities in the isochrone we initially selected candidates lying up to 1.5 mag from a linear fit to the 15 known late-type members, given by:

$$i_{\text{DENIS}} = 4.098 \times (i - J_{\text{2MASS}}) + 5.65 \quad (2.1)$$

While the true cluster isochrone is almost certainly non-linear, such an approximation is valid at this initial stage due to the uncertainties mentioned above. Because we are interested in the low-mass population we restricted our candidates to  $(i - J) > 1.5$ —corresponding to spectral types  $\sim M3$  and later—and  $(J - H)_{\text{2MASS}} < 0.8$ , to minimise contamination from background giants (Bessell & Brett 1988). Excluding stars with poor 2MASS photometry (14, we kept only stars with AAA photometric quality), known members (5, all recovered) and previously confirmed field stars (3) left 81 photometric candidates. Figure 2.2 shows the distribution of the candidates on the sky. Just one candidate (2MASS J0820-8003) lies within 1.5 deg of the cluster, the radius to which Luhman (2004b) searched using different selection techniques and reported no new members. Our survey is 13 times larger in area than that of Luhman. We also plot in Figure 2.2 the distribution of interstellar material in the region around  $\eta$  Cha, as traced by 100  $\mu\text{m}$  observations from the *Infrared Astronomical*

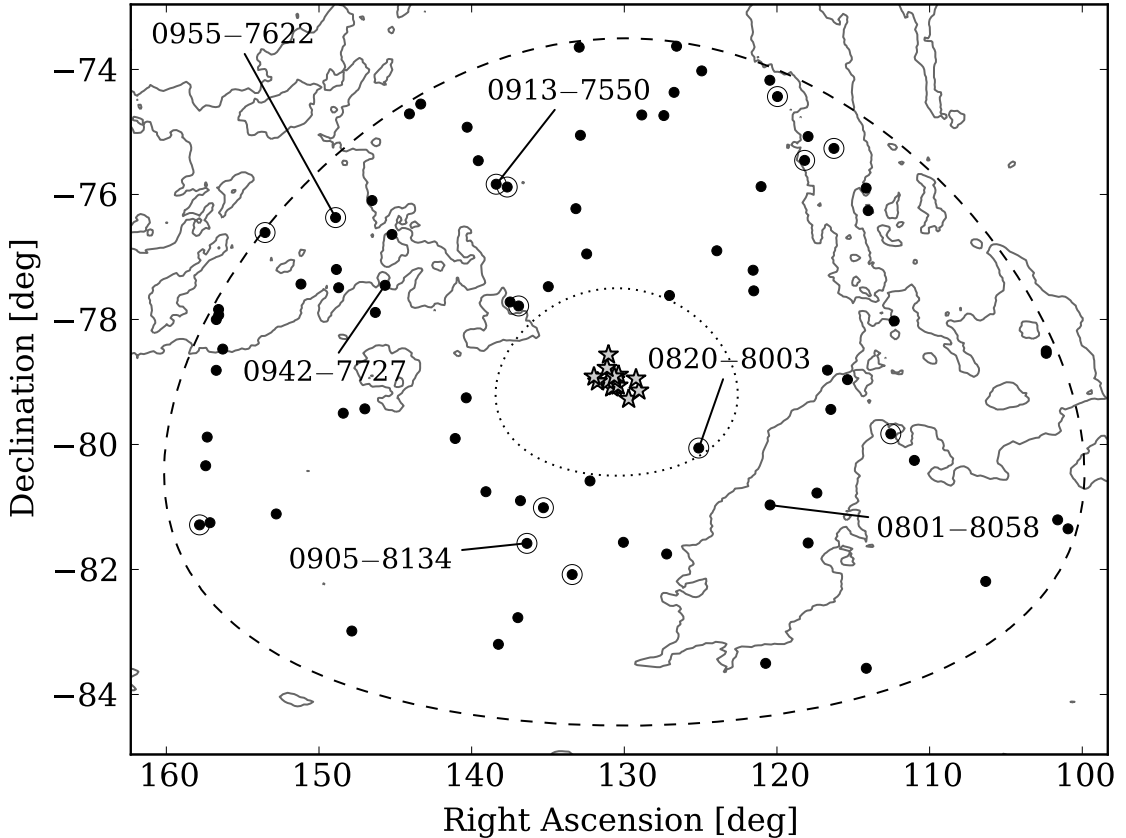


**Figure 2.2** Distribution of candidates on the sky. Symbols are as in Figure 2.1. The area enclosed by the dotted line is that searched by Luhman (2004b), the dashed line is the 5.5 deg radius of this study. Contours correspond to an IRAS 100  $\mu\text{m}$  flux level of 10 MJy  $\text{sr}^{-1}$ .  $\eta$  Cha lies in a region devoid of gas and dust which is responsible for the negligible reddening towards the cluster.

*Satellite* (IRAS). The positions of the candidates are not particularly correlated with the 100  $\mu\text{m}$  emission. The cluster itself sits in a region devoid of significant interstellar material, explaining its negligible reddening ( $E(B - V) \simeq 0.00$ , Westin 1985; Mamajek et al. 2000). A full listing of the photometric candidates is given in Table 2.1.

### 2.2.2. Proper motions

As Chapter 1 attests, kinematics have been vital in confirming membership of the many young associations in the solar neighbourhood. In the absence of radial velocities and accurate distances, proper motions are the sole means of investigating the kinematics of our candidates. We therefore cross-matched the 81 stars in Table 2.1 against the Naval Observatory Merged Astrometric Dataset (NOMAD<sup>7</sup>). Although NOMAD includes astrometry from the *Hipparcos*, Tycho-2, UCAC2 and USNO-B1 catalogues, all of the candidates had USNO-B1 or UCAC2 proper motions. To a matching limit of 10'' only one of the photometric candidates was not found in NOMAD—this was the second faintest star in the sample ( $i = 18.12$ ). Eighteen candidates returned a null proper motion of  $(0, 0) \pm (0, 0)$  mas  $\text{yr}^{-1}$ . These correspond to highly uncertain proper motion measurements explicitly set to zero (D. Monet, private communication). NOMAD proper motions for the photometric candidates can be

<sup>7</sup><http://www.nofs.navy.mil/nomad/>; Virtual Observatory identifier ivo://astronet.ru/cas/nomad

**Table 2.1** Photometric candidates within 5.5 deg of  $\eta$  Cha

2MASS ID	<i>J</i>	<i>H</i>	<i>K<sub>s</sub></i>	DENIS ID	<i>i</i>	<i>J</i>	<i>K</i>	NOMAD ID	$\mu_\alpha \cos \delta$	$\sigma_{\mu_\alpha \cos \delta}$	$\mu_\delta$	$\sigma_{\mu_\delta}$
		[mag]				[mag]				[mas yr <sup>-1</sup> ]		
06434426–8120578	12.54	11.98	11.75	J064343.8–812058	14.3	12.66	11.62	0086–0022191	+236.0	29.0	+50.0	1.0
06462710–8112221	11.39	10.73	10.48	J064626.9–811222	12.95	11.36	10.37	0087–0021147	+90.0	14.0	+40.0	3.0
06492625–7832302	13.97	13.34	12.97	J064926.1–783230	16.33	13.91	13.2	0114–0022673	0.0	0.0	0.0	0.0
06492684–7830096	11.81	11.21	10.95	J064926.7–783009	13.35	11.88	10.95	0114–0022675	+10.7	6.5	+61.6	6.0
07051818–8212197	15.34	14.97	14.45	J070517.9–821130	18.12	15.67						
07235966–8015179	11.3	10.82	10.44	J072359.5–801517	13.42	11.33	10.34	0097–0023438	-400.0	13.0	+726.0	15.0
07291649–7801257	11.14	10.54	10.31	J072916.5–780125	12.7	11.08	10.18	0119–0028000	0.0	0.0	0.0	0.0
07301029–7949465	11.79	11.2	10.88	J073010.2–794946	13.38	11.79	10.83	0101–0024103	+2.0	13.0	+40.0	6.0
07360613–7615306	11.98	11.35	11.07	J073606.1–761530	13.78	11.89	11.1	0137–0038802	-66.0	5.0	+188.0	29.0
07363553–8334516	11.76	11.26	10.91	J073635.5–833451	13.47	11.69	10.84	0064–0017785	-88.0	2.0	+92.0	1.0
07363787–7553548	15.11	14.53	14.04	J073637.7–755354	17.71	15.04	13.73	0141–0043715	0.0	0.0	0.0	0.0
07413127–7857463	12.31	11.73	11.4	J074131.2–785746	14.22	12.24	11.41	0110–0025049	-26.0	42.0	+70.0	14.0
07450450–7515483	13.76	13.34	13.2	J074504.7–751550	16.33	13.78		0147–0056811	-2.5	6.7	+23.6	7.1
07455327–792617	12.18	11.54	11.28	J074553.7–792621	13.82	12.39	11.29	0105–0025051	0.0	0.0	0.0	0.0
07464520–7848403	15.03	14.41	13.97	J074645.2–784841	17.84	15.18		0111–0025239	0.0	0.0	0.0	0.0
07493223–8046366	12.01	11.43	11.11	J074932.5–804638	13.73	12.17	11.05	0092–0023931	-176.0	2.0	+216.0	3.0
07514986–8134348	10.79	10.15	9.94	J075150.0–813435	12.35	10.96	9.94	0084–0029863	-6.1	6.1	-2.9	6.0
07515088–7504221	11.95	11.4	11.07	J075150.9–750421	13.59	12.2	11.22	0149–0060296	+8.1	6.1	+15.7	6.2
07524497–7527172	9.74	8.98	8.73	J075245.1–752717	11.28	9.88	8.76	0145–0053268	-4.7	6.0	+17.7	6.0
07595212–7426018	11.62	10.97	10.76	J075952.1–742601	13.39	11.66	10.81	0155–0073794	-10.0	6.0	+8.9	6.2
08014860–8058052	11.29	10.6	10.23	J080148.6–805805	13.17	11.31	10.23	0090–0024145	-10.0	3.0	+26.0	10.0
08015214–7410216	11.7	11.13	10.85	J080152.1–741021	13.22	11.72	10.76	0158–0079617	0.0	0.0	0.0	0.0
08025781–8330076	10.67	10.04	9.71	J080257.7–833007	12.52	10.58	9.65	0064–0019143	-116.0	17.0	+124.0	5.0
08040986–7552265	15.17	14.42	14.08	J080409.6–755226	18.06	15.12		0141–0046221	0.0	0.0	0.0	0.0
08060539–7732313	12.85	12.29	11.98	J080605.3–773232	14.73	12.84	11.9	0124–0045366	-40.0	13.0	-78.0	9.0
08061506–7712441	11.82	11.23	10.98	J080614.9–771244	13.32	12.15	11.25	0127–0047178	-6.8	6.4	-5.4	6.5
08154563–7654027	11.4	10.89	10.58	J081545.5–765403	12.96	11.41	10.62	0130–0047650	+32.0	6.5	+108.9	6.2
08194309–7401232	10.06	9.43	9.2	J081943.1–740123	11.67	10.01	9.23	0159–0086496	-18.7	6.0	+37.9	6.0
08202975–8003259	11.3	10.73	10.43	J082029.9–800325	12.96	11.2	10.32	0099–0027452	-36.0	14.0	+34.0	8.0
08261843–7337418	12.15	11.52	11.25	J082618.5–733742	13.8	12.13	11.22	0163–0105857	-104.0	8.0	+116.0	0.0
08265778–7421593	11.36	10.71	10.49	J082657.7–742159	12.9	11.35	10.59	0156–0079527	+56.3	6.0	+3.6	6.2
08280966–7736574	14.22	13.58	13.17	J082809.6–773658	16.8	14.13	13.15	0123–0045758	+40.0	12.0	+190.0	10.0
08285425–8145094	13.77	13.2	12.83	J082854.3–814509	15.96	13.77	12.63	0082–0032706	-68.0	15.0	+34.0	7.0
08293859–7444155	14.58	13.98	13.91	J082938.7–744415	17.73			0152–0070533	0.0	0.0	0.0	0.0
08352539–7443428	12.71	12.15	11.84	J083525.3–744343	14.54	12.6	11.85	0152–0071222	+52.0	20.0	+108.0	6.0
08401433–8133555	13.64	13.14	12.72	J084014.4–813355	16.13	13.6	12.84	0084–0033355	-20.0	2.0	-6.0	4.0
08485911–8035017	10.42	9.79	9.5	J084859.5–803501	12.06	10.43	9.51	0094–0029124	0.0	0.0	0.0	0.0
08495184–7657072	11.68	11.12	10.77	J084952.2–765708	13.32	11.7	10.84	0130–0052425	-264.0	19.0	+198.0	17.0
08513016–7503119	11.36	10.76	10.5	J085130.2–750312	12.93	11.22	10.41	0149–0068148	-14.2	6.3	+36.6	6.0
08514891–7338397	12.28	11.7	11.39	J085148.9–733839	14.06	12.14	11.32	0163–0109404	0.0	0.0	0.0	0.0
08524138–7613377	11.69	11.11	10.81	J085241.4–761338	13.27	11.6	10.68	0137–0047278	0.0	0.0	0.0	0.0
08533950–8204523	11.47	10.83	10.62	J085339.6–820452	12.98	11.48	10.51	0079–0035296	-38.2	6.0	+11.5	6.0
08595512–7728298	11.78	11.22	10.91	J085955.1–772830	13.45	11.81	10.82	0125–0055097	-81.3	9.0	+32.0	9.0
09011161–8100433	13.85	13.26	12.9	J090111.7–810043	16.03	13.83	12.74	0089–0030427	-36.0	7.0	+18.0	8.0
090503087–8134572	12.16	11.6	11.3	J090531.2–813458	14.16	12.21	11.21	0084–0035278	-52.0	19.0	+8.0	17.0
09071270–8053594	12.5	11.88	11.54	J090712.8–805400	14.28	12.49	11.6	0091–0030281	-188.0	19.0	+166.0	32.0
09074165–7747024	11.96	11.35	11.22	J090741.5–774703	13.8	11.98	11.23	0122–0047685	-21.6	6.1	+20.4	6.1
09075370–8246148	15.01	14.5	14.21	J090753.5–824616	17.63	14.99		0072–0028031	0.0	0.0	0.0	0.0
09095558–7743129	14.78	14.04	13.54	J090955.7–774313	17.68	14.7	13.17	0122–0047974	0.0	0.0	0.0	0.0
09104094–7552528	13.62	12.98	12.59	J091041.0–755253	15.82	13.56	12.48	0141–0054372	-58.0	23.0	+30.0	9.0
09125959–8311515	11.56	10.98	10.69	J091259.8–831152	13.4	11.57	10.55	0068–0024433	-390.0	5.0	+712.0	11.0
09133435–7550099	11.86	11.32	11.0	J091334.3–755010	13.82	11.8	10.89	0141–0054888	-36.0	8.0	+14.0	15.0
09161589–8045205	14.64	14.04	13.71	J091616.6–804518	17.44			0092–0030513	0.0	0.0	0.0	0.0
09181593–7527342	11.46	10.86	10.63	J091815.9–752734	12.98	11.37	10.52	0145–0064601	-96.0	9.0	+126.0	11.0
09211098–7455270	11.74	11.46	11.41	J092111.2–745525	14.08	11.92	11.5	0150–0074388	+2.2	6.0	-2.8	6.0
09212550–7915133	12.62	12.1	11.73	J092125.5–791513	14.7	12.66	11.68	0107–0035021	-52.0	13.0	+40.0	10.0
09241480–7954161	15.41	14.71	14.32	J092414.8–795416	18.12	15.28		0100–0033465	+63.1	9.0	-272.8	9.0
09332070–7433127	10.93	10.37	10.08	J093320.6–743313	12.55	10.97	10.21	0154–0085970	-14.0	11.0	+34.0	6.0
09361819–7442386	12.0	11.44	11.14	J093618.2–744238	13.57	11.94	11.18	0152–0081294	-66.0	5.0	+62.0	12.0
09405280–7638233	12.86	12.22	11.92	J094052.9–763823	14.92	12.82	11.95	0133–0057137	-32.0	22.0	+92.0	11.0
09424157–7727130	12.38	11.79	11.52	J094241.5–772714	14.11	12.36	11.56	0125–0062122	0.0	0.0	0.0	0.0
09451445–7753150	13.89	13.23	12.79	J094514.5–775315	16.84	13.82	12.83	0121–0050831	-32.0	47.0	+168.0	28.0
09460586–7605479	12.98	12.4	12.12	J094605.8–760548	14.89	12.86	12.08	0139–0056858	-2.0	30.0	+196.0	34.0
09475915–7925481	14.96	14.36	13.96	J094759.4–792548	17.8	14.95	13.88	0105–0036743	0.0	0.0	0.0	0.0
09512392–8259057	12.04	11.5	11.19	J095124.1–825906	13.86	12.13	11.32	0070–0028766	-36.0	3.0	+40.0	4.0
09533862–7929598	11.48	10.94	10.65	J095338.7–792959	13.08	11.48	10.52	0105–0037380	-38.4	6.1	+43.1	6.2
09545099–7729327	11.32	10.74	10.43	J095451.0–772933	12.92	11.27	10.41	0125–0064071	-23.4	6.2	+31.3	6.4
09552669–7712005	10.65	9.88	9.61	J095526.6–77								

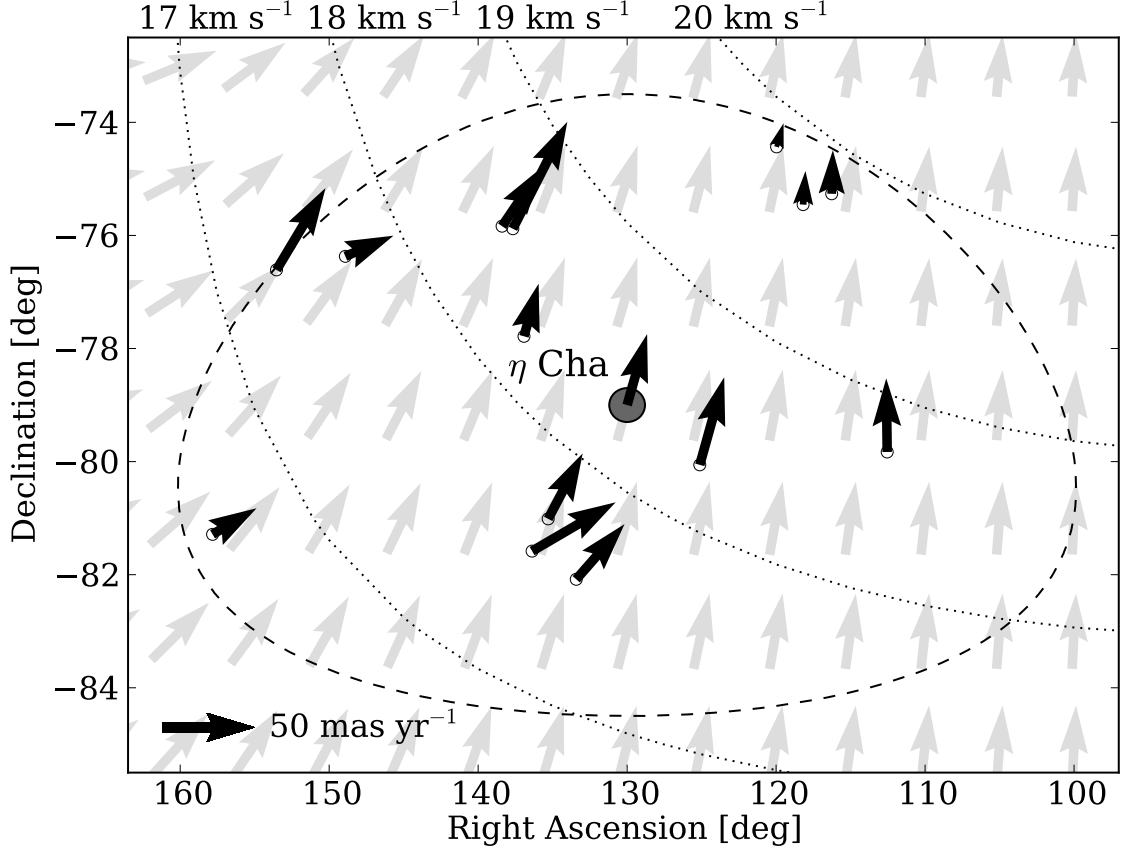


**Figure 2.3** The  $\eta$  Cha space motion decomposed into transverse and radial velocities over the plane of the sky. Arrows show the expected proper motion vectors while dotted contours give the variation in radial velocity over the 5.5 deg radius field (dashed perimeter). Proper motion candidates are shown with their NOMAD proper motion vectors. Vectors in this schematic diagram do *not* take into account the convergence of right ascension at the pole, so that direct visual comparison is possible over the survey area.

found in Table 2.1. All 18 known  $\eta$  Cha members were also found in NOMAD, 14 of which had non-zero proper motions. The four outstanding members are located close to bright stars or diffraction spikes, making proper motion measurements unreliable.

For a given  $UVW$  space motion, the resultant proper motion vector (and radial velocity) depends on both sky position and distance. Given the large angular extent of our survey area, this can have a substantial effect on the expected proper motions and radial velocities of the candidates. Figure 2.3 illustrates the variation in proper motion and radial velocity fields as a function of sky position for the updated cluster kinematics in Table 2.4. Both the magnitude and direction of the expected proper motion vectors change substantially over the field. Using the canonical cluster space motion,  $(U, V, W) = (-11.8, -19.1, -10.5)$  km s $^{-1}$  (Mamajek et al. 2000), we calculated the expected proper motion of each candidate at a distance of 97 pc, following the formalism of Johnson & Soderblom (1987)<sup>8</sup>. For each component of the NOMAD proper motion we then determined how many times its quoted uncertainty the observed value was from the expected motion. These differences are plotted in Figure 2.4 for both the candidates and confirmed  $\eta$  Cha members. As expected, the core members cluster closely around the origin with a small offset of  $(+0.5, -1.4) \pm (1.4, 1.2) \sigma$ . We selected as proper motion candidates the 14 DENIS/2MASS stars that lay within  $\pm 3\sigma$  of this point.

<sup>8</sup>with updated Galactic coordinate transformations from §1.5.11 of Perryman & ESA (1997)

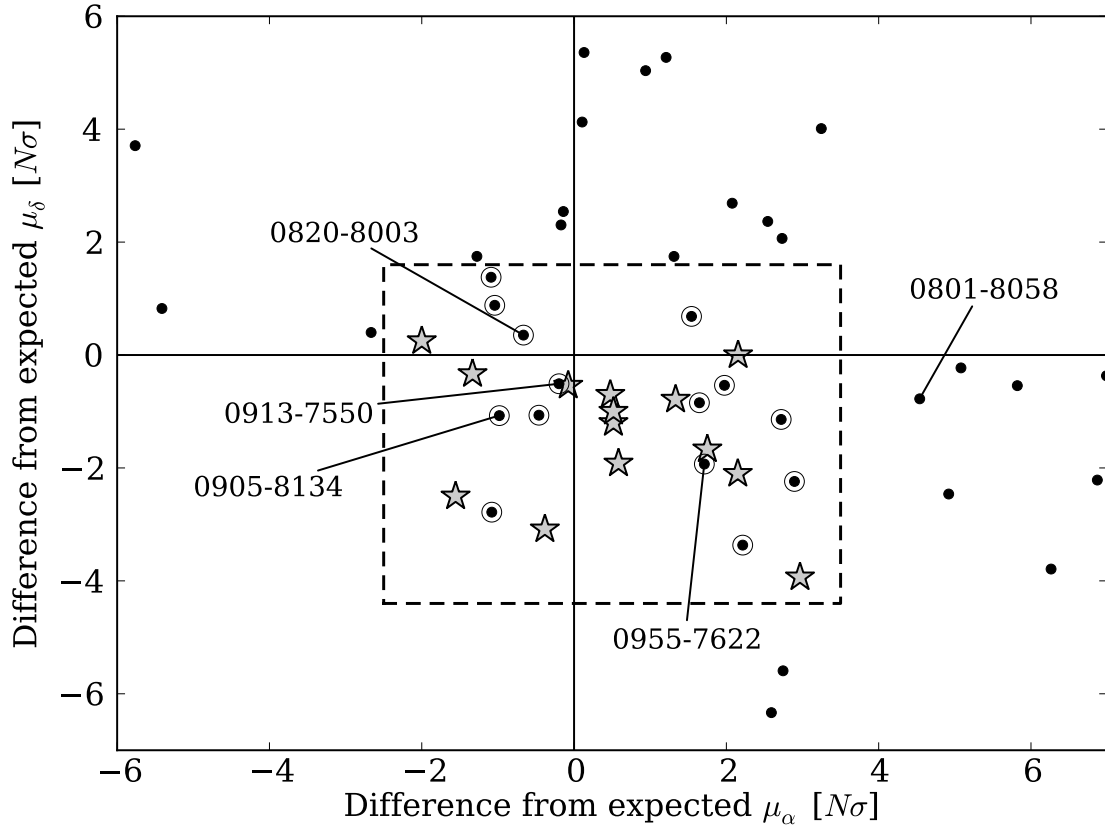


**Figure 2.4** Selection diagram for the 14 proper motion candidates (open circles). Each axis shows the number of standard deviations the star lies from its expected proper motion. This was calculated from the projected cluster space velocity at 97 pc. Known cluster members are also plotted (filled stars). The dashed box shows the  $3\sigma$  selection criterion. Most photometric candidates lie outside the limits of this diagram.

All 14 known members fell within the selection box. In a search for dispersed members of a cluster such as this, a candidate that has been ejected will have a distance and space motion (and hence projected proper motion and radial velocity) that are slightly different from the cluster proper. It is therefore likely that some of the photometric candidates lying just outside the  $3\sigma$  proper motion selection box could be cluster members imparted with larger ejection velocities. To ensure we were not biased against such events we made sure to include stars up to  $10\sigma$  away from the cluster mean in the spectroscopic observations described in the next section.

One final caveat to consider is the effect of the *solar reflex motion* (or conversely, the motion of the Local Standard of Rest in a heliocentric frame), whereby stars in the solar neighbourhood at rest with respect to the LSR will reflect the solar motion in their observed (heliocentric) proper motions and radial velocities. The solar reflex motion is notoriously difficult to determine empirically and generally depends on the population of stars used to define it. From a sample of 573 southern M-dwarfs, Hawley et al. (1996) determined a solar reflex motion of  $(U, V, W) = (-10, -21, -8)$  km s $^{-1}$ . This can be compared to the  $(-10, -5, -7)$  km s $^{-1}$  reflex motion of Dehnen & Binney (1998), derived from a kinematically unbiased sample of *Hipparcos* stars. The Hawley et al. (1996) velocity is more appropriate in this case as we are considering a similar stellar population. At the position and distance of  $\eta$  Cha, this reflex motion corresponds to a radial velocity of 17 km s $^{-1}$  and a proper motion of  $(\mu_\alpha \cos \delta, \mu_\delta) = (-24, +31)$  mas yr $^{-1}$ , very similar to those observed for the cluster (Table 2.4).

This means that a *solely* proper motion selected sample would no doubt include a large number of older field stars at similar distances to  $\eta$  Cha. However, such stars would be considerably fainter and fall outside our photometric selection band. Because of the youth and proximity of  $\eta$  Cha, main sequence stars would need to lie at  $\sim 40$  pc to overlap the cluster sequence, a distance at which their proper motions would be some 2.3 times larger.

Preibisch et al. (1998) found a similar problem in their proper motion-selected sample of X-ray quiet stars in the 5 Myr Upper Scorpius OB association. From a spectroscopic sample of 115 proper motion candidates, *none* could be classified as pre-main sequence stars. At 90 percent confidence they inferred  $<2$  percent of the total proper motion-selected sample were young. Clearly proper motions alone are not particularly efficient in identifying young stars, but when combined with other observational data, such as X-ray fluxes, multi-colour photometry and spectroscopy, they are a powerful discriminant (e.g. Mamajek 2005b).

### 2.3. DBS low-resolution spectroscopy

During 2009 March we obtained low-resolution spectra of the proper motion candidates and a selection of photometric candidates using the now-decommissioned *Double Beam Spectrograph (DBS)* on the ANU 2.3-m telescope at Siding Spring Observatory. With the 316R grating our spectra covered the wavelength range 5920–9750 Å at a resolution of 5 Å ( $1.9 \text{ \AA pixel}^{-1}$ ). The slit was set to  $2''$  and oriented to the parallactic angle to minimize differential atmospheric extinction. Each night we also observed flux standards, smooth spectrum stars for telluric correction and a selection of Gliese dwarf standards from Lyo et al. (2004a, 2008) for spectral typing and gravity estimation. Exposure times ranged from 30 s to 900 s for the fainter targets. Of the 14 proper motion candidates, 11 were observed in this mode. The remaining three were faint and two had DENIS *i*-band fluxes more than a magnitude below the cluster isochrone. These stars are not considered likely members. We also observed 17 additional photometric candidates that lay close to the cluster isochrone and had null proper motions or a proper motion just outside the  $3\sigma$  selection box of Figure 2.4.

The spectra were reduced and extracted in IRAF<sup>9</sup> using APALL and other standard routines. Accurate flux calibration is necessary for the computation of synthetic photometry and spectral typing. Using a set of smooth spectrum stars observed each night from the list of Bessell (1999), we determined the telluric absorption spectrum and corrected the candidate spectra using the TELLURIC routine, which scales the normalised telluric spectrum based on airmass ( $\sec z$  for zenith distance  $z$ ) and divides it into the target spectrum. Spectra were ‘relative–absolute’ flux calibrated using flux standards observed each night (again from the list of Bessell 1999) and the SENSFUNC and CALIBRATE routines. They are suitable for the computation of synthetic colours but not absolute flux measurements. Two examples of flux-calibrated DBS spectra can be seen in Figure 2.5, for the M4.5 Gliese dwarf GL 493.1 and the proper motion candidate 2MASS J0820–8003.

---

<sup>9</sup>IRAF is distributed by the National Optical Astronomy Observatory, which is operated by the Association of Universities for Research in Astronomy under cooperative agreement with the National Science Foundation.

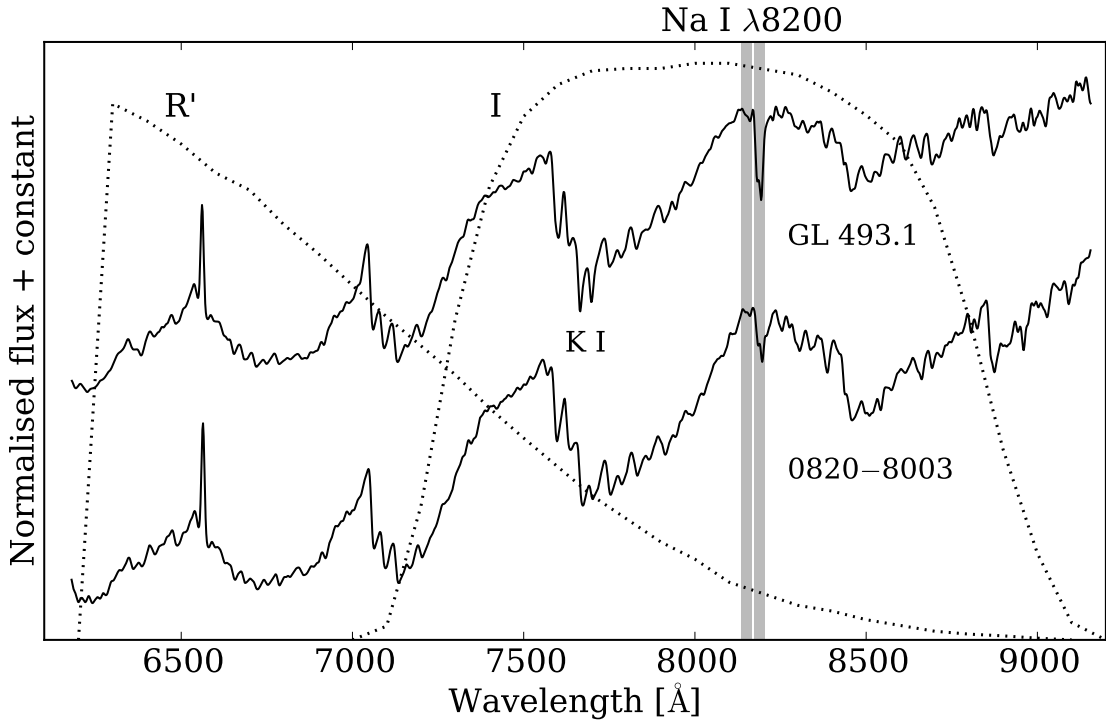


**Figure 2.5** DBS 316R spectra of the Gliese dwarf GL 493.1 and  $\eta$  Cha candidate 2MASS J0820–8003. Both stars share the same approximate spectral type ( $\sim$ M4.5). The strength of neutral alkali metal absorption lines like Na I and K I are much weaker in the (supposed) pre-main sequence object. This gravity sensitivity can therefore be used as an age proxy. The shaded regions show the extent of the integration used to form the Na I index (see §2.3.2). The  $I$  and truncated  $R'$  bands used in the synthetic photometry are also plotted.

### 2.3.1. Spectral types

To garner spectral types we first performed synthetic photometry on the flux-calibrated spectra to calculate broadband  $(R - I)_C$  colours. Lyo et al. (2004a) used a similar method on their DBS 158R spectra. Because of the low signal-to-noise in the spectra blueward of 6300 Å we were forced to truncate the Cousins  $R$  filter of Bessell (2005) to form the  $R'$  filter seen in Figure 2.5. Unfortunately, the Gliese standards we intended to use to calibrate the colour and spectral type transformations are much brighter than the candidates and suffered from severe fringing at wavelengths longer than  $\sim$ 8000 Å, probably as a result of scattered light inside the spectrograph. The fringing could not be removed even when using bright flat-field exposures taken immediately before and after each observation. The DBS was upgraded after the observations of Lyo et al. (2004a) and the new CCD chips were particularly prone to fringing. Using the Gliese dwarfs to calibrate the candidate photometry resulted in a systematic 0.05–0.15 mag excess in  $(R - I)$  for the known  $\eta$  Cha members. We therefore calibrated the photometry of the Gliese dwarfs and candidates separately. The instrumental  $(R' - I)$  colours of the two groups were transformed onto the Cousins system using published photometry for the Gliese dwarfs from Bessell (1990) and the 14 late-type members of  $\eta$  Cha from Lyo et al. (2004a, 2008), respectively. In both cases the insensitivity of the  $(R - I)$  colour to wavelengths blueward of 6300 Å meant the transformation was well-fitted by a low-order polynomial with an RMS residual of 0.03 mag. The Lyo et al.  $\eta$  Cha stars were calibrated using the same Gliese sample and colours we used, so the two calibrations are equivalent.

Spectral types for the candidates were finally obtained from the  $(R - I)$  colour using the M-dwarf transformation of Bessell (1991). Lyo et al. (2004a, 2008) have shown that the  $(R - I)$  colours and various narrow-band spectral indices of intermediate-age pre-main sequence stars are indistinguishable from Gyr-old field dwarfs and that they closely follow a dwarf temperature (spectral type) sequence. The  $(R - I)$ -derived spectral types of the Gliese M-dwarfs and known  $\eta$  Cha members agree with published values at the 0.1 subtype level. We also checked each candidate by eye, comparing its spectrum to the dwarf standards and known  $\eta$  Cha members. In most cases these visual inspections agreed with the  $(R - I)$  spectral types but in a few cases the latter were clearly in error by a few tenths of a subtype. Finally, we also computed a selection of narrow-band spectral type indices from the compilation of Riddick et al. (2007). We did not adopt these molecular index-derived spectral types as we found tighter relations when using the  $(R - I)$  colour (but see later chapters).

No attempt has been made to correct the spectra or photometry for the effects of reddening—we assume it to be minimal at these distances. The maximum reddening at the candidate positions from the Schlegel et al. (1998) dust maps is  $E(B - V) = 0.5$  mag, although the majority of this material is probably associated with the Chamaeleon complex and thus behind the candidates. Whittet et al. (1997) and Knude & Hog (1998) estimated 0.1 mag as a likely upper limit to foreground ( $d \lesssim 150$  pc) extinction in the region. To include the effects of any residual reddening and our piecewise colour-spectral type conversion, we adopt a spectral type uncertainty of half a subtype. Reddening will be revisited in later chapters.

### 2.3.2. Gravity estimation

Pre-main sequence stars are in the process of contracting towards their eventual main sequence radii. As a result they have slightly lower surface gravities than main sequence stars (but still much closer to dwarfs than giants). The neutral alkali metal lines in their spectra, such as the K I ( $\lambda 7665/7699$ ) and Na I ( $\lambda 8183/8195$ ) doublets, are highly sensitive to gravity. At spectral types later than mid-M there is a marked difference in Na I absorption strength between M-dwarfs, pre-main sequence stars and M-giants. Many authors have used the strength of the Na I doublet to gauge the surface gravities of late-type pre-main sequence candidates and assign coarse ages. Recently, Lawson et al. (2009) used the Na I doublet and FeH  $\lambda 9896$  band-head strengths to rank the ages of several young associations in the solar neighbourhood at an age resolution of 1–2 Myr. They were able to resolve  $\eta$  and  $\epsilon$  Cha in gravity (age) and confirmed that age rankings using gravity estimation agree with the isochronal age ranking of the groups.

We adopt the spectral index defined by Slesnick et al. (2006a) to measure the strength of Na I absorption. It is formed by integrating<sup>10</sup> the spectrum over two 30 Å bands, one on the doublet, the other sampling the adjacent pseudo-continuum:

$$\text{Na I index} = \frac{F_{8174-8204}}{F_{8135-8165}} \quad (2.2)$$

The location of the bands is shown in Figure 2.5, where we compare the intermediate-gravity  $\eta$  Cha candidate 2MASS J0820–8003 to an older main sequence dwarf of the same spectral type. The Na I and K I doublets are significantly weaker in the (presumably) younger star.

<sup>10</sup>Since publication of this work we have discovered that Slesnick et al. (2006a) formed the *average* of the flux in each band, not the sum as we have computed. As Figure 2.6 attests, the choice of index is of little importance.

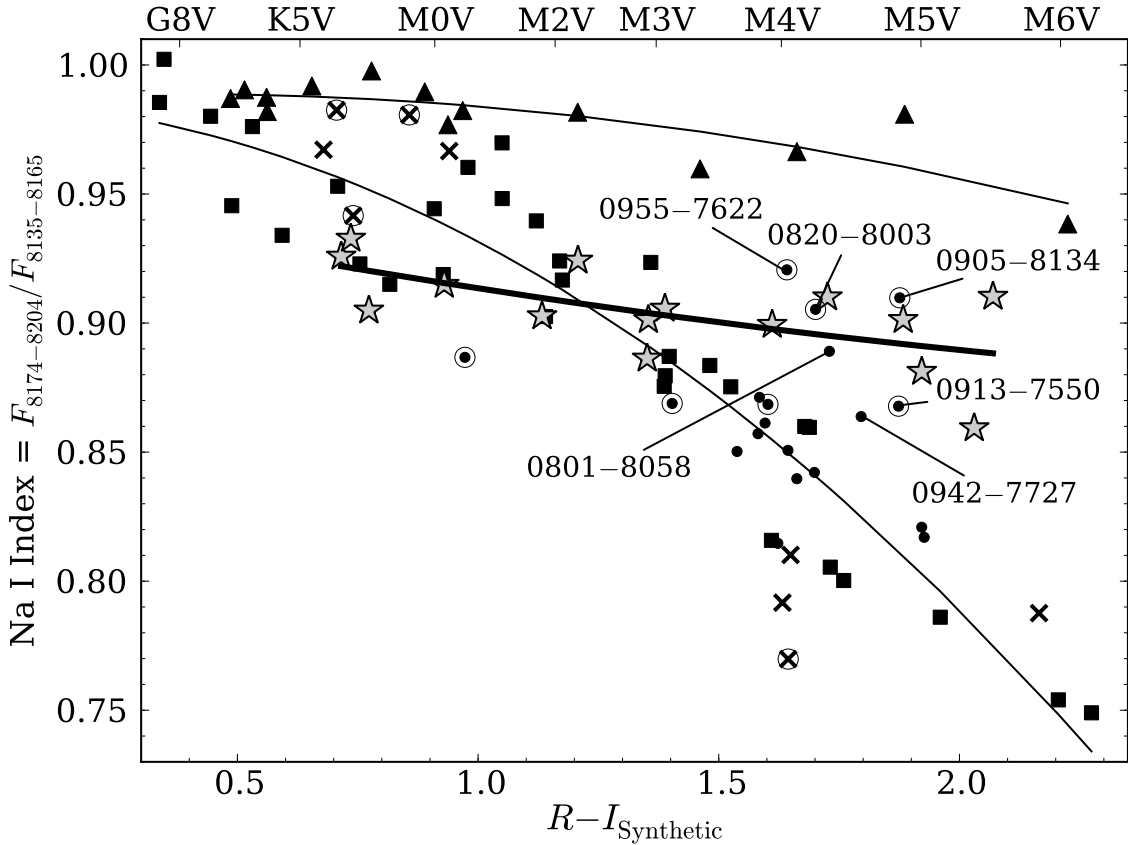


**Figure 2.6** Gravity–temperature diagram for the DBS targets. Thin lines are fits to the observed K and M-type dwarfs (squares) and Pickles giants (triangles). The thick line is a fit to the late-type cluster members (filled stars). Candidates with H $\alpha$  emission are denoted by filled circles, those without are crosses. Proper motion candidates are identified with open circles.

Figure 2.6 shows the Na I index versus synthetic ( $R - I$ ) colour for our DBS targets, known  $\eta$  Cha members, Gliese field dwarf standards and KM giants from the Pickles (1998) library. Because of the small width of the bands defining the index it is not affected by the fringing in the Gliese spectra. At spectral types later than M3, the locus of  $\eta$  Cha members clearly diverges from the dwarf sequence and assumes an intermediate position between dwarfs and giants (which show no Na I absorption). This in part motivated the  $(i - J) > 1.5$  limit of the photometric selection. Six candidates (labelled) also occupy this region on the diagram. They are likely to be pre–main sequence stars with ages similar to  $\eta$  Cha.

As noted by Slesnick et al. (2006b), the presence of a telluric water absorption band at  $\lambda 8161$ – $8282$  can contaminate the Na I index, leading to artificially high index values if telluric correction is insufficient. This underlines the importance of observing smooth spectrum stars for accurate telluric correction. As a check we verified the gravities of all our candidates by eye. True intermediate-gravity objects are readily distinguishable from the older field dwarfs under such inspection (see Figure 2.5). All six intermediate-gravity candidates passed visual inspection and we did not find any other spectra with such gravities.

Four of the eleven proper motion candidates we observed had intermediate gravities. Concerning the two remaining intermediate-gravity candidates, 2MASS J0801–8058 sits on the cluster isochrone with a proper motion just outside the selection box of Figure 2.4 and 2MASS J0942–7727 has a null proper motion in NOMAD and an  $i$ -band magnitude that

**Table 2.2** DBS observations of the photometric candidates

2MASS J <sup>‡</sup>	$i_{\text{DENIS}}$ [mag]	$(i - J)$ [mag]	$(R - I)_{\text{syn}}$ [mag]	Na I index	Sp. Type [ $\pm 0.5$ ]	Int. grav.?	H $\alpha$ em.?
<i>Proper motion candidates</i>							
07291649–7801257	12.70	1.56	1.60	0.861	M3.9		yes
07524497–7527172	11.28	1.54	0.86	0.981	K8.9		
07595212–7426018	13.39	1.77	0.71	0.982	K6*		
08202975–8003259	12.96	1.65	1.70	0.905	M4.3	yes	yes
08533950–8204523	12.98	1.51	1.40	0.869	M3.1		yes
09053087–8134572	14.16	2.01	1.88	0.910	M4.9	yes	yes
09074165–7747024	13.80	1.84	0.74	0.942	K7*		
09133435–7550099	13.82	1.96	1.87	0.868	M4.9	yes	yes
09553919–7622119	13.12	1.85	1.64	0.921	M4.0	yes	yes
10140807–7636327	11.32	1.58	1.60	0.869	M3.9		yes
10311806–8117112	14.06	1.82	0.97	0.887	M0.5		yes
<i>Other photometric candidates</i>							
07301029–7949465	13.38	1.59	1.64	0.770	M4.0		
07360613–7615306	13.78	1.80	1.65	0.810	M4.1		
07413127–7857463	14.22	1.92	1.92	0.821	M5.0		yes
08014860–8058052	13.17	1.88	1.73	0.889	M4.4	yes	yes
08194309–7401232	11.67	1.61	1.64	0.851	M4.0		yes
08285425–8145094	15.96	2.20	2.17	0.788	M5.8		
08485911–8035017	12.06	1.64	1.63	0.792	M4.0		
08513016–7503119	12.93	1.56	1.54	0.850	M3.7		yes
08595512–7728298	13.45	1.67	1.58	0.857	M3.8		yes
09212550–7915133	14.70	2.08	1.93	0.817	M5.1		yes
09332070–7433127	12.55	1.62	1.66	0.840	M4.1		yes
09424157–7727130	14.11	1.73	1.80	0.864	M4.6	yes	yes
09512392–8259057	13.86	1.82	1.70	0.842	M4.3		yes
09533862–7929598	13.08	1.60	1.62	0.815	M4.0		yes
09545099–7729327	12.92	1.60	1.58	0.871	M3.8		yes
10261679–7755442	13.47	1.59	0.68	0.967	K5.5*		
10265445–7800055	13.08	1.52	0.94	0.967	M0.3		

<sup>‡</sup> 2MASS identifier has the format ‘2MASS Jhhmmssss±ddmmssss’ (J2000)

\*  $(R - I)$  colour outside the range of the Bessell (1991) relation. Spectral type estimated by comparison against Gliese standards and the relation of Kenyon & Hartmann (1995).

places it at the bottom of the photometric selection band. It lies more towards the dwarf trend than the other candidates in Figure 2.6 which suggests it could be slightly older than  $\eta$  Cha. We will meet this interesting object again in later sections.

### 2.3.3. H $\alpha$ emission

All of the known late-type members of  $\eta$  Cha exhibit H $\alpha$   $\lambda 6563$  emission, with equivalent widths ranging from  $-1$  Å to  $-110$  Å for the accreting T Tauri star ECHA J0843.3–7905 (Lawson et al. 2002). As an additional signature of youth, we required that candidates also show H $\alpha$  emission. These stars are plotted as filled circles in Figure 2.6 and listed in Table 2.2. As expected, all of the intermediate-gravity stars also presented H $\alpha$  emission.

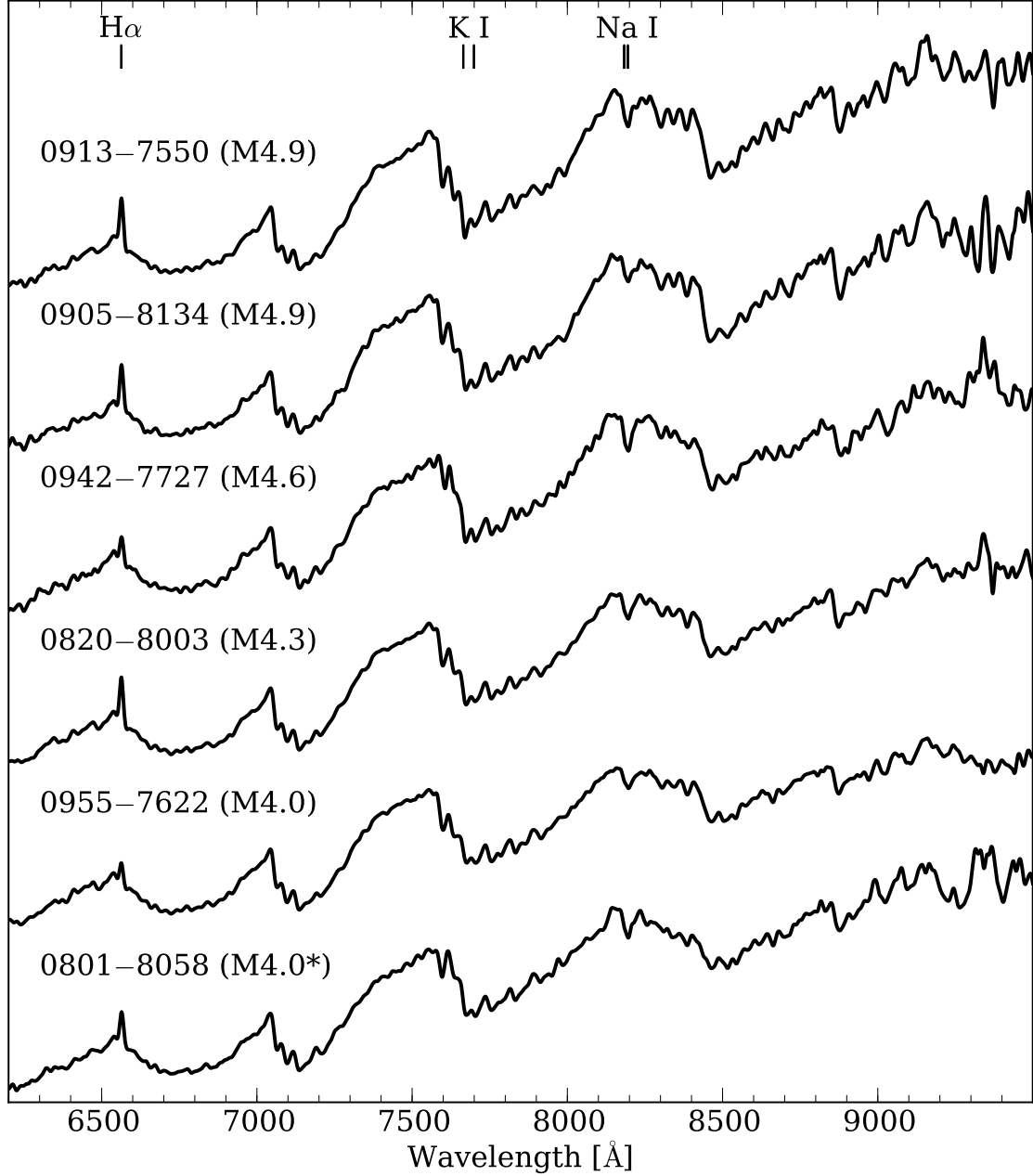


**Figure 2.7** DBS 316R spectra of the six intermediate-gravity  $\eta$  Cha candidates from Table 2.2. All spectra have been normalised around 7500 Å and smoothed for clarity. Note the H $\alpha$  emission and weak absorption doublets of Na I and K I. Although 2MASS J0801–8058 has an ( $R - I$ ) spectral type of M4.4, its spectrum is affected by a reddening of  $E(B - V) \approx 0.3$  mag (see Chapter 3). An M4.0 spectral type is a better match to the DBS spectrum.

However, because of the potential contamination from older field dwarfs whose emission is driven by active chromospheres, this is a necessary, but insufficient indicator of youth. Over the range of spectral types considered in this survey, 30–60 percent of old disk M-dwarfs have been shown to possess some level of H $\alpha$  emission (Hawley et al. 1996).

In summary, Table 2.2 lists the 28 stars with DBS 316R observations, along with their photometry, spectral types and youth indicators. Spectra of the six intermediate-gravity candidates are presented in Figure 2.7. Before we can confirm these stars as *bona fide*  $\eta$  Cha members it is necessary to observe them at higher spectral resolution, to check for lithium absorption and obtain radial velocities. These observations are presented in the next section.

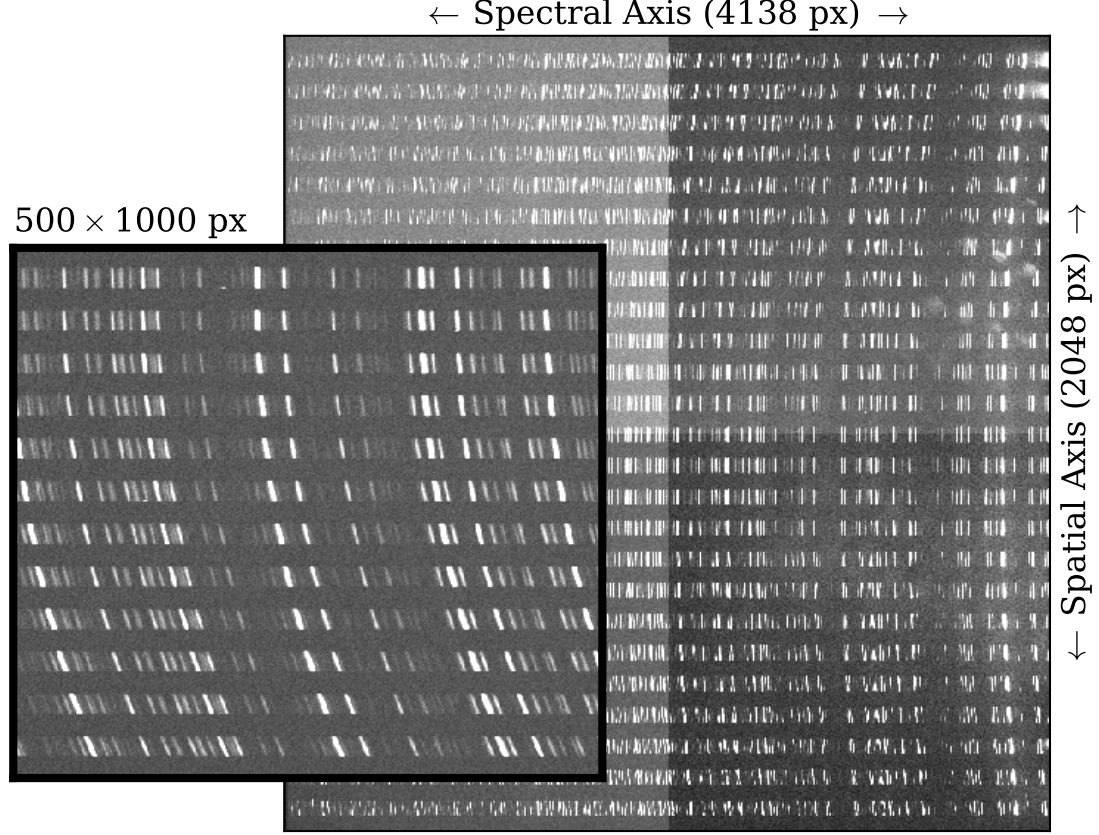


**Figure 2.8** WiFeS raw data format. The image shows a raw 1×2 binned NeFeAr arc frame taken with the R7000 grating and RT480 dichroic. The quadrant pattern is the result of the four amplifiers. Due to electronic problems in late 2010, images taken in 2011 were only read out from the top half of each frame (13 slitlets) through a single amplifier. *Inset:* A section of the chip from the bottom-left quadrant. The tilt of the dispersion across and between each slitlet is immediately obvious in the arc lines.

## 2.4. WiFeS medium–resolution spectroscopy

To determine radial velocities and check for the presence of Li I  $\lambda 6708$  absorption, we obtained medium-resolution ( $R \simeq 7000$ ) spectra of the intermediate-gravity stars in Table 2.2 with the *Wide Field Spectrograph* (WiFeS) at the ANU 2.3-m during 2010 January–2011 April. We also observed several other candidates with congruent photometry, proper motions or H $\alpha$  emission. WiFeS (Dopita et al. 2007, 2010) is a new double-beam, image-slicing integral-field spectrograph which replaces the venerable DBS. It nominally provides a  $25'' \times 38''$  field of view with  $0.5''$  pixels along each of its  $25\ 38'' \times 1''$  slitlets. We consider only the red spectra in this thesis. Our choice of the RT480 dichroic is optimised for the R7000 grating and provides wavelength coverage from 5300–7060 Å, at a resolution of 1 Å ( $0.44\text{ Å px}^{-1}$ ). We used 2× binning in the spatial dimension on the detector to decrease read-out times. This reduced the size of the spatial pixels to  $1''$  across the slitlets, of minimal consequence for point sources. The resultant images (see Figure 2.8) are similar in format to echelle orders, with each slice sampling a different  $38'' \times 1''$  strip of the stellar disk. Because of electrical problems in three of the red amplifiers in late-2010, it was necessary to read the entire chip out through the sole remaining amplifier. To maintain reasonable read-out times we elected to use only the top half of each chip (13 slices with full spectral coverage). All observations

taken in 2011 used this half-chip mode. The factor of two decrease in spatial coverage (down to  $12.5'' \times 38''$ ) is again of minimal consequence for our point-source observations.

For each observation we reduced the images and extracted the central 3–5 slices (3–5'' around the star)—which essentially contain all the stellar flux—using custom Figaro<sup>11</sup>, IRAF and Python<sup>12</sup> routines. As seen in Figure 2.8, the image slicer tilts and shifts the spectra in each slice as a function of position along the spatial axis of the detector. These distortions were automatically removed slice-by-slice using an arc frame and the Figaro IARC integral-field spectroscopy routine. Corrected slices were then treated like long-slit spectra and individually extracted and wavelength calibrated. The wavelength fits generally had an RMS residual of  $\sim 0.02 \text{ \AA}$ , corresponding to a velocity precision of  $\sim 1 \text{ km s}^{-1}$  at  $6000 \text{ \AA}$ . The wavelength-calibrated slices were then summed to form the final spectrum. Since we already had spectrophotometry for these stars from the *DBS* observations, we did not observe flux standards nor make any attempt to flux calibrate the spectra. Each candidate was observed on multiple epochs over the 16 months to improve the derived radial velocity (see §2.4.2) and check for variable H $\alpha$  emission. The utility of these multiple observations is evident in the next chapter.

#### 2.4.1. Lithium equivalent widths

Stars that achieve core temperatures greater than  $\sim 2.5 \times 10^6 \text{ K}$  will start to burn lithium via nuclear reactions which convert  $^6\text{Li}$  or  $^7\text{Li}$  and a proton to two alpha particles. The deep convection zones inside low-mass stars ( $\lesssim 1 M_\odot$ ) ensure that once lithium burning has begun it will rapidly (<15 Myr, see Figure 2.9) deplete lithium throughout the entire star. In higher mass stars with radiative cores, provided the temperature at the base of the convection zone is lower than the critical burning temperature, photospheric lithium abundances can be maintained for many Gyr. For very low-mass stars and brown dwarfs, core temperatures take longer to reach this critical point, so these stars also retain their primordial lithium longer than more massive objects. Below masses of  $65 M_{\text{Jup}}$  ( $0.065 M_\odot$ ), brown dwarfs never achieve interior temperatures high enough to burn lithium and therefore retain their entire primordial supply of the element.

Detection of Li I  $\lambda 6708$  in the spectrum of a K or M-type star is therefore a strong indicator of youth, although because of the strong dependence of lithium depletion on both mass and age, a negative detection does not necessarily imply the star is old (see the discussion of the Lithium Depletion Boundary below). Moreover, Yee & Jensen (2010) are only the latest study to demonstrate that current lithium depletion models fail to match observational isochrones of young associations, perhaps due to the erroneously small stellar radii predicted by pre-main sequence evolutionary models<sup>13</sup>.

Despite these caveats, lithium measurements are still useful for the comparative age-dating of young clusters and associations. We present such a comparison in Figure 2.9, where we plot the *WiFeS* Li I  $\lambda 6708$  equivalent widths of our candidates against those of other young,

---

<sup>11</sup><http://www.ao.gov.au/figaro/>

<sup>12</sup><http://www.python.org> — In particular the excellent SciPy (<http://www.scipy.org>), PyFITS and PyRAF packages (both available from [http://www.stsci.edu/institute/software\\_hardware/](http://www.stsci.edu/institute/software_hardware/)).

<sup>13</sup>Baraffe & Chabrier (2010) have also recently suggested it may be possible to accelerate lithium depletion in fast circumstellar disk accretion events, leading to overestimates in ages derived from lithium abundances.

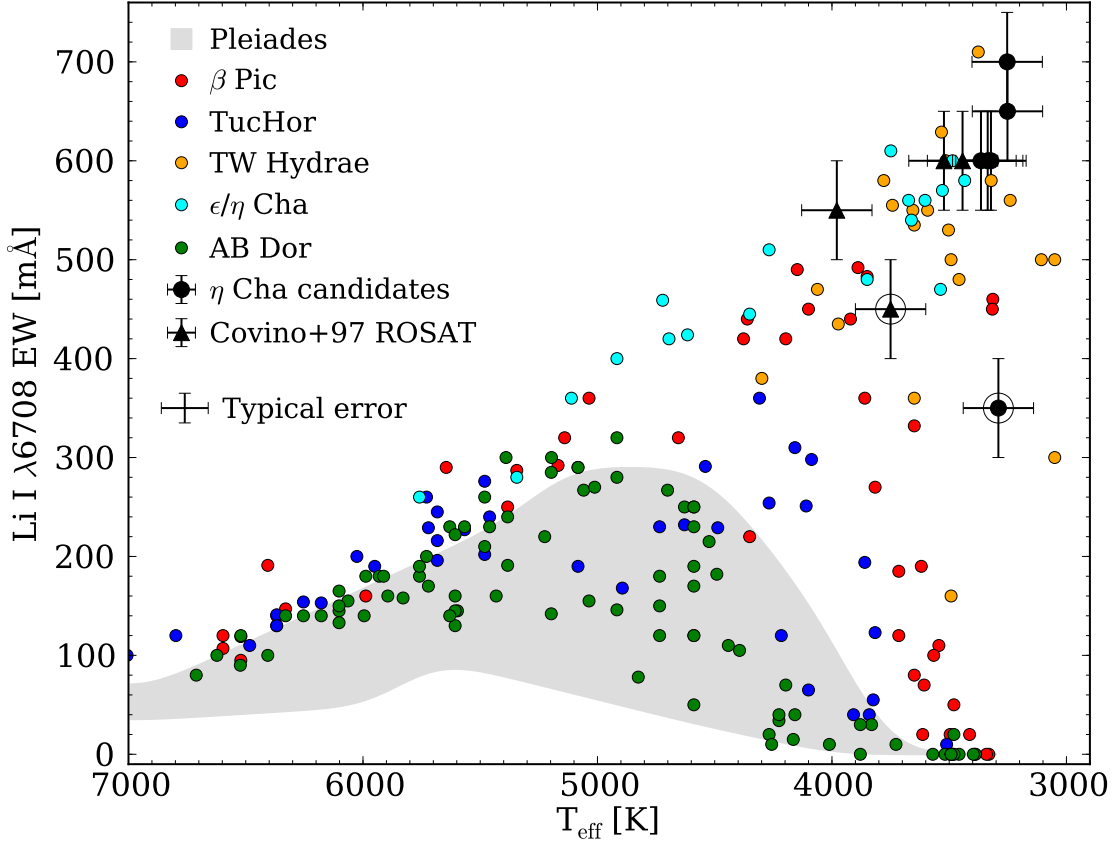


**Figure 2.9** Lithium equivalent widths of our  $\eta$  Cha candidates compared to known  $\eta$  and  $\epsilon$  Cha members and other young associations from da Silva et al. (2009);  $\beta$  Pic (12 Myr), TW Hydreae (8–10 Myr), Tucana-Horologium ( $\sim$ 30 Myr) and AB Doradus ( $\sim$ 70–120 Myr). The envelope of EW values observed in the Pleiades ( $\sim$ 120 Myr) by Neuhauser (1997) is also shown. Temperatures for the  $\eta$  Cha candidates were estimated from ( $R - I$ ) photometry and the relations of Bessell (1991) (synthetic photometry for our candidates and from Alcalá et al. (1995) for the ROSAT sources). Components of the potential wide binary near RA =  $09^{\circ}42'$  are circled.

nearby associations from the high-resolution study of da Silva et al. (2009). Only the six intermediate-gravity stars in Table 2.2 were observed to have lithium in their spectra. All but one of the candidates occupy a region on the plot with known  $\eta$  Cha members and the similarly aged  $\epsilon$  Cha (6–8 Myr) and TW Hydreae (8–10 Myr) Associations.

The sensitivity of lithium depletion to both stellar age and mass is clearly seen in the older associations. Even by an age of  $\sim$ 12 Myr, lithium is already heavily depleted in early M-type members of  $\beta$  Pictoris. The discontinuity in EW for  $\beta$  Pic members around 3300 K is the so-called Lithium Depletion Boundary (LDB), where at a given age a small increase in temperature (mass) can lead to the disappearance of the Li I  $\lambda$ 6708 feature.

The effects of lithium depletion move to hotter temperatures as a coeval group of stars ages, as clearly demonstrated by comparing the trends for the  $\beta$  Pic ( $\sim$ 12 Myr), Tucana-Horologium ( $\sim$ 30 Myr) and AB Doradus ( $\sim$ 70–120 Myr) associations. However, as can be seen in the  $\eta$  Cha and TW Hydreae members, even at a fixed age and temperature there is still considerable scatter in the equivalent widths. Although this is most likely due to a combination of processes, the main culprits appear to be variations in rotational velocity and their effect on interior mixing (e.g. Jeffries 2000) and a spread in stellar radii due to varying levels of surface activity (King et al. 2010; Pinsonneault 2010).

The lithium equivalent width for 2MASS J0942–7727 is far outside the spread seen in  $\eta/\epsilon$  Cha and TW Hydriæ members of similar temperature. This confirms the suspicions we raised about the age of the star in §2.3.2 and we can therefore rule it out as a possible member of  $\eta$  Cha. It may however be associated with the *ROSAT* source RX J0942.7–7726 (see §2.5), which also has a smaller than expected equivalent width.

#### 2.4.2. Radial velocities

Radial velocity measurements are vital for examining the dynamics of the potentially ejected cluster members, as we shall describe in §2.6. To ensure robust radial velocities we took NeFeAr arc frames immediately after each exposure and also observed 4–7 M-type velocity standards each night from the list of Nidever et al. (2002). To obtain a radial velocity, each spectrum was cross-correlated using the IRAF task `FXCOR` against all the standards from that night over the region 6000–6500 Å. This wavelength interval was chosen to avoid interference from the H $\alpha$  and Na I D lines and strong telluric features. Prior to cross-correlation, each spectrum was continuum normalised by subtracting a 31-pixel boxcar twice-smoothed version of itself, following the method of Dawson & De Robertis (2005). The final velocity for each observation was taken as the mean of these measurements, after transforming to a heliocentric frame using the corrections provided by the telescope in the image headers.

Every star was observed on multiple nights during the 16 months and we adopted the mean of these values as the radial velocity. None of the candidates showed systematic trends in velocity indicative of a spectroscopic binary system. Multiple measurements and over 600 cross-correlations between standards demonstrate we are easily able to attain a radial velocity precision of 1.5–2 km s $^{-1}$  per epoch from the instrument at signal-to-noise levels above  $\sim 20$  (see Appendix C). This is also confirmed by other careful users of the instrument (D. Bayliss, private communication). For the fainter candidates the velocity precision drops to around 2–3 km s $^{-1}$ , as demonstrated by the increased scatter around their mean velocity.

Table 2.3 summarises the lithium and radial velocity measurements of the six intermediate-gravity objects with lithium detections. The uncertainties in the radial velocities are the standard errors in the mean velocity ( $\sigma_{\text{RV}} / \sqrt{N_{\text{obs}}}$ ). The raw standard deviation of the measurements can be obtained simply by inverting the above equation, given  $N_{\text{obs}}$  from the table. Compared to 2MASS J0820–8003 and 2MASS J0955–7622, 2MASS J0801–8058 has a velocity spread far larger than that expected from its brightness and  $N_{\text{obs}} = 36$  independent measurements. Its position in the cluster colour-magnitude diagram (Figure 2.12) suggests it may be a near equal-mass binary system. 2MASS J0955–7622 may also be a binary on account of its lower than expected radial velocity and elevated position in the cluster colour-magnitude diagram. These stars will be examined further in §2.6.

#### 2.4.3. H $\alpha$ emission

Table 2.3 also lists the *WiFeS* H $\alpha$  equivalent widths of the six intermediate-gravity candidates. The large uncertainties in these measurements reflect the difficulty in defining a continuum level at the moderate ( $R=7000$ ) spectral resolution of *WiFeS* with such broad lines. As expected from their *DBS* spectra, all of the lithium-rich candidates also showed moderate levels of H $\alpha$  emission, with equivalent widths generally less than 10 Å. Most of the stars

Table 2.3 WiFeS observations of  $\eta$  Cha candidate members

2MASS designation	$N_{\text{obs}}$	H $\alpha$ EW [ $\pm 1 \text{ \AA}$ ]	Li EW [ $\pm 0.05 \text{ \AA}$ ]	RV [ $\text{km s}^{-1}$ ]	$\sigma_{\text{RV}}^{\dagger}$ [ $\text{km s}^{-1}$ ]	$\mu_{\alpha} \cos \delta$ [ $\pm 9 \text{ mas yr}^{-1}$ ] <sup>†</sup>	Membership?
<b>DENIS/2MASS intermediate-gravity candidates</b>							
2MASS J0801–8058	35	−27<EW<−6	0.60	18.3	0.5	−28	+39
2MASS J0820–8003	19	−40<EW<−10	0.60	18.3	0.4	−33	+30
2MASS J0905–8134	11	−8	0.65	16.6	0.9	−35	+27
2MASS J0913–7550	6	−9	0.70	14.2	1.0	−40	+34
2MASS J0942–7727	10	−7	0.35	18.0	0.9	−16	+23
2MASS J0955–7622	12	−5	0.60	9.3	0.7	−30	+19
<b>Covino et al. (1997) ROSAT candidates</b>							
RX J0902.9–7759 <sup>*</sup> (M3) <sup>#</sup>	5	−2	0.60	18.9	0.4	−35	+31
RX J0915.5–7608 (K7)	5	−1	0.55	24.0	0.6	−32	+16
RX J0942.7–7726 (M0)	7	−3	0.45	20.7	0.4	−24	+17
RX J1005.3–7749 (M1)	5	−4	0.60	19.6	0.8	−30	+17

<sup>\*</sup> ROSAT identifier<sup>#</sup> Spectral types from Covino et al. (1997)<sup>†</sup> Proper motions from the PPMXL catalogue (Roeser et al. 2010)<sup>‡</sup> Standard error on the mean,  $\sigma_{\text{RV}} = \sigma / \sqrt{N_{\text{obs}}}$

showed no variation in emission strength across the multi-epoch spectra. Two candidates however, 2MASS J0801–8058 and 2MASS J0820–8003, exhibited a large range of equivalent widths, sometimes changing significantly on timescales of hours to days. At maximum strength their equivalent widths and velocity profiles were comparable to known accreting members of  $\eta$  Cha. The possible accretion and disk properties of these two interesting objects are the subject of Chapter 3.

## 2.5. Other young stars in the region

As described in §1.3, the region surrounding  $\eta$  Cha is rich in pre–main sequence stars of various ages. Alcalá et al. (1995, 1997) used *ROSAT* All-Sky Survey (RASS) X-ray detections to identify 77 new Weak-lined T Tauri Stars (WTTS) over a vast region of southern sky towards the Chamaeleon cloud complex. In a follow-up study, Covino et al. (1997) presented rotational and radial velocities, as well as H $\alpha$  and Li I  $\lambda$ 6708 equivalent widths for these stars derived from high-resolution spectra. It was the clustering of four such sources prompted Mamajek et al. (1999) to investigate the region and eventually propose the  $\eta$  Cha cluster. Another four *ROSAT* detections lie in the eastern half of our survey area and have spectral types and lithium equivalent widths similar to the late-type population of  $\eta$  Cha. These stars are shown in Table 2.3 and Figure 2.9 with measurements derived from our *WiFeS* observations. Spectral types are taken from Covino et al. (1997).

One of the stars, RX J0902.9–7759, has a published radial velocity that differs significantly from our *WiFeS* value. This is a possible indication of (spectroscopic) binarity. Covino et al. (1997) reported a velocity of  $11 \pm 2$  km s $^{-1}$ , compared to our value of  $18.9 \pm 0.4$  km s $^{-1}$  from five observations. Over a baseline of almost one year we found no appreciable trend in the radial velocity measurements. We therefore adopt the mean *WiFeS* velocity for the star in Table 2.3 and the dynamical simulations of §2.6. If RX J0902.9–7759 is in fact a binary its systemic radial velocity will likely be different from this value.

Köhler (2001) reported the results of their speckle interferometry and direct imaging observations of many of the Chamaeleon *ROSAT* sources, including RX J0902.9–7759. They detected no companions around the star over separations of 0.13–6.0''. A null detection can provide an upper limit on the brightness difference (contrast) of any undetected companions—from simulations Köhler (2001) calculated this to be 3.25 mag in K-band at 0.13'' separation. Using 10 Myr Baraffe et al. (1998) and Chabrier et al. (2000) isochrones, the contrast limit for RX J0902.9–7759 corresponds to a mass limit of  $0.02 M_\odot$ , with a primary mass of  $\sim 0.2 M_\odot$  from its observed  $(V - I_C)$  colour (Padgett et al. 2006). The radial velocity semi-amplitude  $K$  is related to the stellar masses (assuming circular orbits) by:

$$K = \frac{M_c \sin i}{\sqrt{(M_\star + M_c)a/G}} \quad (2.3)$$

For the masses above and  $a = 13$  AU (0.13'' at 100 pc) we find  $K = 0.3 \sin i$  km s $^{-1}$ . Using a 5 Myr isochrone instead, the masses become  $0.27 M_\odot$  and  $0.025 M_\odot$ , with  $K = 0.4 \sin i$  km s $^{-1}$ . The corresponding orbital periods would be  $\sim 100$  yr. In order to explain the  $\sim 8$  km s $^{-1}$  difference in radial velocities, any as-yet undetected companion must therefore be much closer to RX J0902.9–7759 than the limits set by the null detection of Köhler (2001), or the system must lie significantly closer than 100 pc.

Our M4.6 candidate 2MASS J0942–7727 has a null NOMAD proper motion and a DENIS *i*-band magnitude that placed it at the bottom of the photometric selection band. Intriguingly however, it is situated only 42'' from the ROSAT source RX J0942.7–7726. Both stars have similar radial velocities and PPMXL proper motions that agree within uncertainties (Table 2.3). Furthermore, their lithium equivalent widths are lower than those seen in confirmed  $\eta$  and  $\epsilon$  Cha members of similar temperatures (Figure 2.9). As seen in Figure 2.12, the stars lie  $\sim 1$  mag below the  $\eta$  Cha isochrone defined by single stars (or high mass-ratio binaries). If they were a similar age to  $\eta$  Cha this would correspond to a distance of  $\sim 150$  pc. However, from their lower lithium equivalent widths and the more dwarf-like gravity of 2MASS J0942–7727 (see §2.3.2) it seems likely that the stars are older than  $\eta$  Cha and therefore slightly closer than 150 pc. The possibility that these two objects may form a wide, pre–main sequence binary is discussed in Chapter 4.

### 2.5.1. ROSAT completeness

Finally, we note that such an X-ray-selected sample is grossly incomplete for the spectral types covered by our photometric survey. The typical limiting flux of the RASS in the 0.5–2.5 keV energy band is  $\sim 2 \times 10^{-13}$  erg cm $^{-2}$  s $^{-1}$  (Schmitt et al. 1995). At a distance of 100 pc this corresponds to an X-ray luminosity of  $\log(L_X) = 29.4$  erg s $^{-1}$ . Assuming the saturated (e.g. Fleming et al. 1993, 1995) ratio of X-ray to bolometric luminosities typically seen in young stars,  $\log(L_X/L_{\text{bol}}) \simeq -3.0$  (Zuckerman & Song 2004) we arrive at a limiting luminosity of  $\sim 0.062 L_\odot$ . Based on a 10 Myr Baraffe et al. (1998) isochrone this corresponds to a temperature of  $\sim 3360$  K, or an approximate spectral type of M3–M4 depending on the adopted conversion. This agrees quite well with the  $\sim$ M2 limit of RASS detections for known  $\eta$  Cha members (equivalent to an upper X-ray luminosity limit of  $\log(L_X) \simeq 30.0$  erg s $^{-1}$ , Mamajek et al. 2000) and the non-detection in the RASS of any of our DENIS/2MASS lithium-rich candidates, which are spectral type M4 and later.

## 2.6. Dynamics

If the remaining candidates are in fact ejected members of  $\eta$  Cha then we do not expect their space motions to be identical to that of the cluster proper. They will have each been imparted some ejection velocity which acts over time to disperse the star away from the cluster core. To determine the possible epoch and magnitude of this impulse we modelled the space motion of each candidate as a function of ejection time and distance. In the absence of a trigonometric parallax, this kinematical distance can then be compared to a photometric distance based on the position of the star in the cluster colour-magnitude diagram.

For such work it is important to be able to correctly trace a star's position back in time. In Murphy et al. (2010) we used a simple linear (sometimes called *ballistic*) approximation, where the heliocentric position of a star ( $X, Y, Z$ ) moving with constant velocity  $(U, V, W)_0$  may be given at time  $t$  by:

$$(X, Y, Z) = (X, Y, Z)_0 + (U, V, W)_0 \times t \quad (2.4)$$

where  $X$  is positive towards the Galactic centre,  $Y$  is positive in the direction of Galactic rotation and  $Z$  is normal to the Galactic plane and completes the right-handed triad. Similarly,

$(U, V, W) = (\dot{X}, \dot{Y}, \dot{Z})$ . While such a linear approximation is generally valid for timescales of  $< 10$  Myr, it neglects the effects of rotation and the Galactic gravitational potential. In the dynamical simulations described below a full integration of the stellar equations of motion under the influence of a multi-component Galactic potential (e.g. Hoogerwerf et al. 2001; Fernández et al. 2008) would prove computationally expensive. We instead use the *epicyclic approximation* (Binney & Tremaine 2008; Mo et al. 2010) which assumes nearly circular orbits in an axisymmetric potential about the Galactic centre. A full derivation of the epicyclic approximation can be found in Appendix B.

### 2.6.1. The epicyclic approximation

We adopt the formulation of Makarov et al. (2004), who have solved the stellar equations of motion (Eqn. B.1) to give the position of a star moving under the epicyclic approximation in heliocentric XYZ coordinates as a function of time:

$$\begin{aligned} X &= X_0 + \frac{U_0}{\kappa} \sin \kappa t + \frac{1}{2B}(V_0 - 2AX_0)(1 - \cos \kappa t) \\ Y &= Y_0 - \frac{U_0(1 - \cos \kappa t)}{2B} \\ &\quad + \frac{V_0}{\kappa B}[A\kappa t - (A - B)\sin \kappa t] \\ &\quad - \frac{2AX_0}{\kappa B}(A - B)(\kappa t - \sin \kappa t) \\ Z &= Z_0 \cos \nu t + \frac{W_0}{\nu} \sin \nu t \end{aligned} \tag{2.5}$$

and similarly for the instantaneous velocities:

$$\begin{aligned} U &= \frac{dX}{dt} = \frac{\kappa V_0}{2B} \sin \kappa t + U_0 \cos \kappa t - X_0 \frac{\kappa A}{B} \sin \kappa t \\ V &= \frac{dY}{dt} = \frac{V_0}{B}[A - (A - B)\cos \kappa t] - \frac{\kappa U_0}{2B} \sin \kappa t \\ &\quad - 2AX_0 \frac{(A - B)}{B}(1 - \cos \kappa t) \\ W &= \frac{dZ}{dt} = W_0 \cos \nu t - Z_0 \nu \sin \nu t \end{aligned} \tag{2.6}$$

where  $(X, Y, Z)_0$  and  $(U, V, W)_0$  are the position (in pc) and velocity (in km s<sup>-1</sup>) at the reference time  $t$  (in Myr). In contrast to the linear approximation (Eqn. 2.4), both the position *and* instantaneous velocity of the star change as a function of time.  $A$  and  $B$  are the Oort constants of Galactic dynamics and  $\kappa$  and  $\nu$  are the epicyclic and vertical frequencies of oscillation. For these we adopted the updated values from Binney & Tremaine (2008, Table 1.2):

$$\begin{aligned} A &= 0.0148 \text{ km s}^{-1} \text{ pc}^{-1} \\ B &= -0.0124 \text{ km s}^{-1} \text{ pc}^{-1} \\ \kappa &= \sqrt{-4B(A - B)} = 0.0367 \text{ km s}^{-1} \text{ pc}^{-1} \\ \nu &= \sqrt{4\pi G\rho_0} = 0.070 \text{ km s}^{-1} \text{ pc}^{-1} \end{aligned} \tag{2.7}$$

The angular frequencies  $\kappa$  and  $\nu$  correspond to epicyclic and vertical periods of  $2\pi/\kappa = 171$  Myr and  $2\pi/\nu = 90$  Myr (where  $1 \text{ Myr}^{-1} \simeq 0.978 \text{ km s}^{-1} \text{ pc}^{-1}$ ).

**Table 2.4** Updated kinematic parameters for  $\eta$  Cha

Property	Value	Source
Position (J2000)	$08^h 40^m 48.24^s - 79^\circ 00' 24.8''$	Tycho-2 <sup>†</sup>
Distance	$94.3 \pm 1.1$ pc	<i>Hipparcos</i> <sup>‡</sup>
Proper Motion ( $\alpha, \delta$ )	$(-29.35, +27.41) \pm (0.13, 0.13)$ mas yr <sup>-1</sup>	Tycho-2 + Hipp. <sup>#</sup>
Radial Velocity	$18.3 \pm 0.1$ km s <sup>-1</sup>	A. Brandeker <sup>##</sup>
<i>Derived quantities</i>		
Heliocentric position	$(X, Y, Z) = (+33.4, -81.0, -34.9) \pm (0.4, 1.0, 0.4)$ pc	
Heliocentric velocity	$(U, V, W) = (-10.2, -20.7, -11.2) \pm (0.2, 0.1, 0.1)$ km s <sup>-1</sup>	

<sup>†</sup> Weighted average of  $\eta$  Cha, RS Cha, RECX 1 and HD 75505 Tycho-2 positions

<sup>‡</sup> Weighted average of  $\eta$  Cha and RS Cha new *Hipparcos* parallaxes (van Leeuwen 2007)

<sup>#</sup> Weighted average of  $\eta$  Cha, RS Cha (*Hipparcos*), RECX 1 and HD 75505 (Tycho-2)

<sup>##</sup> Weighted average of RECX 1,3,4–6,9,10–13 (A. Brandeker, private communication)

As the epicyclic approximation is based on a low-order Taylor expansion of the effective potential around the guiding centre (see Appendix B), it is only valid for  $|X|/R_\odot \ll 1$  and  $|V|/R_\odot \ll \Omega_\odot$ , i.e. orbits with an angular momentum close to that of the corresponding circular orbit at  $R_\odot$ . Furthermore, the assumptions made about the potential imply a constant mass density in the  $Z$ -direction, which is only satisfied near the Galactic mid-plane,  $|Z| \lesssim 300$  pc. The phase space considered in this thesis—stars very close to the Sun traveling with low relative velocities, combined with trace-back times very much less than the vertical or epicyclic periods—means the epicyclic equations (Eqn. 2.5 and 2.6) should provide a good approximation to the true behaviour of stars under the action of the full Galactic potential.

### 2.6.2. Dynamical simulations

In simulations described below we use the new cluster distance of 94.3 pc from revised *Hipparcos* astrometry by van Leeuwen (2007), proper motions from Tycho-2 and *Hipparcos* and an improved cluster radial velocity,  $V_R = 18.3$  km s<sup>-1</sup> (A. Brandeker, private communication). These new kinematics are listed in Table 2.4. They yield an updated cluster space motion of  $(U, V, W) = (-10.2, -20.7, -11.2)$  km s<sup>-1</sup>. This differs from the canonical cluster motion (Mamajek et al. 2000) by 2.4 km s<sup>-1</sup>, primarily due to the improved radial velocity.

Proper motions from the PPMXL catalogue<sup>14</sup> (Roeser et al. 2010) are also now available for our candidates. We use them here and in Table 2.3 in preference to the original NOMAD values. PPMXL is a re-reduction of USNO-B1 and 2MASS astrometry and contains absolute proper motions for over 900 million objects on the International Celestial Reference System (ICRS). Although they quote slightly larger standard errors than NOMAD, PPMXL is better able to replicate the mean proper motion of known  $\eta$  Cha members, as demonstrated in Figure 2.10. As a check we have repeated the analysis of §2.2.2 using the PPMXL values and find no change in the final proper motion candidate list.

Using the epicyclic approximation (Eqns. 2.5 and 2.6) we modelled the space motion of each candidate as a function of ejection time and current distance, between 0 and −12 Myr

<sup>14</sup>Virtual Observatory identifier: ivo://org.gavo.dc/ppmxml/q/cone

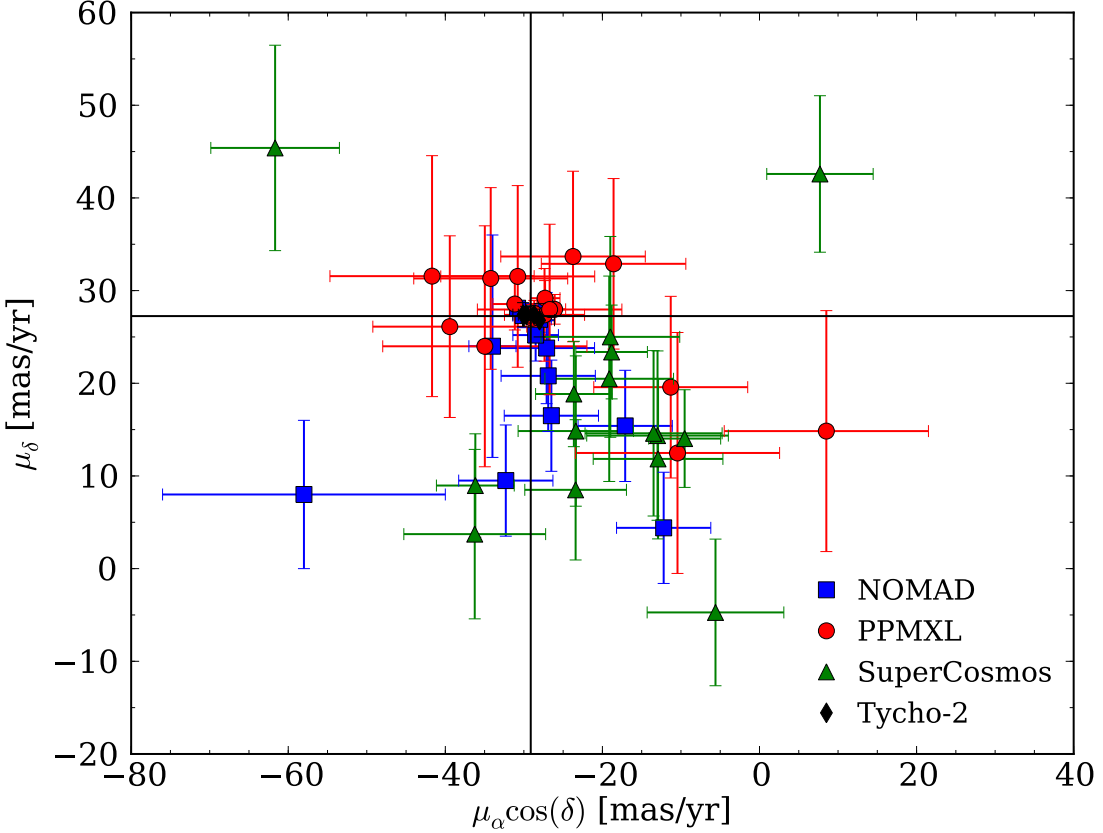


**Figure 2.10**  $\eta$  Cha members as found in the NOMAD (blue squares), PPMXL (red circles), SuperCosmos (green triangles) and Tycho-2 (black diamonds) proper motion catalogues. In addition to having absolute ICRS proper motions and recovering three more faint members than NOMAD, PPMXL more accurately replicates the canonical cluster motion as traced by the mean of the Tycho-2 stars (black lines).

( $\Delta t = 0.25$  Myr) and 50–150 pc ( $\Delta d = 1$  pc). Our known quantities were position on the sky, proper motion and radial velocity. Figure 2.11 and Table 2.5 show the results of such simulations for the stars in Table 2.3. At each simulated ejection time the cluster was first back-traced to its heliocentric position and space velocity at that epoch. For each (current) distance we then calculated the XYZ location of the candidate and the corresponding space motion required to move it there since ejection. This was determined by simultaneously solving Equation 2.5 for  $(U, V, W)_0 = (U, V, W)_k$ , knowing the current position of the star ( $X, Y, Z$ ) (at the assumed distance) and the position of the cluster ( $X, Y, Z$ )<sub>0</sub> at the time of ejection. The three-dimensional impulse imparted to the star at the moment of its ejection is simply the difference between  $(U, V, W)_k$  above and the back-traced cluster velocity.

By transforming the calculated  $(U, V, W)_k$  to  $t = 0$  (present day) we then tested the merit of each solution by comparing the velocity to the *observed*  $(U, V, W)$  derived from proper motion and radial velocity measurements at the assumed distance. The colour mapping in Figure 2.11 indicates the magnitude of the difference between the two space velocities:

$$\begin{aligned} \Delta Uvw &= \|(U, V, W)_{\text{obs}} - (U, V, W)_{k,t=0}\| \\ &= \sqrt{(U_{\text{obs}} - U_{k,t=0})^2 + (V_{\text{obs}} - V_{k,t=0})^2 + (W_{\text{obs}} - W_{k,t=0})^2} \end{aligned} \quad (2.8)$$

Empty regions in the diagrams have velocity differences larger than those expected from the error in the space motion (via errors in radial velocity and proper motion) at that distance.

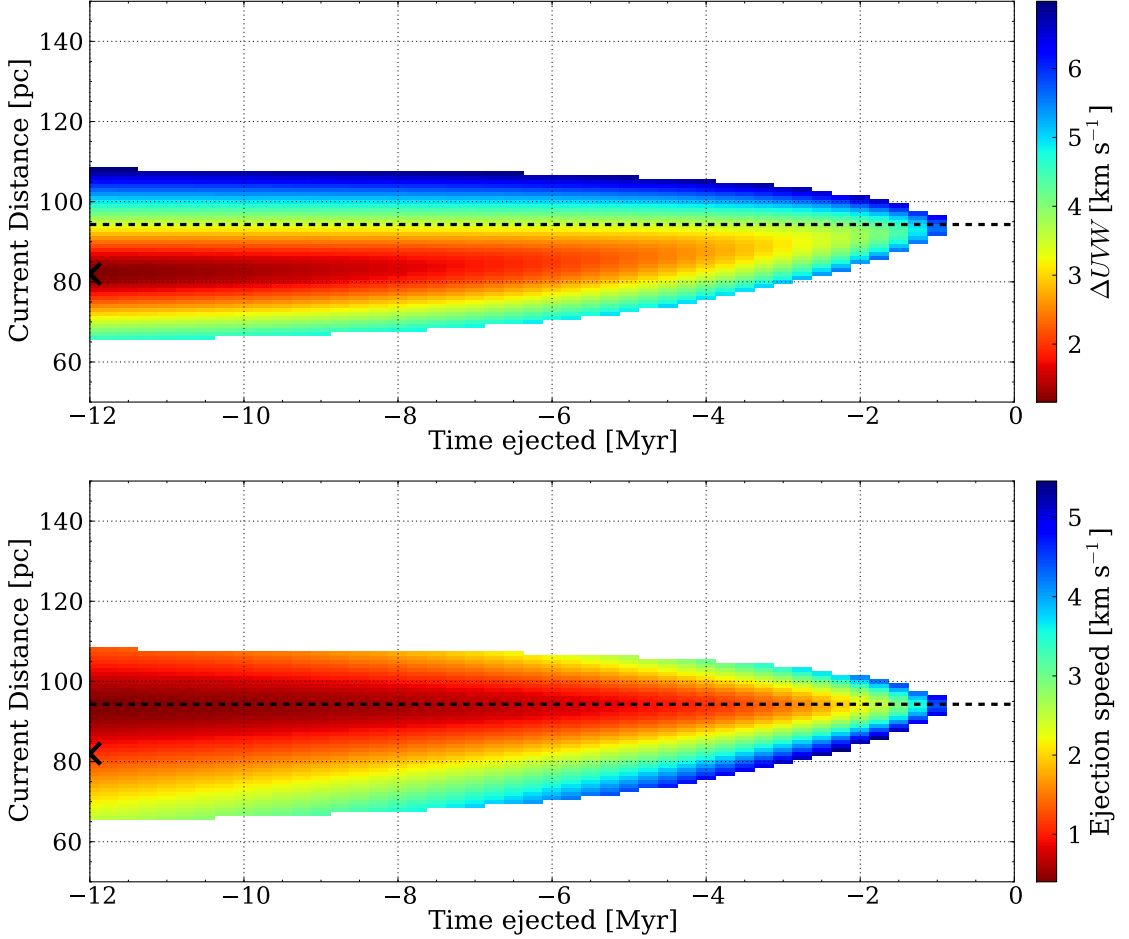


**Figure 2.11** The results of dynamical simulations for 2MASS J0801–8058 as a function of ejection time and current distance. *Top panel:* The magnitude of the vector difference between the observed and expected space motion (see Eqn. 2.8). The minimum is shown by the black cross and summarised in Table 2.5. The dashed line denotes the revised 94.3 pc cluster distance from van Leeuwen (2007). *Bottom panel:* Magnitude of the ejection velocity ‘kick’ over the same space. The cross shows the location of the minimum  $\Delta(UVW)$  from the top panel.

A similar map is also shown for ejection speed ( $\|(U, V, W)_k - (U, V, W)_{\text{cluster}}\|$ ) over the same parameter space. The results of Figure 2.11 and Table 2.5 are very similar to those presented in Murphy et al. (2010), confirming the expected equivalency of the linear and epicyclic approximations over the short trace-back times of the simulations. They are discussed in the context of cluster membership and dynamical evolution in the next section.

## 2.7. Cluster membership

To definitively assign membership in  $\eta$  Cha, the kinematic distances estimated from Figure 2.11 must be checked against those expected from the star’s position in the cluster colour-magnitude diagram. Such a diagram is shown in Figure 2.12, where we separate the known cluster members into single (or high mass-ratio binary) stars and unresolved binary systems (see Table 1.2 and Lyo et al. 2004b). As expected for equal-mass systems, most known or suspected binaries lie around  $2.5 \log_{10}(2) = 0.75$  mag above the single star locus. From comparison of Figures 2.11 and 2.12 we propose four *probable* and four *possible* new members of  $\eta$  Cha, which we describe below and summarise in Table 2.3.

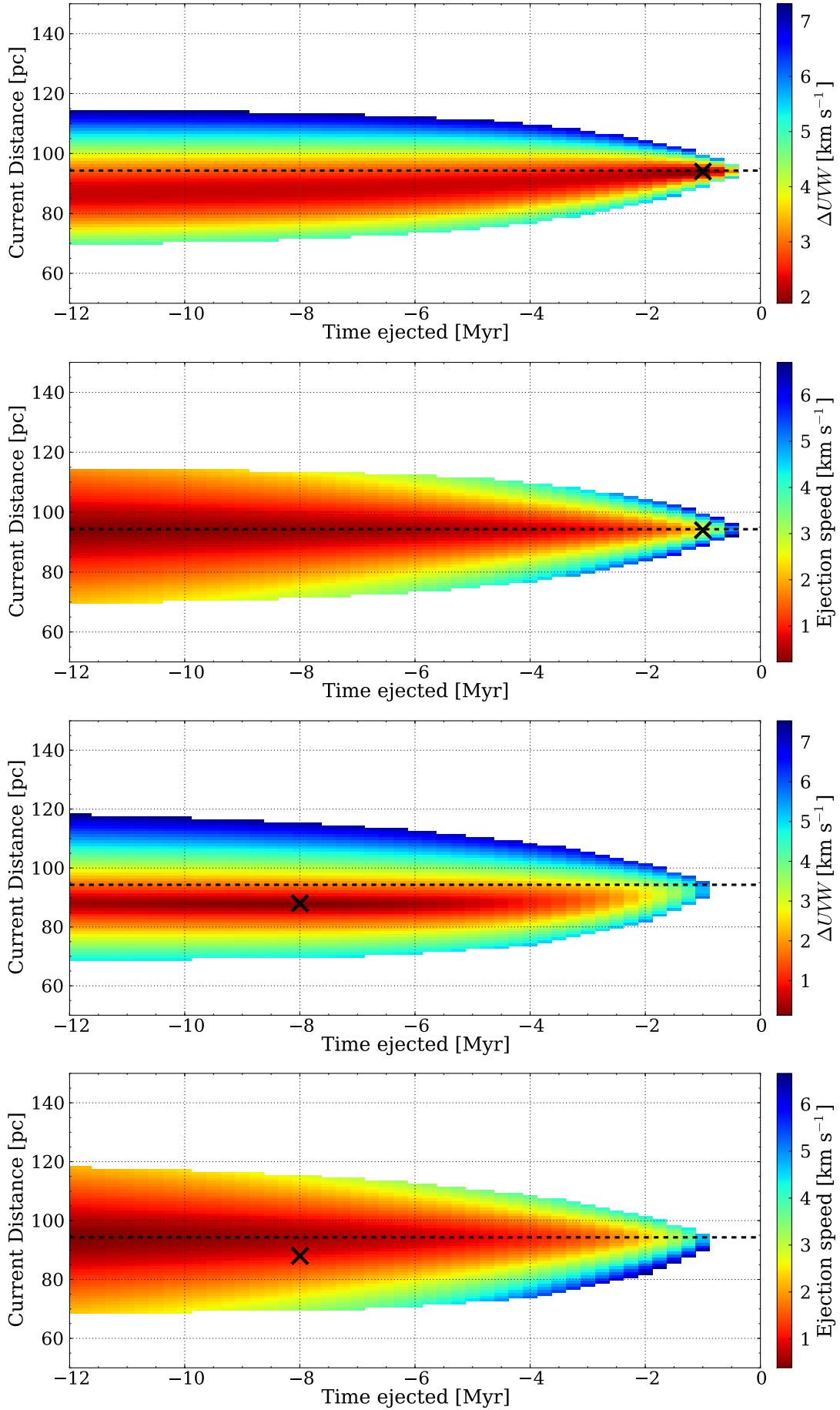


**Figure 2.11** (cont.) Dynamical simulations for 2MASS J0820–8003 (top) and 2MASS J0905–8134 (bottom).

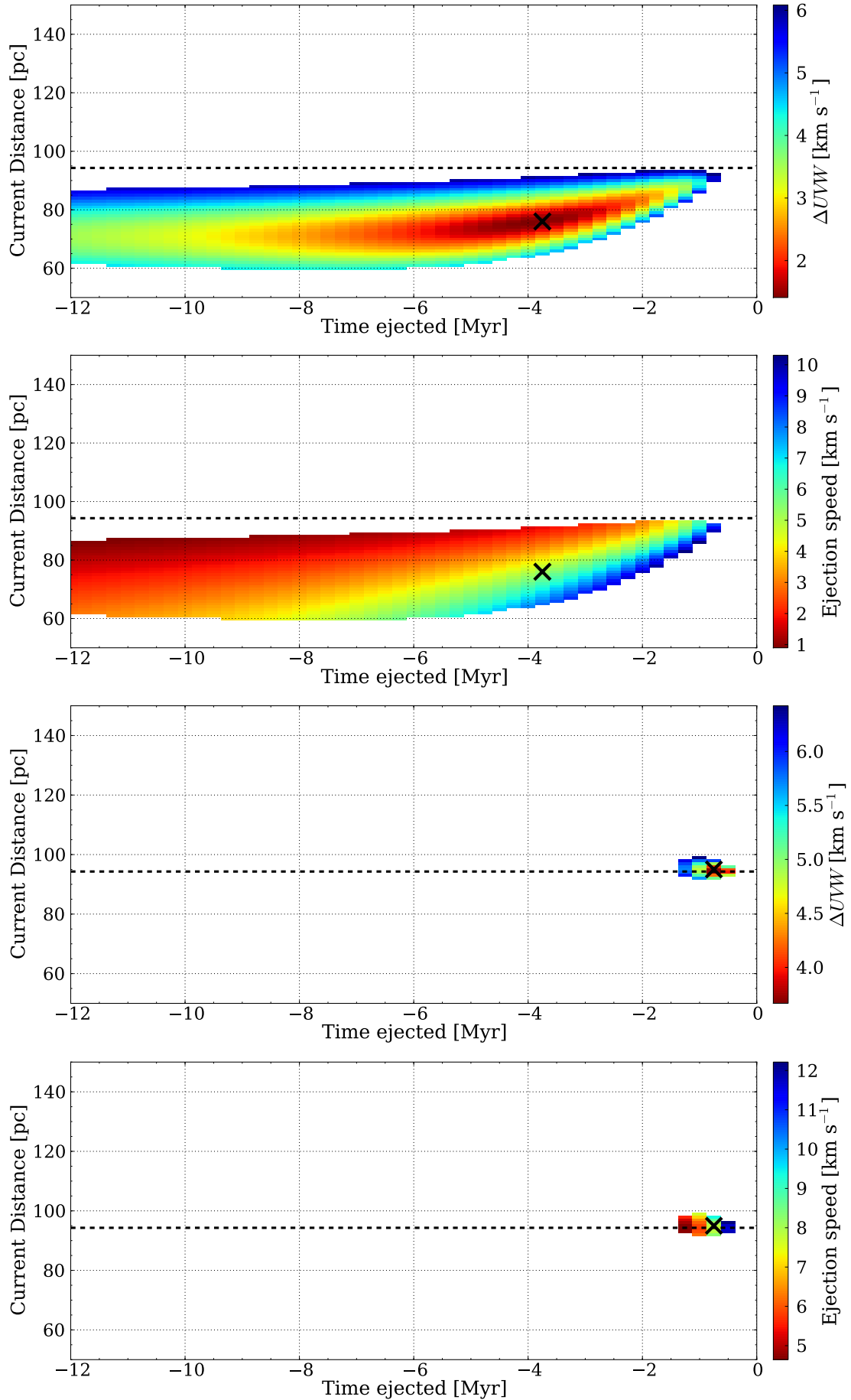
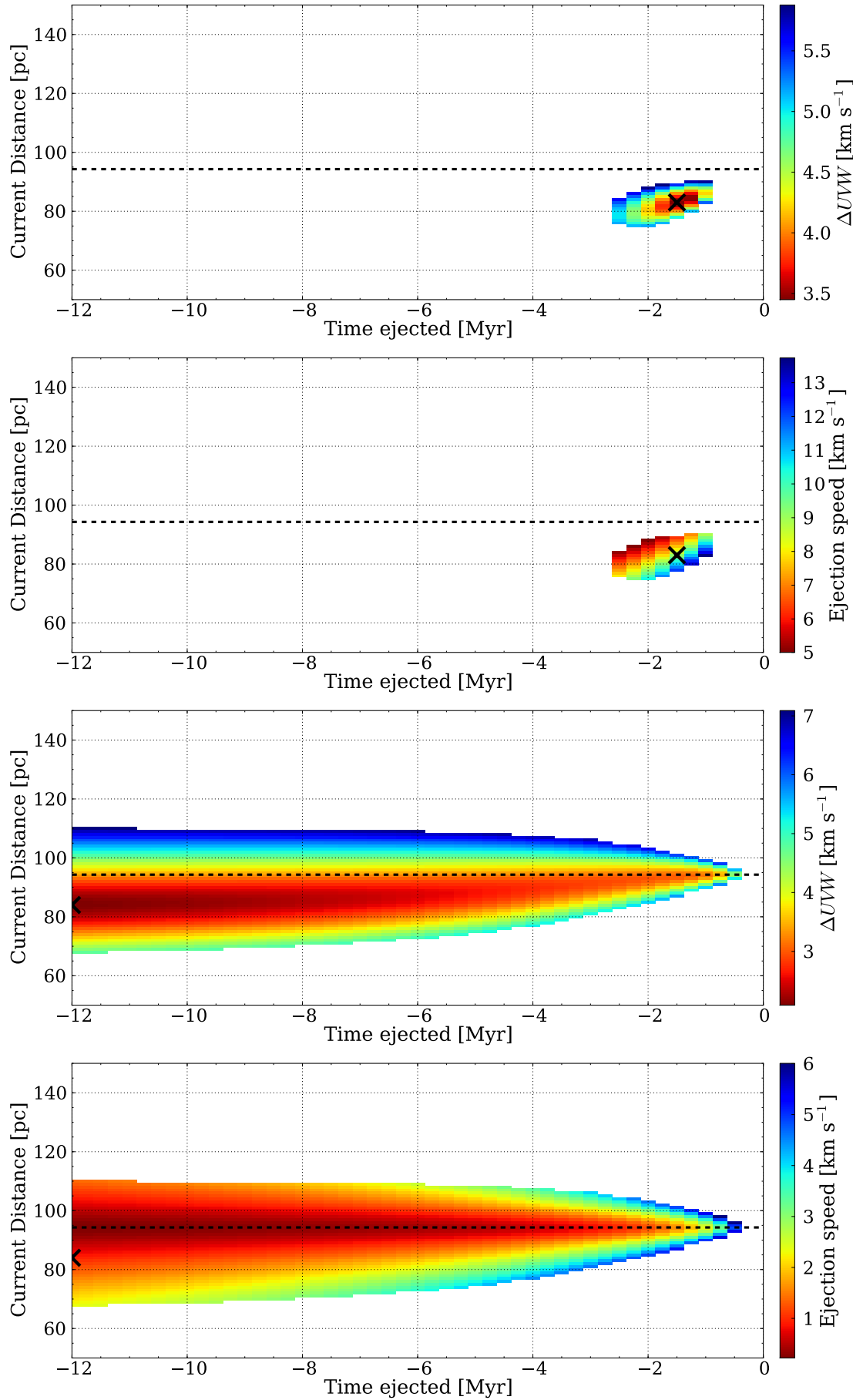


Figure 2.11 (cont.) Dynamical simulations for 2MASS J0913-7550 (top) and 2MASS J0942-7727 (bottom).



**Figure 2.11** (cont.) Dynamical simulations for 2MASS J0955–7622 (top) and RX J0902.9–7759 (bottom).

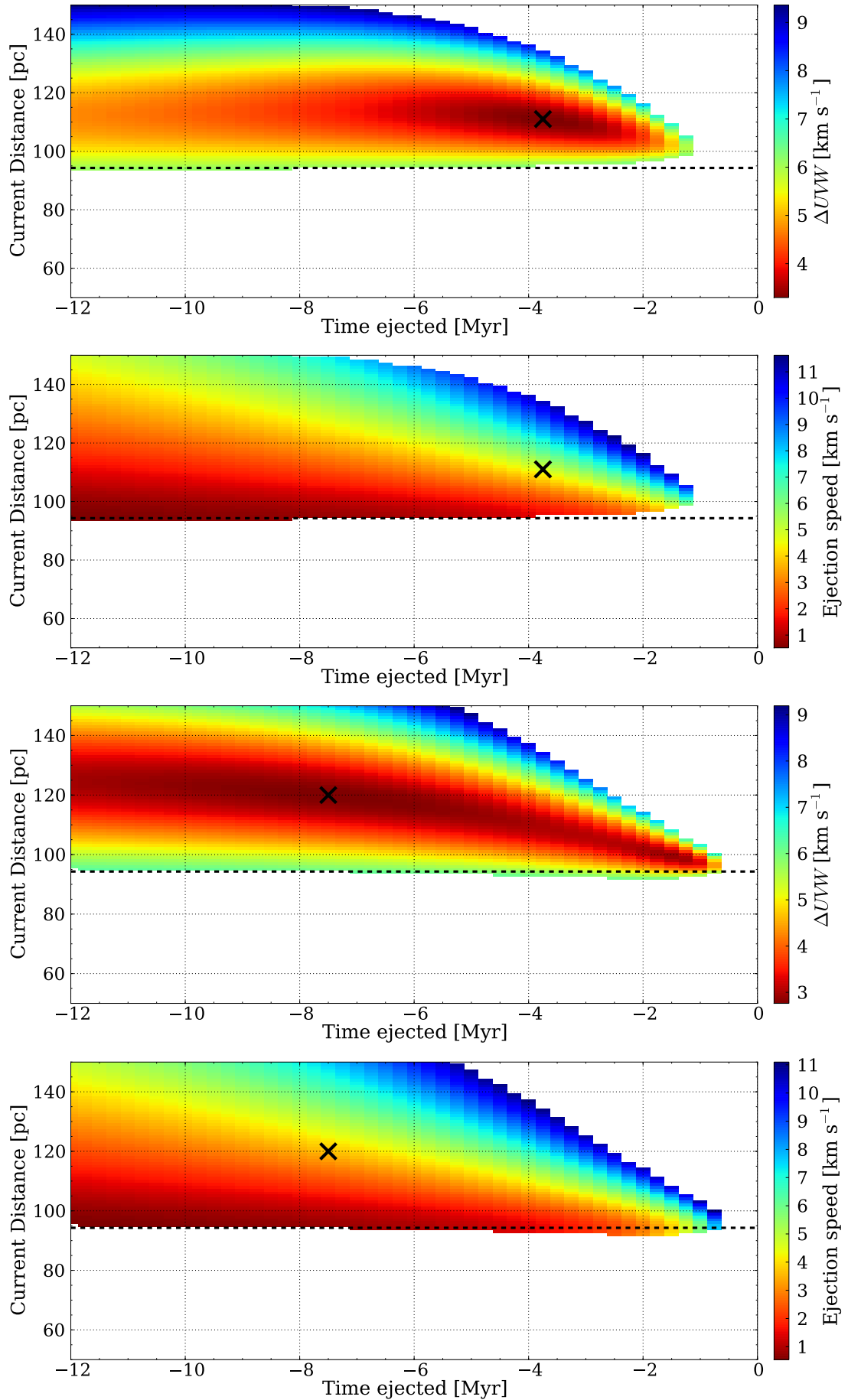
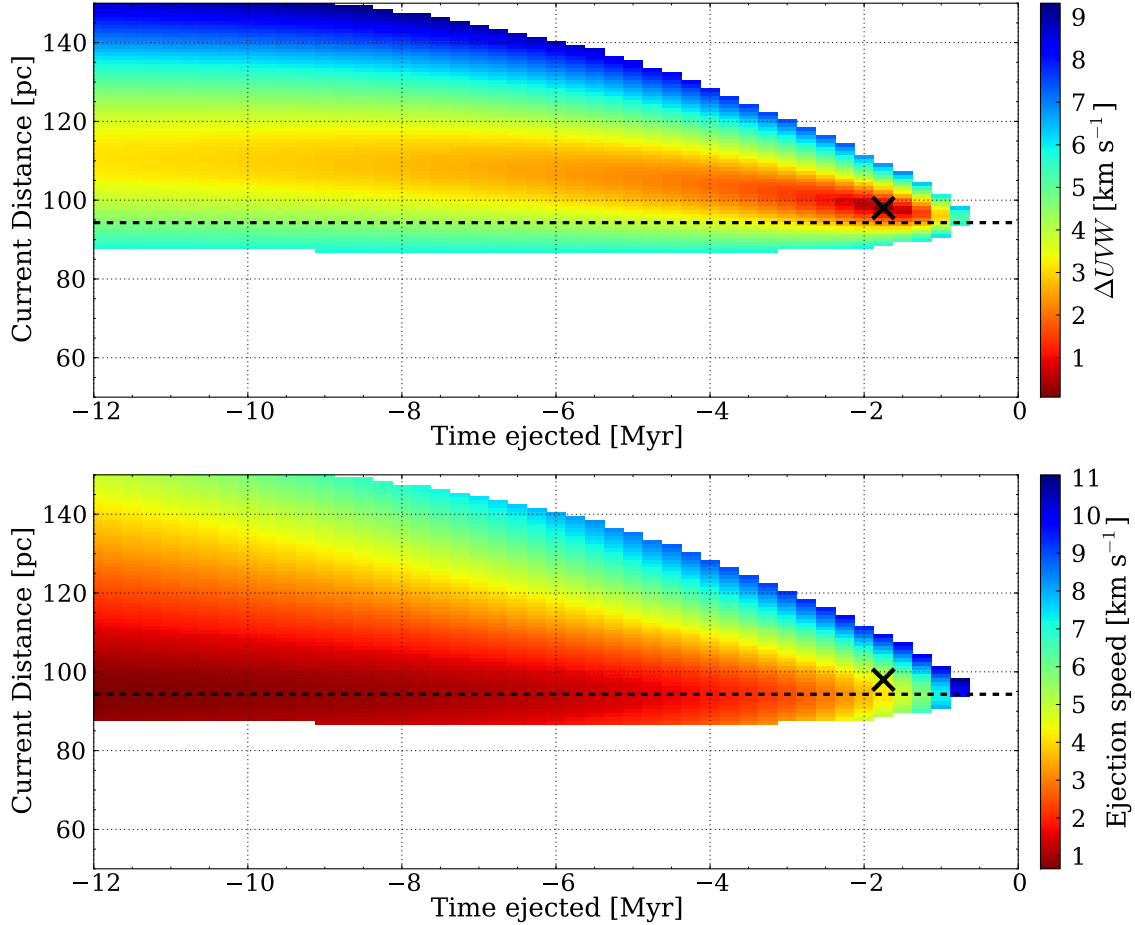
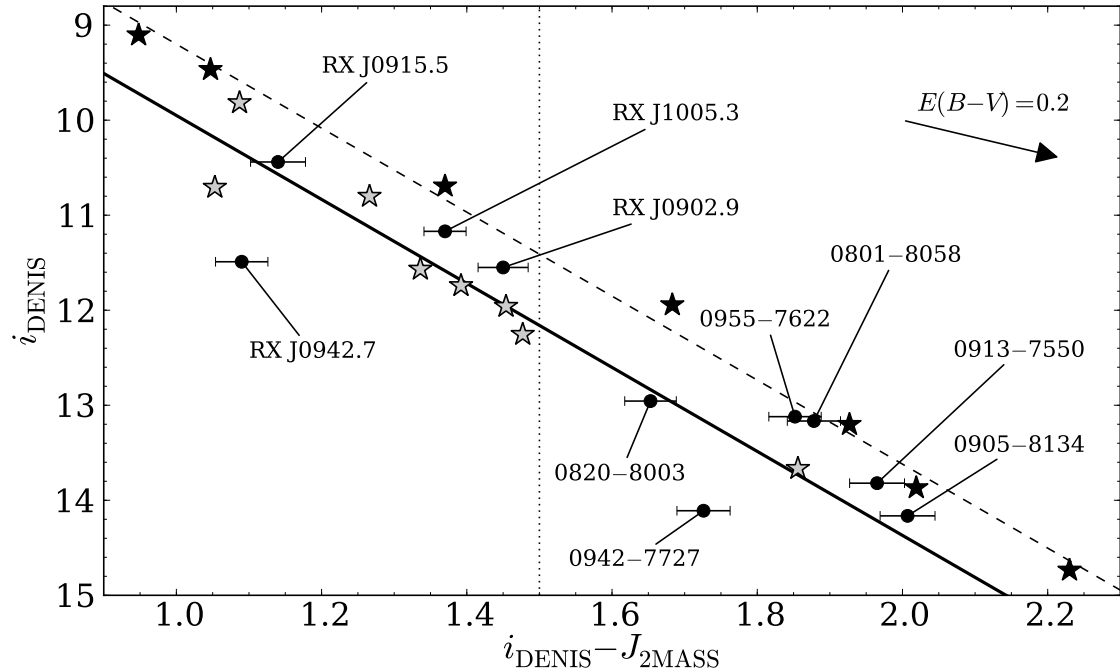


Figure 2.11 (cont.) Dynamical simulations for RX J0915.5-7608 (top) and RX J0942.7-7726 (bottom).



**Figure 2.11** (cont.) Dynamical simulations for RX J1005.3–7749.



**Figure 2.12** The late-type  $\eta$  Cha cluster sequence, for single stars (gray stars, solid fitted line) and known unresolved binaries (filled stars, dashed line). The arrow indicates a reddening vector of  $E(B - V) = 0.2$  mag in this colour-magnitude plane. The vertical line denotes the blue limit of our photometric survey; ROSAT sources lie to the left of this limit, 2MASS/DENIS sources to the right.

**Table 2.5** Summary of the dynamical simulations. See §2.7 for discussion.

	$\Delta UVW_{\min}$ [km s $^{-1}$ ]	$v_{\text{eject}}$ [km s $^{-1}$ ]	$t_{\text{eject}}$ [Myr]	$d_0$ [pc]
<i>DENIS/2MASS intermediate-gravity candidates</i>				
2MASS J0801–8058	1.2	1.1	−12.0	82
2MASS J0820–8003	1.9	2.4	−1.0	94
2MASS J0905–8134	0.1	1.0	−8.0	88
2MASS J0913–7550	1.4	5.2	−3.75	76
2MASS J0942–7727	3.7	7.8	−0.75	95
2MASS J0955–7622	3.4	9.2	−1.5	83
<i>Covino et al. (1997) ROSAT candidates</i>				
RX J0902.9–7759	2.1	0.9	−12.0	84
RX J0915.5–7608	3.3	4.8	−3.75	111
RX J0942.7–7726	2.8	3.6	−7.5	120
RX J1005.3–7749	0.1	4.7	−1.75	98

### 2.7.1. Probable members

**2MASS J0820–8003** This star has the closest angular separation from the cluster core of any candidate (1.44 deg). According to the simulations it has a minimum  $\Delta UVW$  corresponding to ejection only 1 Myr ago. This is unlikely given the current dynamical state of the cluster. However, excellent agreement can still be found at almost all trace-back times, with ejection velocities around 1 km s $^{-1}$  and current distances of 88–94 pc. This places 2MASS J0820–8003 near the single-star sequence, as observed. Multiple *WiFeS* observations show the star possesses strong and highly variable H $\alpha$  emission, indicative of accretion from a circumstellar disk. 2MASS J0820–8003 will be examined in greater detail in Chapter 3.

**2MASS J0905–8134** This candidate shows excellent agreement ( $\Delta UVW = 0.13$  km s $^{-1}$ ) between its kinematic distance of ∼88 pc and a slightly elevated position above the  $\eta$  Cha single-star sequence. The simulations indicate it was ejected from the cluster around 8 Myr ago at a speed of 1 km s $^{-1}$ , although a broad range of ejection times are also acceptable.

**2MASS J0913–7550** This star also shows excellent agreement between its kinematic and photometric distances. It appears to have been ejected 3–4 Myr ago at a speed of 5 km s $^{-1}$  and currently lies in front of the cluster at a distance of 76 pc. Stellar two-body encounters would be so rare and weak at this epoch that the most plausible mechanism for such dynamics is the three-body disruption of an unstable multiple system, perhaps RS Cha or another of the close binaries observed in the cluster (Köhler & Petr-Gotzens 2002).

**RX J0902.9–7759** This M3 star from Covino et al. (1997) lies just inside the 1.5 deg radius surveyed by Luhman (2004b). It has a kinematic distance of ∼85 pc and would have been ejected at 1–2 km s $^{-1}$  early in the cluster’s history. This distance does not fully explain the ∼0.4 mag elevation above the single-star cluster sequence, which could be accounted for by a close binary companion. Binarity is also implied by the difference in radial velocity between our *WiFeS* measurement and that reported by Covino et al. (1997) (see §2.5).

### 2.7.2. Possible members

**2MASS J0801–8058** The radial velocity variations described in §2.4.2 and the elevation of the star above the cluster isochrone are hints that it may be a binary. The dynamical simulations show very good agreement between the current space motion at a distance of 82 pc and ejection early in the cluster’s history at a speed of 1–2 km s<sup>−1</sup>. This would account for nearly half of the elevation above the single-star sequence in Figure 2.12. As we will argue in Chapter 3, the star is probably not a high mass ratio binary and is instead reddened by  $E(B - V) \approx 0.3$  mag. Correcting for this extinction, 2MASS J0801–8058 falls 0.3 mag below the single-star sequence, whereas its dynamical distance of 82 pc implies it should lie that much *above* the line. Because of the uncertainty in the lower-main sequence cluster isochrone, we classify the star as a *possible*  $\eta$  Cha member.

**2MASS J0955–7622** Also a probable binary from its elevated position in Figure 2.12 and unusually low radial velocity. Twelve velocity measurements during 2010 January–December did not show any variation outside the expected instrumental errors. The radial velocity greatly constrains the permitted distances and ejection times in Figure 2.11. If the observed velocity is not systemic this parameter space would obviously change. From the simulations the star would have been ejected from the cluster at nearly 10 km s<sup>−1</sup> only 1.5 Myr ago. Even the implied current distance of 83 pc would not be close enough to match its position in Figure 2.12 without including binarity. High resolution spectroscopy and imaging will be necessary to confirm the binarity and derive a systemic velocity.

**RX J0915.5–7608** The dynamical simulations for this star suggest a current distance of 111 pc, whereas its position in Figure 2.12 indicates it should lie at a similar distance to the cluster. Binarity could explain an elevated position in the CMD and indeed Köhler (2001) detect a close companion at 0.11'' with a K-band brightness ratio of 0.26. This also likely explains the larger than expected (and thus probably not systemic) radial velocity, which is responsible for the large minimum  $\Delta UVW$  of 3.3 km s<sup>−1</sup>. If the velocity is systemic RX J0915.5–7608 would have been ejected from  $\eta$  Cha at nearly 5 km s<sup>−1</sup> only 3.75 Myr ago. Covino et al. (1997) derived a radial velocity of  $21 \pm 2$  km s<sup>−1</sup>, which improves the  $\Delta UVW$  to 2.3 km s<sup>−1</sup> and has the effect of ejecting the star from the cluster ~8 Myr ago at ~2 km s<sup>−1</sup>. Guenther et al. (2007) also observed the star and found a velocity of  $20.3 \pm 0.1$  km s<sup>−1</sup> ( $\Delta UVW \approx 2$  km s<sup>−1</sup>). We conservatively assign RX J0915.5–7608 *possible* membership status until its systemic velocity can be determined.

**RX J1005.3–7749** Figure 2.12 suggests a distance slightly in front of the cluster, however the best fitting kinematic distance is 98 pc (+0.08 mag), corresponding to an ejection of 4–5 km s<sup>−1</sup> only 1.75 Myr ago. The difference between the expected and observed space motions at this distance is less than 0.1 km s<sup>−1</sup>. The star lies in the midst of the 100  $\mu$ m IRAS flux contours in Figure 2.2 so it is possible that it may be reddened slightly, affecting its position in the CMD. Covino et al. (1997) and Guenther et al. (2007) both also observed RX J1005.3–7749. Their velocities ( $17 \pm 2$  km s<sup>−1</sup> and  $16.3 \pm 0.2$  km s<sup>−1</sup>, respectively) have little effect on the dynamical results. In both cases the star was apparently ejected less than 2 Myr ago at speeds of ~5 km s<sup>−1</sup>, presumably due to an interaction with a close binary.

### 2.7.3. Non-members

**2MASS J0942–7727 and RX J0942.7–7726** These stars are unlikely to be  $\eta$  Cha members due to their position far below the cluster sequence and lower lithium equivalent widths. 2MASS J0942–7727 does not fit any plausible cluster ejection scenario. RX J0942.7–7726 does better ( $\Delta UVW = 2.8 \text{ km s}^{-1}$ ), but even at the 120 pc given by the simulations it still lies well below the single cluster members. As mentioned previously, the pair may form a wide binary and be distant members of another young association in the solar neighbourhood. These stars will be discussed in greater detail in Chapter 4.

## 2.8. Discussion

From photometry, proper motions and extensive optical spectroscopy we have discovered six new low-mass pre–main sequence stars surrounding the  $\eta$  Cha open cluster. Four more candidate cluster members were identified in an X-ray selected sample of pre–main sequence stars from *ROSAT*. After consideration of each candidate’s kinematics we identified four *probable*  $\eta$  Cha members in a halo surrounding the cluster and another four *possible* members requiring further investigation. The remaining two candidates are older pre–main sequence stars that may form a wide binary. These results differ slightly from those presented in Murphy et al. (2010); with updated kinematics RX J0915.5–7608 has now been classified as a *possible* member and 2MASS J0942–7727 explicitly joins RX J0942.7–7726 as a non-member.

Two *probable* members, 2MASS J0820–8003 and RX J0902.9–7759, lie just within the 1.5 deg radius surveyed by Luhman (2004b) (1.48 deg and 1.41 deg away from his adopted field centre, respectively). One may naturally ask why we selected the stars as candidates and Luhman did not? We have used the most-recent Third DENIS Data Release while his study used the Second Release, for which *i*-band photometry was not available over the full 1.5 deg field. Both stars do not appear in this DENIS release but they do have full 2MASS photometry, which Luhman also used to select candidates in the absence of DENIS *i*-band data. In his 2MASS *H* versus (*H* –  $K_s$ ) colour-magnitude diagram both stars lie above the 10 Myr isochrone used to select spectroscopic candidates. While RX J0902.9–7759 occupies a crowded region of colour-magnitude space, 2MASS J0820–8003 is far redder and adjacent to several  $\eta$  Cha members in a sparser region of the diagram. Had Luhman obtained a spectrum of the star its youth would have been immediately obvious. This underscores the importance of a thorough spectroscopic campaign and the efficacy of proper motions and spectroscopy in significantly reducing contaminants, especially over such large fields.

One may also ask if the discovery of these new halo members is consistent with a dynamical origin for the apparent paucity of low-mass objects in  $\eta$  Cha today? To answer this we consider the radial distribution of simulated ejectees presented in Moraux et al. (2007) and in the bottom-left panel of Figure 2.13. Integrating the distribution out to 9 pc (5.5 deg at the cluster distance) we could expect to find up to seven stars across all masses in the survey area. Our blue photometry limit of  $(i - J) > 1.5$  corresponds to an approximate spectral type of M3 and our spectroscopic campaign is complete to  $(i - J) < 2$ , approximately M5. Transforming these colours to masses through an 8 Myr Baraffe et al. (1998) isochrone gives an *approximate* surveyed mass range of  $0.08 < M/M_\odot < 0.3$ . We consider only the

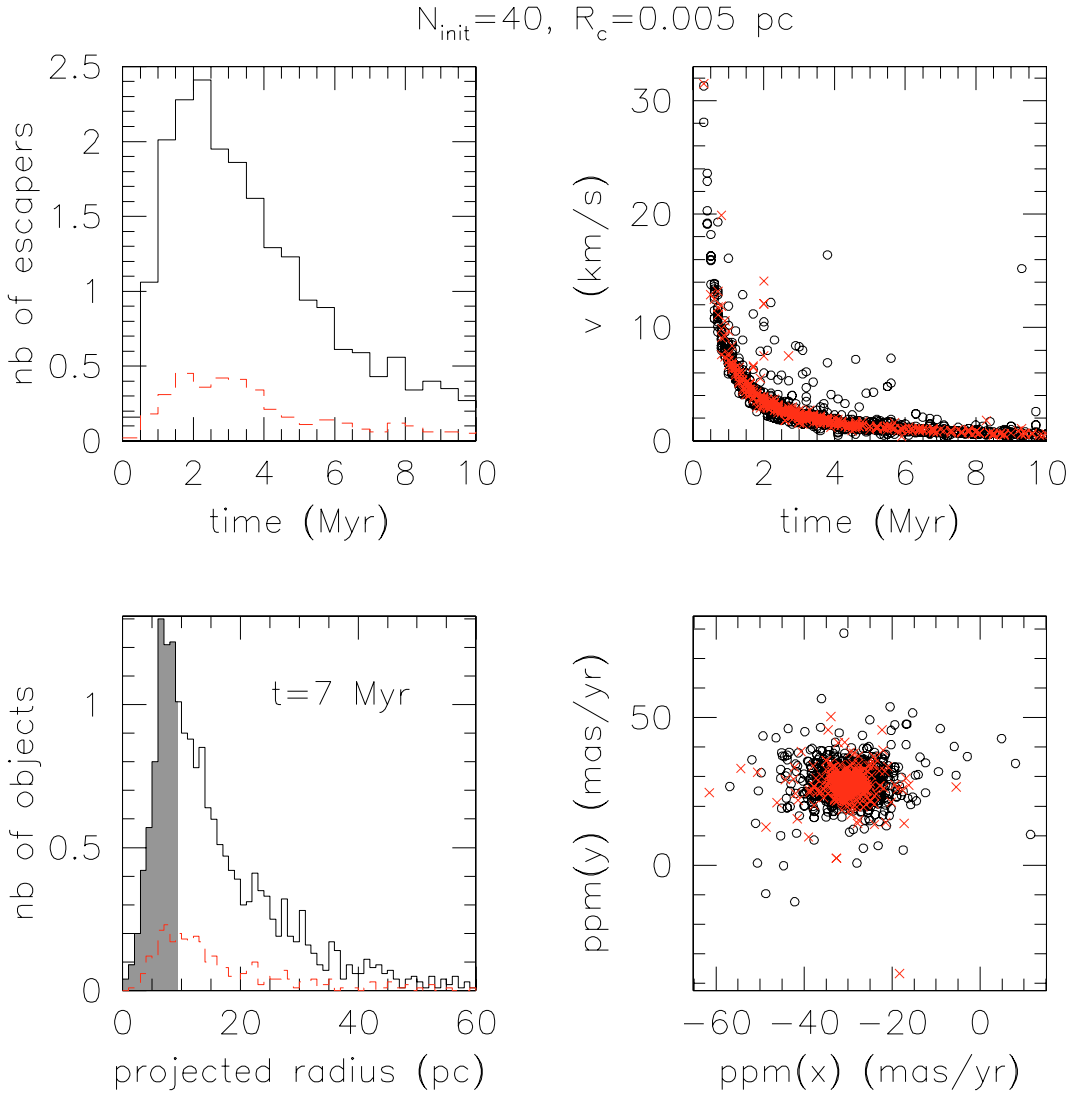


**Figure 2.13** Results of 100 N-body simulations of  $\eta$  Cha by Moraux et al. (2007, used with permission). *Top left:* number of stars ejected with time, at masses  $M > 0.1 M_{\odot}$  (solid line) and  $M < 0.1 M_{\odot}$  (dashed line). The number of objects is averaged over the 100 realisations. *Top right:* ejection velocity of the escapees. Red crosses denote stars with  $M < 0.1 M_{\odot}$ . *Bottom left:* average radial distribution of the escapees at  $t = 7$  Myr. The time scale has its origin at the epoch of gas removal from the proto-cluster, which probably occurred when it was 1–2 Myr old. The dashed line again shows the lower mass sample. The 9 pc (5.5 deg) limit of our survey is shaded. *Bottom right:* proper motion diagram of escapees at  $t = 7$  Myr.

DENIS/2MASS candidates observed spectroscopically because we can be reasonably sure such a sample is complete. On the other hand, the X-ray-selected *ROSAT* sources cannot be guaranteed to be complete as they are, by definition, biased against X-ray-faint stars.

Both Moraux et al. and Weidner et al. (2011) found that the mass function of cluster ejectees was roughly constant with radius and consistent with the input IMF of their simulations. In the case of Moraux et al. the IMF was that of Chabrier (2003). We therefore integrate this IMF over the above mass range to find the fraction of stars at those masses; this is  $\sim 35$  percent. Hence we could expect to find 2–3 ejected  $\eta$  Cha members within the surveyed area and mass range. Our discovery of three probable DENIS/2MASS members is entirely consistent with this prediction. Even including the *possible* members 2MASS J0955–7622

and 2MASS J0801–8058 as true cluster members the results are still consistent, considering the small number of stars in the sample and the sensitivity of the number fraction to the low-end of the adopted mass range. Whether it is possible a suspected close binary like 2MASS J0955–7622 (or RX J0902.9–7759) could have been ejected from the cluster remains an open question. Finally, we note that from the epoch and magnitude of its ejection velocity, the *probable* candidate 2MASS J0913–7550 appears to have been ejected from  $\eta$  Cha by the disruption of an unstable multiple system. The simulations of Moraux et al. (2007) did not include binaries (see below) so the only possible interactions are two-body.

Despite small number statistics invariably influencing these arguments, the overall agreement between the models and our findings is reassuring. We can therefore conclude that dynamical evolution is likely responsible for the current configuration of  $\eta$  Cha and it is not necessary to invoke an IMF deficient in low-mass objects. These new halo members will provide additional strong constraints on future simulations, which must be able to satisfactorily replicate the spatial and mass distributions of *all* cluster members.

### 2.8.1. Postscript: adding binaries to the Moraux et al. (2007) simulations

Becker & Moraux (in preparation) have attempted to improve the simulations of Moraux et al. (2007) by modelling the effects of binaries on the dynamical evolution of  $\eta$  Cha. While Moraux et al. (2007) used single stars with realistic *system* masses, these new simulations assumed the initial cluster to have a 100 percent binary fraction with thermalised eccentricities and random pairings drawn from a log-normal *individual* IMF over the mass range  $0.01 < M/M_{\odot} < 4$ . The new simulations must be able to reproduce the current  $\sim$ 40 percent binary fraction in the central 0.6 pc of the cluster (with no wide binaries,  $a > 20$  AU), in addition to replicating the new halo members at  $>1.5$  deg described in this Chapter. Despite changing a range of initial parameters, including the number of systems, the Plummer radius of the cluster, the virial ratio and the binary mass ratio, they found that no set of parameters can satisfy the observational constraints. The simulations are still being refined, but in all the current models the binary ratio falls dramatically and the number of stars increases as binaries are disrupted by dynamical interactions early in the evolution of the cluster. The continual breaking of binaries ensures the number of low-mass stars does not decrease fast enough to match the observations. The halo criterion does provide a strong constraint on the simulations, which are dominated by the plethora of single low-mass stars in the central 1.5 deg (2.5 pc) around the cluster.

These preliminary results would seem to imply a log-normal IMF with a realistic initial binary population *cannot* reproduce the current state of  $\eta$  Cha, assuming solely dynamical evolution. While we await the final outcome of the simulations, we are left with the Seeger-esque problem posed in §2.1 – *where have all the low-mass stars gone?* The answer to this question may lie in the relationship between  $\eta$  Cha and the nearby  $\epsilon$  Cha Association. We defer discussing the membership and origin of  $\epsilon$  Cha until Chapter 5, but note that there are almost certainly many as-yet undiscovered members of both groups throughout the region. These stars should be visible in contemporary wide-field surveys like 2MASS/DENIS and PPMXL. To this end we are beginning a project to identify new members using more sophisticated selection techniques. This future work is described in Chapter 6.



# CHAPTER 3

---

## Episodic disk accretion in the halo of $\eta$ Chamaeleontis

*Parts of this chapter have been previously published as ‘Episodic disk accretion in the halo of the ‘old’ pre-main-sequence cluster  $\eta$  Chamaeleontis’, Murphy, S. J., Lawson, W. A., Bessell, M. S., Bayliss, D. D. R., 2011, MNRAS, 411, L51. The work is presented here in expanded and updated form<sup>1</sup>.*

### 3.1. Introduction

Young clusters and associations show a steady decline in the number of stars having disks and signatures of accretion with age (Haisch et al. 2001; Hernández et al. 2008). However, these disk dissipation and accretion timescales are not commensurate with each other. On average, by an age of  $\sim 5$  Myr, 90–95 percent of all young cluster members will have stopped accreting material at a significant rate (Fedele et al. 2010; Jayawardhana et al. 2006), yet  $\sim 20$  percent of objects still retain enough dust in their inner disks to produce a mid-infrared excess. The mechanism responsible for these different timescales remains uncertain, but may be related to planet formation and migration in the inner disk (Fedele et al. 2010).

$\eta$  Cha has already been shown to have both an excess of stars with accretion and circumstellar disks compared to clusters of similar age (Megeath et al. 2005; Sicilia-Aguilar et al. 2009). The cluster also *appears* to have an initial mass function deficient in low-mass objects (Lyo et al. 2004b), although this has been disputed by Luhman et al. (2009a). Fedele et al. (2010) is the latest study to point out that dynamical evolution has probably dispersed a large fraction of these ‘missing’ low-mass members to radii beyond that currently surveyed (see also Moraux et al. 2007). The results of the previous Chapter confirm that a significant number of stars have in fact been ejected from the cluster since its birth. One might expect the dispersed members to have experienced strong dynamical interactions which disrupted their disks (Armitage & Clarke 1997), so it is therefore possible the current core membership may be biased towards infrared-excess and strong H $\alpha$  emitting sources. However, as pointed out by

---

<sup>1</sup>This chapter includes data gathered with the 6.5 meter Magellan Telescopes located at Las Campanas Observatory, Chile. Australian access to the Magellan Telescopes was supported through the National Collaborative Research Infrastructure Strategy of the Australian Federal Government.

Lyo et al. (2003) and Lawson et al. (2004), the physical processes which affect circumstellar disk evolution are manifold. Dynamical interactions, binarity and proximity to OB stars among other factors, should all influence the disk destruction rate. By investigating the disk and accretion properties of any new dispersed members of  $\eta$  Cha, we can hope to gain a more unbiased view of the cluster as a whole, as well as addressing the influence cluster dynamics have had on disk evolution.

In the previous Chapter we presented the results of our search for the putative halo of low-mass objects surrounding  $\eta$  Cha. From archival photometry, proper motions and multi-epoch, medium-resolution spectroscopy we identified four *probable* and four *possible* new members, including two stars with large variations in their H $\alpha$  emission line strengths. These stars, 2MASS J0801–8058 (*possible* member) and 2MASS J0820–8003 (*probable* member) are the subject of further investigation in this Chapter.

## 3.2. Multi-epoch spectroscopy

### 3.2.1. Observations

As part of our continued investigation into  $\eta$  Cha, we obtained multi-epoch, medium-resolution ( $R \approx 7000$ ) spectroscopy of 2MASS J0801–8058 and 2MASS J0820–8003 with *WiFeS* on the ANU 2.3-m telescope (see Chapter 2 for more details). To investigate variability of their H $\alpha$  emission profiles we obtained 35 observations of 2MASS J0801–8058 and 19 of 2MASS J0820–8003 from 2010 January to 2011 May. The cadence of observations ranged from hours to months, with nine epochs of 2MASS J0801–8058 taken in one night to constrain any short timescale variability (see §3.4.3). This is an increase of 26 and 6 epochs, respectively, from the observations reported in Murphy et al. (2011). In addition to H $\alpha$ , both stars recurrently showed He I  $\lambda 5876/\lambda 6678$  and Na I D emission, which are often associated with accretion. Details of these observations are given in Tables 3.1 and 3.2.

### 3.2.2. Accretion diagnostics

Traditionally, the equivalent width (EW) of the H $\alpha$  emission line has been used to differentiate between ‘Classical’ T Tauri Stars (CTTSs), whose emission is powered by the in-fall and accretion of circumstellar disk material, and ‘Weak-lined’ (or ‘naked’) T Tauri Stars (WTTSs), which display primarily chromospheric emission. Various EW thresholds have been adopted in the literature, typically with values around 5–10 Å (Appenzeller & Mundt 1989; Bertout 1989). A more physical separation was proposed by Barrado y Navascués & Martín (2003), who considered the saturation limit of chromospheric H $\alpha$  luminosity ( $\log L_{\text{H}\alpha}/L_{\text{bol}} \approx -3.3$ ), transformed to an EW as a function of spectral type. Applying this criterion to the values in Tables 3.1 and 3.2; 2MASS J0820–8003 would be a border-line CTTS in quiescence and 2MASS J0801–8058 would be a CTTS during its three outbursts on 2010 February 19, April 30 and November 23.

Because chromosphere flare activity can also increase line strengths on short timescales, the velocity width of the H $\alpha$  line is usually used in conjunction with the EW to identify accretion (flares mainly increase the height of the line, not its velocity width). White & Basri (2003)

**Table 3.1** *WiFeS* observations of 2MASS J0801–8058

UTC of observation (mid-exposure)	H $\alpha$ EW [Å] <sup>†</sup>	$v_{10}$ width [km s $^{-1}$ ] <sup>‡</sup>	RV [km s $^{-1}$ ] <sup>#</sup>	Other emission lines
2010 Jan 25	13:57	-6	152	13.7
2010 Jan 27	12:35	-6	148	23.7
2010 Jan 28	12:11	-6	153	17.8
2010 Feb 19	11:45	-20	346	21.3
2010 Apr 28	09:04	-6	176	15.7
2010 Apr 29	09:05	-6	160	20.9
2010 Apr 30	10:15	-27	324	23.0
2010 May 01	13:14	-7	178	18.5
2010 Jun 03	09:05	-7	159	20.0
2010 Nov 21	17:24	-6	153	18.0
2010 Nov 23	14:14	-20	206	9.3
2010 Nov 23	17:37	-14	193	17.9
2010 Nov 24	14:47	-8	163	18.2
2010 Dec 16	12:21	-6	145	20.7
2010 Dec 20	11:16	-7	147	22.3
2011 Jan 07	13:07	-7	145	11.9
2011 Jan 08	11:47	-7	145	18.9
2011 Jan 09	11:53	-8	163	18.5
2011 Jan 13	11:13	-7	144	21.2
2011 Feb 10	15:38	-7	148	15.2
2011 Feb 11	16:09	-6	150	18.3
2011 Feb 12	18:16	-6	157	17.0
2011 Feb 24	15:48	-6	148	17.2
2011 Mar 17	13:20	-7	143	15.2
2011 Apr 23	19:48	-7	143	18.0
2011 Apr 27	18:53	-6	145	17.2
2011 May 08	11:22	-7	146	20.3
2011 May 08	12:34	-7	142	16.3
2011 May 08*	16:36	-7	141	19.9
2011 May 08*	17:09	-7	140	20.8
2011 May 08*	17:41	-7	143	18.3
2011 May 08*	18:13	-8	141	19.0
2011 May 08*	18:45	-7	144	18.5
2011 May 08*	19:17	-7	142	17.8
2011 May 09	10:11	-7	163	19.4

<sup>†</sup> Uncertainty  $\pm 1\text{--}2$  Å<sup>‡</sup> Uncertainty  $\pm 10$  km s $^{-1}$ <sup>#</sup> Uncertainty  $\pm 1\text{--}2$  km s $^{-1}$ 

\* Observed consecutively with the same arc frame

**Table 3.2** *WiFeS* observations of 2MASS J0820–8003

UTC of observation (mid-exposure)	$H\alpha$ EW [Å] <sup>†</sup>	$v_{10}$ width [km s <sup>-1</sup> ] <sup>‡</sup>	RV [km s <sup>-1</sup> ] <sup>#</sup>	Other emission lines
<b>ANU-2.3m/WiFeS</b>				
2010 Jan 25	14:45	−23	331	He I
2010 Feb 19	10:28	−40	425	He I, O I, Veiling
2010 Feb 20	10:27	−24	260	He I
2010 Apr 27	12:05	−27	238	He I, Na D
2010 Apr 28	10:14	−17	263	18.9
2010 Apr 28	15:23	−15	262	18.7
2010 Apr 29	10:16	−17	282	20.6
2010 Apr 29	15:05	−16	275	21.4
2010 Apr 30	09:05	−17	237	20.0
2010 Apr 30	11:30	−15	224	17.9
2010 Apr 30	12:50	−16	210	18.4
2010 May 01	12:02	−17	262	17.6
2010 Jun 03	10:15	−17	215	18.9
2010 Nov 21	16:12	−10	197	18.7
2010 Nov 23	15:27	−11	201	19.4
2010 Dec 20	13:36	−12	217	18.4
2011 Jan 07	11:57	−28	237	15.5 He I, Na D, Veiling
2011 Jan 09	13:02	−13	218	15.6
2011 May 09	08:59	−11	203	20.5
<b>Magellan/MIKE</b>				
2010 May 11	23:41	−22	238	17.4 He I

<sup>†</sup> Uncertainty  $\pm 1\text{--}2$  Å<sup>‡</sup> Uncertainty  $\pm 10$  km s<sup>−1</sup><sup>#</sup> Uncertainty  $\pm 1\text{--}2$  km s<sup>−1</sup>

proposed that a velocity full-width at 10 percent flux ( $v_{10}$ ) of 270 km s<sup>−1</sup> could be used to separate veiled, accreting CTTSs from WTTSs. Jayawardhana et al. (2003) likewise found that  $v_{10} \simeq 200$  km s<sup>−1</sup> may be a more physical limit, especially for very low-mass brown dwarfs. Recently, Nguyen et al. (2009) have shown that because of the strong dependence of  $v_{10}$  on the shape of the underlying  $H\alpha$  line profile, the Ca II 8662 Å line flux is perhaps a more reliable quantitative diagnostic of accretion rate. However, the  $H\alpha$   $v_{10}$  width has a well-established record as an accretion indicator and despite the caveats put forward by Nguyen et al. (2009), we use it here for comparison to previous studies and the fact that our wavelength coverage does not extend past 7100 Å. Measurements of the EW and  $v_{10}$  for each star are listed in Tables 3.1 and 3.2.  $H\alpha$  EWs were calculated by direct integration of the line profile, assuming a linear continuum under the line. Similarly, the  $v_{10}$  width was found by first converting the spectrum to a velocity profile and normalising by a linear function fitted to the region outside the line. The exact width was then calculated by interpolating the profile around the 10 percent intensity level. We estimate an uncertainty of  $\pm 1\text{--}2$  Å for the EWs and  $\pm 10$  km s<sup>−1</sup> in  $v_{10}$ , primarily due to uncertainties in defining the pseudo-continuum around the broad  $H\alpha$  lines at this modest spectral resolution.

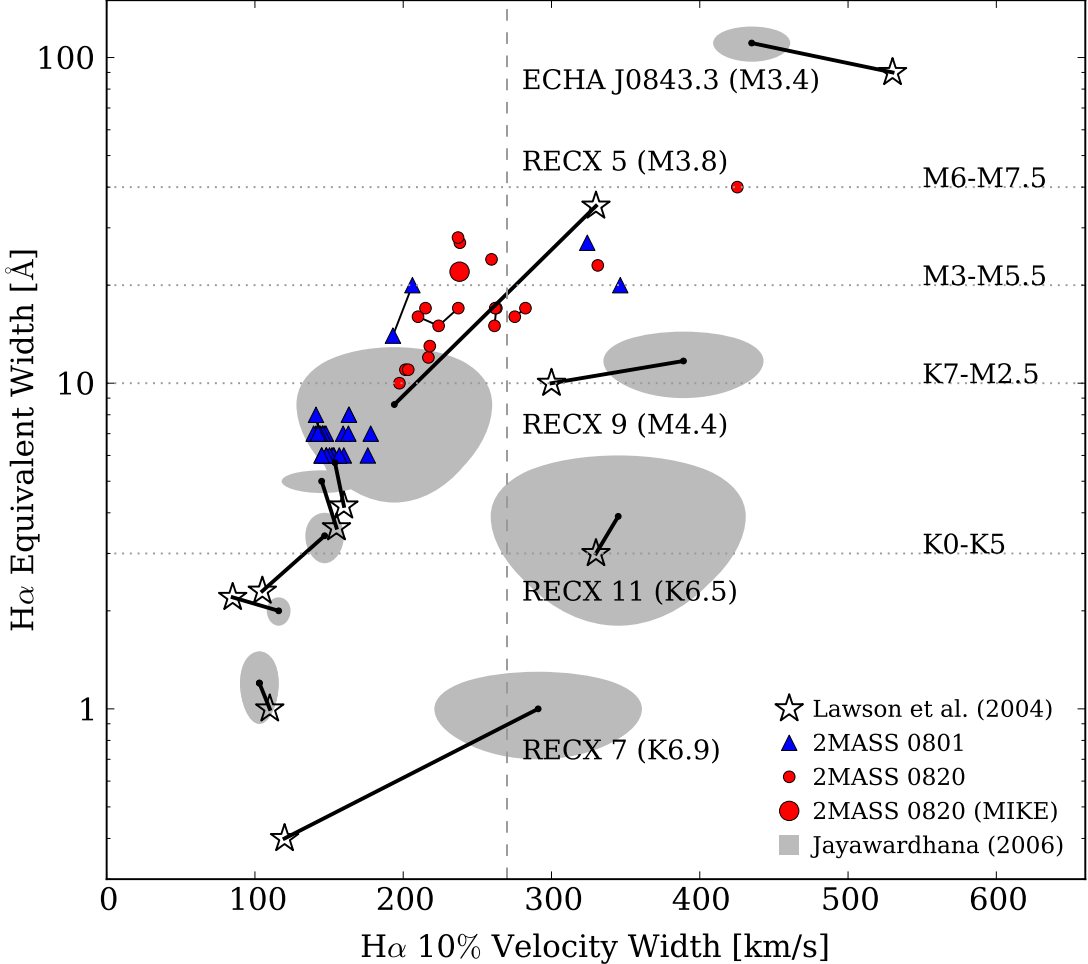


**Figure 3.1** H<sub>α</sub> EW versus the velocity width at 10 percent of peak intensity ( $v_{10}$ ) for 2MASS J0820–8003 and 2MASS J0801–8058. Horizontal lines denote the minimum EW for CTTs in the indicated range of spectral types. The vertical line at 270 km s<sup>-1</sup> separates accreting and non-accreting objects (White & Basri 2003). Shaded regions show the standard deviation of the multi-epoch measurements of Jayawardhana et al. (2006). Comparisons to the single epoch data of Lawson et al. (2004) are also shown. Lines connect the two sets of measurements. For our candidates, lines connect observations taken on the same night.

Following White & Basri (2003), Figure 3.1 shows an EW- $v_{10}$  diagram for our observations of 2MASS J0801–8058 and 2MASS J0820–8003, with  $\eta$  Cha members observed by Jayawardhana et al. (2006) and Lawson et al. (2004) for comparison. Lawson et al. (2004) observed the cluster at high-resolution and found EW variations of 40–300 percent for RECX 5, 9 and 11 when compared to the discovery measurements of Mamajek et al. (1999). Jayawardhana et al. (2006) obtained 3–8 epochs of Magellan/MIKE Echelle data for 11  $\eta$  Cha members during 2004 December–2005 March. They reported variations in EW and  $v_{10}$  in some stars similar to those seen in 2MASS J0801–8058 and 2MASS J0820–8003 with 35 percent  $v_{10}$  and 50 percent EW variations in the maximal cases. The studies are compared in Figure 3.1. Overall there is good agreement between the two sets of measurements. RECX 9, RECX 11 and ECHA J0843.3–7905 are clearly accretors in both studies, using either the criterion of White & Basri (2003) or Jayawardhana et al. (2003). RECX 7 is a known non-accreting double-lined spectroscopic binary (Lyo et al. 2003), which explains the broad line width but low EW in the Jayawardhana et al. observations. Lawson et al. (2004) classified RECX 5 as accreting with  $v_{10} > 300$  km s<sup>-1</sup> from their 2002 observation. Jayawardhana et al., however,

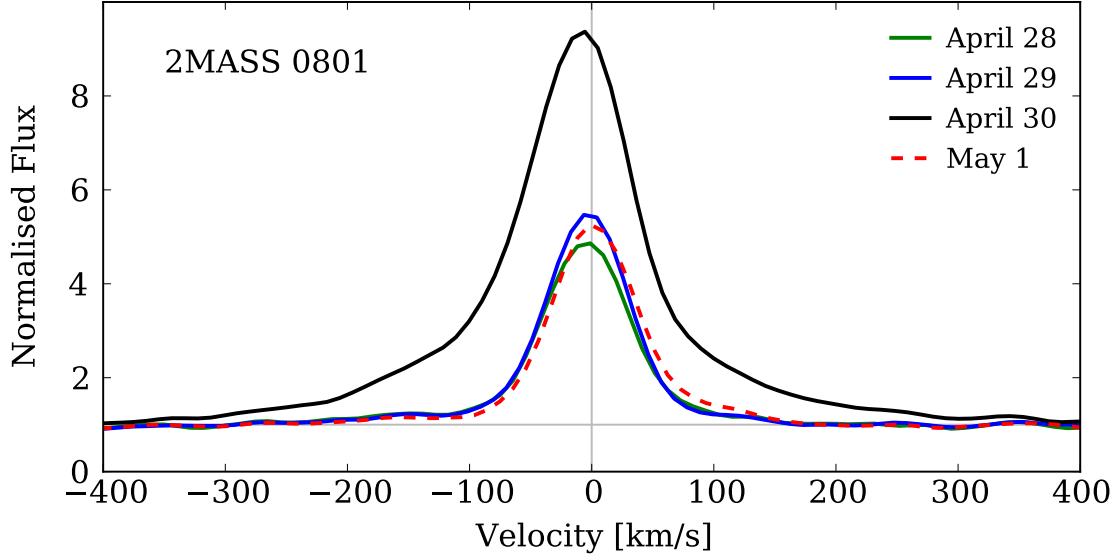


**Figure 3.2** Evolution of the 2MASS J0801–8058 H $\alpha$  velocity profile during the 2010 April outburst. All profiles have been shifted to zero radial velocity. The April 30 profile has been veiling-corrected as described in the text.

failed to detect any accretion, with only one of their five observations showing a broadened H $\alpha$  line. The blue-shifted bump in their 2004 December spectrum could indicate RECX 5 is sporadically accreting at low levels and Lawson et al. serendipitously observed a moderately strong outburst of  $10^{-10} M_{\odot}$  yr $^{-1}$  accretion in 2002. Alternatively, the star may have been in a period of enhanced chromospheric activity at that epoch. Activity and its role as a possible mechanism for the variations seen in our spectra is discussed in detail in §3.2.3.

Both 2MASS J0801–8058 and 2MASS J0820–8003 show substantial variation in the EW- $v_{10}$  space, with the scatter more pronounced for the latter star. While both stars generally lie on the non-accreting side of the 270 km s $^{-1}$  criterion defined by White & Basri (2003), they each make several excursions into the accreting region of the diagram, meeting both the EW and  $v_{10}$  criteria for accreting CTTSs. This is similar to the behaviour of RECX 5 during 2002–2005. Based on the cadence of our observations, the timescale of these excursions appears to be of the order of hours to days. If instead we adopt the  $v_{10}$  criterion of Jayawardhana et al. (2003), then 2MASS J0820–8003 would be a border-line accretor in quiescence (as it is using the EW criterion of Barrado y Navascués & Martín 2003).

In the case of 2MASS J0801–8058, both EW and  $v_{10}$  increase dramatically on 2010 April 30, before returning to quiescent levels the next night. Similar levels of activity are seen on 2010 February 19 and November 23. Figure 3.2 shows the evolution of the H $\alpha$  profile during the 2010 April event. We obtained spectra the day before, during and the day after the event. The pre- and post-event line profiles are remarkably similar, with broad wings developing during the April 30 outburst, giving rise to a velocity width of  $v_{10} > 320$  km s $^{-1}$ . The EW similarly quadruples to  $-27 \text{ \AA}$ . The central velocity of the line also evolves with time (see Figure 3.5). A similar, but somewhat weaker change in profile was observed before and after the 2010 November 23 event. A spectrum taken  $\sim 3$  hours after the strong emission ( $v_{10} \approx 200$  km s $^{-1}$ , EW =  $-20 \text{ \AA}$ ) shows the EW decreasing to  $-14 \text{ \AA}$  on its way back to the quiescent range of  $-8 < \text{EW} < -6 \text{ \AA}$ , while the velocity width remains constant at  $\sim 200$  km s $^{-1}$ . When observed the next night the star had fully returned to quiescence

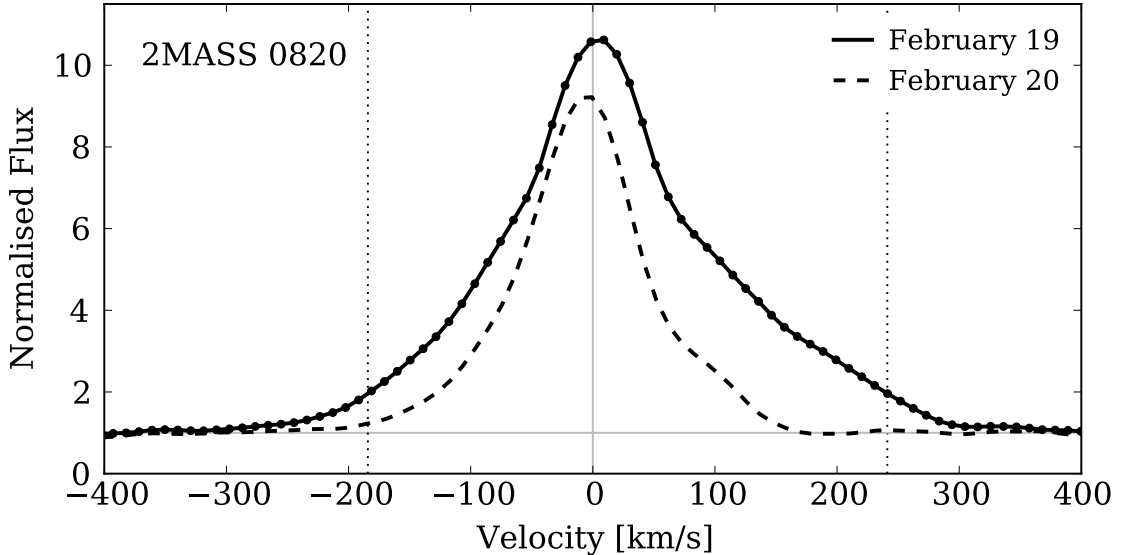


**Figure 3.3**  $\text{H}\alpha$  profiles for 2MASS J0820–8003 during (solid line) and after (dashed line) the strong 2010 February event. Points show the  $10.5 \text{ km s}^{-1}$  pixels of the *WiFeS* R7000 spectra. The  $425 \text{ km s}^{-1}$  velocity width at 10 percent flux ( $v_{10}$ ) is denoted by the dotted lines.

( $v_{10} \approx 150 \text{ km s}^{-1}$ ). The unusually low radial velocity during the event ( $\text{RV} = 9.3 \text{ km s}^{-1}$ ) is probably explained by chromospheric activity skewing the absorption line profiles used for cross-correlation. The low velocity persisted after calibrating the spectrum against multiple arc frames and image slices so it is almost certainly intrinsic to the star and not a consequence of improper data reduction.

As well as exhibiting significantly more scatter in Figure 3.1, 2MASS J0820–8003 appears to have several tiers of activity: a base level at  $\text{EW} \gtrsim -16 \text{ \AA}$ , a somewhat higher level at  $-20 > \text{EW} > -27 \text{ \AA}$ , before increasing to  $-40 \text{ \AA}$  and  $v_{10} = 425 \text{ km s}^{-1}$  on 2010 February 19. The velocity profile of this event is shown in Figure 3.3. The large EW and broad, asymmetric profile compared to 2MASS J0801–8058 immediately suggests that this event could be the result of accretion from a circumstellar disk. With the exception of 2011 January 7, the EW and  $v_{10}$  values for 2MASS J0820–8003 from late-2010 are systematically lower than those taken earlier in the year. Furthermore, we obtained several sets of spectra of both stars taken during the same night. They reveal a scatter of up to  $25 \text{ km s}^{-1}$  in  $v_{10}$  and several Angstroms in EW, i.e. larger than the instrumental errors. Both these long and short-term variations are probably the result of quiescent chromospheric activity (see §3.2.3).

In addition to *WiFeS* spectroscopy, we obtained a high-resolution ( $R \approx 25,000$  with a  $1''$  slit) spectrum of 2MASS J0820–8003 with the *MIKE* spectrograph on the 6.5-m Magellan Clay telescope at Las Campanas Observatory. The star was observed on 2010 May 11 during an unrelated program and reduced using the *MIKE* Python pipeline<sup>2</sup> (D. Bayliss, private communication). The  $\text{H}\alpha$  profile is shown in Figure 3.4 with a contemporaneous *WiFeS* spectrum. The EW and  $v_{10}$  of the higher resolution spectrum are in good agreement with the *WiFeS* values (see Figure 3.1, Table 3.2). The *MIKE* velocity profile shows some self-absorption in the line centre as well as a slight excess of blue-shifted emission at  $v \approx -100 \text{ km s}^{-1}$ . To test how our lower-resolution spectra affect measurements of the EW

<sup>2</sup>Available at <http://obs.carnegiescience.edu/Code/mike>

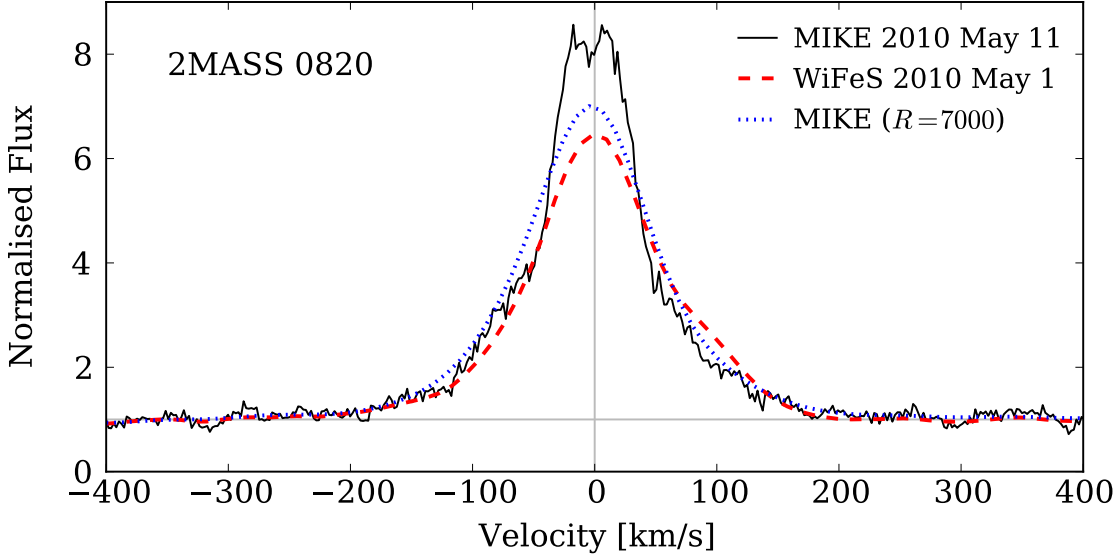


**Figure 3.4** MIKE velocity profile of 2MASS J0820–8003 compared to a contemporaneous *WiFeS* observation. The dotted line shows the  $R \approx 25,000$  MIKE spectrum smoothed to the  $R \approx 7000$  resolution of *WiFeS*.

and  $v_{10}$  we smoothed the *MIKE* spectrum to  $R \approx 7000$  and re-measured both quantities. In each case the smoothed value was slightly smaller (in the absolute sense for EW) than the original. We are thus likely underestimating the EW and  $v_{10}$  from the *WiFeS* observations.

### 3.2.3. H $\alpha$ velocity profile variations

As well as the bulk quantities of EW and  $v_{10}$ , we also investigated the variation in the shape of the H $\alpha$  velocity profile over our observations. The top panels in Figures 3.5 and 3.6 show the average quiescent spectrum for each star, constructed using 14–24 non-outburst spectra. The standard deviation of these spectra around the mean is also shown. As expected from Figure 3.1, 2MASS J0801–8058 presents a very stable mean profile in quiescence, with only three events that could be considered outbursts (2010 February 19, April 30, November 23). Conversely, 2MASS J0820–8003 exhibits considerably more scatter around the mean velocity profile. This is due to variable-strength emission components present in many of the observations. The bottom panels in each Figure show the residual spectra—the difference between the individual spectra and the mean spectrum. Immediately apparent are broad residual profiles at many epochs, tracing velocities up to  $\pm 200$  km s $^{-1}$ . Velocity shifts in the peaks of the residual spectra of up to 50 km s $^{-1}$  are also seen.

The 2010 February 19 observation of 2MASS J0820–8003 shows a residual velocity profile reaching to  $\pm 300$  km s $^{-1}$ , with four distinct components visible and a large red asymmetry. The profile is quite distinct from the others, which are typically much narrower and have less-complex shapes. Similar H $\alpha$  profiles were observed by Jayawardhana et al. (2006) in several members of the TW Hydrae Association (see also Mohanty et al. 2005). Their time-series velocity profiles of TWA5A, TWA10 and TWA3A in particular are remarkably similar to the profile of 2MASS J0820–8003 in Figure 3.3. TWA3A is a known accretor (Muzerolle et al. 2000), whereas although TWA5A and TWA10 meet the EW and  $v_{10}$  accretion criteria, the lack of a detectable disk in *Spitzer Space Telescope* infrared photometry (Low et al. 2005) betrays their H $\alpha$  emission as merely chromospheric in origin.

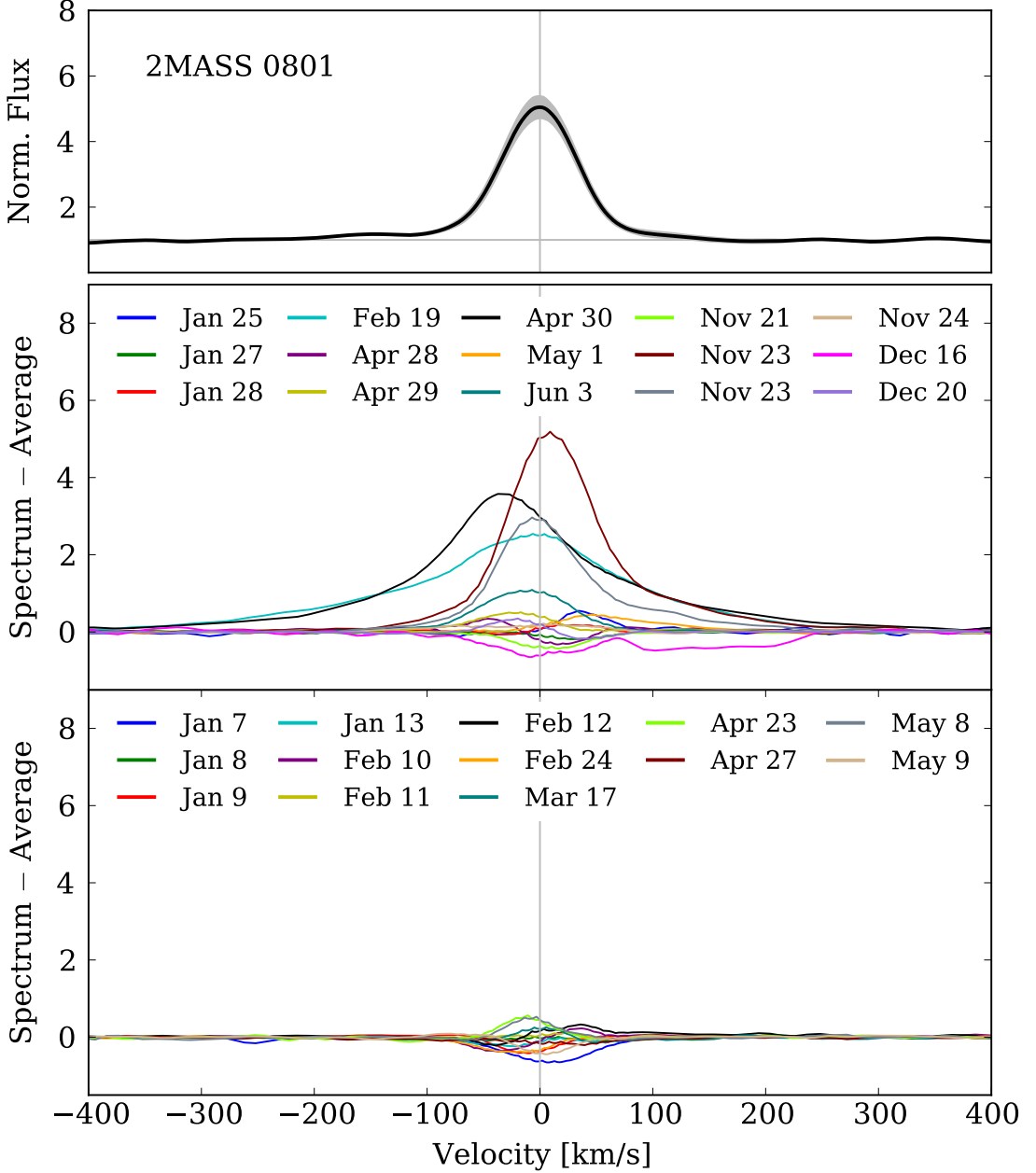


**Figure 3.5** WiFeS H $\alpha$  velocity profiles for 28 observations of 2MASS J0801–8058. For clarity, only a single profile from 2011 May 8 is drawn. The top panel shows the average quiescent spectrum and the standard deviation of quiescent spectra around the mean (shaded). The bottom panels illustrate the variation around the mean spectrum for all epochs. All spectra have been shifted to zero radial velocity.

Instead of invoking accretion, can chromospheric activity also explain the strong and varying H $\alpha$  profiles in 2MASS J0801–8058 and 2MASS J0820–8003? The work of Montes et al. (1998) and Poncet et al. (1998) has shown that in some WTTs the H $\alpha$  line profile cannot be fitted by a single component. Two Gaussians are necessary: a narrow component of full-width half-maximum (FWHM)  $< 100 \text{ km s}^{-1}$  and a much broader component with a FWHM of 150–500 km s $^{-1}$ , sometimes offset in wavelength from the narrow component. Stauffer et al. (1997) observed a similar effect in several of their 30–50 Myr-old IC 2391/2602 and  $\sim 100$  Myr Pleiades targets (which are too old to harbour disks). Montes et al. (1998) attributed these line profiles to *micro-flaring* occurring in the stellar chromosphere. Micro-flares are frequent, short duration magnetic events that are the low-energy analogs of flares.

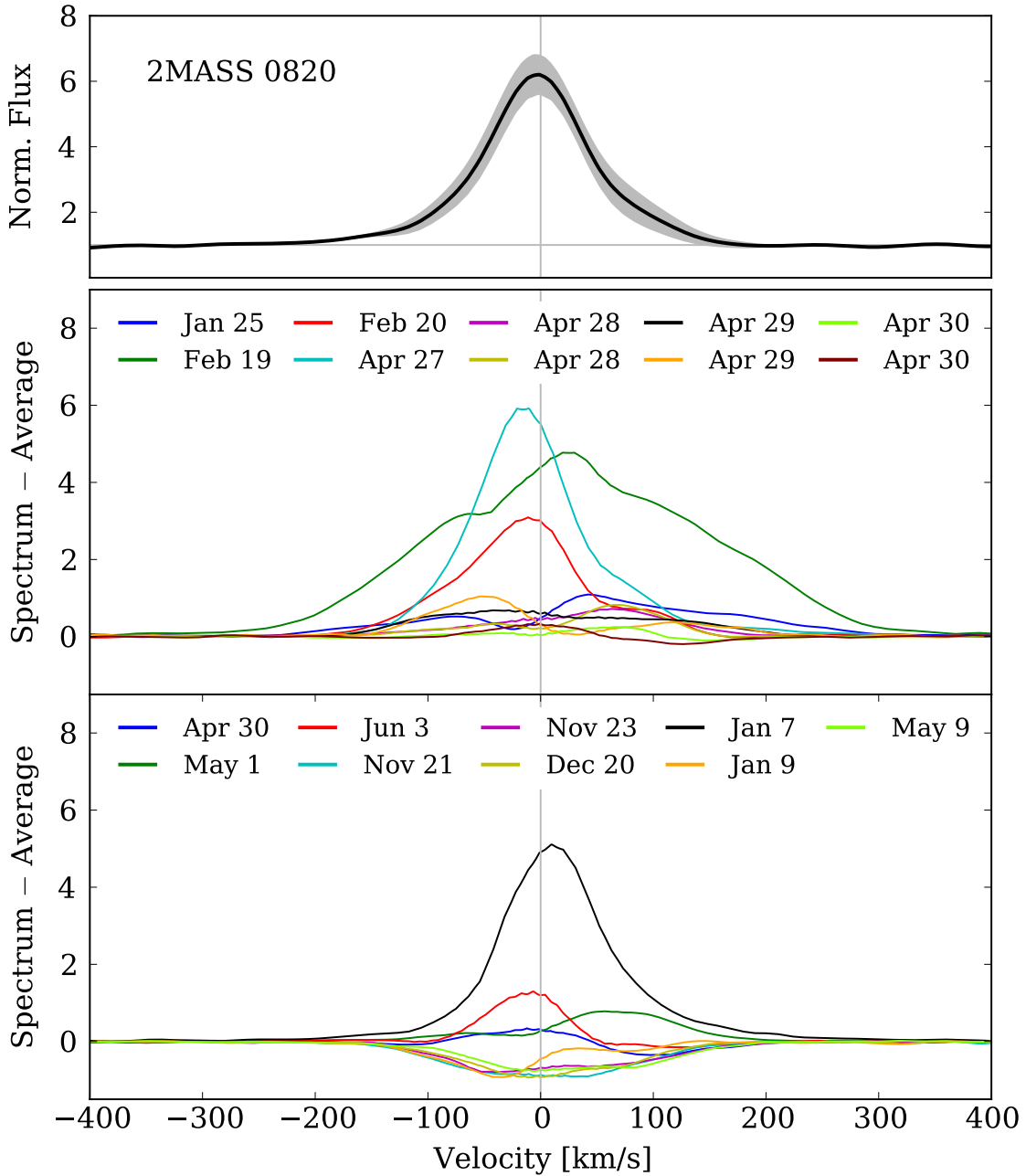


**Figure 3.6** WiFeS H $\alpha$  velocity profiles for the 19 observations of 2MASS J0820–8003. See Figure 3.5 for more information. The average quiescent spectrum was formed from the 14 spectra in Table 3.2 not showing He I or Na D emission. Note the increased scatter in the profile shape compared to 2MASS J0801–8058 and the broad multi-component residual on February 19.

Their large-scale gas motions could explain the broad wings observed in the H $\alpha$  lines and the residual spectra in Figures 3.5 and 3.6. Jayawardhana et al. (2006) also considered a two-component Gaussian fit to an H $\alpha$  velocity profile of TWA5A. They attributed the profile to an unresolved combination of chromospheric activity, rotation and possible binarity. The FWHM of the fitted components ( $100 \text{ km s}^{-1}$ ,  $300 \text{ km s}^{-1}$ ) are consistent with those attributed to micro-flaring. With the exception of the 2010 February 19 spectrum of 2MASS J0820–8003, the non-quiescent *residual* spectra of both stars can likewise be approximated by single Gaussians of various widths. The resultant two-component H $\alpha$  profiles are remarkably similar to those reported by Montes et al. (1998).

Both stars showed He I  $\lambda 6678$  in emission at their peak H $\alpha$  levels (see Tables 3.1 and 3.2). Strong He I emission is an accretion diagnostic as it is generally only present at low-levels ( $\ll 1 \text{ \AA}$ ) in older chromospherically active stars (Gizis et al. 2002; Mohanty et al. 2005). While we do detect strong (1.5  $\text{\AA}$ ) emission in the 2010 April 30 outburst spectrum of 2MASS J0801–8058, at all other epochs where we detect the line it is weak ( $\sim 0.5 \text{ \AA}$ ). Moreover, Martín & Ardila (2001) detected strong (1–4  $\text{\AA}$ ) He I  $\lambda 6678$  emission during a flare of the old M9 field dwarf LHS 2065.

Given the weak He I line strengths generally observed in our stars and the simple Gaussian-like profiles of the residual spectra, we do not have strong evidence for ongoing accretion. Chromospheric activity is a much more likely explanation for the line profiles and EW/ $v_{10}$  variations observed in 2MASS J0801–8058 and 2MASS J0820–8003. Only the 2010 February 19 spectrum of 2MASS J0820–8003 shows the broad, asymmetric residuals characteristic of an accretion event. Multiple components are present at velocities up to  $\pm 300 \text{ km s}^{-1}$ , presumably tracing the ballistic infall of material from several regions around the putative circumstellar disk onto the stellar surface. The strength of the emission was much reduced the next night, suggesting the accretion event was short (<1–2 days), although this is not well-constrained as the only prior observation was January 25.

### 3.2.4. Accretion rates

Natta et al. (2004) have shown that in accreting T Tauri stars of masses 0.04–0.8  $M_\odot$ , a good correlation exists between the H $\alpha$   $v_{10}$  velocity width and the mass accretion rate ( $\dot{M}_{\text{acc}}$ ) from the disk onto the star:

$$\log \dot{M}_{\text{acc}} = -12.89(\pm 0.3) + 9.7(\pm 0.7) \times 10^{-3} \times (v_{10}/\text{km s}^{-1}) \quad (M_\odot \text{ yr}^{-1}) \quad (3.1)$$

If we assume the observed H $\alpha$  emission is solely the result of accretion, we can use the Natta et al. (2004) relation to derive the mass accretion rate without the need to perform detailed magnetospheric radiative transfer fits to the line profile (as in Muzerolle et al. 2000; Lawson et al. 2004). Using Equation 3.1, we derive an average quiescent accretion rate for 2MASS J0820–8003 of  $\log \dot{M} = -10.6 \pm 0.5 M_\odot \text{ yr}^{-1}$ , where the uncertainty reflects both the variation in  $v_{10}$  and uncertainties in the relation parameters. This is similar to the rates reported by Lawson et al. (2004) for RECX 5, 9 and 11 (but see below). If 2MASS J0801–8058 is also accreting, we derive an accretion rate of  $\log \dot{M} = -11.3 \pm 0.3 M_\odot \text{ yr}^{-1}$  in quiescence.

For the multi-component  $v_{10} = 425 \text{ km s}^{-1}$  emission seen in 2MASS J0820–8003 on 2010 February 19 we calculate an accretion rate of  $\log \dot{M} = -8.7 \pm 0.5 M_\odot \text{ yr}^{-1}$ . This is similar to that derived for ECHA J0843.3–7905 ( $\log \dot{M} = -9.0 M_\odot \text{ yr}^{-1}$ , Lawson et al. 2004) and the  $\sim 10 \text{ Myr}$  CTTS (and eponymous TWA member) TW Hya ( $\log \dot{M} = -9.3 M_\odot \text{ yr}^{-1}$ , Muzerolle et al. 2000) from detailed H $\alpha$  profile modelling, but at the low end of the  $\dot{M} \approx 10^{-9} - 10^{-7} M_\odot \text{ yr}^{-1}$  range of accretion rates typically seen in younger CTTSs in regions like Taurus-Auriga,  $\rho$  Oph and Cha I (Calvet et al. 2000; White & Basri 2003).

However, care must be taken in interpreting the results of the Natta et al. (2004) mean trend. Using the  $v_{10}$  velocity for ECHA J0843.3–7905 given by Lawson et al. (2004), Equation 3.1 yields an accretion rate 1.3 dex larger than the corresponding model fit. According to Nguyen et al. (2009), the large scatter in this average relation probably reflects object-to-object variation (possibly due to evolutionary effects) rather than the effects of variability on

the usually single-epoch observations, as previously thought (e.g. Scholz & Jayawardhana 2006). As a single parameter,  $v_{10}$  is strongly dependent on the underlying H $\alpha$  emission profile and could be influenced by fast rotation or binarity. Detailed model fits to higher-resolution spectra should yield better estimates of the accretion rate and inner disk properties (e.g. inclination, magnetospheric radius, temperature). Note that the effect of our lower spectral resolution means we have likely underestimated  $v_{10}$ , so the derived accretion rates are probably slightly higher.

2MASS J0820–8003 showed an 80-fold jump in accretion rate between quiescence and its most active phase. Using the Natta et al. relation on the  $v_{10}$  values of RECX 5 from Lawson et al. (2004) and Jayawardhana et al. (2006) results in a similar 20-fold change in accretion rate. Furthermore, if we suppose that the scatter observed in the quiescent  $v_{10}$  velocities is a result of the accretion rate varying with time, then the variations in 2MASS J0820–8003 are similar in magnitude to those seen in TW Hya (Eisner et al. 2010) and lower-mass accreting brown dwarfs (Scholz & Jayawardhana 2006; Stelzer et al. 2007). The much smaller variations seen in 2MASS J0801–8058 again point to a chromospheric origin for its H $\alpha$  emission.

### 3.3. Infrared photometry

The H $\alpha$  variations seen in 2MASS J0820–8003 are suggestive of at least one episode of  $\sim 10^{-9} M_\odot \text{ yr}^{-1}$  accretion from a circumstellar disk. Infrared photometry, especially at wavelengths greater than 3  $\mu\text{m}$ , is vital in the detection and characterisation of such disks (Williams & Cieza 2011, and references therein).

We plot in Figure 3.7 the 2MASS two-colour diagram for 2MASS J0820–8003, 2MASS J0801–8058 and other  $\eta$  Cha members. 2MASS J0801–8058 displays an excess of around 0.1 mag in  $(J - H)$  and 0.05 mag in  $(H - K_s)$  relative to 2MASS J0820–8003 and other mid-M members of  $\eta$  Cha. This excess emission could indicate the presence of dusty circumstellar material. The star inhabits a region of colour space close to two strong accretors known to possess optically-thick disks; RECX 11 and ECHA J0843.3–7905. Both stars have Class II spectral energy distributions (SED, Evans et al. 2009), with significant excess emission at wavelengths beyond 3  $\mu\text{m}$  (Gautier et al. 2008; Sicilia-Aguilar et al. 2009).

The near-infrared excess seen in 2MASS J0801–8058 could also be the result of reddening (i.e. interstellar dust, see §3.4.1). The recently launched *Wide-field Infrared Survey Explorer* satellite (WISE, Wright et al. 2010)<sup>3</sup> now provides photometry in 3.4, 4.6, 12 and 22  $\mu\text{m}$  bands across much of the sky, including Chamaeleon. Excess emission due to a disk should become apparent over these wavelengths, whereas the effects of reddening are much diminished at longer wavelengths and the SED should trace the photospheric flux. Plotted in Figure 3.8 are 2MASS/WISE SEDs for 2MASS J0801–8058 and 2MASS J0820–8003. Absolute fluxes were calculated assuming an 88 pc dynamical distance to the stars (see Chapter 2) and the zero-magnitude calibrations of Cohen et al. (2003) and Jarrett et al. (2011). Isophotal mean wavelengths were taken from the same authors. While 2MASS J0801–8058 shows no strong excess above the expected photospheric flux, it is immediately obvious that 2MASS J0820–8003 exhibits significant excess emission at wavelengths greater than 5  $\mu\text{m}$ . The

<sup>3</sup>Preliminary Data Release available at <http://irsa.ipac.caltech.edu/Missions/wise.html>

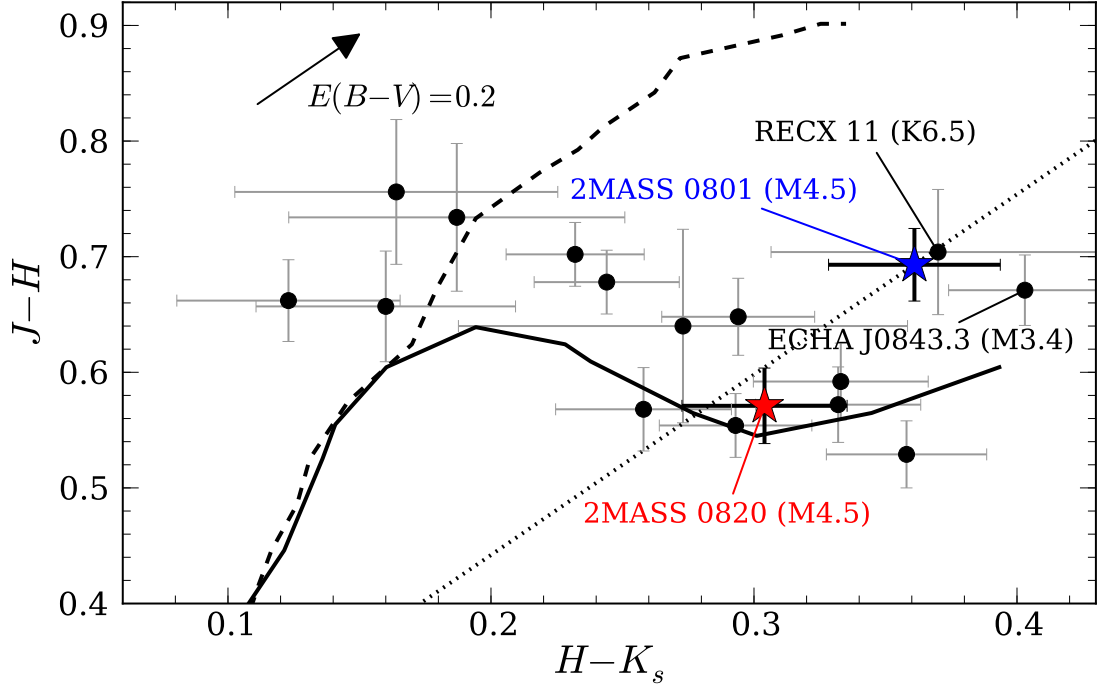


**Figure 3.7** 2MASS two-colour diagram for 2MASS J0801–8058, 2MASS J0820–8003 and known  $\eta$  Cha members. Dwarf (solid line) and giant (dashed) loci from Bessell & Brett (1988) have been transformed onto the 2MASS system. The reddening vector (arrow) is also shown passing through 2MASS J0801–8058 (dotted line). RECX 11 and ECHA J0843.3–7905 (labelled) are both known to possess optically-thick disks (Sicilia-Aguilar et al. 2009).

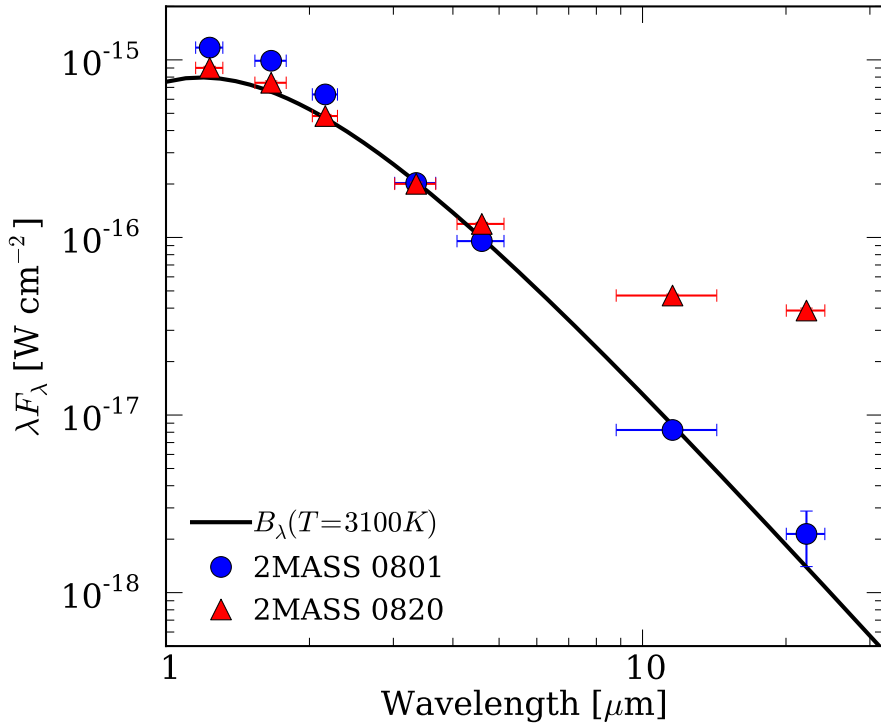


**Figure 3.8** 2MASS/WISE absolute spectral energy distributions of 2MASS J0801–8058 and 2MASS J0820–8003, assuming both stars are 88 pc away. 2MASS J0801–8058 has been dereddened by  $E(B - V) = 0.3$  mag (see text). A 3100 K blackbody is plotted to approximate the underlying photospheric continuum. Horizontal error bars show the bandwidths of the 2MASS and WISE filters.

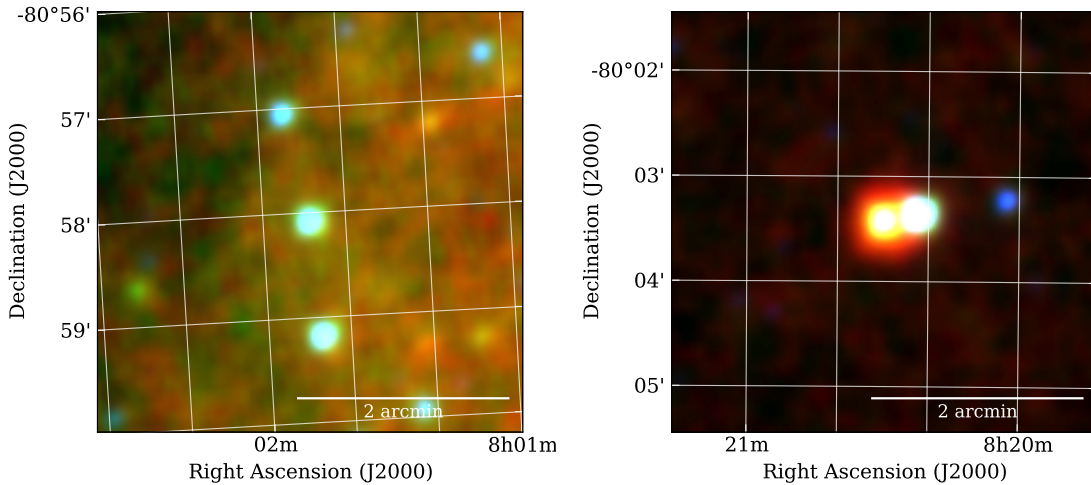


**Figure 3.9** WISE 5/12/22  $\mu\text{m}$  colour composites of 2MASS J0801–8058 (left) and 2MASS J0820–8003 (right). Each channel is linearly scaled between 0.25 and 99.75 percent. Note the bright, dusty environment surrounding 2MASS J0801–8058. The blue source immediately adjacent to 2MASS J0820–8003 is unrelated.

photometry for the star is flagged in the WISE Preliminary Data Release as having been possibly contaminated by halo image artefacts. However, visual inspection of the WISE Atlas images (see Figure 3.9) confirms significant emission from 2MASS J0820–8003 in all four bands (which is responsible for the halo effects), far above that seen in 2MASS J0801–8058 and the other lithium-rich  $\eta$  Cha candidates from Chapter 2. We attribute this excess emission to a dusty circumstellar disk.

To help classify the disk around the star, we plot in Figure 3.10 the WISE W3 (12  $\mu\text{m}$ ) and W4 (22  $\mu\text{m}$ ) magnitudes against 2MASS  $K_s$  (2.2  $\mu\text{m}$ ) for 2MASS J0820–8003, 2MASS J0801–8058 and  $\eta$  Cha members. The other lithium-rich halo candidates from Chapter 2 are also shown. The core members of  $\eta$  Cha have been well-studied with the *Spitzer Space Telescope* (Megeath et al. 2005; Bouwman et al. 2006; Gautier et al. 2008; Sicilia-Aguilar et al. 2009; Bouwman et al. 2010). 2MASS J0820–8003 occupies a similar region of the diagram to cluster members known to possess disks. As mentioned above, RECX 11 and ECHA J0843.3–7905 both have Class II SEDs typical of CTTSs. RECX 11 is thought to have an optically-thick, geometrically flat disk, perhaps due to grain-settling (Sicilia-Aguilar et al. 2009; Megeath et al. 2005). RECX 5, 9, ECHA J0841.5–7853 and ECHA J0844.2–7833 show no excess emission in 2MASS colours and can be classified as having ‘transitional’ disks with inner opacity holes (see discussion in Evans et al. 2009; Williams & Cieza 2011). RECX 5 is particularly interesting as it is thought to harbour a Saturn-mass planet responsible for clearing the inner disk (Bouwman et al. 2010). Its significant 22  $\mu\text{m}$  excess in Figure 3.10 is probably due to large amounts of crystalline silicates (forsterite) present in the disk.

Because of the lack of infrared excess blueward of 5  $\mu\text{m}$  and similar WISE colours to other disk-bearing members of  $\eta$  Cha, we classify 2MASS J0820–8003 as also having a transitional disk. The creation of an inner hole by grain-growth would naturally lead to a lack of near-IR excess, while still preserving sufficient levels of gas necessary for accretion. A ‘patchy’ inner disk region not completely cleared of material would explain the variable H $\alpha$  emission seen in Figures 3.1 and 3.6, with the outburst of 2010 February 19 presumably due to the stochastic accretion of a denser packet of gas-rich material. A similar scenario may also be responsible for the broad H $\alpha$  line in RECX 5 measured by Lawson et al. (2004). The effect

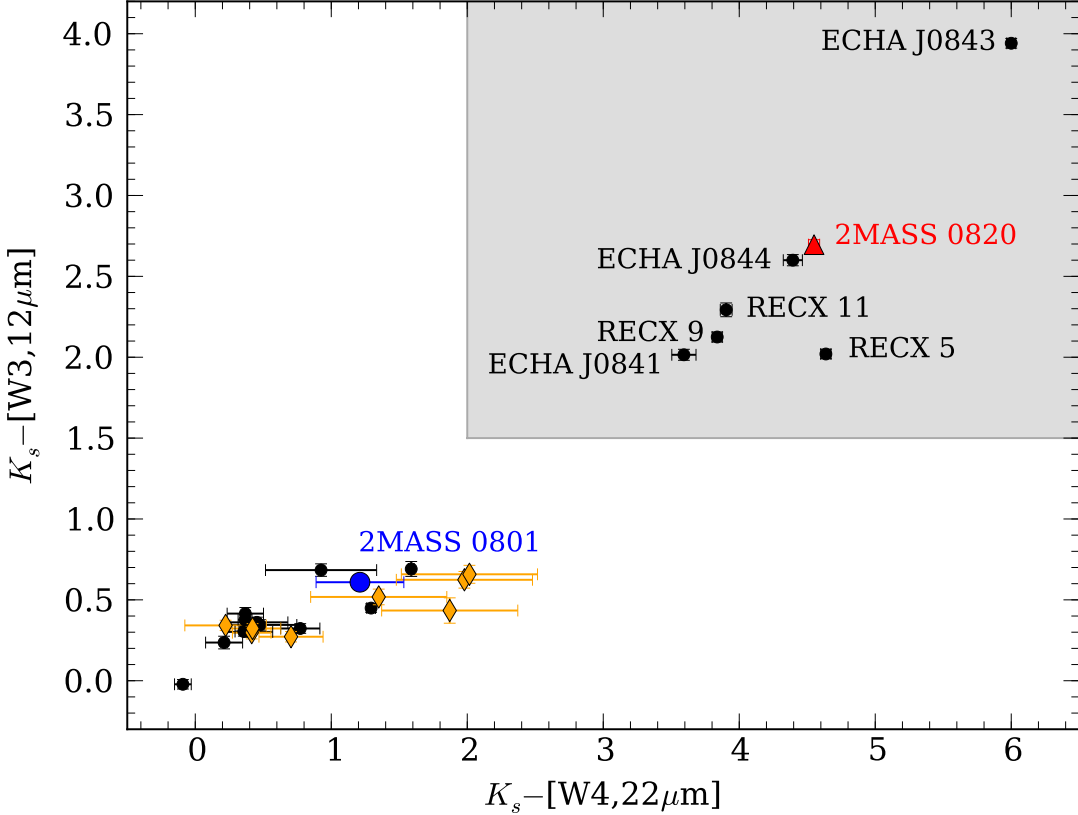


**Figure 3.10** 2MASS/WISE two-colour diagram for known  $\eta$  Cha members (black points), 2MASS J0801–8058 (blue circle), 2MASS J0820–8003 (red triangle) and the rest of the lithium-rich candidates from Chapter 2 (orange diamonds). Several stars have substantial excesses in the WISE 12 and 22  $\mu\text{m}$  bands. The shaded region arbitrarily separates these seven confirmed disk-bearing stars from the other members. The strong excess source ECHA J0843.3–7905 is an actively accreting CTTS (Lawson et al. 2002).

is also seen in other young clusters. For example, from deep  $U$ -band observations, Sicilia-Aguilar et al. (2010) implied strong levels of accretion in several members of the  $\sim 4$  Myr-old cluster Trumpler 37 (IC 1396) with transitional disks that were previously shown to have narrow, non-accreting  $\text{H}\alpha$  profiles (Sicilia-Aguilar et al. 2006). They attributed this change to a short-term increase in accretion rate during the photometric observations. Because of their younger age, disks in Trumpler 37 will be less depleted than in  $\eta$  Cha, resulting in accretion bursts that should be longer and more frequent.

## 3.4. Discussion

### 3.4.1. Reddening

The reddening vector in the 2MASS two-colour plane (dotted line in Fig. 3.7) shows 2MASS J0801–8058 appears reddened by  $0.2 \lesssim E(B - V) \lesssim 0.4$  mag compared to other mid-M type members of  $\eta$  Cha. A similar level of reddening was implied from the colour-magnitude diagram in Figure 2.12. The Schlegel et al. (1998) reddening along a line of sight to 2MASS J0801–8058 is  $E(B - V) = 0.4$  mag and the star sits on a ridge of prominent dust emission visible in IRAS maps of the region (Figure 3.11). The stellar colours will therefore be affected by reddening if the dust lies in front of the star.

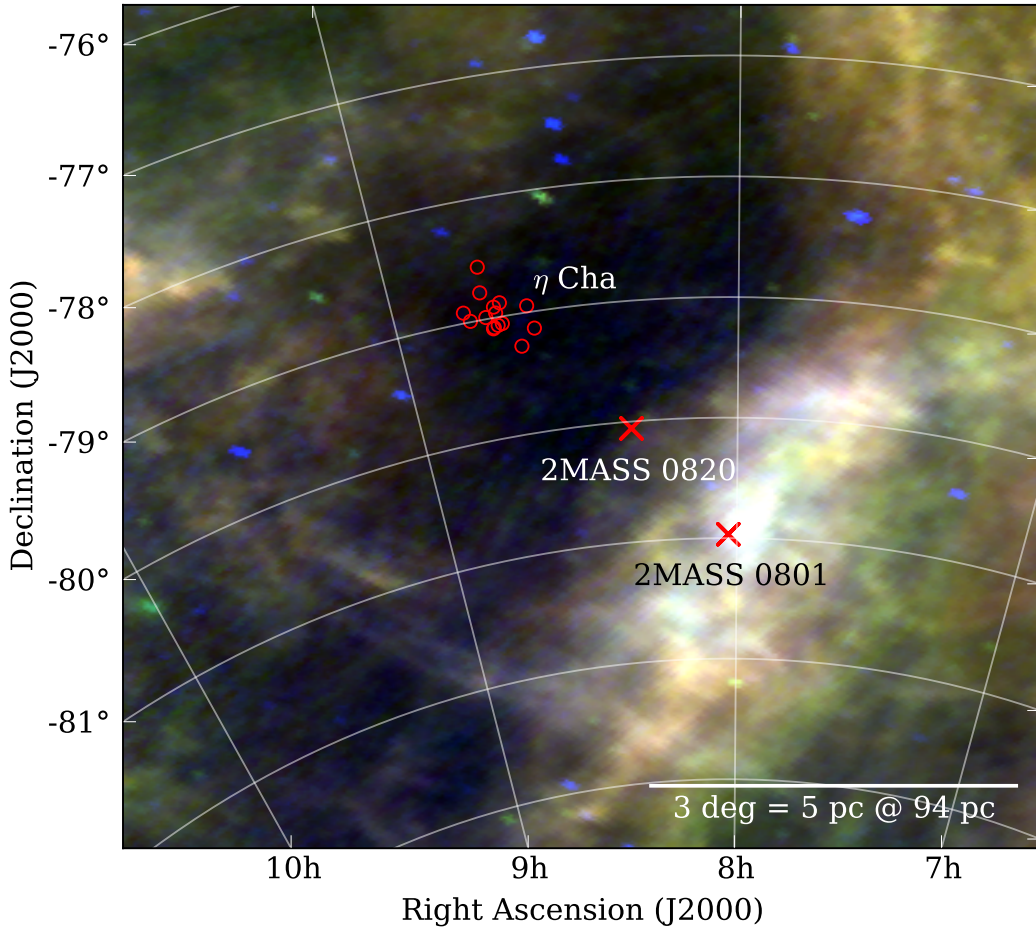


**Figure 3.11** IRAS 12/25/60  $\mu\text{m}$  colour mosaic of the region surrounding  $\eta$  Cha.

Mamajek et al. (2000) and de Geus (1992) have discussed the interstellar environment surrounding  $\eta$  Cha and the broader Scorpius-Centaurus OB Association. The dust ridge in Figure 3.11 is associated with a loop of neutral hydrogen that forms the southern extension of a wind-blown bubble surrounding Sco-Cen. From optical polarisation studies the distance to the ridge has been estimated to be  $\sim 115$  pc (Cleary et al. 1979), 40 percent larger than the 82 pc dynamical distance to 2MASS J0801–8058 estimated in Chapter 2. Nevertheless, visualising the ridge as part of a spherical shell (Mamajek et al. 2000), material from the edge closest to the Sun may lie in front of the star and redden it by  $0.2 < E(B - V) < 0.4$ .

Such a reddening is supported by Figure 3.12, where we plot the 2.3-m/DBS spectra of 2MASS J0801–8058 and 2MASS J0820–8003. We find a good match between the M3.8  $\eta$  Cha member RECX 5 (Lyo et al. 2004a) and 2MASS J0801–8058 if we de-redden the latter by  $E(B - V) = 0.3$  mag. Whatever the adopted reddening, 2MASS J0801–8058 has a noticeably earlier spectral type than 2MASS J0820–8003, which is well-matched to the M4.4  $\eta$  Cha member RECX 9 with no reddening. 2MASS J0820–8003 also appears to be of slightly earlier spectral type than the M4.7  $\eta$  Cha member ECHA J0841.5–7853.

The only previous spectral type for 2MASS J0801–8058 (M4.4), was determined by us (Chapter 2, Murphy et al. 2010) solely from  $(R - I)$  synthetic photometry. The emergence of molecular bands (e.g. TiO, VO, CaH) in the spectra of late-type stars enables a more precise spectral type determination (e.g. Kirkpatrick et al. 1991; Reid et al. 1995; Martín et al. 1999). With a judicious choice of molecular indices, a spectral type can be obtained that is almost

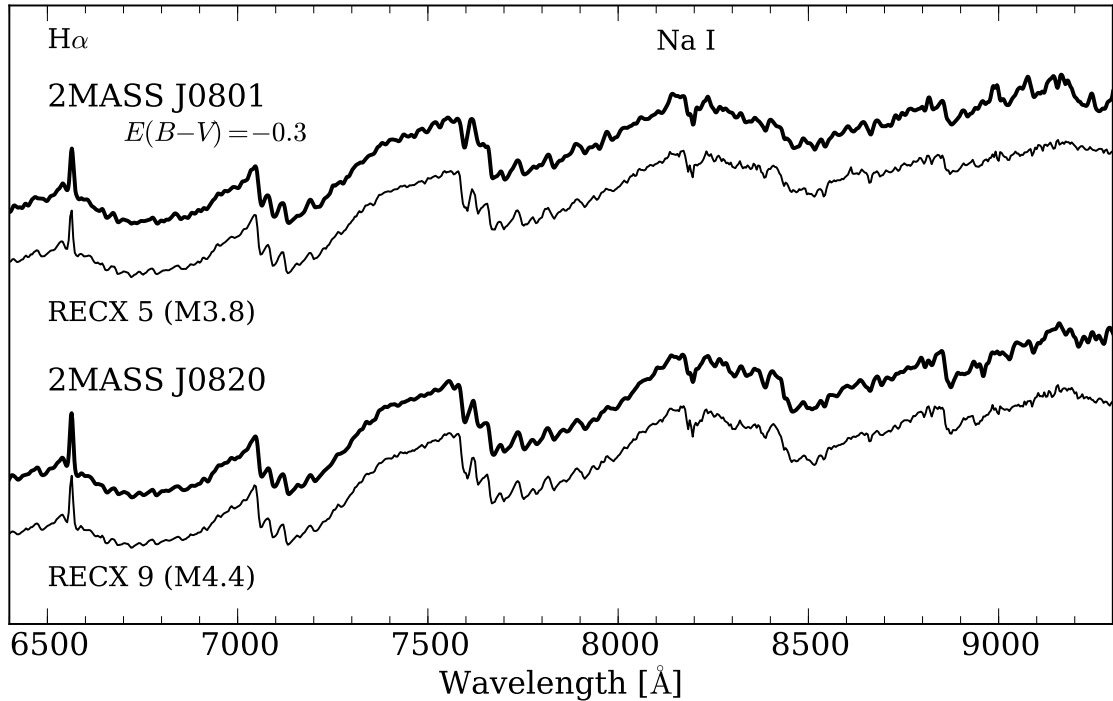


**Figure 3.12** 2.3-m/DBS spectra of 2MASS J0801–8058 and 2MASS J0820–8003, compared to  $\eta$  Cha members observed by Lyo et al. (2004a)—RECX 5 (M3.8) and RECX 9 (M4.4). 2MASS J0801–8058 has been dereddened by  $E(B - V) = 0.3$  mag. All the spectra have been normalised at 7500 Å and the DBS spectra were smoothed to match the resolution of the Lyo et al. observations.

reddening-independent, unlike photometric colours and the so-called “pseudocontinuum” indices (Martin et al. 1996), which trace broadband spectral shape.

We adopted a selection of molecular indices from the compilation of Riddick et al. (2007), which have been shown to vary smoothly with spectral type across the M spectral subclasses<sup>4</sup>. The seven indices gave an average spectral type of  $M4.1 \pm 0.5$  for 2MASS J0801–8058 and  $M4.7 \pm 0.3$  for 2MASS J0820–8003, confirming the types estimated by visual inspection. The slightly later spectral types found using the indices probably reflect a small residual dependence on reddening at large values. We therefore conclude that 2MASS J0801–8058 has a spectral type of approximately M4.0 and lies along a line of sign with an approximate reddening of  $E(B - V) \approx 0.3$  mag. 2MASS J0820–8003 appears unreddened and has a spectral type of around M4.5.

### 3.4.2. Continuum veiling

The 2010 April 30 spectrum of 2MASS J0801–8058 presented a Li I  $\lambda 6708$  equivalent width of 450 mÅ, significantly smaller than the value seen in quiescence (600 mÅ). This is the effect of continuum veiling, where enhanced continuum emission fills in absorption lines and reduces the measured EW. Following Hessman & Guenther (1997), the veiling  $V$  at a particular absorption line is defined by

$$V = \frac{F_{\text{obs}}}{F_{\star}} - 1 = \frac{\text{EW}_{\star}}{\text{EW}_{\text{obs}}} - 1 \quad (3.2)$$

<sup>4</sup>The adopted indices were drawn from the high-fidelity list of Riddick et al. (2007): VO2, c81, TiO8465, R1, R2, R3 and VOb (see their Figure 3 and Table 3)

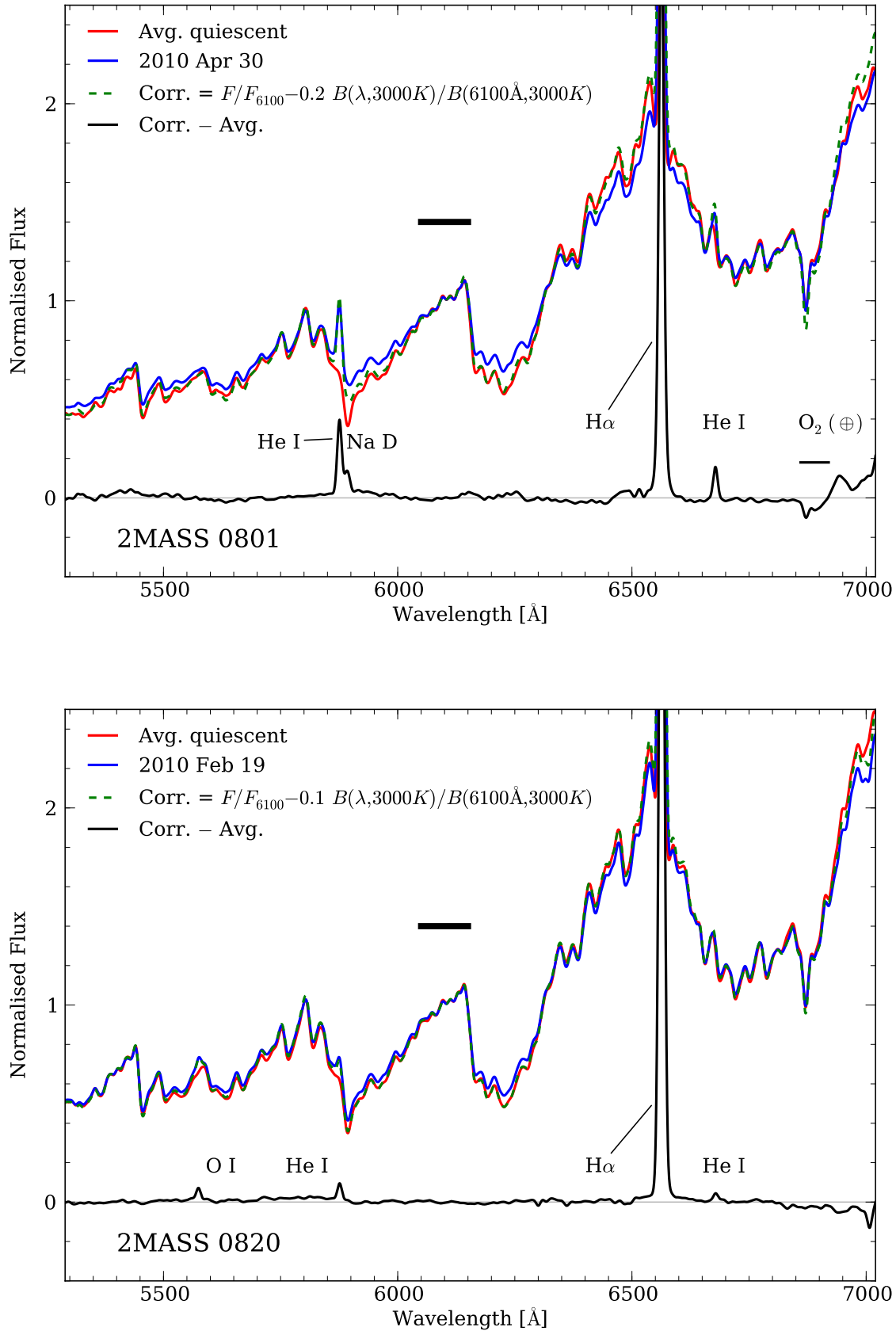


**Figure 3.13** The effects of continuum veiling on the 2010 April 30 spectrum of 2MASS J0801–8058 (top) and the 2010 February 19 spectrum of 2MASS J0820–8003 (bottom). All the spectra are smoothed by a 20-pixel Gaussian kernel and are normalised over the 6050–6150 Å region (heavy line). The green dashed line shows the final veiling-corrected spectrum (see text), while the solid black line is the difference between the average quiescent and the veiling corrected-spectra.

where  $F_{\text{obs}} = F_{\star} + F_{\text{veil}}$  is the observed flux,  $\text{EW}_{\text{obs}}$  is the observed (veiled) equivalent width, and the underlying photospheric quantities are  $F_{\star}$  and  $\text{EW}_{\star}$ . For the Li I EW values above we find  $V \approx 0.33$ . This is modest compared to the strongly-veiled ( $V \gg 1$ ) spectra seen in many CTTSSs (e.g. Basri & Batalha 1990; Hessman & Guenther 1997). Magnetospheric infall models predict the presence of veiling from accretion shocks, as matter from the accretion flow reaches the stellar surface (e.g. Muzerolle et al. 2003). Figure 3.13 shows the *WiFeS* spectrum of 2MASS J0801–8058 on 2010 April 30, compared to the average quiescent spectrum. Veiling is readily apparent as an enhancement of the continuum in the CaH  $\lambda 6200$  band and depression of the continuum around H $\alpha$  (due to the normalisation at 6100 Å).

The *WiFeS* R7000 spectra were not flux-calibrated so the change in spectral shape could be the result of sensitivity variations between observations (however, this would not affect the line veiling). The individual quiescent spectra show little variation around the mean spectrum so any night-to-night correction is likely to be small. Prior to plotting in Figure 3.13 we calibrated the average *WiFeS* spectrum using the previously flux-calibrated *DBS* spectrum of 2MASS J0801–8058. As the *DBS* spectra only extend to  $\sim 6200$  Å, we were forced to extrapolate the correction down to the 5250 Å limit of the *WiFeS* spectra. As expected, the corrections were smooth and well-fitted by a low-order polynomial. We then applied this correction to the 2010 April 30 spectrum to flux-calibrate it.

Using the average quiescent spectrum as a reference we find the excess continuum present on 2010 April 30 can be well-modelled by a black-body of temperature  $T = 3000 \pm 500$  K. The observed flux  $F$  was veiling-corrected using the following prescription:

$$F_{\text{corr}} = F_{\star} = F/F_{6100\text{\AA}} - 0.20 \times B(\lambda, T)/B(6100\text{\AA}, T) \quad (3.3)$$

where  $B(\lambda, T)$  is the Planck black-body function and  $T = 3000$  K. Once corrected, the continuum and Li I  $\lambda 6708$  EW match the quiescent levels and the only excess is now due to line emission from H $\alpha$ , He I and Na D (see Figure 3.13). With the lower, solely stellar continuum, the H $\alpha$  EW increases from  $-20$  Å to the  $-27$  Å given in Table 3.1.

2MASS J0801–8058 and 2MASS J0820–8003 also showed smaller levels of veiling ( $V_{\text{LiI}} \lesssim 0.2$ ) on several other occasions of enhanced activity. These are listed in Tables 3.1 and 3.2. We plot in the bottom panel of Figure 3.13 the veiling seen in the 2010 February 19 spectrum of 2MASS J0820–8003, after flux-calibrating as above. The veiling emission is once again well-fitted by a black-body of  $T = 3000$  K, albeit at a much lower level ( $V_{6100} \approx 0.1$ ). The residual forbidden [O I] emission in Figure 3.13 is commonly seen in CTTSSs and accreting WTTSs. However, at such a low level, in this case it is probably the result of insufficient subtraction of the strong sky emission.

In both cases, the temperature of the veiling emission is of order the photospheric temperature. This implies the veiling most likely originated there and not the chromosphere or an accretion shock, which generally emit at much higher temperatures (5000–20000 K). Stempelets & Piskunov (2003) have suggested that magnetic activity and spots brought on by the strong magnetic fields of accretion columns may have an influence on veiling. Both 2MASS J0801–8058 and 2MASS J0820–8003 are active (and almost certainly heavily spotted) in the absence of accretion, so could presumably supply the requisite magnetic fields themselves. In a similar vein, after ruling out chromospheric emission and flares, Amado & Byrne (1997) proposed that white-light emission from photospheric faculae—with temperatures

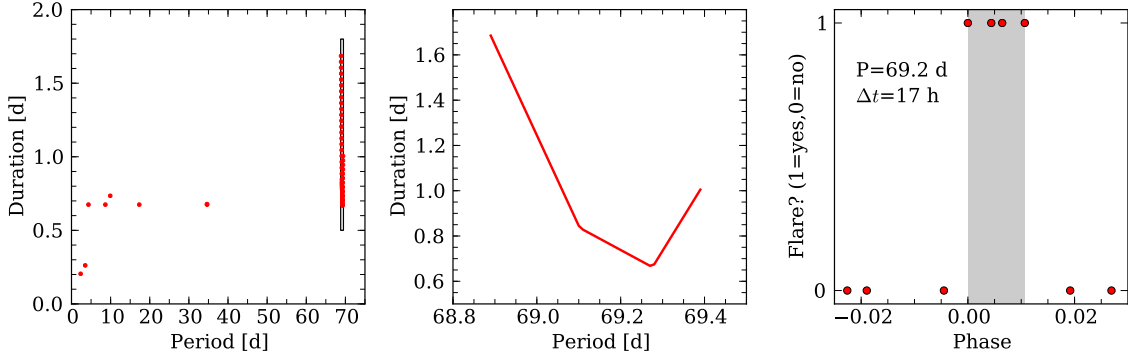


**Figure 3.14** Periodicity analysis of the flare activity seen in 2MASS J0801–8058. *Left:* The distribution of allowed periods and event durations. A large number of periods around 69 days are acceptable. Harmonics of this value are seen around 35, 17, 8 and 4 days. *Middle:* Close-up of the region around 69 days. *Right:* Phased flare profile for a period of 69.2 days. The event duration (shaded) is around 17 hours.

a few 100 K above the photosphere and surface filling factors up to 100 percent—could be responsible for ultraviolet activity seen in dMe stars. We can only speculate that the concentration of magnetic fields during the 2010 April 30 flare event of 2MASS J0801–8058 (or possibly weak accretion columns in the case of 2MASS J0820–8003) could have created swarms of dark spots and bright faculae on the photosphere of the stars, which subsequently veiled the emergent flux.

### 3.4.3. Periodic flares in 2MASS J0801–8058?

2MASS J0801–8058 exhibited three outbursts during our observations. The time between the first two flares in Table 3.1 was 69.9 days. The next outburst occurred 207.2 days later. The ratio of these times is  $2.96 \approx 3$ . While three events in our sparse data are by no means convincing evidence of periodicity, the near-integer quotient is nevertheless intriguing.

Traditional period-finding methods like the Lomb-Scargle periodogram (Lomb 1976; Scargle 1982) or Phase Dispersion Minimisation (Stellingwerf 1978) are not optimal for the analysis of non-sinusoidal ‘burst’-like variations, where the star spends a majority of its time in a non-varying, quiescent state. We therefore tried a much simpler approach to test for any periodicity in the H $\alpha$  emission of 2MASS J0801–8058. The H $\alpha$  EW values were first parameterised as {0, 1}, where the four observations with  $|EW| > 10 \text{ \AA}$  were set to unity. This encodes the shape of the outburst as a box profile in time. Although the two 2010 November 23 observations showed substantially smaller  $v_{10}$  velocities than the other outburst epochs, we consider only the EWs in this analysis.

For a range of trial periods,  $0.1 < P/\text{days} < 100$  ( $\Delta P = 0.01 \text{ d} = 14 \text{ min}$ , half the smallest exposure time), we phased the encoded EWs over the phase range  $-0.5 < \phi < 0.5$ , such that  $\phi = 0$  corresponded to the first outburst on 2010 February 19. This ensured we were not influenced by phase wrapping of outbursts around  $\phi \in \{0, 1\}$ . Finally, we tested each period by requiring that the four outburst epochs were contiguous in phase-space, i.e. we assume they all corresponded to a single, repeating flare of a certain duration, with no quiescent epochs within that phase range. This method is conceptually similar to the box-fitting algorithm developed by Kovács et al. (2002) for detecting short duration transit events in light curves (presumably due to extrasolar planets).

The results of the periodicity investigation are summarised in Figure 3.14. A broad range of periods around 69 days are permitted (centre panel), with outburst durations  $\Delta t < 2$  days. A phased profile for a period of 69.2 days is shown in the right-hand panel. The duty-cycle of this outburst is around 1 percent (17 hours). This is consistent with the variation seen over 2010 April 29–May 1 (Figure 3.2) and the decrease in EW during 2010 November 23–24. By randomly assigning outburst epochs over our current sampling, we find that only 0.03 percent of random realisations at this period yield acceptable profiles. This is evidence—*albeit weak given the sparse sampling*—that the flares did not occur by chance.

Further observations of 2MASS J0801–8058 in outburst are necessary to prove any 69 day periodicity. A large increase in EW outside of the predicted flare epochs (2010 November 11, 2011 January 11, March 20, ...) would immediately falsify the hypothesis. If confirmed, the periodicity is unlikely to be driven by rotation (e.g. a long-lived magnetic feature on the stellar surface), as young, low-mass stars typically have rotational periods of days to weeks (Lamm et al. 2004; Messina et al. 2010). Instead, we speculate that the variation may be caused by a close binary companion in an eccentric orbit that enhances chromospheric activity in 2MASS J0801–8058 every 69 days around periastron. The mass, orbital semi-major axis and eccentricity of any putative companion are currently unknown, but could be inferred statistically if the 69-day signal is confirmed by further observations.

### 3.4.4. Radial velocity variations

Our multi-epoch observations provide insight into any radial velocity variations in the two stars. The measurement of velocities from the *WiFeS* spectra is described in Chapter 2 and the resultant RV values are given in Tables 3.1 and 3.2. From over 600 observations of M-type velocity standards we have established that *WiFeS* is capable of an RMS velocity precision of  $1\text{--}2 \text{ km s}^{-1}$  per epoch at a resolution of  $R \approx 7000$  (Appendix C). The standard deviation of 19 RV measurements of 2MASS J0820–8003 is  $1.9 \text{ km s}^{-1}$ , consistent with a flat velocity curve. The RV derived from the high-resolution *MIKE* spectrum ( $17.4 \pm 0.5 \text{ km s}^{-1}$ ) is also consistent with the mean *WiFeS* value of  $18.3 \pm 0.4 \text{ km s}^{-1}$ . In contrast, 2MASS J0801–8058 has a standard deviation of  $2.9 \text{ km s}^{-1}$  from 35 measurements. The eight spectra of the star taken on 2011 May 8 again confirmed the stability of the instrument ( $\sigma_{\text{RV}} = 1.4 \text{ km s}^{-1}$ ), so the long-term RV variation must be intrinsic to the star.

In Chapter 2 we suggested that in conjunction with its elevated position in the cluster colour-magnitude diagram, the velocity variation of 2MASS J0801–8058 suggested binarity. The periodicity analysis above also hints at such a prospect, although at a much longer period. The elevation of 2MASS J0801–8058 above the single-star isochrone can be explained by a reddening to the star of  $E(B - V) \approx 0.3$  (see §3.4.1). To check for periodic variation we tried phasing the RV data over a range of periods, but none gave a strong signal. This is not surprising, considering the amplitude of the expected variation is similar to the velocity precision of *WiFeS*. High resolution spectroscopy and adaptive optics imaging (e.g. Köhler & Petr-Gotzens 2002) will be necessary to resolve a companion, if one exists.

A more likely scenario is that the velocity variation seen in 2MASS J0801–8058 is induced by activity or co-rotating surface features. Magnetic ‘starspots’ on the stellar surface can add RV noise by causing temporal changes in the profiles of absorption lines used to measure the

velocity (Vogt et al. 1987; Saar & Donahue 1997). The problem has been studied extensively in recent years because of its implications for the detection of extrasolar planets around low-mass stars via the radial velocity technique (e.g. Barnes et al. 2011; Reiners et al. 2010).

Several authors have observed long-lived activity-induced RV variations similar to those seen in 2MASS J0801–8058. Martín et al. (2006) detected a  $7 \text{ km s}^{-1}$  amplitude (peak-to-peak), 3.7 hr periodicity in the optical RV data of the M9 brown dwarf LP 944–20, which they attributed to rotationally modulated surface features. Mahmud et al. (2011) reported a similar  $2.8 \text{ km s}^{-1}$  amplitude sinusoidal RV variation in the K7 WTTS Hubble I 4. An extrasolar planet could be excluded as the cause of the signal in both cases as the variations were smaller or undetectable (in the case of LP 944–20) in the near-infrared. This is expected from spots because of the smaller temperature contrast between the spot and the surrounding photosphere at longer wavelengths (Reiners et al. 2010).

Using a toy model with a single spot 100–200 K cooler than the photosphere covering  $\sim 10$  percent of the stellar surface, Reiners et al. (2010) could generate a velocity variation with an amplitude of a few  $\text{km s}^{-1}$ . This is similar to the signal seen in LP 944–20 and 2MASS J0801–8058. Similarly, Mahmud et al. (2011) found a single 25 deg radius (5 percent filling factor) spot 1200 K cooler than the photosphere could reproduce their observed  $2.8 \text{ km s}^{-1}$  variation. Chaotic spot configurations with larger filling factors are more likely to produce random RV ‘jitter’ than a well-phased sinusoidal signal (Barnes et al. 2011).

Spots, or other magnetic surface activity—compounded by the modest spectral resolution of *WiFeS*—are a natural explanation for the RV variations seen in 2MASS J0801–8058. We do not find any correlation between the velocity and either the H $\alpha$  EW or  $v_{10}$  so the variation is probably driven by rotation not chromospheric flaring. An notable exception to this rule may be the anomalously low  $9.3 \text{ km s}^{-1}$  velocity measured during the event of 2010 November 23. The rotational period of 2MASS J0801–8058 has not been measured, but is likely to be on the order of days, similar to the other late-type members of  $\eta$  Cha (Lawson et al. 2001) and the timescale of the observed velocity variation.

### 3.4.5. Dynamical evolution—a solution to the high disk fraction problem?

$\eta$  Cha is well-known to have an excess of stars with disks compared to other similarly aged clusters (e.g. Mamajek 2009; Fedele et al. 2010). Gautier et al. (2008) and Sicilia-Aguilar et al. (2009) summarised the current disk census of the cluster. As well as the six stars in Figure 3.10, RECX 3 and 4 show  $33 \mu\text{m}$  excess (Bouwman et al. 2006) and RECX 7 has a weak excess at that wavelength (Gautier et al. 2008). Large inner holes are implied in the disks around these stars. The eponymous B8 star  $\eta$  Cha shows a weak excess at long wavelengths, which is probably due to a (second-generation) debris disk (Sicilia-Aguilar et al. 2009). In summary, 10/18 members (55 percent) possess some level of IR excess over  $2\text{--}160 \mu\text{m}$ . For the late-type (K and M) members this fraction is 9/15 (60 percent). These values are more typical of a 2–5 Myr-old population like  $\sigma$  Ori (Hernández et al. 2007) or Trumpler 37 (Sicilia-Aguilar et al. 2006, 2010) than a 5–10 Myr cluster like  $\eta$  Cha.

Of the four *probable* halo members of  $\eta$  Cha we identified in Chapter 2, only one had an appreciable excess in WISE photometry (2MASS J0820–8003). If we ignore the possibility that the other stars may have excesses beyond the  $22 \mu\text{m}$  limit of WISE, this is a 25 percent

disk fraction. Since none of the four *possible* members show disk emission either, it appears that the dynamical processes responsible for their ejection are also not conducive to long-term disk survival. Armitage & Clarke (1997) found that the ejection of a star from a small cluster at velocities of only a few  $\text{km s}^{-1}$  can strip all but the inner circumstellar disk and greatly accelerate the evolution of the remaining material. The disk surrounding 2MASS J0820–8003 may not have been so adversely affected by dynamics. The star is the closest halo member to the cluster core (1.44 deg) and would only need to have been ejected at  $\lesssim 1 \text{ km s}^{-1}$  very early on to move to its current position. The other *probable* member within 1.5 deg, RX J0902.9–7759, is a suspected close binary (see §2.7). Bouwman et al. (2006) found that binarity is a key factor influencing the retention of disks in  $\eta$  Cha. They showed a strong anti-correlation between binarity and the presence of a disk and from this implied that the mean disk dissipation timescale in  $\eta$  Cha binaries was half that of the single stars.

Fedele et al. (2010) claimed that the current census of  $\eta$  Cha members may be biased towards IR excess/accreting stars, presumably due to dynamical evolution removing the bulk of the low-mass members. How this would bias the remaining core members remains unclear, as they would presumably have also undergone significant dynamical interactions which could disrupt (at least outer) disks. The simulations of Moraux et al. (2007) showed that  $\eta$  Cha was initially compact ( $R_0 \sim 1000 \text{ AU}$ ) and extremely dense (average number density  $\sim 10^8 \text{ stars pc}^{-3}$ ), with star-to-star separations on the order of 100–200 AU. This is the typical size of observed protoplanetary disks (Williams & Cieza 2011). Brandeker et al. (2006) also reported a lack of wide ( $a > 20 \text{ AU}$ ) binaries in the cluster, which hints at a more dynamically violent past. The implied primordial density is several orders of magnitude higher than what is observed or produced in simulations, so its accuracy may be called into question, especially given the large uncertainties in the simulations (e.g. see §2.8.1).

Irrespective of the dynamical history of the inner members, we have shown that a significant population of ejected members exists outside the central core. These stars must be counted in any disk census. If we include just the four *probable* members from Chapter 2, the fraction of late-type disk-bearing stars falls to 10/19 (~50 percent). In the minimal case, where we also include the four *possible* members and reject the weak-excess members RECX 3, 4 and 7 as having second-generation (i.e. non-primordial) debris disks, then we can only push the disk fraction as low as 7/23 (30 percent). A similarly-aged cluster should have a disk fraction of only 5–10 percent (Hernández et al. 2008; Mamajek 2009). This would require an initial population of 50–100 cluster members, assuming that few of the dispersed stars harbour disks today, as seen in our (small) sample of halo candidates. The number of required cluster members is a factor of 2–3 times larger than that proposed by Moraux et al. (2007) to explain the current configuration of the cluster ( $N_{\text{init}} \approx 40$ ). However, given the uncertainties in the dynamical modelling, such a difference is trivial. Because of the small number of stars involved, and the fact that a significant population of dispersed  $\eta$  Cha members exists outside the core with a much smaller disk frequency, it is likely that the true cluster disk fraction is much closer to that seen in other 5–10 Myr-old clusters.

The effects of sensitivity and environment must also be considered.  $\eta$  Cha is compact, nearby and unobscured, allowing easy access to its low-mass members for disk studies. This is especially true of the mid and far-infrared observations by *Spitzer* that are crucial for constraining the frequency of primordial disks with large inner holes. The few other clusters

in the crucial 5–10 Myr age range are much further away, and surveys are limited to their brighter, core members. They could also be influenced by extinction. We may be therefore *underestimating* the disk fraction in these (and older) clusters. Young, local associations like TW Hydreae (8–10 Myr) and  $\beta$  Pictoris (12 Myr) can help in this regard. The recent availability of all-sky WISE photometry should enable an efficient disk census of all the young stars within a distance of 100 pc at high sensitivity.

### 3.5. Conclusion

Our multi-epoch observations have shown that H $\alpha$  variability in ~8 Myr-old pre–main sequence stars can be substantial on both short (hours–days) and long (months) timescales. Based on the shape and strength of this variation, it is probably driven primarily by chromospheric activity, which can generate broad H $\alpha$  profiles mimicking accretion during short, discrete events. However, we also have evidence for at least one accretion event in 2MASS J0820–8003. The implied accretion rate of  $\sim 10^{-9} M_{\odot}$  yr $^{-1}$  is similar to those seen in accreting T Tauri stars in younger star-forming regions. 2MASS J0820–8003 has a pronounced infrared excess beyond 5  $\mu$ m, which we attribute to a ‘transitional’ circumstellar disk with an inner opacity hole. The star joins ten other  $\eta$  Cha members known to possess disks, most of which are also transitional. 2MASS J0801–8058 does not have a detectable infrared excess out to the 22  $\mu$ m limit of WISE photometry, supporting a chromospheric origin for its short-duration H $\alpha$  outbursts. The star may show 69 day periodic flaring, potentially due to a close companion in an eccentric orbit.

We detected only one event during 16 months of observations of 2MASS J0820–8003 which we could attribute to accretion from a circumstellar disk. This discrete, episodic accretion is presumably due to an inner disk cleared of dust but not completely free of gaseous material. The infall of volatile-rich solid bodies (i.e. comets) could also be a possibility (e.g. de Winter et al. 1999). Similar events have been observed in the  $\eta$  Cha member RECX 5, which may be a sign of episodic accretion around that star. Assuming the duty-cycle of accretion events is low (we estimate the 2MASS J0820–8003 event lasted no more than 2 days), single-epoch surveys for accreting objects—especially in the critical age range 5–10 Myr when inner disks are being cleared and giant planet formation takes place—are likely missing a large fraction of accreting objects. Gas depletion timescales derived from the fraction of accretors are therefore likely underestimated. This may provide a more natural explanation for the difference in the characteristic timescales of gas accretion and dust dissipation found by Fedele et al. (2010) (2.3 Myr and 3 My respectively), without the need to invoke planet formation and/or migration in the inner disk as a mechanism for prematurely halting accretion. More detailed investigation of the true accreting fraction in pre–main sequence clusters of various ages from *multi-epoch* surveys is needed to resolve the discrepancy.

## CHAPTER 4

---

# The young, wide binary system RX J0942.7–7726AB

*This work has been prepared for publication in the Monthly Notices of the Royal Astronomical Society. It will be submitted in early-2012 with authors Murphy, S. J., Bessell, M. S. and Lawson, W. A.*

### 4.1. Introduction

Since the discovery of a group of young stars associated with the ‘isolated’ T Tauri star TW Hydrae (de la Reza et al. 1989; Gregorio-Hetem et al. 1992; Kastner et al. 1997) it has become clear that the solar neighbourhood is bestrewn with sparse associations of stars with ages substantially less than the Pleiades (Zuckerman & Song 2004; Torres et al. 2008). Although members of these young, local associations share similar kinematics, ages and distances, their proximity to the Sun means they are spread over vast swathes of sky.

The youngest and best-characterised of these groups are associated with the bright stars TW Hydrae ( $\sim$ 10 Myr; Kastner et al. 1997; Webb et al. 1999),  $\beta$  Pictoris ( $\sim$ 12 Myr; Barrado y Navascués et al. 1999; Zuckerman et al. 2001a),  $\eta$  Cha (5–8 Myr; Mamajek et al. 1999, 2000) and  $\epsilon$  Cha ( $<$ 8 Myr; Feigelson et al. 2003; Luhman 2004b). All four associations are located in the southern hemisphere near the Scorpius-Centaurus OB Association (Figure 4.1), the closest site of large-scale massive star formation (Blaauw 1964; de Zeeuw et al. 1999).

Much work has been done to understand the origins of these groups (e.g. Mamajek et al. 2000; Mamajek & Feigelson 2001; Sartori et al. 2003; Makarov 2007; Fernández et al. 2008). Most recently, Ortega et al. (2009) undertook a detailed kinematic study of TW Hydrae,  $\beta$  Pic,  $\epsilon$  Cha and  $\eta$  Cha. They concluded the groups were likely formed in small molecular ‘cloudlets’ on the outskirts of the Lower Centaurus Crux and Upper Centaurus Lupus subgroups of Sco-Cen (Figure 4.1), thrown into star formation by the bulk flows and shocks formed by colliding supernovae-driven bubbles around the subgroups. The cloudlets later dispersed to reveal loose associations of stars with similar ages and velocities. Fernández et al. (2008) proposed a similar scenario, with the star-formation agent being the passage of a spiral density wave through the Sco-Cen region (also see Sartori et al. 2003).

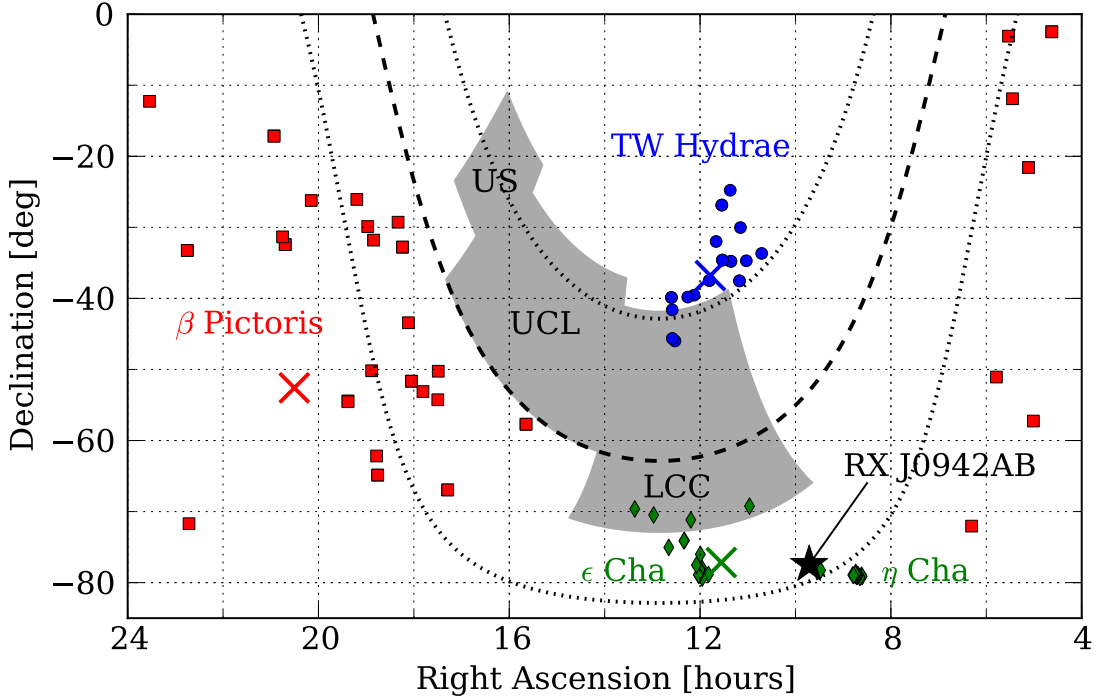


**Figure 4.1** RX J0942.7–7726AB on the sky with members of  $\epsilon$  Cha (green diamonds), TWA (blue points) and  $\beta$  Pic (red squares) from Torres et al. (2008). Crosses denote the mean ( $X, Y, Z$ ) position of each group projected onto the sky. The subgroups of the Scorpius-Centaurus OB Association (as defined by de Zeeuw et al. 1999) dominate the field around the Galactic equator (dashed line, with  $b = \pm 20^\circ$  dotted).

This is reminiscent of the ‘in-situ’ star formation scenario proposed by Feigelson (1996) to explain the discovery of younger isolated T Tauri stars around the Chamaeleon and Taurus-Auriga dark clouds. Under this scenario, groups of stars born in different parts of a molecular cloud inherit the region’s turbulent velocity dispersion, which can be up to  $10 \text{ km s}^{-1}$  on scales of 10–100 pc (Larson 1981). A population of 10 Myr old stars can therefore end up dispersed  $\sim 100$  pc away from the main cloud ( $1 \text{ km s}^{-1} \approx 1 \text{ pc Myr}^{-1}$ ). In the absence of further dynamical interactions however, when traced back in time their motions should converge to a common birthplace of minimal physical size (e.g. Ortega et al. 2002; Song et al. 2003; de la Reza et al. 2006).

In this Chapter we describe the discovery and characterisation of a pair of isolated, young, low-mass stars with common ages, distances and kinematics. They are situated to the southwest of LCC, between the  $\eta$  Cha open cluster and  $\epsilon$  Cha Association (Figure 4.1). We will show they do indeed form a wide (4000–6000 AU) pre-main sequence binary which may have been born in the region surrounding the Scorpius-Centaurus OB Association, or near one of the young groups described above.

#### 4.1.1. RX J0942.7–7726 and 2MASS J0942–7727

RX J0942.7–7726 (=2MASS J09424962–7726407) and 2MASS J09424157–7727130 (hereinafter 2MASS J0942–7727) were serendipitously identified in Chapter 2 as an isolated pair of young stars 3.5 deg from  $\eta$  Cha lying only  $42''$  apart. Both stars appeared to have ages greater than the cluster ( $\sim 8$  Myr) and similar distances, proper motions and radial velocities. Moreover, their kinematics did not match ejection from a young  $\eta$  Cha at any realistic age or distance. We therefore ruled them out as  $\eta$  Cha members but their origin remains uncertain.

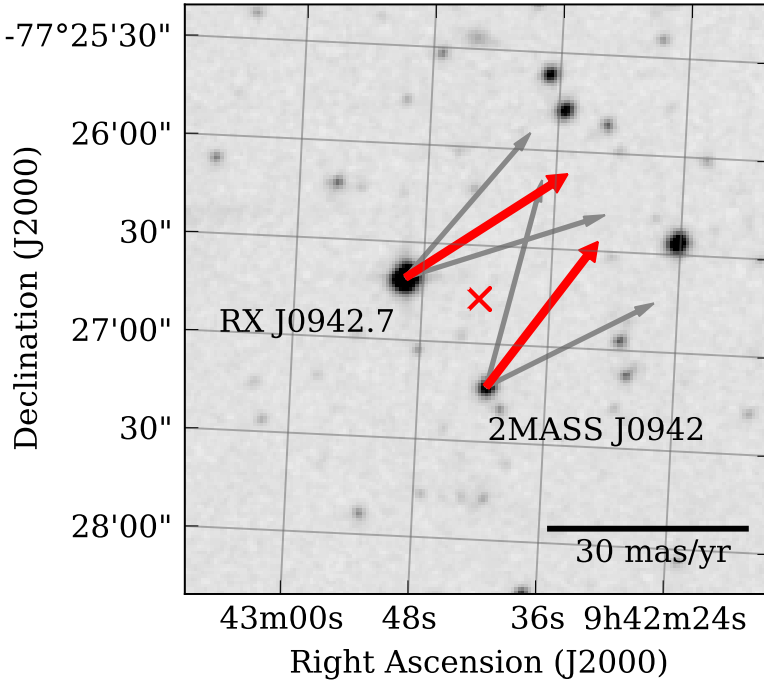


**Figure 4.2**  $3' \times 3'$  DSS2-IR finder chart centred on the ROSAT X-ray position of RX J0942.7–7726 (red cross). The optical sources of RX J0942.7–7726 and 2MASS J0942–7727 are  $42''$  apart. Their PPMXL proper motion vectors are shown in red. The vectors trace the expected motion on the sky over a period of approximately 2000 years. Thin grey arrows depict the proper motion  $1\sigma$  error bounds.

RX J0942.7–7726 was found to be the Weak-lined T Tauri Star (WTTS) counterpart to a ROSAT X-ray detection by Alcalá et al. (1995, 1997), during their survey of Chamaeleon X-ray sources. They obtained low-resolution spectroscopy which confirmed the youth of the star and assigned a spectral type of K7–M0. Covino et al. (1997) refined the spectral type to M0 and from a high-resolution ( $R \approx 20,000$ ) spectrum derived a stellar rotational velocity ( $v \sin i \approx 9 \text{ km s}^{-1}$ ), radial velocity ( $16.4 \pm 2 \text{ km s}^{-1}$ ) and strong lithium absorption ( $\text{EW} = 490 \text{ m}\AA$ ). Köhler (2001) surveyed many of the X-ray-selected young stars in Chamaeleon for close companions, including RX J0942.7–7726. No companions were found around the star, down to separations of  $0.13''$  and a K-band contrast of  $<3.8$  mag.

2MASS J0942–7727 is not as well characterised. Aside from the photometry and spectroscopy presented in Chapter 2 (see also Murphy et al. 2010) the M4.6 star remains largely unstudied. Its PPMXL (Roeser et al. 2010) proper motion,  $(-16, +23) \pm (9, 9) \text{ mas yr}^{-1}$ , agrees with that of RX J0942.7–7726 within the errors (see Figure 4.2) and the two stars have *WiFeS* radial velocities that differ by only  $2.7 \text{ km s}^{-1}$  (Table 2.3). A finder chart for the pair is given in Figure 4.2, along with their PPMXL proper motion vectors. For the sake of brevity we hereinafter refer to the system as RX J0942.7–7726AB.

## 4.2. Other stars in the region

Because RX J0942.7–7726AB lay at the bottom of the  $\pm 1.5$  mag selection band in the  $\eta$  Cha colour-magnitude diagram (Figure 2.1), there may be other young stars in the vicinity of the pair that we missed in Chapter 2. Figure 4.3 shows the 768 stars within  $10'$  of RX J0942.7–7726 with DENIS and 2MASS photometry and PPMXL proper motions. Only

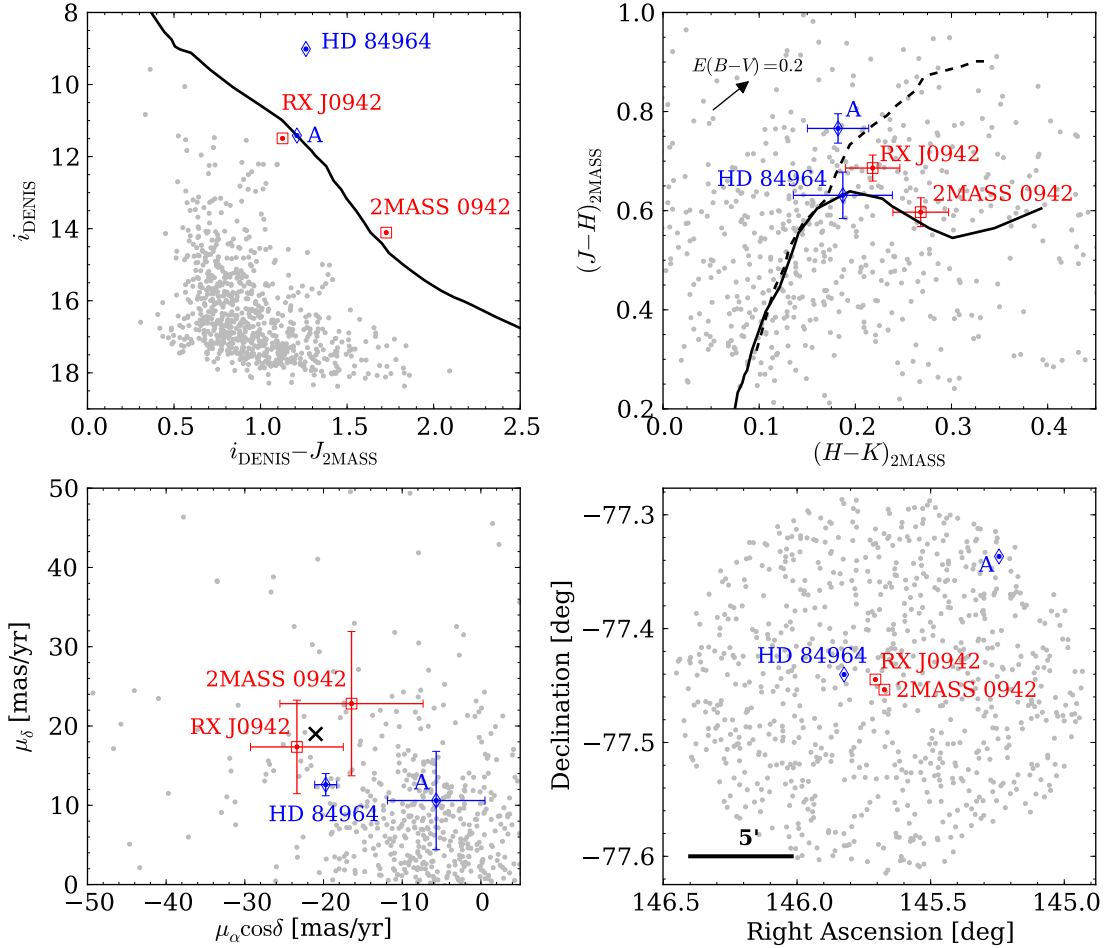


**Figure 4.3** The 768 stars within 10' of RX J0942.7–7726AB with  $iJHK$  photometry and PPMXL proper motions. The two blue labelled points are discussed in the text. *Top-left:* Colour-magnitude diagram with a 40 Myr Baraffe et al. (1998) isochrone at 90 pc for reference. *Top-right:* 2MASS two-colour diagram with dwarf (solid line) and giant (dashed) locii from Bessell & Brett (1988), transformed to 2MASS colours. *Bottom-left:* PPMXL proper motions. The cross shows the weighted average proper motion of RX J0942.7–7726AB. *Bottom-right:* The 10' radius field on the sky. HD 84964 is only 1.5' from RX J0942.7–7726.

two stars have positions in the CMD similar to RX J0942.7–7726AB. Star A (labelled) lies at the edge of the 10' field but has similar photometry to RX J0942.7–7726. However, its 2MASS colours are giant-like and its proper motion is significantly smaller than RX J0942.7–7726AB. HD 84964 is classified as a K1 star (Houk & Cowley 1975) that Olsen (1994) identified as a giant from Stromgren photometry. We note it has 2MASS colours consistent with an early K-giant reddened by  $E(B-V) \approx 0.2$ , the reddening attributed to the region surrounding RX J0942.7–7726AB (see §4.3). Although HD 84964 is only 1.5' from RX J0942.7–7726AB and has a PPXML (and Tycho-2) proper motion vector near both stars, it is likely unrelated.

To confirm this we observed HD 84964 and Star A with *WiFeS/R7000* in 2011 July and found them both to be mid-K stars (from visual comparison to radial velocity standards) with strong H $\alpha$  absorption and negligible ( $\lesssim 50$  mÅ) Li I  $\lambda 6708$  equivalent widths. Their radial velocities ( $67 \pm 1.5$  km s $^{-1}$  and  $1.4 \pm 1.5$  km s $^{-1}$ , for HD 84964 and Star A respectively) are also inconsistent with either RX J0942.7–7726 or 2MASS J0942–7727 (weighted mean velocity  $19.9 \pm 0.5$  km s $^{-1}$ ). To the limits of DENIS and 2MASS photometry we conclude that RX J0942.7–7726AB are an isolated pair of young stars with no other close companions.

### 4.2.1. Probability of chance alignment

We now address the likelihood that RX J0942.7–7726AB is a true wide binary, rather than a chance alignment of unrelated young stars. The canonical method of finding wide binaries is to search for pairs of stars with small angular separation on the sky. As orbital motions are generally negligible ( $\lesssim 1 \text{ km s}^{-1}$ ) in this regime, the components of true wide binaries are expected to have distances, proper motions and radial velocities that agree within errors. Chance alignments will likely have *different* distances and kinematics.

By comparing the *Hipparcos* and LSPM-North (Lépine & Shara 2005) catalogues, Lépine & Bongiorno (2007) defined the following empirical criterion to separate true wide binaries from unrelated chance alignments:

$$\Delta\theta\Delta\mu \lesssim (\mu/0.15)^{3.8} \quad (4.1)$$

where  $\Delta\theta$  is the angular separation of the pair (in arcseconds),  $\Delta\mu$  is the relative proper motion,  $\sqrt{(\mu_{\alpha 1} - \mu_{\alpha 2})^2 + (\mu_{\delta 1} - \mu_{\delta 2})^2}$ , (in " yr $^{-1}$ ) and  $\mu$  is the mean proper motion of the pair (in " yr $^{-1}$ ). In the case of RX J0942.7–7726AB,  $\Delta\theta = 42''$ ,  $\Delta\mu = 0.01'' \text{ yr}^{-1}$ ,  $\mu = 0.03'' \text{ yr}^{-1}$  (PPMXL, Table 2.3) and so:

$$\Delta\theta\Delta\mu = 0.42 \gg \left(\frac{0.03}{0.15}\right)^{3.8} = 0.0022 \quad (4.2)$$

According to the Lépine & Bongiorno criterion, RX J0942.7–7726AB would be classed as a chance alignment and not a physical binary system. However, this criterion is implicitly valid only for the large proper motions found in LSPM-North (where  $\sigma_\mu \ll \mu$ ). For the above values of  $\Delta\theta$  and  $\mu$ ,  $\Delta\mu$  would need to be  $< 0.05 \text{ mas yr}^{-1}$  to satisfy Equation 4.1. The PPMXL proper motion errors are too large to draw a useful conclusion from this test.

Matters are more difficult when considering young, dispersed populations, whose members are all expected to lie at similar distances, with similar kinematics and ages. The confirmation of most wide binaries therefore usually involves calculating the probability of a chance alignment (e.g. Dhital et al. 2010; Luhman et al. 2009b; Kraus & Hillenbrand 2007b). Ignoring the obvious youth of 2MASS J0942–7727 and RX J0942.7–7726 for the time being, to quantify the probability that they are the coincidental alignment of two unrelated stars we considered the  $\sim 2.5 \times 10^5$  cross matched 2MASS/DENIS stars within 3 deg of their location. We wish to know the average separation of two stars ‘similar’ to RX J0942.7–7726 and 2MASS J0942–7727. If this is significantly larger than 42" then it is likely that RX J0942.7–7726AB is a true binary system.

To this end we selected the 1599 stars in a band  $\pm 1$  mag around both stars in the field colour-magnitude diagram (Figure 4.4, top-left) with  $(i_{\text{DENIS}} - J_{\text{2MASS}}) > 1$ . The sample was cross-matched against PPMXL, keeping the 819 stars with proper motions within  $20 \text{ mas yr}^{-1}$  of the mean proper motion of RX J0942.7–7726AB;  $(-21, +19) \pm (5, 5) \text{ mas yr}^{-1}$  (Figure 4.4, top-right). These constraints define a sample of photometrically and astrometrically ‘similar’ stars to RX J0942.7–7726 and 2MASS J0942–7727. Their spatial distribution is shown in the bottom-left panel of Figure 4.4. The increased density of sources towards the north-east is due to the lower Galactic latitudes in that region and an excess of sources with colours  $1 < (i - J) < 1.5$ . These are likely background stars reddened by the dusty material in the quadrant, which is visible in IRAS images (see Figures 1.8 and 2.2).

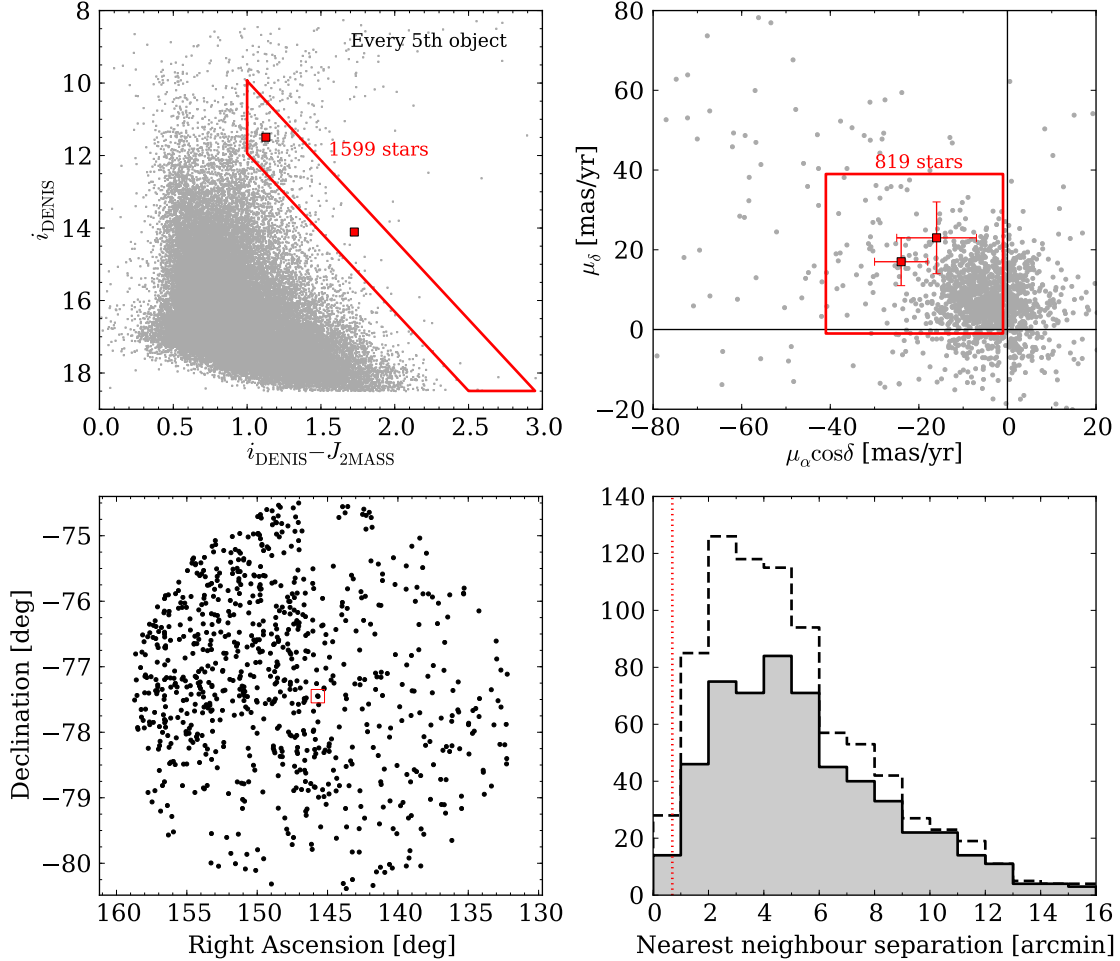


**Figure 4.4** *Top panels:* Colour-magnitude and proper motion selection of ‘similar’ stars to RX J0942.7–7726AB (red squares, see text). *Bottom-left panel:* Spatial distribution of the 819 remaining stars used in the chance alignment calculation. RX J0942.7–7726AB is marked by the red square. *Bottom-right panel:* Nearest neighbour separation of all stars (dashed line) and after correction for isolated pairs (solid fill). The red dotted line marks the 42'' separation of RX J0942.7–7726AB.

The bottom-right panel of Figure 4.4 depicts the separation of each of the 819 stars and its nearest neighbour. The dashed line shows the full sample, while the solid bars are corrected for duplicate values due to isolated pairs (where  $d_{AB} = d_{BA}$ ). If the original sample was wholly constructed of isolated pairs the corrected sample would be half the size. There is a broad maximum in both distributions around 2–5' separation. Of the 567 *unique* nearest-neighbour distances only four are less than 42'', the separation of RX J0942.7–7726AB. This implies that the chance alignment probability of RX J0942.7–7726 and 2MASS J0942–7727 is only  $P(d < 42'') = 4/567 = 0.7 \pm 0.4$  percent (Poisson error). This value agrees with the probability found from a uniform distribution of 819 stars over a 3 deg radius field (again correcting for isolated pairs),  $P(d < 42'') = 0.9 \pm 0.4$  percent, where the error was estimated from multiple random realisations.

Combined with the fact that both stars have *strong* lithium absorption and H $\alpha$  emission, these results show it is virtually impossible for RX J0942.7–7726AB to be the coincidental alignment of two unrelated young M-dwarfs. To confirm binarity requires showing that RX J0942.7–7726 and 2MASS J0942–7727 are coeval, lie at the same distance and have kinematics that agree within errors and the (small) differences expected from orbital motion.

### 4.3. Spectral types and reddening

The reddening towards RX J0942.7–7726AB is currently ill-constrained. Assuming an M0 spectral type, Alcala et al. (1997) used the  $(V - I_C)$  colour of RX J0942.7–7726 to derive a reddening to the star of  $E(B - V) = 0.27$  mag. Sartori et al. (2003) found a slightly lower value,  $E(B - V) = 0.17$  mag, from comparison to updated model atmosphere colours by Bessell et al. (1998), again assuming an M0 spectral type. In Murphy et al. (2010) (see also Chapter 2) we estimated the reddening towards 2MASS J0942–7727 to be  $<0.1$  mag from the 2.3-m/DBS synthetic  $(R - I)_C$  colour. The Schlegel et al. (1998) dust maps provide an upper limit to the reddening along the line of sight to RX J0942.7–7726AB—this is  $E(B - V) = 0.34$  mag.

#### 4.3.1. Observations

To obtain a robust reddening towards the system we took spectra of RX J0942.7–7726 and 2MASS J0942–7727 with *WiFeS* on the ANU 2.3-m during 2011 July. The R3000 grating and RT560 dichroic yielded a spectral resolution of  $R = 3000$  with wavelength coverage from 5300–9600 Å. We did not use the blue-arm spectra, which cover 3200–5900 Å. Because *WiFeS* is an integral-field spectrograph, care was taken to align each star on the same image slices to ensure accurate flux calibration. The frames were reduced in a similar manner to that described in §2.3 and §2.4. After flat-fielding against a quartz-iodine lamp, extraction and wavelength calibration, each spectrum was corrected for telluric absorption using a contemporaneous observation of the DC white dwarf EG 131 (after Bessell 1999). Prior to forming the telluric spectrum, the weak H $\alpha$  and He I  $\lambda 5876$  stellar lines were removed from the otherwise featureless white dwarf spectrum. The spectra were finally flux calibrated to remove the remaining instrumental effects, again using EG 131 as a flux standard<sup>1</sup>. *WiFeS* R3000 spectra of RX J0942.7–7726 and 2MASS J0942–7727 are plotted in Figure 4.5 with  $\eta$  Cha members for comparison from Lyo et al. (2004a).

#### 4.3.2. RX J0942.7–7726

To determine a spectral type for RX J0942.7–7726 we compared its flux-calibrated spectrum to the SDSS M-dwarf template spectra of Bochanski et al. (2007) and the  $\eta$  Cha members observed by Lyo et al. (2004a). A visual comparison immediately showed the putative M0 spectral type was a poor match to the observed spectrum, irrespective of the assumed reddening to the star. The M1 SDSS template and the M1.3  $\eta$  Cha member RECX 4 both gave excellent matches (see Figure 4.5). We tried de-reddening the observed spectrum following the extinction law of Cardelli et al. (1989) but in all cases it was best fitted by the M1 templates and negligible reddening,  $E(B - V) < 0.05$  mag.

The broad-band photometry of Alcala et al. (1995) and Padgett et al. (2006) also suggest little or no reddening when compared to the average M1 colours of Bessell (1991). The previous M0 spectral type gave inconsistent redshifts of  $-0.02 < E(B - V) < +0.17$  mag, depending on the colour index used. In light of these updated observations, we reclassify RX J0942.7–7726 as an M1 star with negligible reddening.

---

<sup>1</sup>Fluxed spectrum available at <http://www.mso.anu.edu.au/~bessell/FTP/Spectrophotometry/>

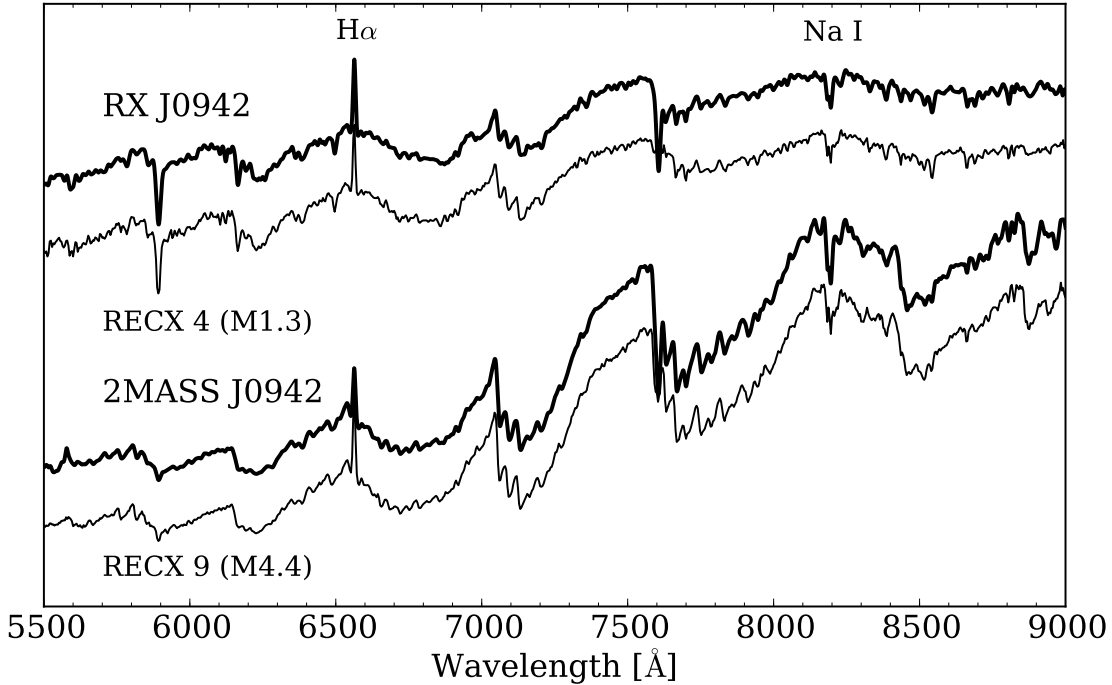


**Figure 4.5** *WiFeS* R3000 spectra of RX J0942.7–7726 and 2MASS J0942–7727. Shown for comparison are two members of  $\eta$  Cha, as observed by Lyo et al. (2004a); RECX 4 (M1.3) and RECX 9 (M4.4). All the spectra have been normalised at 7500 Å. The *WiFeS* spectra are smoothed to the same resolution as the Lyo et al. observations.

#### 4.3.3. 2MASS J0942–7727

The only previous spectral type for 2MASS J0942–7727 (M4.6), was determined by us (Murphy et al. 2010, Chapter 2) solely from  $(R - I)_C$  synthetic photometry. As described in Chapter 3, the emergence of molecular bands in the spectra of M-dwarfs enable a spectral type determination that can be effectively reddening-independent. To obtain a spectral type for 2MASS J0942–7727 we adopted the selection of molecular indices from Riddick et al. (2007) listed in Chapter 3. These are generally valid for determining spectral types later than M2–3. The seven indices gave an average spectral type of  $M4.6 \pm 0.2$ . The agreement between this and the spectral type derived from synthetic photometry immediately suggests any reddening towards 2MASS J0942–7727 must be small.

Indeed, visual comparison of 2MASS J0942–7727 to the M4.4  $\eta$  Cha member RECX 9 (Lyo et al. 2004a) shows an excellent match (Figure 4.5), with an upper limit for the reddening of  $E(B - V) \lesssim 0.05\text{--}0.1$  mag. 2MASS J0942–7727 appears to have a spectral type earlier than both ECHA J0841.5–7853 (M4.7) and the M5 SDSS standard (Bochanski et al. 2007), but demonstrably later than the M4 standard, regardless of reddening.

Finally, we computed synthetic photometry on the *WiFeS* spectrum using the passbands of Bessell (2005) and the absolute calibrations of Bessell et al. (1998). This gave  $(R - I)_C = 1.85$  and a spectral type of M4.8, based on the transformation of Bessell (1991). An M4.6 star has an intrinsic colour of  $(R - I)_C \approx 1.80$ , again confirming that any reddening towards 2MASS J0942–7727 must be small. The new colour agrees with the one derived from the DBS spectrum in Table 2.2 ( $1.80 \pm 0.03$ ). The literature colours of EG 131 (Koen et al. 2010) and RX J0942.7–7726 also agree with the synthetic colours to within 0.03 mag, which we adopt as the error on our photometry.

From the molecular indices and synthetic photometry we confirm that 2MASS J0942–7727 has a spectral type of  $\sim$ M4.5 and like RX J0942.7–7726, lies along a line of sight with negligible reddening. We estimate a spectral type uncertainty of  $\pm 0.3$  subclasses for both stars. This includes any residual reddening, photometric and flux calibration errors, and variation in the colour-spectral type conversions.

#### 4.3.4. Reddening in Chamaeleon

Negligible reddening towards RX J0942.7–7726AB is consistent with the study of Knude & Hog (1998), who estimated the reddening in the Chamaeleon region as a function of distance using *Hipparcos* data. While RX J0942.7–7726AB lies just outside their surveyed area, they found that the reddening within 150 pc is small ( $\lesssim 0.1$  mag) but increases by a factor of four at the distance of the clouds (160–200 pc). This is consistent with an *integrated* reddening of  $E(B - V) = 0.34$  mag towards RX J0942.7–7726AB from dust maps (Schlegel et al. 1998). Similar results were presented by Whittet et al. (1997). Furthermore, the position of RX J0942.7–7726AB in the 2MASS two-colour diagram (Figure 4.3) does not support large reddenings. Based on their photometry and that of (unreddened)  $\eta$  Cha members we again confirm  $E(B - V) \lesssim 0.1$  mag as an upper limit on the reddening to the system.

### 4.4. Age of RX J0942.7–7726AB

We noted in Chapter 2 that 2MASS J0942–7727 and RX J0942.7–7726 appeared to be slightly older than the  $\eta$  Cha cluster. This was based on their smaller than expected Li I  $\lambda 6708$  equivalent widths and the more dwarf-like gravity of 2MASS J0942–7727 when compared to  $\eta$  Cha members. Obtaining a robust estimate of their ages (and demonstrating their coevality) is crucial in confirming the true binary nature of RX J0942.7–7726AB.

Comparison of stars in a Hertzsprung-Russell diagram to empirical or model isochrones is one of the most commonly used pre-main sequence age indicators. Age is degenerate with distance in this diagram however, so in the absence of accurate trigonometric parallaxes for RX J0942.7–7726AB the derived age is a function of distance. For example, in the colour-magnitude diagram of Figure 4.3, the stars are well characterised by a 40 Myr Baraffe et al. (1998) isochrone at a distance of 90 pc. However, they could be equally well-fitted by a 20 Myr isochrone at 120 pc, or a 100 Myr isochrone at 65 pc. Luckily, there are several distance-independent age indicators, described below, which may be used to constrain the age of RX J0942.7–7726AB, and in turn, its distance and kinematics.

#### 4.4.1. Low-gravity features

As described in §2.3.2, the strength of the Na I  $\lambda 8183/8195$  doublet is highly dependent on surface gravity in M-type stars. It can therefore be used as an age proxy for stars contracting towards their main sequence radii. Lawson et al. (2009) used Na I doublet strengths to rank the ages of several young associations in the solar neighbourhood at an age resolution of 1–2 Myr. While there is some scatter in the gravity indices for each association, the mean trends (Figure 4.6) agree completely with the isochronal age ranking of the groups.

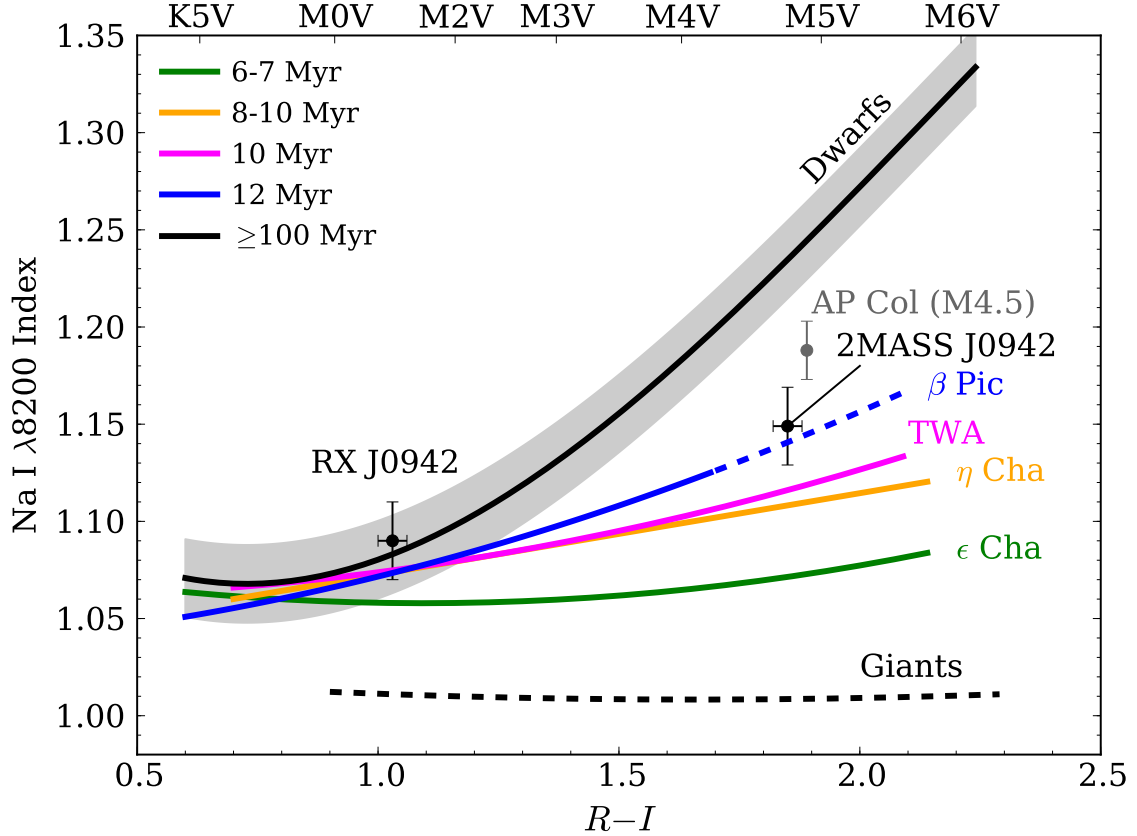


**Figure 4.6** Mean  $\text{Na I } \lambda 8200$  indices for RX J0942.7–7726AB and members of young local associations from Lawson et al. (2009), compared to field dwarf and giant loci. The recently discovered  $\sim 40$  Myr-old Argus member AP Col (Riedel et al. 2011) is also plotted. 2MASS J0942–7727 has a similar intermediate gravity, suggestive of an age around 12 Myr. Errors were estimated from differences in the telluric correction, smoothing, and multiple observations (in the case of 2MASS J0942–7727 and AP Col). The scatter around each mean trend is similar to that seen in the field dwarfs (shaded region).

To place RX J0942.7–7726AB in Figure 4.6 we computed the same  $\text{Na I}$  index,  $\int F_{8148-8172} / \int F_{8176-8200}$ , after smoothing the *WiFeS* spectra to the  $R \approx 800$  resolution of the Lawson et al. data and resampling to the same wavelength scale. As expected for an M1 star, RX J0942.7–7726 is not discernible from older field dwarfs in this diagram. In contrast, 2MASS J0942–7727 has a gravity index between the dwarfs and  $\eta$  Cha, consistent with an age equal or greater than that of the  $\beta$  Pictoris Association ( $\sim 12$  Myr, Torres et al. 2008). We estimate an approximate upper age limit for 2MASS J0942–7727 in this diagram of 40–50 Myr by comparing the star to AP Col, a recently identified, nearby (8.4 pc) member of the Argus/IC 2391 Association (Riedel et al. 2011). Both stars have similar spectral types ( $\sim \text{M4.5}$ ) but AP Col has the stronger doublet strength, indicative of a slightly older age. This has been well-established as 40–50 Myr through a variety of methods, including HR-diagram placement, lithium depletion and accurate kinematics.

#### 4.4.2. Lithium measurements

The amount of lithium depletion in low-mass stars can serve as a mass-dependent clock (see §2.4.1). We plot in Figure 4.7  $\text{Li I } \lambda 6708$  equivalent widths (EW) for 110 K and M-dwarfs from the high-resolution study of da Silva et al. (2009), who investigated lithium

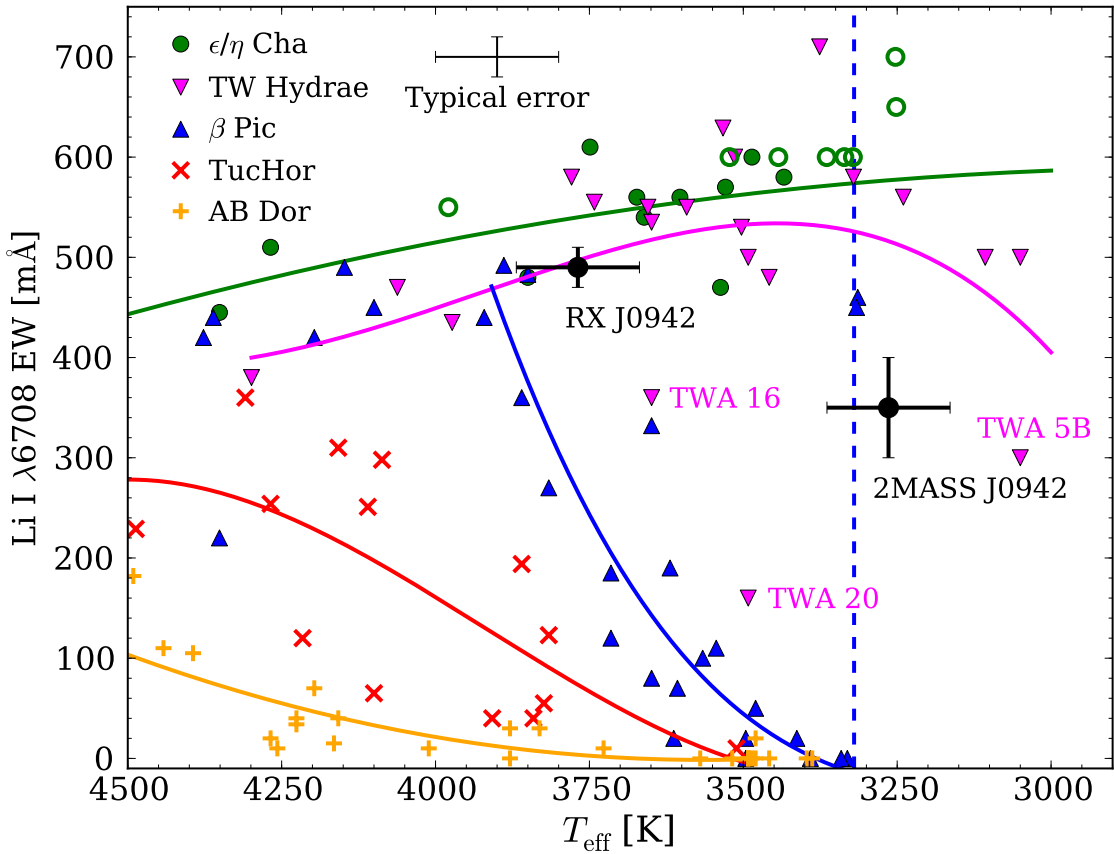


**Figure 4.7** Lithium equivalent widths of RX J0942.7–7726AB compared to other young associations from da Silva et al. (2009);  $\eta/\epsilon$  Cha (5–10 Myr), TW Hydreae (8–10 Myr),  $\beta$  Pic (~12 Myr), Tucana-Horologium (~30 Myr) and AB Doradus (70–120 Myr). Open symbols are the new  $\eta$  Cha candidates from Chapter 2. Low-order polynomial fits are shown for each association. The dashed line is the  $\beta$  Pic lithium depletion boundary.

depletion in many of the recently-identified young associations reviewed by Torres et al. (2008). A similar sample and diagram was presented by Mentuch et al. (2008). Equivalent widths for RX J0942.7–7726AB are plotted, with the high-resolution value of Covino et al. (1997) ( $\text{EW} = 490 \pm 15$  mÅ) used for RX J0942.7–7726. Following the work of da Silva et al., effective temperatures were estimated from  $(V - I_C)$  (RX J0942.7–7726) and  $(R - I)_C$  (2MASS J0942–7727) colours and the transformation of Kenyon & Hartmann (1995), who adopted the temperature scales of Schmidt-Kaler (1982) and Straižys (1992). Comparison in the observed colour space is not possible since neither da Silva et al. (2009) nor Torres et al. (2008) tabulated the  $(V - I_C)$  colours of their full sample. We note that over the early-M spectral types the Kenyon & Hartmann scale yields temperatures that are 100–250 K hotter than those presented by Bessell (1991). While improved contemporary M-dwarf temperature scales exist in the literature (e.g. Casagrande et al. 2008; Luhman et al. 2003), for consistency with the da Silva et al. sample we adopt the Kenyon & Hartmann (1995) scale. The exact choice of transformation used in Figure 4.7 is unimportant as we are interested only in *relative* ages. However, care must be taken to choose an appropriate, modern  $T_{\text{eff}}$  scale when deriving bolometric corrections and estimating *absolute* ages from model isochrones.

RX J0942.7–7726 has a Li I  $\lambda 6708$  EW consistent with the 8–10 Myr-old TW Hydreae Association, some of whose late-type members have already begun to show significant depletion. We discuss the three TWA members with  $T_{\text{eff}} < 3700$  K and  $\text{EW} < 400$  mÅ (TWA 16, 20 and

5B) briefly below. TWA 16 is among the group of members proposed by Zuckerman et al. (2001c) (TWA 14–19) that lie south of TW Hya near the A0 member HR 4796 (TWA 11A). By comparing photometric rotational periods, Lawson & Crause (2005) claimed TWA 14–19 are in fact background members of the LCC subgroup of Sco-Cen (although they did not directly observe TWA 16). TWA 20 was originally proposed as a member by Reid (2003), but later rejected by Song et al. (2003) and Zuckerman & Song (2004) based on its low lithium EW. The star is also a suspected spectroscopic binary (Jayawardhana et al. 2006). Mamajek (2005a) and Torres et al. (2008) have computed kinematic distances to TWA 16 and TWA 20. Compared to the 90–110 pc distance to the inner edge of LCC, the ~70 pc distance to the stars means both are very likely true TWA members<sup>2</sup>. TWA 5B is a confirmed member with a distance of 45 pc (Mamajek 2005a). The accelerated lithium depletion seen in these three stars is likely related to surface activity or rotation (see discussion in §2.4.1). In particular, TWA 20 has a  $v \sin i$  of 30 km s<sup>-1</sup> (da Silva et al. 2009). Only two TWA members (TWA 5A and the early-type TWA 11A) have larger measured rotational velocities.

Lithium depletion is already well advanced in the ~12 Myr  $\beta$  Pictoris Association, with a steep decline in equivalent widths down to the lithium depletion boundary (LDB, dashed blue line). RX J0942.7–7726 is not as depleted as the early-M type members of  $\beta$  Pic. We therefore estimate an upper age limit of ~12 Myr from Figure 4.7. Lithium ages for single stars must be interpreted with caution however, as star-to-star variations within an association (see above) can imply vastly different ages for a coeval population.

Like RX J0942.7–7726, 2MASS J0942–7727 also has a level of lithium depletion consistent with a TWA-like age, and appears older in this diagram than  $\eta$  Cha and  $e$  Cha members. The star lies redward of the  $\beta$  Pic LDB so we cannot use  $\beta$  Pic to constrain its age. Jeffries & Oliveira (2005) determined that the LDB of the  $35 \pm 3$  Myr-old open cluster NGC 2547 falls at  $(R - I)_C = 1.77 \pm 0.03$ <sup>3</sup>. 2MASS J0942–7727 ( $R - I = 1.85$ ) lies between this LDB and that of the young cluster IC 2391, which Barrado y Navascués et al. (2004) found to be slightly redward of the star, at  $(R - I)_C \approx 1.90$  (spectral type ~M5, around 3200 K in Figure 4.7). The detection of significant lithium absorption in 2MASS J0942–7727 implies it must be younger than the lithium age of IC 2391, which both Barrado y Navascués et al. (2004) and Jeffries & Oliveira (2005) find to be 50 Myr, with an uncertainty of 3–5 Myr.

#### 4.4.3. Activity: X-ray emission, H $\alpha$ , variability and rotation

Young, low-mass stars are known to possess active coronae and chromospheres, which are responsible for the copious X-ray emission, continuum and line emission (in particular H $\alpha$  and Ca II H&K) and flares commonly seen in such objects. These characteristics are manifestations of the fast rotation rates and strong magnetic fields typical in pre–main sequence stars (see Zuckerman & Song 2004; Feigelson & Montmerle 1999, and references

<sup>2</sup>As noted by Torres et al. (2008), the possibly binarity of TWA 20 may influence the radial velocity and kinematic distance. Mamajek (2005a) confirmed TWA 17,18 and 19 as background LCC members, in addition to TWA 12 and TWA 24. Given its right ascension, TWA 14 is a borderline case. (see their Figure 3).

<sup>3</sup>Jeffries & Oliveira (2005) rightly point out that because of the uncertainties in transforming colours to temperatures and inconsistencies between various model temperatures, it is better to calculate the luminosity or absolute magnitude of the LDB. Without an accurate distance to RX J0942.7–7726AB however we are left with only colour (or temperature) information.

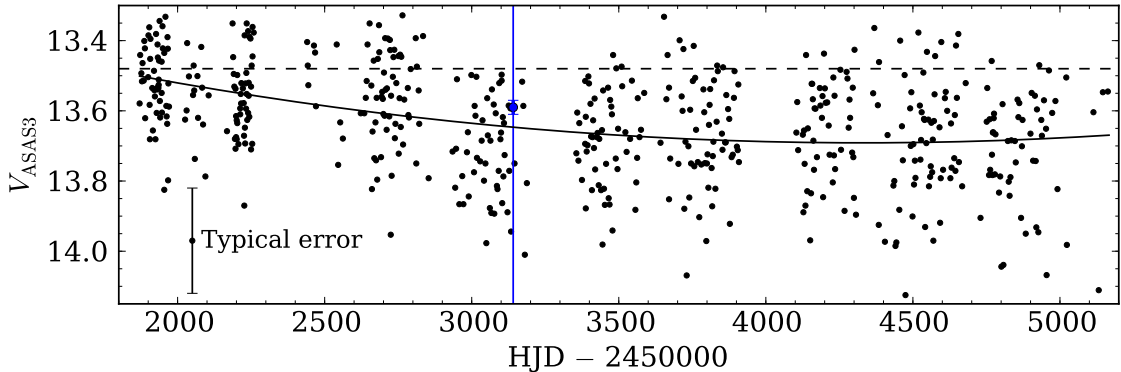


**Figure 4.8** ASAS3  $V$ -band light curve for RX J0942.7–7726. Single-epoch measurements by Padgett et al. (2006) ( $13.59 \pm 0.02$ , blue line) and Alcalá et al. (1995) ( $13.48 \pm 0.01$ , dashed line, pre-ASAS3) are also shown. Photometric errors from the 8 cm ASAS3 telescopes are large ( $\sim 0.15$  mag) at these magnitudes. The solid line is a quadratic fit to the data.

therein). Unfortunately, M-dwarfs have a long adolescence, with enhanced chromospheric and coronal activity that can last for many Gyr (Fleming et al. 1995; Hawley et al. 1996). The diagnostics below are therefore *necessary* but *insufficient* indicators of youth.

X-ray emission from RX J0942.7–7726<sup>4</sup> was identified from *ROSAT* observations by Alcalá et al. (1995) and later characterised by Alcalá et al. (1997). They found a saturated ratio of X-ray to bolometric luminosity typical for young, low-mass stars,  $\log(L_X/L_{\text{bol}}) = -2.66 \pm 0.18$ . No X-rays have yet been detected from 2MASS J0942–7727, though as we demonstrated in §2.5.1, an M4.5 star would need to lie within  $\sim 30$  pc (10 Myr) or  $\sim 20$  pc (40 Myr) to have been detected by the *ROSAT* All-Sky Survey<sup>5</sup>. As mentioned above, old field M-dwarfs can also possess similar levels of X-ray emission, around the coronal saturation of  $\log(L_X/L_{\text{bol}}) \approx -3$ .

Both stars exhibited weak  $H\alpha$  emission throughout the *WiFeS* observations (Table 2.3). No emission variability was detected within the measurement uncertainties on timescales of days to months. The low levels of emission detected ( $|EW| \leq 7$  Å) are the result of quiescent chromospheric activity, not flares or accretion from a circumstellar disk, which are characterised by strong, variable emission (see Chapter 3).

RX J0942.7–7726 has been monitored as part of the ASAS3 photometric survey<sup>6</sup> (Pojmanski 2002). We plot in Figure 4.8 the 2002–2010  $V$ -band light curve. Despite the large photometric errors (0.15 mag near the limit of the survey) washing out any rotationally-modulated short-term variations, a small ( $\sim 0.2$  mag) long-term trend can be seen. This is also reflected in the significant difference between  $V$  magnitudes reported by Padgett et al. (2006) ( $13.59 \pm 0.02$ ) and Alcalá et al. (1995) ( $13.48 \pm 0.01$ ). Recent work (e.g. Messina et al. 2010; Buccino et al. 2011) shows that such long-term variability may be common in low-mass stars.

Finally, the rotation of a star ( $v \sin i$ ) may be used as a crude clock, as young stars are expected to rotate rapidly and spin-down as they age. From their echelle spectrum, Covino et al. (1997) measured a  $v \sin i$  of  $9 \pm 3$  km s<sup>−1</sup> for RX J0942.7–7726. In a sample of 123 M-dwarfs,

<sup>4</sup> Also cross-identified in the *ROSAT* Faint Source Catalogue as 1RXS J094240.7–772637 (Voges et al. 2000)

<sup>5</sup> Given the uncertainty in the X-ray position (see Figure 4.2), it is possible *ROSAT* detected emission from both RX J0942.7–7726 and 2MASS J0942–7727. In the absence of flares however, its flux-limited survey (and the distance arguments above) suggests it more likely observed only the brighter M1 primary.

<sup>6</sup> All Sky Automated Survey: <http://www.astroww.edu.pl/asas/>

Browning et al. (2010) found only seven stars rotating more rapidly than their detection threshold of  $v \sin i \approx 2.5 \text{ km s}^{-1}$ . They estimated less than 10 percent of early-M stars are detectably rotating (see also Jenkins et al. 2009). While gyro-chronology relations exist for solar-type stars (e.g. Mamajek & Hillenbrand 2008), none have been developed for late-type stars. Nevertheless, the detection of significant rotation in RX J0942.7–7726 is yet more (albeit qualitative) evidence of its youth.

#### 4.4.4. Infrared observations

RX J0942.7–7726 was observed as part of the *Spitzer Space Telescope* Cores to Disks (c2d) programme (Padgett et al. 2006; Wahhaj et al. 2010). *Spitzer* photometry, combined with 2MASS and optical VRI data, showed no excess emission above photospheric levels out to  $30 \mu\text{m}$ , which would otherwise indicate the presence of a dusty disk. Similarly, both stars show no excess emission out to  $22 \mu\text{m}$  in the WISE Preliminary Data Release (see Chapter 3). This generally implies an age greater than 5–10 Myr, the time by which almost all inner disks are observed to have dissipated (Haisch et al. 2001; Hernández et al. 2008).

#### 4.4.5. Age of the system

The two most quantitative age indicators—surface gravity and lithium absorption—yield a consistent age for both stars of around 8–12 Myr. While the gravity index of Figure 4.6 cannot constrain the age of RX J0942.7–7726 (and hence the coevality of the system), the star’s position in Figure 4.7 restricts its age to  $\lesssim 12 \text{ Myr}$ . The lithium data for 2MASS J0942–7727 is also consistent with this value, which agrees with the gravity-derived age of the star. None of the other, more qualitative age indicators (X-ray and H $\alpha$  emission, measurable rotation, lack of IR excess) contradict these estimates. On balance, we conclude that RX J0942.7–7726AB are a pair of coeval pre–main sequence stars with an approximate age of 8–12 Myr. Their exact age and origin must await consideration of their kinematics.

### 4.5. Distance and kinematics

Distances to pre–main sequence stars without trigonometric parallaxes are generally estimated either by comparison to empirical or model isochrones via the distance modulus, or some sort of kinematic distance estimate (sometimes called a statistical or moving-cluster parallax) based on the proper motion and/or radial velocity of the star.

To estimate the distance to RX J0942.7–7726AB, we first used the theoretical pre–main sequence isochrones of Baraffe et al. (1998) and Siess et al. (2000), after transforming them to the observed ( $i_{\text{DENIS}}, i - J_{\text{2MASS}}$ ) colour-magnitude space (see Appendix A). Distances were found by minimising the square of the residuals between the isochrone and the observed photometry. For the Baraffe et al. (1998) models, the estimated distances ranged from 121–250 pc, depending on the adopted age (20–5 Myr). The Siess et al. (2000) isochrones gave significantly smaller distances, 99–176 pc for the same range of ages<sup>7</sup>. Both stars appeared

<sup>7</sup>Lawson & Feigelson (2001) found that the Baraffe et al. models were less consistent with observations of the  $\sim 8 \text{ Myr } \eta \text{ Cha cluster}$  than the Siess et al. models. This is likely due to missing opacity sources at wavelengths less than  $1 \mu\text{m}$  giving incorrect synthetic fluxes for models cooler than  $T_{\text{eff}} \approx 3700 \text{ K}$  (Baraffe et al. 1998).

to be co-distant in each set of models. In the extreme case, an age of 1 Myr (100 Myr) yielded distances of 570 pc and 400 pc (65 pc and 35 pc), respectively. Such extreme ages are all but ruled out by the spectroscopic indicators. Furthermore, the low reddening to the system restricts its distance to within 150–200 pc (see §4.3.4). Reddening the isochrones by the maximum allowable  $E(B - V) = 0.1$  increased the derived distances by 5–15 percent, depending on the models and age.

#### 4.5.1. Orbital motion

Assuming circular orbits, the orbital velocity of a star in a binary system is related to the separation of the stars  $a$  and their masses by:

$$v_1 = \sqrt{\frac{M_2^2 G}{(M_1 + M_2)a}} \quad (4.3)$$

The models of Siess et al. (2000) realise a mass of  $0.5 M_\odot$  for RX J0942.7–7726 and  $0.2 M_\odot$  for 2MASS J0942–7727 (from broad-band colours and an age of 10 Myr). If we assume that the physical separation of the stars is close to their angular separation of 4200 AU ( $42''$  at 100 pc), the orbital period is  $\sim 325,000$  years and 2MASS J0942–7727 has an orbital velocity of  $\sim 0.3 \text{ km s}^{-1}$ . The Baraffe et al. (1998) models give similar results, with masses of  $0.95 M_\odot$  and  $0.05 M_\odot$ , respectively. Statistically, the orbital semi-major axis is likely to be slightly larger than the projected separation, yielding an even longer period and smaller orbital velocity (Fischer & Marcy 1992). A change in relative velocity of even  $\sim 1 \text{ km s}^{-1}$  would be enough to perturb 2MASS J0942–7727 out of such a wide orbit. To have avoided disruption, RX J0942.7–7726AB must therefore have been born in a quiescent dynamical environment and never interacted closely with other stars over its short lifetime. Such reasoning is confirmed by  $N$ -body simulations. For instance, Kroupa (1998) found binary systems with periods around  $10^8$  days ( $3 \times 10^5$  yr) that survive the dissolution of a young cluster will have been bestowed a velocity of *at most*  $1\text{--}2 \text{ km s}^{-1}$ , independent of the cluster density. Velocities above this limit would result in disruption.

#### 4.5.2. Space motion

Having estimated a distance to the system, its heliocentric  $UVW$  space motion can be determined. Plotted in Figure 4.9 are the velocities derived for RX J0942.7–7726AB from 5–20 Myr isochronal distances and the weighted average PPMXL proper motion ( $-21, +19 \pm (5, 5) \text{ mas yr}^{-1}$ ) and *WiFeS* radial velocity ( $19.9 \pm 0.5 \text{ km s}^{-1}$ ). Error bars on the velocities correspond to uncertainties in the observed proper motion and radial velocity at each distance. Figure 4.9 clearly shows that, irrespective of the assumed distance (age) to the stars or the model isochrones, the space motions do not agree with any of the known young kinematic groups in the solar neighbourhood. This is perhaps not surprising after considering the location of the system. Ruling out membership in any of the nearby Chamaeleon groups ( $\eta$  Cha,  $\epsilon$  Cha, Cha I, II) due to their younger ages, only the TW Hydrae and  $\beta$  Pictoris Associations have ages congruent with RX J0942.7–7726AB ( $\sim 8\text{--}12$  Myr). However, the system lies many tens of degrees on the sky from the main concentration of either group,

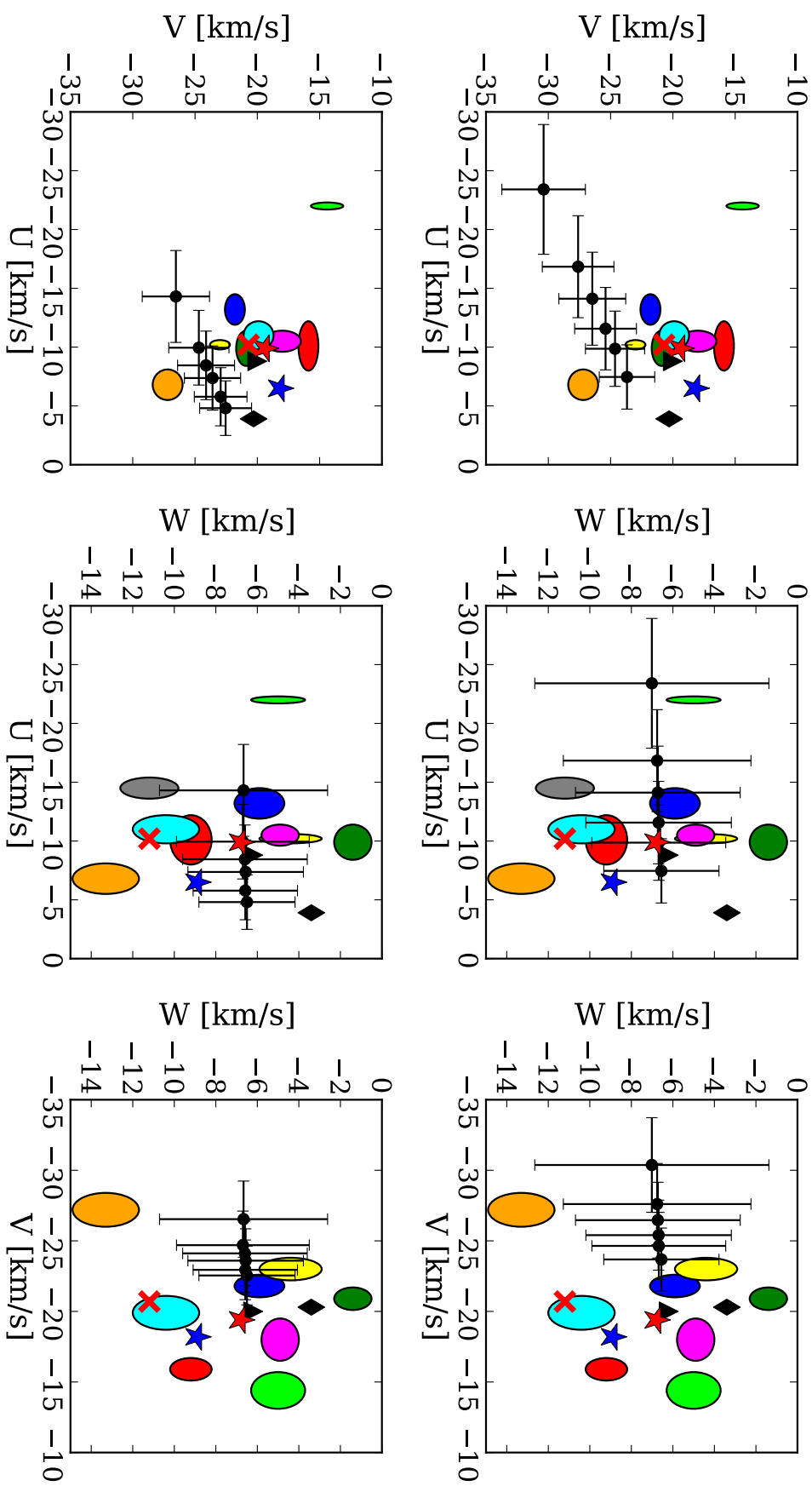


**Figure 4.9** UVW space velocities for RX J0942.7–7726AB. Distances are derived from (left to right) 5, 8, 10, 12, 16 and 20 Myr Baraffe et al. (1998) (top) and Siess et al. (2000) (bottom) unreddened isochrones. Ellipses show the mean velocities and dispersions of young associations from Torres et al. (2008) – Argus (light green), Columba (blue), Tucana-Horologium (green), TW Hydrae (magenta), Carina (yellow), Octans (grey),  $\epsilon$  Cha (cyan),  $\beta$  Pictoris (red) and AB Doradus (orange). Also plotted are the mean velocities of the LCC (triangle) and UCL (diamond) Sco-Cen subgroups (Mamajek et al. 2000),  $\eta$  Cha (red cross; §2.6.2), Cha I (blue star) and Cha II (red star; E. Mamajek, private communication).

**Table 4.1** Results of dynamical simulations for RX J0942.7–7726AB and nearby associations

Association	RX J0942.7–7726AB				RX J0942.7–7726 only			
	$\Delta UVW_{\min}$ km s <sup>-1</sup>	$v_{\text{eject}}$ km s <sup>-1</sup>	$t_{\text{eject}}$ Myr	$d_0$ pc	$\Delta UVW_{\min}$ km s <sup>-1</sup>	$v_{\text{eject}}$ km s <sup>-1</sup>	$t_{\text{eject}}$ Myr	$d_0$ pc
TW Hydrae	2.5	7.1	−13.0	114	1.6	8.7	−10.0	111
$\beta$ Pictoris	... <sup>†</sup>	...	...	...	2.0	8.5	−11.25	106
LCC	3.4	4.0	−20.0	131	3.5	5.6	−12.0	135
UCL	1.0	8.1	−15.25	127	1.6	10.3	−11.75	132

<sup>†</sup>  $\Delta(UVW)$  exceeds the expected velocity error at all distances and times

and at a much greater distance. Given the fragile orbital configuration and the dearth of high-density regions and/or high-mass stars in TWA or  $\beta$  Pic to power any interactions, it is implausible RX J0942.7–7726AB was ejected from either of the groups early in its evolution.

Alternatively, we note that RX J0942.7–7726AB has a similar age, distance and lies adjacent to the nearby Lower Centaurus Crux subgroup of Sco-Cen (see Figure 4.1), whose southern extent may be as young as 11–12 Myr (Preibisch & Mamajek 2008). However, the space motion of the system in Figure 4.9 also does not agree with that previously determined for the subgroup (filled triangle), so it is possible that some sort of ejection process may be at work. As emphasised above, the dynamical impulse provided to RX J0942.7–7726AB would need to be sedate ( $\lesssim 1$  km s<sup>-1</sup>) to avoid breaking the fragile binary. In addition to N-body interactions, this could also be provided by bulk turbulent motions in the primordial molecular cloud, which we explore further in §4.6.1.

To test the ejection hypothesis and obtain kinematic distances and ejection velocities, we performed further trace-back simulations, following the epicyclic method described in §2.6. The simulations were computed over the same range of current distances ( $50 < d/\text{pc} < 150$ ), but a larger range of trace-back times,  $−20 < t/\text{Myr} < 0$ . We used the present-day mean velocities and positions of TW Hydrae and  $\beta$  Pic from Torres et al. (2008) and those of the LCC and UCL Sco-Cen subgroups from Mamajek et al. (2000)<sup>8</sup>. Because the proper motion and radial velocity of RX J0942.7–7726 dominate the weighted average of the pair, we ran the simulations for both the average values and those of RX J0942.7–7726 alone. The results are plotted in Figures 4.11 and 4.10 and summarised in Table 4.1.

For TW Hydrae and  $\beta$  Pic, the simulations reveal RX J0942.7–7726AB could have been ejected at a time roughly coincident with the groups' reported ages. However, Table 4.1 shows that this would require a 7–9 km s<sup>-1</sup> change in velocity at birth to move the system to its current location. Such velocities are absolutely excluded by the fragile orbital configuration, again confirming the implausibility of such a scenario. The simulations gave similar results for LCC and UCL, although the former only required a 4–5 km s<sup>-1</sup> velocity kick (but with  $\Delta UVW \approx 3.5$  km s<sup>-1</sup>). In the next section we examine in greater detail the role of Sco-Cen in the birth of RX J0942.7–7726AB and compare the system to other wide binaries associated with young kinematic groups in the solar neighbourhood.

<sup>8</sup>Unlike  $\eta$  Cha, which can be considered a point source, the other young groups have considerable three-dimensional extent ( $\sigma_{XYZ} \approx 10\text{--}50$  pc). The simulations assume the mean position and velocity of the association is representative of the ejection point and can be used to trace the group back in time. Ejection from a position other than the centre of the group would necessarily change the implied velocity, distance and ejection time.

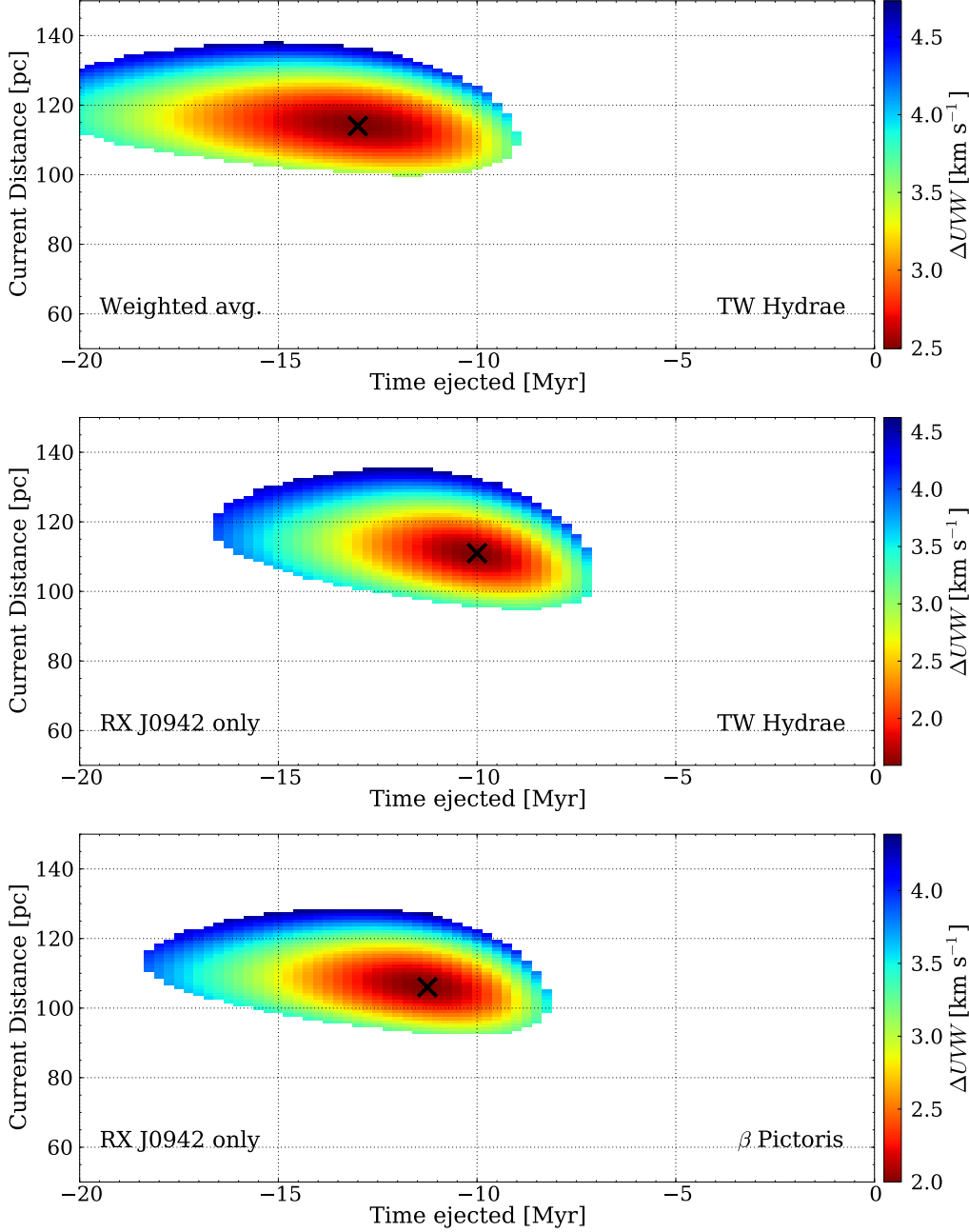


**Figure 4.10** Dynamical simulations for RX J0942.7–7726AB and the TW Hydreae (top plots) and  $\beta$  Pictoris (bottom) Associations. The colour scale gives the value of  $\Delta UVW$ , the match between the observed and predicted space motion at that ejection epoch and current distance. Crosses mark the position of the minimum  $\Delta UVW$ . Ejection parameters at this point are summarised in Table 4.1.

## 4.6. Discussion

### 4.6.1. Origin of RX J0942.7–7726AB

The simulations yielded kinematic distances and ejection times from UCL and LCC similar to the distances and ages of the subgroups (110–140 pc, 11–17 Myr, Preibisch & Mamajek 2008). Ages at the upper end of this range are ruled out by the lithium data for RX J0942.7–7726, which suggests an age no older than  $\beta$  Pictoris (~12 Myr, Figure 4.7). A significant age spread in the subgroups could alleviate this problem. From their survey of solar-type

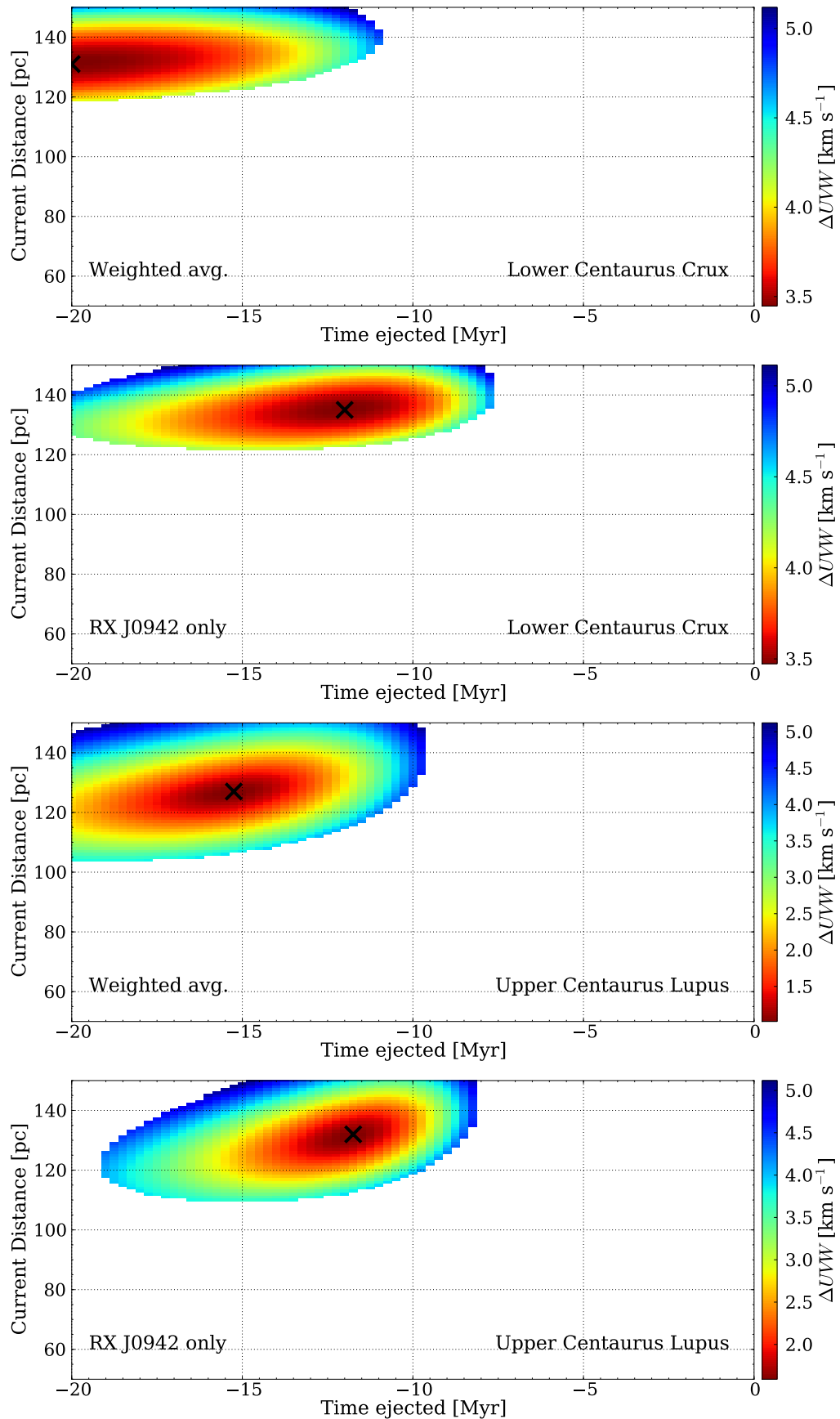


**Figure 4.11** Dynamical simulations for RX J0942.7–7726AB and the Sco-Cen subgroups of Lower Centaurus Crux (top plots) and Upper Centaurus Lupus (bottom plots).

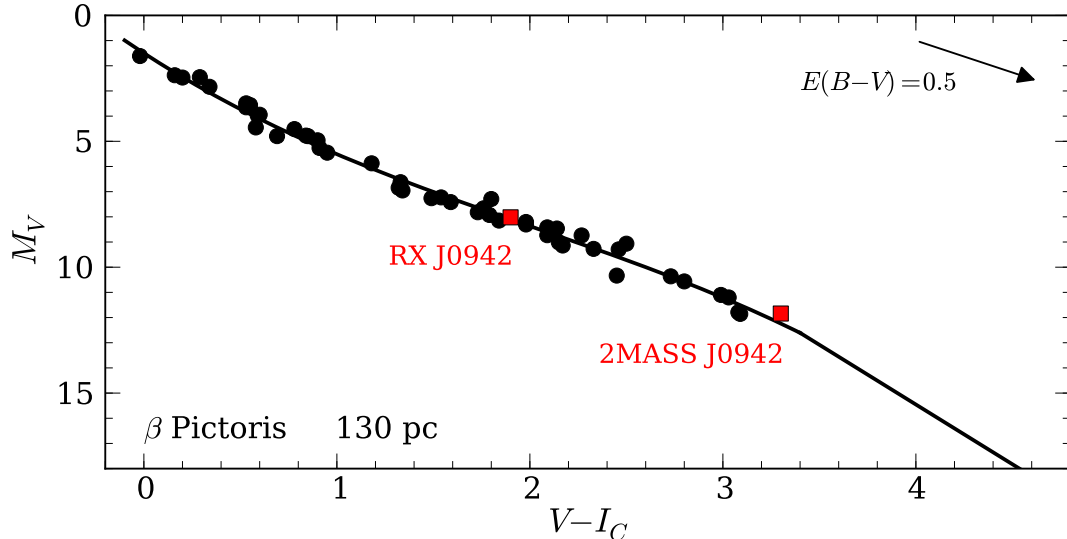


**Figure 4.12** Colour-magnitude diagrams for confirmed members of the  $\beta$  Pictoris Association with trigonometric or kinematic distances from Torres et al. (2008). Photometry from Torres et al. (2006), *Hipparcos* (van Leeuwen et al. 1997) and DENIS. Photometry for 2MASS J0942–7727 was converted from DENIS  $i$  and the synthetic  $(R - I)_C$  colour (via Bessell 1991). The empirical 10 Myr isochrone from Torres et al. (2008) is plotted.

members of LCC and UCL, Mamajek et al. (2002) estimated that star formation in the groups ceased around 5–10 Myr ago, so it is possible that some members may be younger than the quoted age. The velocities required by the simulations ( $4\text{--}10 \text{ km s}^{-1}$ ) are typical of the bulk turbulent or thermal motions in molecular clouds. It is *possible* that RX J0942.7–7726AB was formed in such a turbulent flow associated with one of the subgroups. If the flow was laminar over scales of several thousand AU it could presumably impart a large velocity to the system whilst keeping it intact. Birth near UCL 12 Myr ago with a velocity impulse of  $\sim 10 \text{ km s}^{-1}$  could move RX J0942.7–7726AB to a position 130 pc from the Sun with kinematics only slightly different to those observed ( $\Delta(UVW)_{\min} = 1.6 \text{ km s}^{-1}$ , Table 4.1). Such a scenario parallels the ‘in-situ’ star formation mode proposed by Feigelson (1996), in which stars born in different parts of a molecular cloud inherit the region’s turbulent velocity spread and disperse into the field over timescales of several Myr.

In any case, we are hampered by a paucity of low-mass Sco-Cen members against which to compare. Preibisch & Mamajek (2008) listed only seven M-dwarfs in their compilation of  $\sim 200$  LCC/UCL members. If the subgroups follow a standard initial mass function then there are likely to be several thousand low-mass stars awaiting discovery. As a proxy for recent low-mass star formation in the subgroups, we plot in Figure 4.12 the colour-magnitude diagram of the similarly aged  $\beta$  Pic Association. At the  $\sim 130$  pc distance suggested by the simulations, RX J0942.7–7726AB is a good fit to the 10 Myr empirical isochrone adopted by Torres et al. (2008), despite the uncertainties in transforming the DENIS photometry and synthetic  $(R - I)_C$  colour to  $V$  and  $(V - I_C)$  (via Bessell 1991). This is further evidence that RX J0942.7–7726 and 2MASS J0942–7727 are coeval and indeed co-distant.

Moeckel & Bate (2010) and Kouwenhoven et al. (2010) found that their  $N$ -body simulations could produce wide ( $a > 10^{3\text{--}5} \text{ AU}$ ) binary systems in the halos of dynamically evolving young clusters when two stars were coincidentally ejected with similar velocity vectors and become weakly mutually bound. Kroupa (1998) also reported seeing a similar event in one of their  $N$ -body simulations. Alternatively, Moeckel & Clarke (2011) showed that a small,

transient population of wide binaries can exist in an evolving cluster and be ‘frozen out’ into the field when the cluster dissolves. Old, wide binaries are rare (only a few per cent of systems have  $a > 10^4$  AU in the solar-type sample of Duquennoy & Mayor 1991), but a weakly-bound system could explain why RX J0942.7–7726 and 2MASS J0942–7727 have radial velocities that differ by  $2.7 \text{ km s}^{-1}$ . Given the errors on the mean *WiFeS* velocities, this is a  $2.7\sigma$  difference and well above the maximum variation due to orbital motion ( $0.3 \text{ km s}^{-1}$ ).

The clusters in the  $N$ -body simulations described above are typically very rich. For instance, Moeckel & Bate (2010) evolved a cluster of  $\sim 1200$  stars (stellar mass  $\sim 200 M_\odot$ ) with a half-mass radius of only  $10^4$  AU (0.05 pc). There is no observational evidence that  $\beta$  Pic or TW Hydrae were *ever* in such a rich, dense configuration. In contrast, dynamical models show that  $\eta$  Cha may have been initially very dense ( $10^8$  stars  $\text{pc}^{-3}$ ; Moraux et al. 2007), but likely only possessed  $< 100$  members at birth and is spectroscopically older than RX J0942.7–7726AB. In lieu of a nearby rich cluster, the early dynamical evolution of the Sco-Cen OB Association—perhaps via the dissolution of non-hierarchical few-body ( $N < 10$ ) systems (e.g. Sterzik & Durisen 1995)—appears to be the best scenario for the creation of RX J0942.7–7726AB from the ejection and weak binding of two single stars.

On balance, improved kinematics (ideally from trigonometric parallaxes) and better knowledge of the low-mass population of Sco-Cen are needed to ultimately determine the origin of RX J0942.7–7726AB. Contemporary high-resolution radial velocities will make it possible to discriminate between the coincidental ejection of two stars from Sco-Cen and the ‘in-situ’ turbulent star formation scenario of Feigelson (1996).

#### 4.6.2. Further multiplicity?

Our *WiFeS* radial velocity for RX J0942.7–7726 ( $20.7 \pm 0.4 \text{ km s}^{-1}$ , Table 2.3), differs significantly from that reported by Covino et al. (1997) ( $16.4 \pm 2 \text{ km s}^{-1}$ , c. 1995). The variation is well outside that expected from orbital motion around 2MASS J0942–7727 and may be evidence of binarity. Since a large fraction of stars are born in multiple systems (e.g. Duquennoy & Mayor 1991; Fischer & Marcy 1992), it is not unreasonable to expect that many of the primaries of wide binaries are in fact close multiple systems. Recent surveys (e.g. Makarov et al. 2008; Faherty et al. 2010; Law et al. 2010) have confirmed this and it is also seen in  $N$ -body cluster simulations including primordial binaries (Kouwenhoven et al. 2010). Moreover, there are hints that the frequency of hierarchical systems may increase with separation, at least for M-dwarf systems (Law et al. 2010).

Köhler (2001) did not detect a companion around RX J0942.7–7726 in their speckle interferometry and direct imaging survey of Chamaeleon *ROSAT* sources. Their  $0.13''$  (3.81 mag) detection threshold, the singly-peaked cross-correlation function reported by Covino et al. (1997) and the good fit to the CMD in Figure 4.12 put strong constraints on the orbit and mass of any companion. For instance, a  $0.1 M_\odot$  star in a 5 AU ( $0.05''$  at 100 pc) orbit would induce an orbital velocity in RX J0942.7–7726 of only  $1.7 \text{ km s}^{-1}$  with a period of  $\sim 14$  years. Such a companion could explain the velocity difference without being observed directly.

RX J0942.7–7726 was observed 19 times during 1999–2005 with *FEROS* on the ESO-1.5m and 2.2m telescopes at La Silla<sup>9</sup>. We have obtained the reduced spectra (E. Guenther,

---

<sup>9</sup>Including ESO programmes 075.C-0399, 073.C-0355, 072.A-9012, (PI: E. Covino)

private communication) and derive a mean velocity of  $18.5 \pm 0.6 \text{ km s}^{-1}$ . Velocities were computed by cross-correlation over the region 5900–6500 Å against the M1V star HD 36395, using an archival *ELodie* (Prugniel & Soubiran 2004) spectrum and the SIMBAD velocity ( $7.6 \pm 0.5 \text{ km s}^{-1}$ , White et al. 2007). A similar velocity ( $17.7 \pm 0.9 \text{ km s}^{-1}$ ) was obtained against a *UVES* spectrum of the M1III star HD 210066 (Bagnulo et al. 2003), although the uncertainty on the velocity standard is larger ( $\pm 0.9 \text{ km s}^{-1}$ , Wilson 1953). No evidence of a companion was visible in the cross-correlation functions and the individual velocities show no trend over the six years of *FEROS* data. Some scatter outside the instrumental errors is present, probably as a result of chromospheric activity (see previous Chapter).

Intriguingly, these mean velocities for RX J0942.7–7726 bisect the Covino et al. (1997) and our 2010–2011 *WiFeS* values. They also agree within errors with the velocity derived for 2MASS J0942–7727. While at first this may indicate that the two stars are co-moving, the *WiFeS* velocity for RX J0942.7–7726 ( $20.7 \pm 0.4 \text{ km s}^{-1}$ ) is inconsistent with both values. It is possible we are seeing temporal variation in the radial velocity between 1995, 1999–2005 and 2010–2011. The long period and small amplitude of the variation, if it exists, means further radial velocity monitoring of RX J0942.7–7726 is necessary to confirm any binarity.

#### 4.6.3. Comparison to other wide binaries

Finally, we compare RX J0942.7–7726AB to other young, wide binaries. Such an isolated pre-main sequence system is not unprecedented—Feigelson et al. (2006) reported the discovery of the  $\sim 10$  Myr, 2000 AU F0/M0 binary 51 Eri/GJ 3305. With a distance of 30 pc, they ascribed the pair to the  $\beta$  Pictoris Association. The system lies some 100 deg distant on the sky (110 pc in space) from the supposed birthplace of  $\beta$  Pic, the LCC subgroup of Sco-Cen. 51 Eri/GJ 3305 would need to have been born in gas displaced by  $\sim 10 \text{ km s}^{-1}$  from the LCC group velocity to move to its current location in 10–12 Myr. We have proposed a similar scenario for the birth of RX J0942.7–7726AB.

RX J0942.7–7726AB and 51 Eri/GJ 3305 join a small number of isolated, wide ( $a \gtrsim 1000$  AU) binaries in the young groups associated with Sco-Cen. These include the  $\beta$  Pictoris members HD 172555/CD–64 1208 (A7+K7, 2000 AU; Zuckerman et al. 2001a), V4046 Sgr/GSC7396-0759 (K6+M1, 12300 AU, whose components may be equal-mass binaries; Kastner et al. 2011), the hierarchical double binary HD 199143/HD 358623 (F8+K7,  $\sim 15000$  AU; Kaisler et al. 2004) and the possible triple system HR 7329AB/HD 181327 (A0/M7+F6,  $\sim 20000$  AU). The nearby ( $d \approx 10$  pc) equal-mass M4 binary AT Mic AB also appears to be co-moving with fellow  $\beta$  Pic member AU Mic (M1,  $\sim 47000$  AU; Caballero 2009). TW Hydrae hosts two wide doubles; TWA 1/28 (K6+M8.5,  $\sim 41000$  AU; Scholz et al. 2005; Teixeira et al. 2008), TWA 30AB (M5+M4, 3400 AU;Looper et al. 2010a) and the triple system TWA 11 (A0/M2+M4.5, 13500 AU; Kastner et al. 2008). TWA 19AB (G5+K7, 4200 AU; Zuckerman et al. 2001c) was shown by Mamajek (2005a) to be a background member of LCC at a *Hipparcos* distance of 104 pc. Further south, HD 104237 is the nearest (116 pc) Herbig Ae star and a member of the  $\epsilon$  Cha Association (Chapter 5; Feigelson et al. 2003). It hosts a complex multiple system, with two wide pre-main sequence companions, HD 104237D (M3, 1200 AU) and E (K4, 1700 AU), and two suspected young stars at separations of 160 AU and 600 AU (Grady et al. 2004).  $\epsilon$  Cha may contain at least one other wide binary, the hierarchical system RX J1158.5–7754AB (K4+M3, 1500–2000 AU, see next chapter).

RX J0942.7–7726AB has one of the lowest total masses ( $0.7 M_{\odot}$  by the models of Siess et al. 2000) of all the systems listed above, second only to TWA 30AB (and excluding AT/AU Mic and TWA 1/28, whose  $\sim 0.2$  pc separations mean they are almost certainly no longer bound). While RX J0942.7–7726AB lies near the maximal mass-separation relation seen in field binaries (Reid et al. 2001), in a survey of Taurus and the 5 Myr Upper Scorpius subgroup of Sco-Cen, Kraus & Hillenbrand (2007a, 2009) found that a 4000–6000 AU separation is not unusual for a  $0.7 M_{\odot}$  binary in a young, low-density population. Conversely, the recent SLoWPoKES<sup>10</sup> survey of wide, low-mass binaries (Dhital et al. 2010) showed that while the separation and M1 primary of RX J0942.7–7726AB is typical of the field population, the observed mass ratio ( $M_2/M_1 \approx 0.4$ ) is unusually low. This can be explained by *dynamical shaping* (Kraus & Hillenbrand 2009). It is reasonable to expect that most field stars were born in denser environments than Sco-Cen, where the widest, lowest mass companions will be preferentially stripped over time, increasing the observed field mass ratio.

## 4.7. Conclusion

We have shown that RX J0942.7–7726 and 2MASS J0942–7727 are coeval ( $\sim 10$  Myr), co-distant (100–150 pc) pre–main sequence stars which almost certainly form a physical wide binary with a separation of 4000–6000 AU. Both stars have PPMXL proper motions that agree within errors and similar radial velocities. Their exact origin is currently uncertain, but they were likely born in or near the Lower Centaurus Crux or Upper Centaurus Lupus subgroups of the Scorpius-Centaurus OB Association, approximately 10 Myr ago. Similar birthplaces have been proposed for the  $\beta$  Pictoris, TW Hydreae and  $\epsilon$  Cha associations, as well as other isolated wide binaries. Alternatively, the small but significant radial velocity difference we observed ( $2\text{--}3 \text{ km s}^{-1}$ ) could imply the system is weakly bound, possibly as a result of the coincidental ejection of two single stars from said regions with similar velocity vectors. We speculate that RX J0942.7–7726 may itself also be a binary, but such a claim requires further confirmatory observations.

The very existence of RX J0942.7–7726AB and the other wide binaries associated with Sco-Cen suggests associations like  $\beta$  Pictoris and TW Hydreae may have undergone a different star formation process to denser pre–main sequence groups like  $\eta$  Cha. The well-documented lack of wide ( $a > 20$  AU) binaries in  $\eta$  Cha (Köhler & Petr-Gotzens 2002; Brandeker et al. 2006) is clearly dynamical in origin (Moraux et al. 2007), whereas the fragile nature of systems like RX J0942.7–7726AB forbids any strong dynamical interactions over the past 10 Myr. While all the groups probably formed as a result of a spiral density wave colliding with nearby molecular material (Sartori et al. 2003; Fernández et al. 2008), or bulk flows and shocks from supernovae and wind-driven shells around Sco-Cen (Ortega et al. 2009),  $\eta$  Cha was likely formed in a smaller, denser ‘knot’ of material. This is responsible for its current compact size and resemblance to a classical open cluster, although it is much sparser. The stars that now comprise  $\beta$  Pic and TWA were probably born in a more distended turbulent flow, which would impart a larger spread of natal velocities. Isolated systems like RX J0942.7–7726AB, 51 Eri/GJ 3305 and TWA 19AB presumably formed in a similar manner, from smaller ‘micro’-cloudlets in and around Sco-Cen.

---

<sup>10</sup>Sloan Low-mass Wide Pairs of Kinematically Equivalent Stars – egads!



# CHAPTER 5

---

## An improved membership of the $\epsilon$ Chamaeleontis Association

*This work has been prepared for publication in the Monthly Notices of the Royal Astronomical Society, with authors Murphy, S. J., Lawson, W. A. and Bessell, M. S. It will be submitted in early-2012.*

### 5.1. Introduction

The southern constellation of Chamaeleon is abundant with pre-main sequence stars of various ages. It is dominated in the east by the Chamaeleon molecular cloud complex (see reviews by Luhman 2008; Schwartz 1992) and the extensive population of T Tauri stars associated with the Cha I ( $\sim 2$  Myr, Luhman 2004a, 2007) and Cha II (2–4 Myr, Spezzi et al. 2008) dark clouds. With a total mass of  $\sim 5000 M_{\odot}$  and a distance of 160–200 pc, the complex is one of the nearest large star-forming regions to the Sun.

In addition to the young stars physically associated with the clouds, there exists a sizeable number of foreground ( $d \approx 90$ –110 pc) Weak-lined T Tauri Stars (WTTs) between and around the clouds, with inferred ages of 5–10 Myr. Initially detected by the ROSAT All-Sky Survey, they have been extensively discussed by Alcalá et al. (1995, 1997), Covino et al. (1997) and Frink et al. (1998), among others. Once thought to be the result of ejection from the Chamaeleon complex (e.g. Sterzik & Durisen 1995), many of these isolated, older pre-main sequence stars are now believed to form a distinct co-moving association with the young early-type stars HD 104237 (Herbig A8e star), HD 104036 (A7) and  $\epsilon$  Cha (=HD 104174, B9).

The so-called  $\epsilon$  Chamaeleontis Association<sup>1</sup> ( $\epsilon$  Cha, Feigelson et al. 2003) may be related to the young open cluster  $\eta$  Chamaeleontis (Mamajek et al. 1999, 2000), only 10 degrees to the west. The groups share similar ages, distances and kinematics, suggesting a common history. Like many of the young, local associations in the southern sky (Zuckerman & Song 2004; Torres et al. 2008),  $\eta$  Cha and  $\epsilon$  Cha were almost certainly formed near the Lower Centaurus Crux subgroup of the Scorpius-Centaurus OB Association 5–10 Myr ago (Jilinski et al. 2005; Fernández et al. 2008; Ortega et al. 2009). However, their evolution and relationship today

<sup>1</sup>Following Feigelson et al. (2003) and Torres et al. (2008), we also adopt the nomenclature of the  $\eta$  Cha open cluster and name the association  $\epsilon$  Cha after its most massive member.

remains unclear. As detailed in Chapter 2,  $\eta$  Cha has a sparse halo of low-mass members that extends at least halfway to  $\epsilon$  Cha and probably beyond (Moraux et al. 2007; Murphy et al. 2010). It is possible the two groups are one and the same (Torres et al. 2008), although they exhibit subtle spectroscopic trends indicative of a slight age difference (Lyo et al. 2008).

Differing, often disparate, memberships for  $\epsilon$  Cha have been proposed by various authors in the decade since its discovery. Unfortunately, many candidates lack radial velocities necessary for confirming membership in a kinematic group and several proposed members have no spectroscopy at all. In this chapter we provide an updated membership of the low-mass population of  $\epsilon$  Cha from new low and medium-resolution spectroscopy of candidates from the literature. We then discuss several new accreting T Tauri stars in  $\epsilon$  Cha and compare the confirmed membership to the nearby  $\eta$  Cha cluster.

### 5.1.1. The many faces of $\epsilon$ Cha

The  $\epsilon$  Cha Association has existed in the literature in various guises for over a decade. Frink et al. (1998) discovered that, as well as the population of X-ray-bright young stars associated with the Cha I molecular cloud ( $d \approx 150\text{--}200$  pc), there were several older stars between the cloud and nearby Cha II with larger proper motions that placed them much closer to the Sun ( $d \approx 90$  pc). Terranegra et al. (1999) subsequently found 13 stars (including several from Frink et al.) between the clouds with similar proper motions, which they claimed formed a distinct kinematic association. From the four stars with *Hipparcos* parallaxes, they derived a distance to the association of 90–110 pc and an isochronal age of 5–30 Myr.

At the same time Mamajek et al. (2000) was characterising  $\eta$  Cha they also investigated stars in the vicinity of  $\epsilon$  Cha and HD 104237 (Terranegra et al. 1999). They identified five candidates in the *Hipparcos* and *Tycho-2* catalogues (including  $\epsilon$  Cha itself) with congruent proper motions and photometry, and used them to derive a space motion for the group.

Feigelson et al. (2003) obtained *Chandra X-Ray Observatory* snapshots of two fields around HD 104237 and found four low-mass companions to the Herbig A8e star, two of which (components D and E) had H $\alpha$  emission and strong lithium absorption. Components B and C lie within a few arcsec of the  $V = 6.6$  primary and were not observed spectroscopically. From *Hubble Space Telescope* data, Grady et al. (2004) later showed HD 104237B has a strong near-infrared excess suggestive of youth. HD 104237A itself has a  $\sim$ K3 spectroscopic companion at 0.15 AU separation (Böhm et al. 2004; Testa et al. 2008). The six stars probably form a bound multiple system, as commonly seen around other Herbig AeBe stars (Testi et al. 1999). In addition to HD 104237A–E and  $\epsilon$  Cha (which itself may be triple system), Feigelson et al. (2003) also discovered three  $\sim$ M5 stars in their *Chandra* fields with strong lithium absorption and H $\alpha$  emission. They named the nine-star aggregate the  $\epsilon$  Cha Association after its most massive member. Soon after, Luhman (2004b) surveyed a 30' radius around  $\epsilon$  Cha using 2MASS photometry and added three more lithium-rich, low-mass candidates.

In their review of young stars near the Sun, Zuckerman & Song (2004) proposed an association of stars distinct from that around  $\epsilon$  Cha, which they called “Cha-Near”. No details were given on the group, which included six new candidates and 11 stars from Terranegra et al. (1999) and Mamajek et al. (2000). Around the same time, Sartori et al. (2003) proposed an OB association in Chamaeleon containing at least 21 OB and A-type stars from *Hipparcos*,

including HD 104237 and  $\epsilon$  Cha. They claimed the association is an extension of the adjacent Scorpius-Centaurus OB Association (also see Eggen 1998), but this was convincingly disputed by Mamajek (2003), who showed they are more likely to be field stars.

Finally, while investigating the disk properties of Cha I members with the *Spitzer Space Telescope*, Luhman et al. (2008) identified four stars with proper motions consistent with membership in the  $\epsilon$  Cha Association defined by Feigelson et al. (2003), and three new *ROSAT* sources not previously attributed to  $\epsilon$  Cha. Three of the seven new candidates had Type II spectral energy distributions, typical of accreting Classical T Tauri Stars (CTTSs).

### 5.1.2. Literature candidates

Collating the above studies, there are 41 potential members of the putative  $\epsilon$  Cha Association in the literature. Torres et al. (2008) reviewed  $\epsilon$  Cha as part of their ongoing program to identify new members of young, local associations (Torres et al. 2003a,b, 2006). Combining the candidate lists with radial velocities from the literature and their own observations, they proposed 24 high-probability members with congruent kinematics, photometry and lithium absorption (their Table 8). Their membership included four core members of the open cluster  $\eta$  Cha (RECX 1, 8, 12 and  $\eta$  Cha itself). Torres et al. (2008) considered  $\eta$  Cha to be a part of  $\epsilon$  Cha and while the two groups have similar ages, distances and kinematics, in this chapter we consider only the 20 stars they classified as  $\epsilon$  Cha ‘field’ members. We will discuss the relationship between  $\eta$  and  $\epsilon$  Cha in greater detail in §5.4.5.

Accurate kinematics are vital to the convergence selection method used by Torres et al. (2008) (see also Torres et al. 2006). However, since many of the low-mass candidates lack radial velocities, their solution was somewhat biased towards X-ray-bright solar and early-type stars. It included eight stars from Terranegra et al. (1999), two from Mamajek et al. (2000), two from Feigelson et al. (2003)<sup>2</sup>, two from Luhman et al. (2008) and six new members drawn from the observations of Covino et al. (1997) and Torres et al. (2006). Of the 27 stars in our sample not included by Torres et al. (2008), they rejected only three; RX J1150.4–7704 (Terranegra et al. 1999) has kinematics far from the convergent solution, the F5 star HIP 55746 (Zuckerman & Song 2004) was reclassified as a member of the AB Doradus Association and RX J1158.5–7754A (Terranegra et al. 1999) shows poorly matching kinematics at its *Hipparcos* distance. The star lies only 16'' from the high-probability member GSC 9415–2676 ( $\epsilon$  Cha 20, Luhman et al. 2008) and its kinematics (and perhaps its parallax) may be affected by a close (0.07'') companion (Köhler 2001). The remaining stars did not have radial velocities necessary for application of the convergence method. Measuring velocities for these stars is one of the key contributions of this work.

We consider only the low-mass (K and M spectral type) stars in this study. The 21 low-mass candidates are listed in Table 5.1, with spectral types and  $V$  magnitudes from the literature, where available. The astrometry has been resolved against 2MASS Atlas images and our own spectroscopic observations. For the *ROSAT* sources, the 2MASS coordinates should be used in preference to the X-ray-derived values, which can be up to an arcminute away

---

<sup>2</sup>The two high-probability members proposed by Feigelson et al. (2003) ( $\epsilon$  Cha 6 and 7), are HD 104237D and E. Radial velocities for the primary and component D were published by Grady et al. (2004), who also claimed component E shares a similar velocity, although it was not listed in their paper (see their Table 5).

**Table 5.1** Late-type  $\epsilon$  Cha candidates from the literature

Name	Right Ascension (J2000)	Declination (J2000)	Spectral Type	V [mag]	Membership <sup>†</sup> reference
$\epsilon$ Cha 13	11 18 35.72	-79 35 54.8	M4.75	14.91	6
$\epsilon$ Cha 14	11 22 55.62	-79 24 43.8	M1	13.71	6
$\epsilon$ Cha 15	11 33 49.26	-76 18 39.9	M4.5		6
RX J1137.4-7648	11 37 31.30	-76 47 59.0			2
$\epsilon$ Cha 16	11 40 49.67	-74 59 39.4	M5.75	17.28	6
$\epsilon$ Cha 17	11 43 26.69	-78 04 45.4	M5	17.33	6
RX J1147.7-7842	11 47 48.10	-78 41 52.0			2
RX J1150.4-7704	11 50 28.30	-77 04 38.0	K4	12.0	1
RX J1150.9-7411 <sup>‡</sup>	11 50 45.20 <sup>‡</sup>	-74 11 13.0 <sup>‡</sup>	M4	14.4	1
RX J1158.5-7754A	11 58 28.15	-77 54 29.6	K4	10.9	1
$\epsilon$ Cha 1	11 59 07.98	-78 12 32.2	M4.75		3
$\epsilon$ Cha 3 (HD 104237C)*	12 00 03.60	-78 11 31.0			3
$\epsilon$ Cha 4 (HD 104237B)*	12 00 04.00	-78 11 37.0	M3/4	15.1	3
$\epsilon$ Cha 10	12 00 55.17	-78 20 29.7	M5.75		4
$\epsilon$ Cha 11	12 01 43.43	-78 35 47.2	M2.25		4
$\epsilon$ Cha 8	12 01 44.42	-78 19 26.8	M5		3
$\epsilon$ Cha 9	12 01 52.52	-78 18 41.4	M4.75		3
RX J1202.8-7718	12 02 54.61	-77 18 38.2	M3.5	14.4	1
$\epsilon$ Cha 12	12 07 45.98	-78 16 06.5	M3.75		4
RX J1207.7-7953	12 07 48.30	-79 52 42.0	M4	14.5	2
RX J1243.1-7458 <sup>‡</sup>	12 42 53.00 <sup>‡</sup>	-74 58 49.0 <sup>‡</sup>	M3	15.1	1

<sup>†</sup> Membership references: (1) Terranegra et al. (1999), (2) Zuckerman & Song (2004), (3) Feigelson et al. (2003), (4) Luhman (2004b), (5) Mamajek et al. (2000), (6) Luhman et al. (2008)

<sup>‡</sup> Updated coordinates to those presented by Alcalá et al. (1995). See Figure 5.3.

\* Not observed in this work; too close to HD 104237A ( $V = 6.6$ )

**Table 5.2** Early and solar-type  $\epsilon$  Cha candidates from the literature

Name	Right Ascension (J2000)	Declination (J2000)	Spectral Type	V [mag]	Membership <sup>†</sup> reference
TYC 9414-191-1	11 16 29.03	-78 25 20.8			5
HIP 55746*	11 25 18.10	-84 57 16.0	F5	7.6	2
TYC 9238-612-1	11 41 27.70	-73 47 03.0	G5	10.7	2
TYC 9420-676-1	12 04 57.43	-79 32 04.7	F0	10.28	5
HD 105234	12 07 05.50	-78 44 28.1	A9	7.4	5
HIP 59243	12 09 07.80	-78 46 53.0	A6	6.9	2

<sup>†</sup> Membership references: (2) Zuckerman & Song (2004), (5) Mamajek et al. (2000)

\* Suspected member of the AB Doradus Association (Torres et al. 2008)

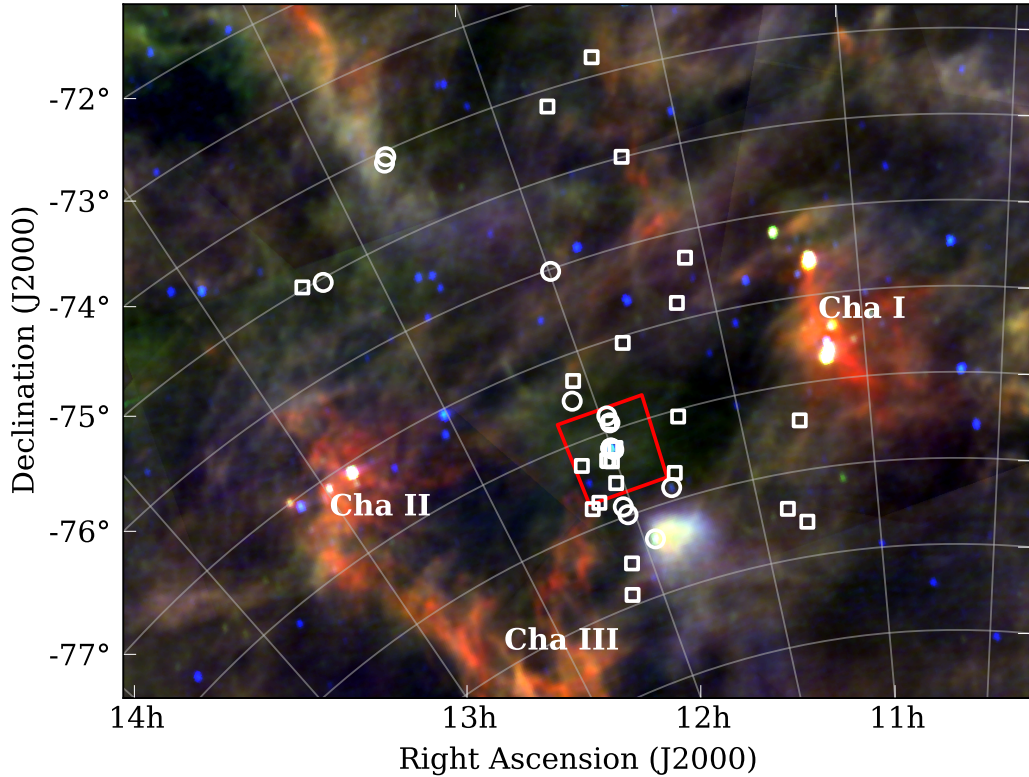


**Figure 5.1** Members of the  $\epsilon$  Cha Association from the literature (squares) and confirmed members from Torres et al. (2008) (circles).  $\eta$  Cha members, HD 82879, the likely AB Doradus member HIP 55746 and several members north of  $-72^\circ$  are not shown (see Figures 5.7 and 5.12). The background map is a 25/60/100  $\mu\text{m}$  IRAS colour composite. The red square shows the 1  $\deg^2$  field around  $\epsilon$  Cha (see Fig. 5.2).

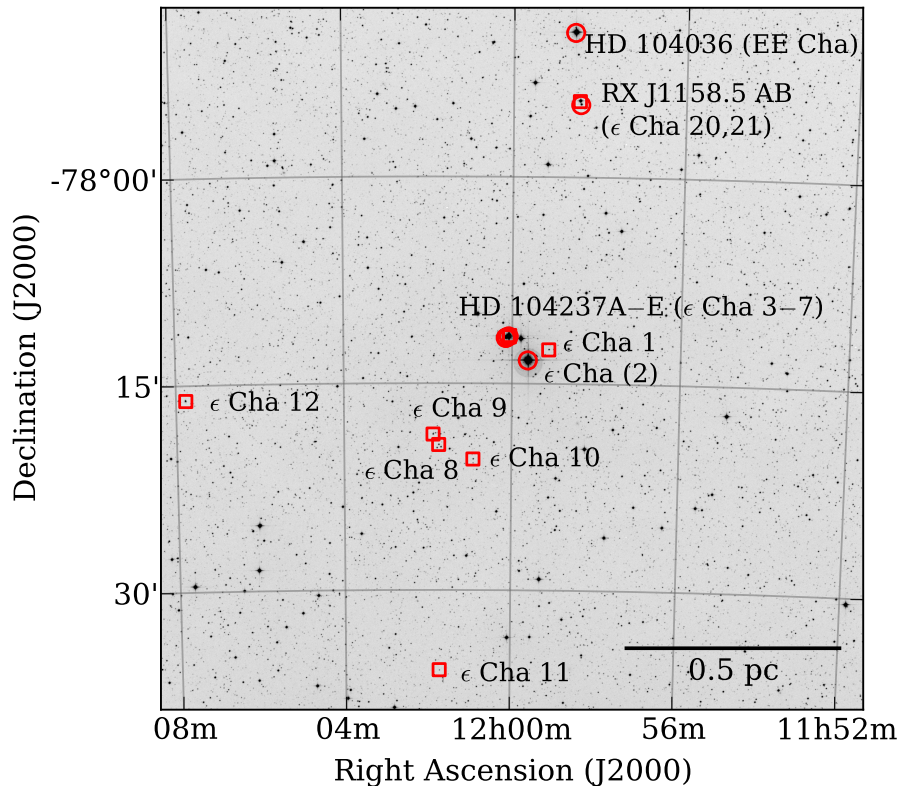


**Figure 5.2** POSS2-IR 1  $\deg^2$  image of the core association members, centred on the eponymous star  $\epsilon$  Cha. Symbols are as in Figure 5.1. The scale assumes a distance of 111 pc, the *Hipparcos* distance to  $\epsilon$  Cha.

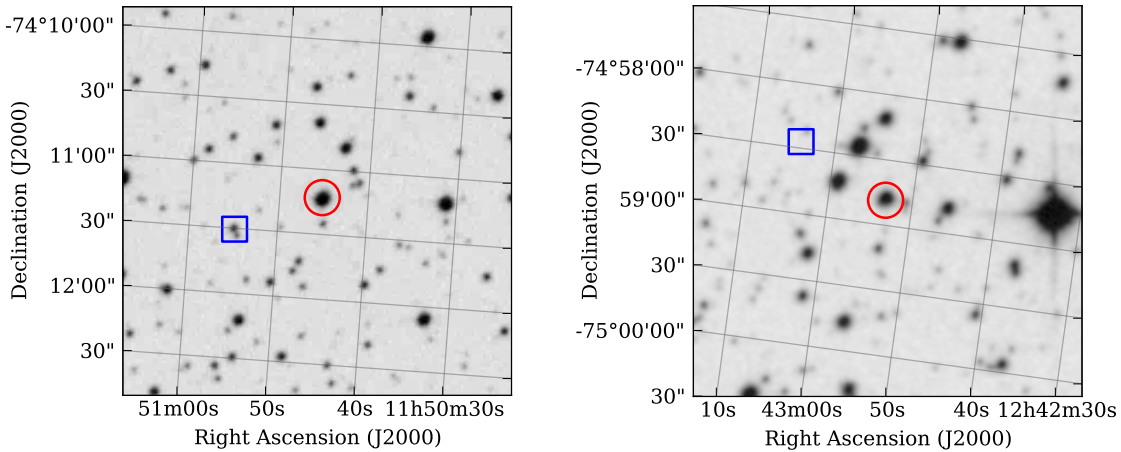


**Figure 5.3** POSS2-Red 3'×3' finding charts for RX J1150.9–7411 (left) and RX J1243.1–7458 (right). The new optical positions (Table 5.1) are circled, while SIMBAD ROSAT X-ray positions are shown by the blue squares.

from the true optical positions (Figure 5.3). We have included the two late-type candidates rejected by Torres et al. (2008) as they warrant further investigation. The six early and solar-type stars are listed in Table 5.2 and will be examined in a later work.

The various studies described above (frustratingly) use different—often inconsistent—naming schemes for their respective candidates. In Table 5.1 we adopt the nomenclature of the paper which originally proposed the candidate. In practice this reduces to two schemes; the ‘ $\epsilon$  Cha’ nomenclature<sup>3</sup> of Feigelson et al. (2003) and Luhman, and *ROSAT* RX J identifiers.

Figures 5.1 and 5.2 show the distribution of candidates and confirmed members on the sky. In addition to the four low-mass stars associated with HD 104237 (Feigelson et al. 2003; Grady et al. 2004), there is a clustering of candidates around this star and the eponymous B9 member  $\epsilon$  Cha (Figure 5.2), with the remainder of the low-mass stars dispersed around the region. This is reminiscent of  $\eta$  Cha, which has a distinct division between core and halo members (Chapter 2). However, unlike  $\eta$  Cha, the distribution of  $\epsilon$  Cha candidates is largely the result of observational bias. The region around  $\epsilon$  Cha and HD 104237A has been very well studied (Feigelson et al. 2003; Luhman 2004b) whereas the majority of the dispersed population are isolated *ROSAT* sources (Terranegra et al. 1999; Zuckerman & Song 2004) or incidental observations of stars around the Cha I cloud (Luhman et al. 2008). Given the shallow depth of the *ROSAT* All Sky Survey (§2.5.1), future wide-field surveys will likely reveal an extensive population of low-mass, X-ray-faint members in the region.

## 5.2. Observations

To obtain radial velocities and assess the youth of the candidates, we observed all but two of the stars in Table 5.1 on the ANU 2.3-m telescope between 2010 February and 2011 June. We could not observe  $\epsilon$  Cha 3 or 4 as they were too close to their primary HD 104237. In order to constrain any velocity variations and measure Li I  $\lambda$ 6708 equivalent widths, each candidate was observed 3–7 times over timespans of 60–500 days with the *WiFeS* spectrograph and *R*7000 grating ( $R \approx 7000$ ). Exposure times ranged from 900 to 5400 seconds. To estimate spectral types and reddenings we also obtained single-epoch *R*3000

<sup>3</sup>SIMBAD (<http://simbad.u-strasbg.fr/simbad/>) identifier: “[FLG2003] EPS CHA X”.

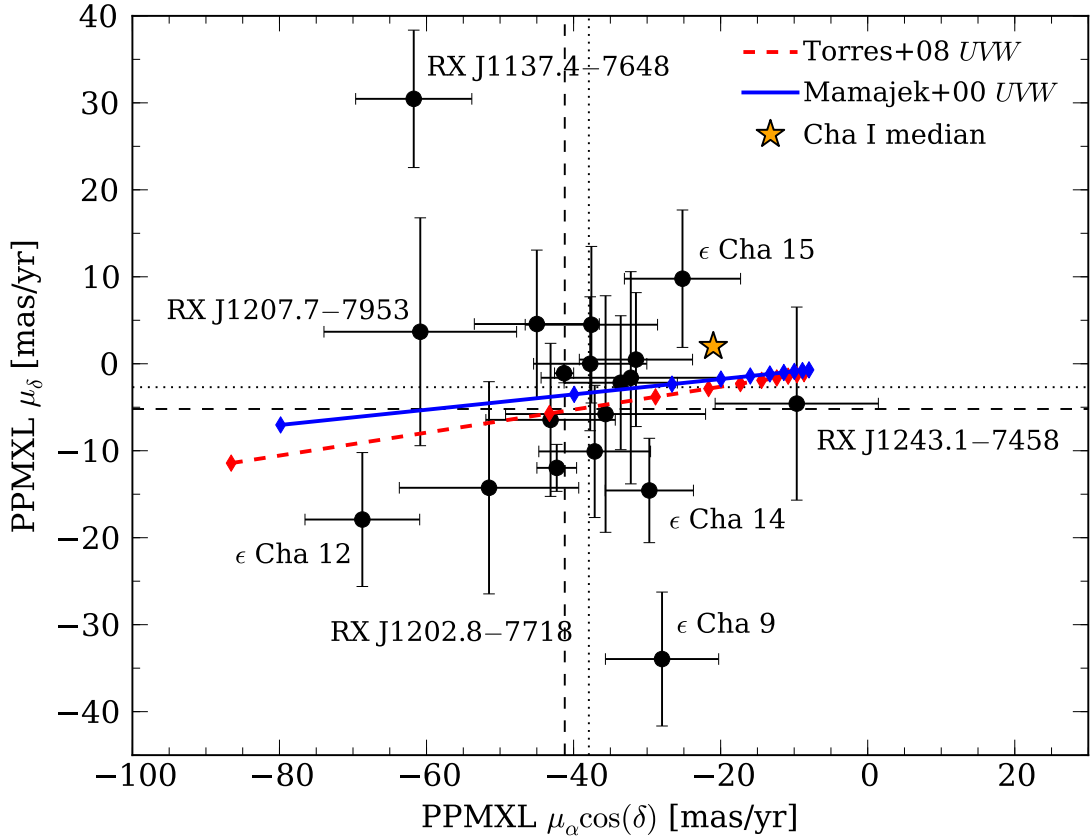


**Figure 5.4** PPMXL proper motions for the late-type members of  $\epsilon$  Cha from Table 5.1. Outliers mentioned in the text are labelled. Dotted lines mark the mean motion of the non-outlying stars. Dashed lines show the mean Tycho-2 proper motion of early and solar-type stars (see text). Red and blue lines give the  $\epsilon$  Cha space motion projected onto the sky at  $(\alpha, \delta) = (180^\circ, -78.25^\circ)$  and 50–500 pc (left to right, 50 pc increments). The orange star denotes the median proper motion of Cha I sources from Luhman et al. (2008),  $(-21, +2)$  mas yr $^{-1}$ .

spectra for  $\epsilon$  Cha 13–17 and the *ROSAT* candidates during 2011 July 30–31. All the spectra were observed and reduced as described in Chapters 2 and 4. Note that RX J1137.4–7648 is a 3'' visual binary that was barely resolved in the typical 2–2.5'' seeing. During a night of exceptional  $\lesssim 1''$  seeing on 2011 May 16 we resolved the pair in the *WiFeS* field and extracted minimally-blended spectra. Both components of RX J1137.4–7648 are non-members and will be discussed further in §5.3.3. Details of the observations are given in Table 5.3.

### 5.2.1. Proper motions

Many proposed members of  $\epsilon$  Cha were initially selected as co-moving with HD 104237 and  $\epsilon$  Cha itself. To confirm this we cross-matched the candidates in Table 5.1 against the recently-released PPMXL proper motion catalogue (Roeser et al. 2010). Only  $\epsilon$  Cha 3 and 4 were not recovered. As described in Chapter 2, we chose to use PPMXL as it offers the largest homogeneous collection of proper motions on the International Celestial Reference System (ICRS) currently available. Other contemporary astrometric catalogues such as UCAC3 (Zacharias et al. 2010) gave similar results, though fewer successful matches<sup>4</sup>. The 19 low-mass candidates with PPMXL proper motions are listed in Table 5.3 and shown in Figure 5.4, with projections of the Mamajek et al. (2000) and Torres et al. (2008)  $\epsilon$  Cha

<sup>4</sup>Also note that, although it is formally on the ICRS, Roeser et al. (2010) found that UCAC3 contains plate-dependent distortions in its proper motion system north of  $-20^\circ$  declination.

space motions. While the mean proper motion of background Cha I sources is around  $(\mu_\alpha \cos \delta, \mu_\delta) \approx (-21, +2)$  mas yr $^{-1}$  (Luhman et al. 2008), the majority of  $\epsilon$  Cha candidates cluster around a mean of  $(-38, -3)$  mas yr $^{-1}$  (dotted lines). Their motion is a good match to both space velocities at distances of 100–120 pc, as expected. Several stars have proper motions far from the mean values. These outliers will be discussed in later sections.

We also compared the PPMXL proper motions of the candidates to those derived by Terranegra et al. (1999) and Ducourant et al. (2005). Five stars overlap the former study, including RX J1150.9–7411 and RX J1243.1–7458<sup>5</sup> (Figure 5.3). All five proper motions agree with the PPMXL values within the quoted errors. Terranegra et al. (1999) noted that RX J1243.1–7458 is a kinematic (but not spatial) outlier to their proposed moving group. We also see this in the PPMXL proper motions (Figure 5.4). Ducourant et al. (2005) measured proper motions for four of the *ROSAT* candidates (RX J1150.4–7704, RX J1150.9–7411, RX J1158.5–7754A, RX J1202.8–7718). All but one of their proper motions match the Terranegra et al. (1999) and PPMXL values within the errors. Their proper motion for RX J1150.9–7411,  $(+15, +37) \pm 16$  mas yr $^{-1}$ , differs significantly from other published values. The coordinates and proper motion of the source they attributed to RX J1150.9–7411 are in fact for the faint (non-PMS) star at the X-ray position of Alcala et al. (1995) in Figure 5.3. This underscores the importance of accurate astrometry when deriving proper motions and cross-matching.

Of the 41 candidates identified in the literature, 13 have proper motions in the Tycho-2 catalogue (also on the ICRS; Høg et al. 2000); the six early and solar-type candidates from Table 5.2, RX J1158.5–7754A and six members of the Torres et al. (2008) sample. The dashed lines in Figure 5.4 mark the mean proper motion of these stars,  $(-41.2, -5.2) \pm (1.7, 3.2)$  mas yr $^{-1}$ , after removing the kinematic outliers HIP 55746 (probable AB Dor member) and TYC 9238-612-1. The mean PPMXL and Tycho-2 proper motion vectors for  $\epsilon$  Cha agree within the errors, as do the individual proper motions for the 13 stars.

### 5.2.2. Spectral types and reddenings

Spectra for many of the candidates in Table 5.1 have been presented by Luhman (2004b, 2007), Lyo et al. (2008), Covino et al. (1997) and Alcala et al. (1995). Our *WiFeS* R3000 spectra allow us to refine their spectral types and estimate any reddening along the line of sight. Updated spectral types are listed in Table 5.3. As in previous chapters, they were derived using molecular indices from the list of Riddick et al. (2007) and comparison to the  $\eta$  Cha/ $\epsilon$  Cha spectra of Lyo et al. (2004a, 2008). We also used the grid of Allen & Strom (1995) to extend our classification to K and early-M spectral types. The *WiFeS*/R3000 values agree with those previously determined at the 0.5 subtype level. However, for the four stars in common with Luhman (2007), our spectral types are systematically 0.2–0.3 subtypes earlier. This is probably due to the giant/dwarf average classification scheme adopted by Luhman, where we have used a dwarf scheme. We note that Lyo et al. (2004a, 2008) have shown that the broadband colours and narrow-band spectral indices of intermediate-age pre-main sequence stars are indistinguishable from Gyr-old field dwarfs and that they closely follow a dwarf temperature (spectral type) sequence.

<sup>5</sup>Note that Terranegra et al. (1999) adopt the erroneous X-ray positions of Alcala et al. (1995) for these two stars. The remaining three candidates in common to our sample (RX J1150.4–7704, RX J1158.5–7754A, RX J1202.8–7718) have reliable coordinates.

**Table 5.3** *WiFeS* observations of  $\epsilon$  Cha candidates from the literature

Name	Sp. Type	Li I $\lambda 6708$ [ $\pm 0.05 \text{ \AA}$ ]	RV [ $\text{km s}^{-1}$ ]	$\sigma_{\text{RV}}^{\dagger}$ [ $\text{km s}^{-1}$ ]	Ha EW [ $\pm 1 \text{ \AA}$ ]	$N_{\text{obs}}$	$\Delta t$ [days]	$\mu_{\alpha} \cos \delta$ PPMXI [mas yr $^{-1}$ ]	$\mu_{\delta}$ PPMXI [mas yr $^{-1}$ ]	$\sigma_{\mu}$	Comments
$\epsilon$ Cha 13	M4.5	0.60	19.3*	1.6*	-18 ... -30	7	477	-45	+5	9	SB1?, CTTS, Type II SED <sup>†</sup>
$\epsilon$ Cha 14	M1.5	0.15	2.7*	2.9*	-2	6	477	-30	-15	6	SB1, LCC member?
$\epsilon$ Cha 15	M4.5	0.65	16.7*	1.5*	-6	5	413	-25	+10	8	SB1?, Cha I member
RX J1137.4-7648	M2	0.00	~14	...	-1.5	1	...	-62	+30	8	old non-member
$\epsilon$ Cha 16	M5.5	0.70	10.3	1.0	-11 ... -35	4	411	-37	-10	8	SB1?
$\epsilon$ Cha 17	M4.7	0.70	15.6	1.0	-60 ... -120	6	480	-38	+0	8	CTTS, Type II SED <sup>†</sup>
RX J1147.7-7842	M3.5	0.65	16.1	0.9	-4 ... -7	5	409	-38	+4	9	
RX J1150.4-7704	K4	0.50	6.1*	1.6*	-1	5	479	-42	-12	3	SB1, LCC member?
RX J1150.9-7411	M3.6	0.50	15.0*	1.2*	-8	4	59	-32	-2	12	SB1?, close companion <sup>#</sup>
RX J1158.5-7754A	K4	0.50	19.9	0.8	-0.5	4	480	-41	-1	1	SB1, close companion <sup>#</sup>
$\epsilon$ Cha 1	M4.75#	0.65	15.1	0.2	-5	3	356	-36	-6	14	
$\epsilon$ Cha 10	M5.75##	0.60	10.7*	1.3*	-10 ... -20	6	411	-34	-2	8	WTTS, SB1?
$\epsilon$ Cha 11	M2.25##	0.70	20.0	0.6	-70 ... -140	3	370	-43	-6	9	CTTS, SB1?
$\epsilon$ Cha 8	M5.0##	0.50	14.9	1.1	-20 ... -45	4	60	-32	+0	8	CTTS
$\epsilon$ Cha 9	M4.75##	0.65	16.5	1.1	-8	4	411	-28	-34	8	bad kinematics
RX J1202.8-7718	M3.4	0.30	17.1	1.4	-5 ... -12	4	411	-52	-14	12	LCC member
$\epsilon$ Cha 12	M3.75##	0.50	15.4*	2.3*	-3.5	5	410	-69	-18	8	SB1?, $\beta$ Pic? CMD?
RX J1207.7-7953	M3.5	0.55	15.0	0.8	-4	4	414	-61	+4	13	
RX J1243.1-7458	M3.3	0.60	13.5	0.7	-4 ... -7	4	60	-10	-5	11	SB1?, close companion(s) <sup>#</sup>
											Cha II member

<sup>\*</sup> *WiFeS* velocity time series shows a trend indicative of binarity (see §5.3.2 and Table 5.4)<sup>†</sup> Standard error on the mean,  $\sigma_{\text{RV}} = \sigma / \sqrt{N_{\text{obs}}}$ <sup>#</sup> From the speckle and direct imaging survey of Chamaeleon ROSAT sources by Köhler (2001)<sup>†</sup> From *Spitzer* photometry by Luhman et al. (2008)<sup>##</sup> Spectral type from Luhman (2004b) (not observed with *WiFeS/R3000*)

RX J1137.4–7648 and RX J1147.7–7842 (Zuckerman & Song 2004) have no previously published spectra. We plot in Figure 5.5 their *WiFeS*/R3000 spectra, along with that of  $\epsilon$  Cha 13, whose 2011 July 30 spectrum (and previous R7000 epochs) showed the presence of forbidden lines of oxygen (including the high-excitation [O II]  $\lambda\lambda$ 7320/7331 doublet), sulphur, nitrogen, iron and calcium. Such emission lines are characteristic of the high-temperature, low-density winds commonly seen in CTTSs. The features are obviously transient as the spectrum presented by Luhman (2007) showed only H $\alpha$  in emission. The star has a transitional disk (Manoj et al. 2011) and will be discussed further in §5.4.4 with the other CTTSs in  $\epsilon$  Cha. Only one of the candidates shows any appreciable reddening. Through comparison to (unreddened)  $\eta$  Cha spectra we estimate  $\epsilon$  Cha 15 (Luhman et al. 2008) is reddened by approximately  $E(B - V) \approx 0.15$  mag. Luhman (2007) reported a similar level of reddening from their low-resolution spectrum of the star.

### 5.3. Kinematic membership analysis

After considering the proper motions, velocities, spectral types and lithium measurements of the candidates in Table 5.3, we propose the following improved membership of  $\epsilon$  Cha. In these discussions we adopt the space motions of Torres et al. (2008) for  $\epsilon$  Cha and Mamajek et al. (2000) for the Lower Centaurus Crux (LCC) subgroup of the Sco-Cen OB Association.

#### 5.3.1. Confirmed members

**$\epsilon$  Cha 1** The PPMXL proper motion of the star is an excellent match to the  $\epsilon$  Cha space motion at a distance of 120 pc. The predicted radial velocity differs by only 1 km s $^{-1}$  from that observed. The star is lithium-rich (EW = 650 mÅ) and lies only 1.7' from  $\epsilon$  Cha itself.

**$\epsilon$  Cha 8** The star has strong He I emission and a broad, double-peaked H $\alpha$  line. We find a good match to both the  $\epsilon$  Cha and LCC space motions, at distances of 135 pc and 115 pc, respectively. The predicted radial velocities differ by only 1 km s $^{-1}$  and both agree with the mean *WiFeS* value. While the majority of confirmed  $\epsilon$  Cha members have distances  $\lesssim$ 120 pc, the fact that WISE photometry also reveals an infrared excess indicative of a circumstellar disk (see §5.4.4) suggests  $\epsilon$  Cha 8 is likely to be younger than LCC, where such accreting stars are rare (also see the discussion of MP Mus in §5.4.1).

**$\epsilon$  Cha 11** A CTTS with forbidden line emission, Luhman (2004b) noted that the star appears under-luminous, which they attributed to being observed in scattered light due to an edge-on disk. We find an excellent proper motion match to the  $\epsilon$  Cha space velocity at  $\sim$ 100 pc. However, the predicted radial velocity is 6 km s $^{-1}$  lower than we measured. This may be a sign of spectroscopic binarity. The three *WiFeS* velocities showed no trend over  $\sim$ 1 year, so any companion must be sufficiently distant to induce a period longer than this.

**$\epsilon$  Cha 16** The PPMXL proper motion of the star agrees with that expected from  $\epsilon$  Cha at a distance of  $\sim$ 115 pc. The expected radial velocity (14.3 km s $^{-1}$ ) differs by 4 km s $^{-1}$  from that derived from four *WiFeS* spectra. Again, this may indicate binarity with a period greater than the  $\sim$ 1 yr baseline of our observations.

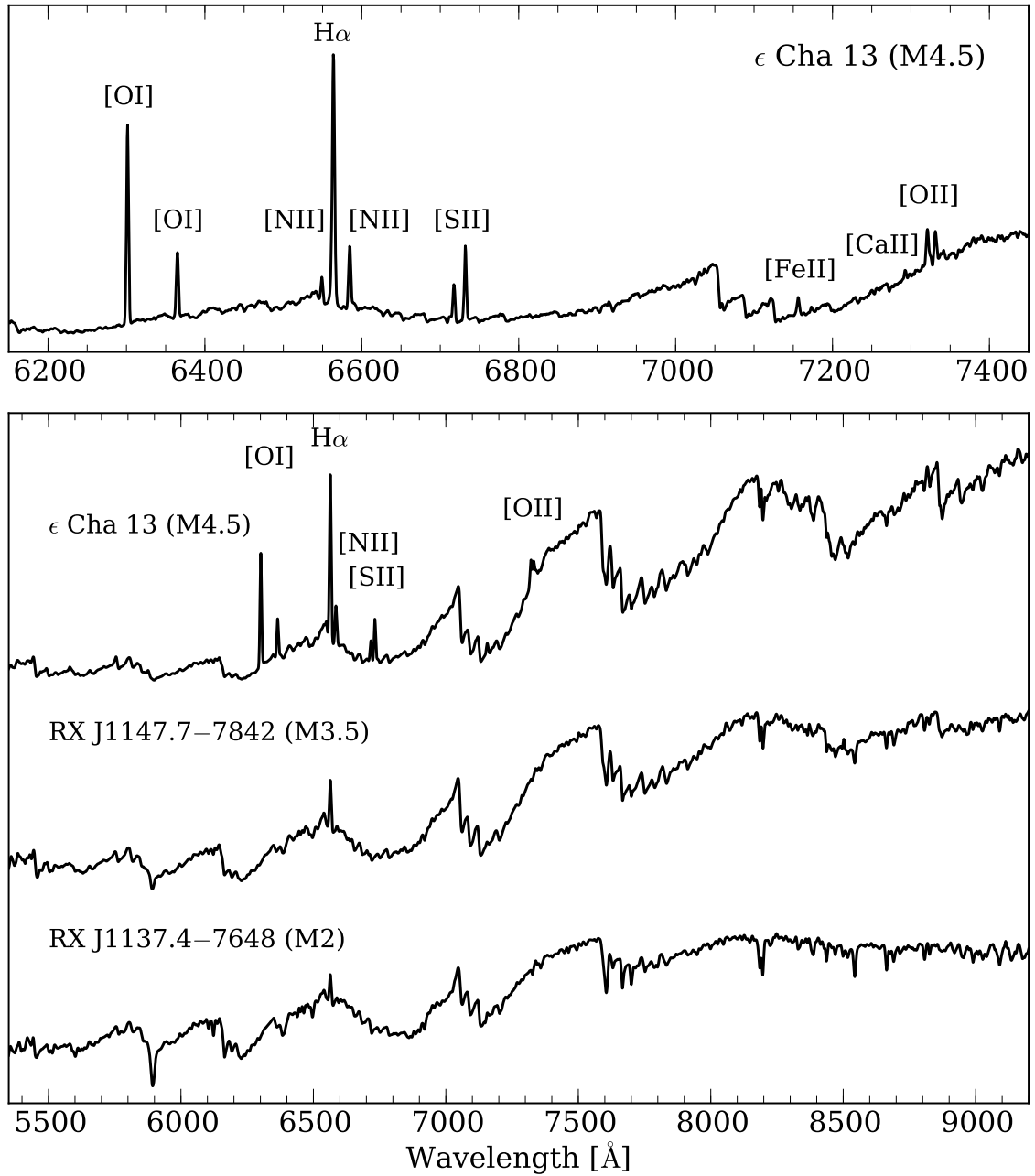


**Figure 5.5** *WiFeS/R3000* spectra of  $\epsilon$  Cha candidates RX J1137.4–7648, RX J1147.7–7842 (Zuckerman & Song 2004) and the CTTS  $\epsilon$  Cha 13 (Luhman 2008). The top panel shows the various forbidden emission lines present in the spectrum of  $\epsilon$  Cha 13, including rarely seen high-excitation forbidden lines of [Fe II], [Ca II] and [O II].

**$\epsilon$  Cha 17** Luhman et al. (2008) reported a Type II SED for the star, which was confirmed by *Spitzer* spectroscopy by Manoj et al. (2011). We detected variable H $\alpha$  emission in our six spectra, with equivalent widths ranging from  $-60$  to  $-120$  Å. At a distance of 115 pc the  $\epsilon$  Cha space motion is well-matched to the PPMXL proper motion and *WiFeS* radial velocity.

**RX J1147.7–7842** We find an excellent match between membership in  $\epsilon$  Cha at 115 pc and the observed proper motion of the star. The  $16.1 \pm 0.9$  km s $^{-1}$  mean *WiFeS* velocity is in good agreement with the predicted velocity of 14.3 km s $^{-1}$ .

**RX J1207.7–7953** After careful comparison to other astrometric catalogues, we find the PPMXL proper motion for this star appears to be in error. The best available proper motion is that of UCAC3,  $(-40, -7) \pm (2, 2)$  mas yr $^{-1}$ . Although the SuperCosmos (Hambly et al. 2001) proper motion disagrees with UCAC3 and PPMXL, the USNO-B1 (Monet et al. 2003) and older UCAC2 reduction both agree with UCAC3 within the errors. Using the latter in our analysis, RX J1207.7–7953 is an excellent match to  $\epsilon$  Cha at distances of 100–110 pc, with an observed radial velocity only 1 km s $^{-1}$  larger than predicted.

### 5.3.2. Spectroscopic binaries

Our multi-epoch radial velocities revealed seven candidates (marked in Table 5.3) with velocity measurements indicative of binarity. Two further candidates, RX J1158.5–7754A and RX J1243.1–7458, showed no trend but have mean velocities that differ significantly from those previously reported in the literature. Multi-epoch velocities of these nine stars and any available literature measurements are listed in Table 5.4.

**$\epsilon$  Cha 14 (=RX J1123.2–7924)** The star shows a clear trend from negative to positive velocities during 2010–2011, varying by nearly 20 km s $^{-1}$  over our observations. Köhler (2001) detected no close companions around  $\epsilon$  Cha 14 down to a *K*-band contrast of 2.9 mag at 0.13'' separation. The low lithium EW we measured means the star is unlikely to be a member of  $\epsilon$  Cha (see Figure 4.7). Instead, it may be an outlying member of the LCC subgroup of Sco-Cen immediately northward. However, the LCC space velocity at 100 pc predicts a proper motion at the star's position of  $(-36, +9)$  mas yr $^{-1}$  ( $RV = 15$  km s $^{-1}$ ), some 25 mas yr $^{-1}$  from the observed values. The UCAC3 (Zacharias et al. 2010) proper motion of the star agrees with PPMXL within the errors. It is unlikely that the unseen companion distorts the observed proper motions as its effects should be minimal over the long baseline of PPMXL (or UCAC3) astrometry. A systemic radial velocity would be extremely helpful in determining the exact kinematics.

**RX J1150.4–7704 (=GSC 9415-1685)** The star was noted by Covino et al. (1997) as being a possible spectroscopic binary, although Köhler (2001) found no visual companion. Binarity is confirmed by the variation in our five velocity measurements and the velocity reported by Guenther et al. (2007),  $-3.3 \pm 1.0$  km s $^{-1}$ . Torres et al. (2008) rejected the star on the basis of this velocity, but it is almost certainly not systemic. Their space motion for  $\epsilon$  Cha predicts a proper motion of  $(\mu_\alpha \cos \delta, \mu_\delta) = (-43, -5)$  mas yr $^{-1}$  at 100 pc and a radial velocity of 14 km s $^{-1}$ . The agreement between this and the observed proper motions (PPMXL, UCAC3, Terranegra et al. 1999; Ducourant et al. 2005), combined with the large lithium EW, point strongly to membership in  $\epsilon$  Cha. Confirmation of the predicted systemic velocity must await a full velocity curve. Wahhaj et al. (2010) classified the star as a CTTS on the basis of a broad H $\alpha$  line, but this is likely the result of binarity (also see Covino et al. 1997).

**RX J1158.5–7754A** This star is the only candidate in our sample with a *Hipparcos* parallax ( $d = 90.4^{+14}_{-11}$  pc; van Leeuwen 2007). Both the *Hipparcos* and Tycho-2 proper motions agree with PPMXL within their quoted errors. Our radial velocity differs significantly from those

**Table 5.4** WiFeS time-series and literature velocities

Epoch	RV [km s <sup>-1</sup> ]	Error <sup>‡</sup> [km s <sup>-1</sup> ]	Epoch	RV [km s <sup>-1</sup> ]	Error <sup>‡</sup> [km s <sup>-1</sup> ]			
<b>— <math>\epsilon</math> Cha 14 —</b>								
2010 Feb 25	-2.6	3.1	2010 Feb 25	+9.0	3.5			
2010 May 02	-5.0	0.1	2010 May 06	+9.7	1.7			
2010 Dec 20	-0.4	1.7	2011 Feb 10	+6.2	0.4			
2011 Feb 10	+2.4	0.4	2011 May 17	+1.0	1.7			
2011 May 16	+7.3	1.8	2011 Jun 19	+4.5	1.4			
2011 Jun 17	+14.1	2.1	Covino et al. (1997)	SB?				
Covino et al. (1997)	+10.0	2.0	Guenther et al. (2007)	-3.3	1.0			
<b>— RX J1158.5–7754A —</b>								
2010 Feb–2011 Jun	+19.9	0.8	2010 May 04	+15.0	1.1			
Covino et al. (1997)	+13.1	2.0	2011 Jan 09	+7.2	0.8			
James et al. (2006)	+10.2		2011 Feb 24	+9.0	2.0			
<b>— RX J1243.1–7458 —</b>								
2011 Apr–Jun	+13.5	0.7	2011 May 09	+13.4	1.1			
Covino et al. (1997)	+7.0	2.0	2011 May 17	+12.0	1.7			
<b>— <math>\epsilon</math> Cha 12 —</b>								
2010 May 05	+23.4	1.5	2010 Feb 25	+19.8	2.6			
2011 Jan 08	+10.7	0.8	2010 May 02	+15.8	0.5			
2011 Jan 13	+15.2	1.9	2010 Dec 20	+14.3	1.9			
2011 May 17	+16.7	1.1	2011 Feb 11	+17.9	1.2			
2011 Jun 19	+11.0	0.5	2011 Feb 12	+17.8	... <sup>#</sup>			
<b>— <math>\epsilon</math> Cha 15 —</b>								
2010 May 02	+13.9	0.6	2011 May 16	+26.7	1.2			
2010 Dec 20	+14.0	1.5	2011 Jun 17	+23.2	2.7			
2011 Feb 11	+15.1	0.7	<b>— RX J1150.9–7411 —</b>					
2011 May 16	+20.4	1.5	2011 Apr 22	+15.6	1.2			
2011 Jun 19	+20.1	0.6	2011 Apr 24	+16.8	0.6			
			2011 May 17	+16.1	1.1			
			2011 Jun 20	+11.6	1.1			

<sup>‡</sup> Errors on the single-epoch WiFeS measurements are the standard deviation of cross-correlations against 4–8 RV standards observed on the same night.

<sup>#</sup> Only one RV standard observation.

reported by Covino et al. (1997) ( $13.1 \pm 2.0$  km s<sup>-1</sup>) and James et al. (2006) (10.2 km s<sup>-1</sup>). Köhler (2001) detected a 0.07'' companion and the star is thought to be associated with the Torres et al. (2008) member GSC9415-2676 (=RX J1158.4–7754B), only 16'' away. These authors rejected RX J1158.5–7754A as a member of  $\epsilon$  Cha on the basis of bad kinematics at its *Hipparcos* distance. However, at the 123 pc ascribed to GSC9415-2676, RX J1158.5–7754A has kinematics well-matched to  $\epsilon$  Cha (and GSC9415-2676). Like Torres et al. (2008), we conclude that, as well as being responsible for the velocity variation, the close companion detected by Köhler (2001) distorted the parallax over the short baseline of *Hipparcos* observations (although the space-based proper motions agree with the long-baseline PPMXL values). The hierarchical wide binary is reminiscent of nearby RX J0942.7–7726AB (Chapter 4).

**RX J1243.1–7458** Covino et al. (1997) measured a radial velocity of  $7 \text{ km s}^{-1}$  for the star, while our four observations over 60 days give a (flat) mean velocity of  $13.5 \text{ km s}^{-1}$ . It is therefore possible the star is a spectroscopic binary with a period longer than  $\sim 1$  yr. Indeed, Köhler (2001) detected a companion at  $0.3''$  and another wide one at  $2.5''$  (which they noted is likely the coincidental alignment of an unrelated field star). Terranegra et al. (1999) derived a proper motion for RX J1243.1–7458 of  $(-20, -6) \pm (6, 5) \text{ mas yr}^{-1}$ , in agreement with both the PPMXL and UCAC3 values (which have large errors in  $\mu_\alpha \cos \delta$ ). If these kinematics are correct then membership in  $\epsilon$  Cha would require an unrealistic distance of  $\sim 200$  pc. The high lithium EW ( $600 \text{ m}\AA$ ) means membership in LCC is also problematic, as its lithium depletion boundary (LDB) should lie around a spectral type of M4–5. However, RX J1243.1–7458 lies a few degrees north of the Cha II dark cloud (see Figure 5.1) and the Terranegra et al. proper motion is an excellent match to the cloud space motion<sup>6</sup> at a distance of  $\sim 200$  pc. This agrees with recent distance estimates to the cloud (170–210 pc; Whittet et al. 1997; Knude 2010). The  $12 \text{ km s}^{-1}$  predicted radial velocity also agrees with the mean WiFeS value, implying we observed the star close to its systemic velocity.

**$\epsilon$  Cha 10** The  $\epsilon$  Cha space motion is good match to the star at a distance of  $\sim 120$  pc. The  $14 \text{ km s}^{-1}$  predicted velocity is slightly larger than the  $10.7 \text{ km s}^{-1}$  mean velocity in Table 5.3. Since we detected strong, variable H $\alpha$  emission and an infrared excess (§5.4.4), this difference (and the variation in Table 5.4) may be due to either an unseen companion, surface activity, accretion or a combination of all three.

**$\epsilon$  Cha 12** The large proper motion of this candidate suggests a distance much closer than the 100–110 pc typically attributed to  $\epsilon$  Cha members. The Torres et al. (2008)  $\beta$  Pic space motion at 55 pc is a good match to the PPMXL (and UCAC3) proper motions, but with a predicted radial velocity  $\sim 5 \text{ km s}^{-1}$  lower than observed. If the velocity in Table 5.3 is close to systemic, then epicyclic trace-back simulations (Figure 5.6) show that birth in  $\beta$  Pic is possible if the star lies at a distance of 54 pc and was given a  $\sim 4 \text{ km s}^{-1}$  kick early on, potentially forming a hard binary (responsible for the velocity variation) after a three-body interaction. Systemic velocities of  $10\text{--}18 \text{ km s}^{-1}$  also gave acceptable results. Membership in  $\epsilon$  Cha or LCC is ruled out by the simulations irrespective of the systemic velocity. Non-detection in the ROSAT All-Sky Survey cannot constrain the distance, as an M4 star with saturated X-ray emission would need to lie within  $\sim 30$  pc to have been detected (see Chapter 2). If  $\epsilon$  Cha 12 is (was?) a member of  $\beta$  Pic it would be by definition just cooler than the group's LDB, which falls near a spectral type of M4 (Song et al. 2002, 2003). We will discuss this star further after constructing the colour-magnitude diagram of candidates in §5.4.2.

**$\epsilon$  Cha 13** This candidate from Luhman et al. (2008) has the spectral characteristics of a CTTS with a transitional disk (Figure 5.5; Manoj et al. 2011). The space motion of  $\epsilon$  Cha is an excellent match to the observed proper motion at a distance of 90–100 pc. The mean WiFeS velocity is  $4.5 \text{ km s}^{-1}$  larger than predicted by membership in  $\epsilon$  Cha. Again, this could be due to a combination of a companion, activity or accretion from the disk.

---

<sup>6</sup> $(U, V, W) = (-9.9, -19.4, -6.8) \pm (1.6, 1.1, 1.3) \text{ km s}^{-1}$  (E. Mamajek, private communication)

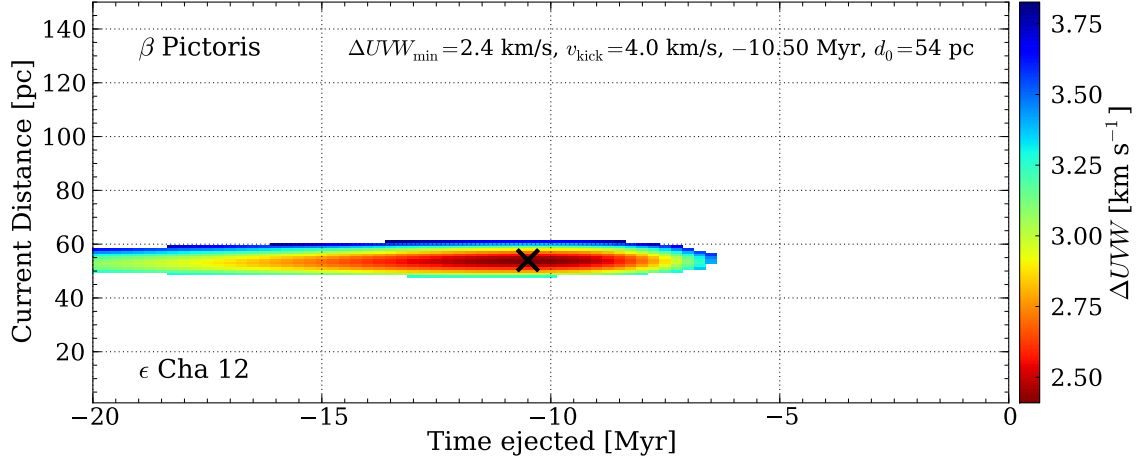


**Figure 5.6** Results of dynamical simulations for  $\epsilon$  Cha 12 and the  $\beta$  Pictoris Association, using the proper motion and radial velocity in Table 5.3 and the mean  $\beta$  Pic position and space motion from Torres et al. (2008). Parameters corresponding to the minimum  $\Delta UVW$  (black cross) are listed at the top of each plot. See Chapter 2 for more information on the simulations.

**$\epsilon$  Cha 15** Located between the Cha I dark cloud and the core of  $\epsilon$  Cha (see Figure 5.1), this star was proposed by Luhman et al. (2008) as having a proper motion more similar to  $\epsilon$  Cha than the cloud sources. The 196/215 confirmed members of Cha I from Luhman (2007) that are recovered in PPMXL have a median proper motion of  $(-22, +6)$  mas yr $^{-1}$ . The PPMXL proper motion of  $\epsilon$  Cha 15 is in excellent agreement with this median value. Furthermore, it is a poor match to the  $\epsilon$  Cha space motion at any realistic distance. The proper motion used by Luhman et al. (2008) to classify the star is not reported in their paper. The star does not appear in the UCAC3 or USNO-B1 catalogues and the SuperCosmos proper motion for the source at its position is a meagre  $(+2, +1)$  mas yr $^{-1}$ . With only the congruent PPMXL proper motion we have no choice but to reclassify  $\epsilon$  Cha 15 as an outlying Cha I member at an estimated distance of  $\sim 160$  pc (Whittet et al. 1997).

**RX J1150.9–7411** Köhler (2001) detected a close 0.9'' companion which may have been responsible for the drop in radial velocity on 2011 June 20. Our observations cover only 59 days so confirming binarity will require further measurements. If the companion does not alter the mean velocity significantly, then the space motion of  $\epsilon$  Cha is a good match to the PPMXL kinematics at a distance of 135 pc. The Terranegra et al. (1999) proper motion,  $(\mu_\alpha \cos \delta, \mu_\delta) = (-39, +4) \pm (4, 3)$  mas yr $^{-1}$ , agrees with PPMXL but with much smaller uncertainties (the UCAC3 proper motion is spurious). Membership in LCC matches the improved proper motion at distances of 90–100 pc. The predicted radial velocity is 14 km s $^{-1}$  in both cases, in good agreement with the mean *WiFeS* velocity. However, the high lithium equivalent width (500 mÅ) and M3.6 spectral type favours  $\epsilon$  Cha (but see discussion in §5.4.1). Improved kinematics and a better understanding of the low-mass population of LCC are necessary to ascertain the true status of this star.

**Other known binaries in  $\epsilon$  Cha**  $\epsilon$  Cha 10, 13, RX J1150.4–7704 and RX J1158.5–7754A join a small but growing number of confirmed or suspected binaries in  $\epsilon$  Cha. Of the confirmed members from Torres et al. (2008), HD 104237 and  $\epsilon$  Cha itself are both well-known

multiple systems and RX J1204.6–7731 (=GSC9416-1029) is a recently confirmed double-lined spectroscopic binary (Doppmann et al. 2007). Both RX J1157.2–7921 (=T Cha) and RX J1201.7–7859 (=HD 104467) are suspected binaries based on the spread in their velocities reported in the literature<sup>7</sup>. RX J1220.4–7407 (=GSC9239-1572) has a 0.3'' companion (Köhler 2001) and a large difference between velocities reported by Covino et al. (1997) ( $18 \pm 2$  km s $^{-1}$ ) and Guenther et al. (2007) ( $12.3 \pm 0.4$  km s $^{-1}$ ). Finally, we add RX J1149.8–7850 (=DZ Cha =  $\epsilon$  Cha 18, Luhman et al. 2008) as a suspected spectroscopic binary. The single *WiFeS* velocity of  $17 \pm 3$  km s $^{-1}$  we obtained in 2010 February differs from those reported by Covino et al. (1997) ( $12.2 \pm 2$  km s $^{-1}$ ) and Torres et al. (2006) ( $13.4 \pm 1.3$  km s $^{-1}$ ), but is similar to an earlier measurement of 18 km s $^{-1}$  by Gregorio-Hetem et al. (1992).

### 5.3.3. Marginal and non-members

**RX J1137.4–7648** Proposed as a “Cha-Near” member by Zuckerman & Song (2004), the near equal-brightness components of this visual binary are separated by only 3'' and barely resolved in typical SSO seeing. The M2 spectral type listed in Table 5.3 is that of the unresolved pair. During a night of exceptional ( $\lesssim 1''$ ) seeing we were able to resolve the components at  $R = 7000$ . While both stars show H $\alpha$  emission ( $EW \approx -1$  Å) and have similar radial velocities ( $\Delta RV < 0.5$  km s $^{-1}$ ), neither shows any appreciable Li I  $\lambda 6708$  absorption and their (unresolved) PPMXL proper motion is far from that predicted by membership in  $\epsilon$  Cha. We classify both stars as nearby, old field stars. Their inclusion in Cha-Near by Zuckerman & Song (2004) was inconsistent with lithium measurements taken at the time by the same authors (B. Zuckerman, private communication).

**$\epsilon$  Cha 9** The PPMXL proper motion of this star differs significantly from the other candidates. The star is lithium-rich (650 mÅ), but its proper motion (particularly the large negative  $\mu_\delta$  component) does not match projections of  $\epsilon$  Cha, LCC, the Cha I/II clouds or other young associations at any distance. There is another source in PPMXL only 0.1'' from its coordinates with a large proper motion,  $(\mu_\alpha \cos \delta, \mu_\delta) = (-21, -293) \pm 10$  mas yr $^{-1}$ , but this is also a very poor match. A similar source exists in the USNO-B1 catalogue but UCAC3 returns no matches. These multiple close sources likely indicate a problem with the proper motion solution.  $\epsilon$  Cha 9 is obviously young and close to the core of  $\epsilon$  Cha (Figure 5.2), but confirming its membership must await improved kinematics.

**RX J1202.8–7718** The large proper motion and 300 mÅ lithium EW suggest membership in  $\beta$  Pictoris at  $\sim 70$  pc. However, the observed radial velocity is  $\sim 6$  km s $^{-1}$  higher than predicted and trace-back simulations imply the star would need to have been given a similar impulse 10 Myr ago to move to its current location. Ducourant et al. (2005), Terranegra et al. (1999) and UCAC3 derived similar proper motions that differ from the lower-precision PPMXL values. These are an excellent match to the LCC space motion at 100 pc, with a radial velocity that differs by only 2 km s $^{-1}$  from that observed. Membership in LCC would also be consistent with the lower lithium EW. Rejecting the discrepant PPMXL proper motion,

---

<sup>7</sup>T Cha is particularly interesting as there is evidence for a substellar object orbiting within the inner gap of its disk (Huélamo et al. 2011) and a wide M4.5 companion at 38,000 AU (Kastner et al. 2012, in press).

we assign membership of RX J1202.8–7718 to LCC. The M3.4 *WiFeS* spectral type agrees with the one found by Riaz et al. (2006), who derived a spectroscopic distance of  $58 \pm 21$  pc assuming the star was an M3.5 main sequence dwarf.

### 5.3.4. New members

Since the compilation of Torres et al. (2008), several new  $\epsilon$  Cha members have been proposed in the literature. By comparing the kinematics and lithium/X-ray properties of stars in the RAVE (*RA*dial *V*elocity *E*xperiment; Steinmetz et al. 2006) database to  $\epsilon$  Cha members, Kiss et al. (2011) proposed 2MASS J12210499–7116493 as a new member at an estimated kinematic distance of 98 pc. The K7 star has strong Li I  $\lambda 6708$  absorption (550 mÅ) and a space motion only  $1.5 \text{ km s}^{-1}$  from that of  $\epsilon$  Cha<sup>8</sup>. It is located slightly north of the majority of  $\epsilon$  Cha members (Figure 5.7), near the southern border of LCC (see §5.4.1).

From a sample of nearby ( $d < 20$  pc) *Hipparcos* stars with good radial velocities, Nakajima et al. (2010) proposed an additional six members of the “Cha-Near” group of Zuckerman & Song (2004). They searched for stars with congruent space motions and used an epicyclic traceback (similar to that presented in Chapter 2) to determine the separation of each candidate from  $\epsilon$  Cha 8 Myr ago, their assumed age for the group. Given the excellent kinematics from *Hipparcos* and the fact that none of their candidates get closer than 48 pc from the core of the  $\epsilon$  Cha, we assign them a low probability of membership. Indeed, their “Cha-Near” sample includes the  $\beta$  Pic member AU Mic, GJ 82 (estimated age 35–300 Myr; Shkolnik et al. 2009), GJ 824 (age  $>600$  Myr; Barrado y Navascués et al. 1999) and the binary EQ Peg, whose M3.5 primary has only a marginal lithium detection (Zboril et al. 1997), implying an age greater than 10 Myr (but see discussion in Barrado y Navascués 1998; Riedel et al. 2011). The remaining two A-type stars likely have space motions coincidental with  $\epsilon$  Cha, unsurprising considering the  $8 \text{ km s}^{-1}$  velocity threshold adopted by the study<sup>9</sup>.

## 5.4. Discussion

### 5.4.1. $\epsilon$ Cha and Lower Centaurus Crux

2MASS J1221–7116 and four stars from the Torres et al. (2008) solution (CP–68 1388, HD 105923, CD–69 1055 and MP Mus) lie north of the majority of  $\epsilon$  Cha members, within the  $b = -10$  deg southern boundary of LCC (de Zeeuw et al. 1999, Figure 5.7). Mamajek et al. (2002) also identified these four stars as LCC members in their survey of Sco-Cen. In this section we reexamine all the stars’ membership in  $\epsilon$  Cha using the best available kinematic and lithium information. We finish by briefly discussing the relationship between  $\epsilon$  Cha and the southern extent of Lower Centaurus Crux.

---

<sup>8</sup>Note that Kiss et al. (2011) swapped the radial velocity of 2MASS J1221–7116 with their  $\beta$  Pic member 2MASS J01071194–1935359 (immediately below 2MASS J1221–7116 in their Table 1). The listed space motions for both stars are correct and consistent with the rectified velocities and tabled UCAC3 proper motions.

<sup>9</sup>Note added during corrections: Nakajima & Morino (2012) have presented an updated study containing seven new Cha-Near candidates within 30 pc. None appear to have ever been closer than  $\sim 20$  pc from  $\epsilon$  Cha. They include GJ 82, EQ Peg and HR 8162 from their earlier study and the older pre-main sequence stars DK Leo (age  $>400$  Myr; Shkolnik et al. 2009), GJ 755 ( $200 \pm 100$  Myr; Barrado y Navascués 1998), HR 3499 ( $>100$  Myr; Wichmann et al. 2003) and the  $\beta$  Pic member AF Lep (Torres et al. 2008).

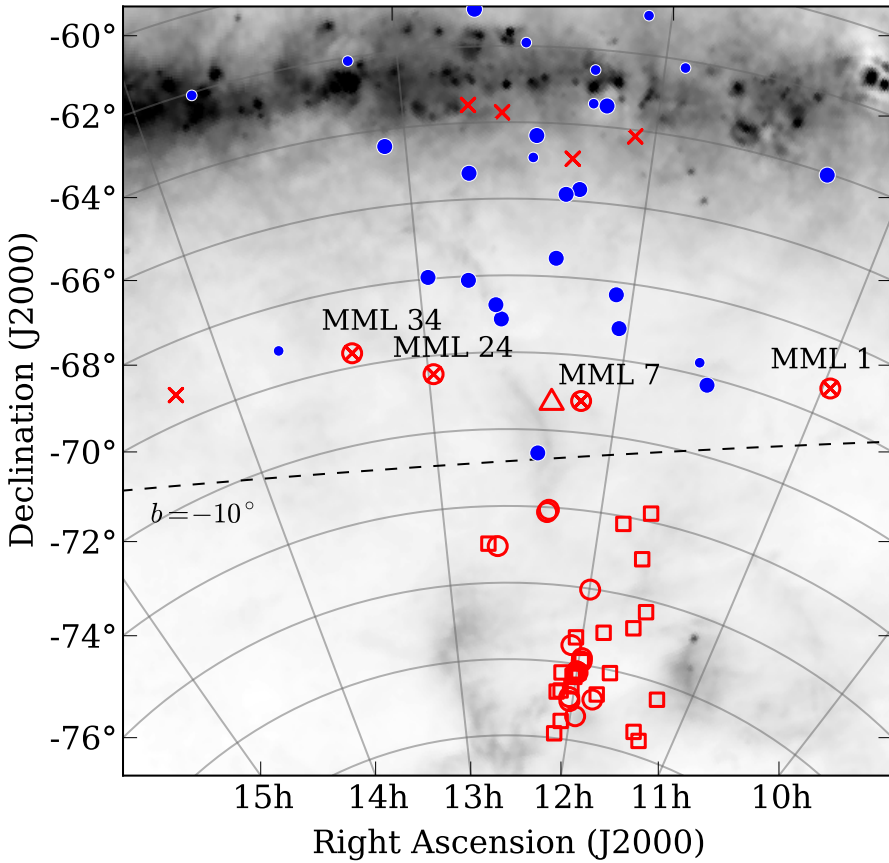


**Figure 5.7** Chamaeleon-Musca extinction map (Schlegel et al. 1998) with proposed  $\epsilon$  Cha members (symbols as in Figure 5.1), the new member 2MASS J1221–7116 (triangle; Kiss et al. 2011) and late-type LCC members from Mamajek, Meyer, & Liebert (2002) (crosses). The four  $\epsilon$  Cha candidates that overlap this study are labelled. Blue filled circles denote the high-probability (>90 percent) early-type (large circles) and late-type (small circles) LCC membership of de Zeeuw et al. (1999), with the  $b = -10^\circ$  ‘boundary’ of the subgroup (dashed line).

All four MML stars have Tycho-2 (Høg et al. 2000) proper motions and high-resolution radial velocities from Torres et al. (2006). For 2MASS J1221–7116, we follow Kiss et al. (2011) and use the UCAC3 (Zacharias et al. 2010) proper motion (which agrees with PPMXL) and their RAVE radial velocity. Table 5.5 compares the observed kinematics with those expected from the  $\epsilon$  Cha and LCC space velocities. For LCC we adopt the recently revised space motion of Chen et al. (2011),  $UVW = (-7.8, -20.7, -6.0) \pm (0.5, 0.6, 0.3) \text{ km s}^{-1}$ , which is similar to that calculated by Mamajek et al. (2000), but differs by  $\sim 8 \text{ km s}^{-1}$  from the canonical value of de Bruijne (1999) (see also de Zeeuw et al. 1999; Madsen et al. 2002). We use it here as it captures the best-available astrometry (van Leeuwen 2007) and observed radial velocities. With the exception of CP–68 1388 (MML 1), which appears to be an LCC member at  $\sim 90 \text{ pc}$ , the observed proper motions and radial velocities are a better match to the  $\epsilon$  Cha space motion at distances of 100–120 pc than to LCC.

High-resolution lithium measurements for the four MML stars were presented by Torres et al. (2006) and Weise et al. (2010). Since at late-G/early-K spectral types there is minimal difference in lithium depletion between pre-main sequence stars of ages  $\lesssim 20 \text{ Myr}$  (da Silva et al. 2009; Mentuch et al. 2008), we are unable to distinguish between membership in LCC and  $\epsilon$  Cha on the basis of lithium alone. However, with a K7 spectral type (Riaz et al. 2006), 2MASS J1221–7116 has a Li I  $\lambda 6708 \text{ EW}$  much greater than  $\sim 12 \text{ Myr}$   $\beta$  Pictoris members of

Table 5.5 Observed and predicted kinematics of northern  $\epsilon$  Cha/LCC members

Star	Observed			$\epsilon$ Cha			LCC					
	$\mu_\alpha \cos \delta^\dagger$	$\mu_\delta^\dagger$	RV <sup>‡</sup>	$\mu_\alpha \cos \delta$	$\mu_\delta$	RV	$d_{\text{best}}$	$\mu_\alpha \cos \delta$	$\mu_\delta$	RV	$d_{\text{best}}$	Memb.?
	[mas yr <sup>-1</sup> ]	[mas yr <sup>-1</sup> ]	[km s <sup>-1</sup> ]	[mas yr <sup>-1</sup> ]	[mas yr <sup>-1</sup> ]	[km s <sup>-1</sup> ]	[pc]	[mas yr <sup>-1</sup> ]	[mas yr <sup>-1</sup> ]	[km s <sup>-1</sup> ]	[pc]	
2MASS J1221-7116	-44.2 ± 1.5	-12.4 ± 1.6	11.5 ± 1.4	-43	-13	13.0	100	-44	-4	14.6	85	$\epsilon$ Cha
CP-68 1388	-36.1 ± 2.4	+5.7 ± 2.4	15.9*	-36	+0	15.4	115	-36	+8	16.7	90	LCC
HD 105923	-38.9 ± 1.4	-8.3 ± 1.4	14.2*	-36	-9	13.3	120	-37	-2	14.9	100	$\epsilon$ Cha
CD-69 1055	-43.1 ± 1.5	-18.7 ± 1.5	12.8*	-42	-20	11.8	100	-44	-12	13.6	85	$\epsilon$ Cha
MP Mus	-40.8 ± 1.5	-23.3 ± 1.5	11.6 ± 0.2	-41	-24	11.0	100	-42	-16	12.9	90	$\epsilon$ Cha

<sup>†</sup> Proper motions from Tycho-2 and UCAC3 (2MASS J1221-7116).

<sup>‡</sup> Radial velocities from Kiss et al. (2011) (2MASS J1221-7116) and Torres et al. (2006).

\* Single-epoch measurements. Torres et al. (2006) claimed 0.3 km s<sup>-1</sup> as a typical velocity error.

a similar temperature (which can be used as a proxy for the similarly-aged LCC). Combined with the excellent kinematic match, its low level of lithium depletion confirms membership in  $\epsilon$  Cha. From the available kinematic information, we confirm the findings of Torres et al. (2008) and place HD 105923, CD–69 1055 and MP Mus in  $\epsilon$  Cha, but suggest CP–68 1388 (MML 1) is better classified as an LCC member at  $\sim 90$  pc. Mamajek et al. (2002) calculated a secular parallax for the star of 102 pc using the space motion of de Bruijne (1999). This also gives an excellent fit to the Tycho-2 proper motion, albeit with a much lower predicted radial velocity ( $8.7 \text{ km s}^{-1}$ ). The new Chen et al. (2011) space motion resolves this discrepancy.

As noted by Torres et al. (2008), the detection of an optically-thick primordial disk surrounding MP Mus (MML 34; Kastner et al. 2010; Silverstone et al. 2006) is consistent with the younger age implied by membership in  $\epsilon$  Cha. Mamajek et al. (2002) estimated an age for LCC of 17–23 Myr, although the southern part of the subgroup may be as young as  $\sim 12$  Myr old (Preibisch & Mamajek 2008). This younger age notwithstanding, primordial disks are exceptionally rare around stars older than 10 Myr (Mamajek 2009; Hernández et al. 2008) and MP Mus is the only CTTS detected by Mamajek et al. (2002) from 110 solar-type members of UCL and LCC. The star would not be an exception in  $\epsilon$  Cha however—Torres et al. (2008) claimed T Cha could also be classified as a CTTS in its most active phases. We have detected a disk around the star and found several new CTTSs amongst  $\epsilon$  Cha candidates from the literature. These are described in §5.4.4.

While a reanalysis of all southern LCC members using updated kinematics is outside the scope of this thesis, it is worth discussing the relationship between LCC and the  $\epsilon$  Cha Association in light of their overlapping memberships and similar distances and space motions. As noted by Preibisch & Mamajek (2008), there are hints of substructure in LCC and it appears that the northern part of the group is somewhat more distant, older, and richer ( $\sim 17$  Myr, 120 pc) than the region south of the Galactic equator ( $\sim 12$  Myr, 110 pc). Furthermore, while Chen et al. (2011) calculated a space motion for all of LCC, there is subtle evidence of a N-S gradient in the  $W$  velocity component. The younger, southern region ( $b < -1$ ) has  $W = -6.9 \text{ km s}^{-1}$ , while for the northern region ( $b > +1$ )  $W \sim -5.3 \text{ km s}^{-1}$  (E. Mamajek, private communication).  $\epsilon$  Cha has a  $W$  velocity component of  $-10.4 \text{ km s}^{-1}$  (Torres et al. 2008). The age, distance and velocity trends mean we could be seeing evidence for a N-S wave of triggered star formation across LCC, ending with the birth of  $\epsilon$  Cha (and possibly the  $\eta$  Cha open cluster, see §5.4.5) only 3–7 Myr ago. In such a picture a useful demarcation between the groups simply may not exist and it would be futile to try and classify stars between LCC and the main concentration of  $\epsilon$  Cha as belonging to either group<sup>10</sup>. For the time being we keep the classifications of Tables 5.3 and 5.5, eagerly awaiting a better understanding of the star formation history across the region.

#### 5.4.2. Updated colour-magnitude diagram

Having estimated kinematic distances to all the candidates, we may now calculate their absolute magnitudes and compare them to known members and model isochrones. To this end, we plot in Figure 5.8 the DENIS/2MASS colour-magnitude diagram for confirmed late-type members and literature candidates. The old field binary RX J1137.4–7648 is not

<sup>10</sup>A similar problem exists at the northern edge of LCC and the TW Hydriæ Association, where TWA stars at 70–150 pc are very likely LCC members. See discussion in Mamajek (2005a) and Lawson & Crause (2005).

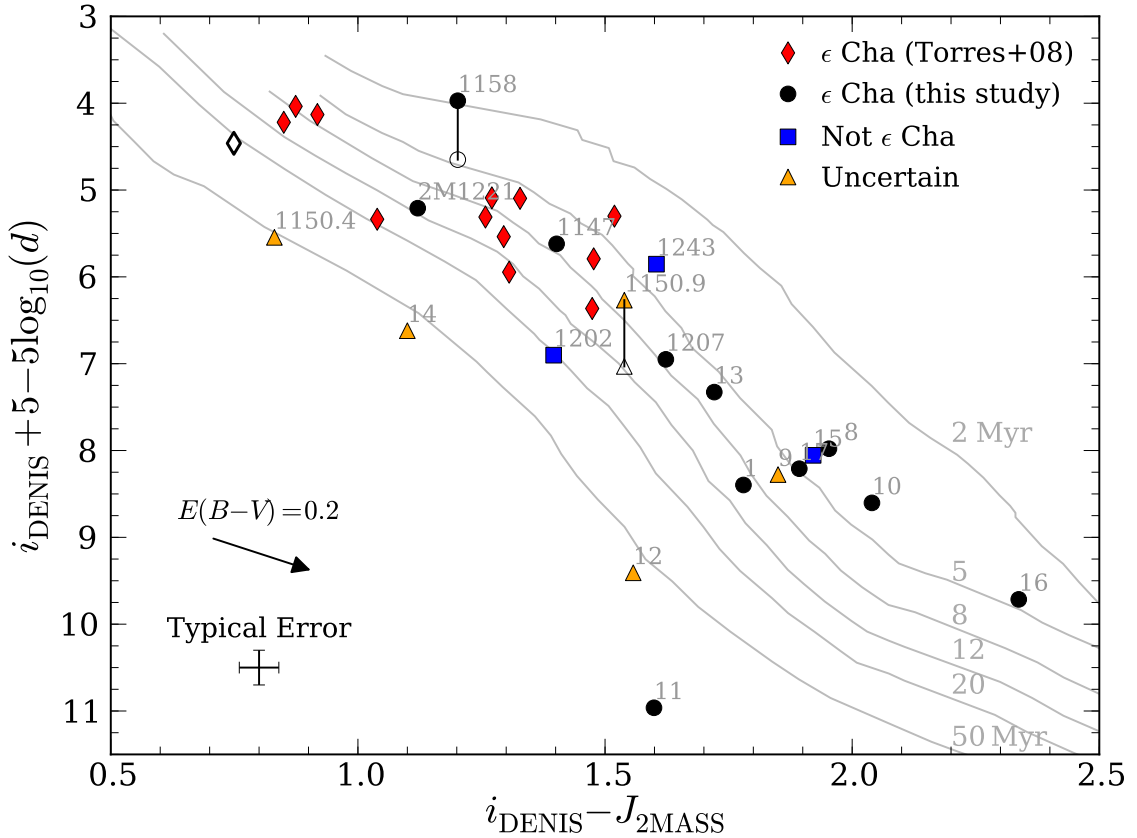


**Figure 5.8** Colour-magnitude diagram for late-type  $\epsilon$  Cha members from Torres et al. (2008) (red diamonds), confirmed candidates from this study (black circles), uncertain candidates (orange triangles) and non-members (blue squares). The open diamond is the new LCC member CP-68 1388 at 90 pc. Transformed 2–50 Myr isochrones from Baraffe et al. (1998) are drawn for comparison. The open circle shows RX J1158.5–7754A at its 90.4 pc *Hipparcos* distance. RX J1150.9–7411 is plotted at the both the 135 pc distance required for membership in  $\epsilon$  Cha and its 95 pc LCC distance (open triangle).  $\epsilon$  Cha 9 is drawn at the group distance of 110 pc.

plotted. Overall, there is broad agreement between both sets of members and a 5–10 Myr age, as estimated from Baraffe et al. (1998) isochrones. However, even considering the large uncertainties implicit in the kinematic distances, there are some notable outliers.

$\epsilon$  Cha 11 is significantly under-luminous for its  $\sim 100$  pc distance. As noted by Luhman (2004b), this is probably due to the star being observed in light scattered from an edge-on disk. The star is a CTTS with a strong infrared excess and will be discussed further in §5.4.4.

RX J1150.4–7704 also appears under-luminous at 100 pc, especially if its unresolved companion contributes significantly to the  $i$ -band flux. Reddening cannot explain the position of the star in Figure 5.8 as the reddening vector is parallel to the isochrones. Using the VRI photometry of Padgett et al. (2006) and assuming the companion contributes negligible luminosity, RX J1150.4–7704 has an absolute magnitude consistent with the Torres et al. (2008)  $\beta$  Pictoris isochrone at 80–100 pc. However, at this distance the star would be an unrealistic  $\sim 80$  pc from  $\beta$  Pic itself and the trace-back simulations provide no plausible ejection scenario. Since  $\beta$  Pictoris and LCC have similar ages ( $\sim 12$  Myr), it is possible that the star is another outlying LCC member with a peculiar velocity, similar to  $\epsilon$  Cha 14.

At the 123 pc kinematic distance of its wide companion, RX J1158.5–7754A is almost a magnitude over-luminous compared to members of similar spectral type. With a  $K$ -band

flux ratio of 0.5, the 0.07'' close companion (Köhler 2001) can explain some but not all of this excess. The 90 pc *Hipparcos* distance is a better match to the  $\epsilon$  Cha isochrone, but yielded a poor match to the association space motion. A combination of binarity and a slightly reduced distance can satisfactorily explain the over-luminosity.

$\epsilon$  Cha 14 and RX J1202.8–7718 appear to be true LCC members, as expected from their low lithium EW measurements (150 and 300 mÅ, respectively). Their photometric and kinematic distances agree to first-order, given the unknown age and shape of the low-mass LCC isochrone, and the uncertain kinematic distance to  $\epsilon$  Cha 14. They are joined at lower luminosities by the possible  $\beta$  Pic member  $\epsilon$  Cha 12, whose 55 pc kinematic distance places it well below confirmed  $\epsilon$  Cha members. However, with  $i_{\text{DENIS}} = 13.11$  and assuming the Luhman (2004b) M3.75 spectral type is correct, this distance yields an absolute  $V$ -band flux nearly 2 mag below the Torres et al. (2008) isochrone of  $\beta$  Pic members. The flux may be suppressed by an edge-on disk but no such structure is detected in WISE photometry (see §5.4.4). Moreover, the under-luminosity is enhanced if its putative close companion contributes a significant fraction of the observed flux. Although clearly not a member of  $\epsilon$  Cha, more observations are required to determine the origin of  $\epsilon$  Cha 12.

The distance used for RX J1150.9–7411 was 135 pc, which gave a kinematic match between  $\epsilon$  Cha and the star's PPMXL proper motion. The location of the star in the CMD and its large lithium EW support this assignment. However, membership in LCC at a smaller distance (~95 pc, open triangle) cannot be ruled out given the improved kinematics from Terranegra et al. (1999).  $\epsilon$  Cha 9 is lithium-rich but has discrepant kinematics. Its position in Figure 5.8 is consistent with membership in  $\epsilon$  Cha at the canonical group distance of 110 pc.

Lastly,  $\epsilon$  Cha 15 and RX J1243.1–7458 both lie on the upper (brighter) envelope of  $\epsilon$  Cha sources in the CMD, consistent with membership in the 1–4 Myr-old Cha I and II clouds at distances of 160 and 200 pc, respectively.

#### 5.4.3. Membership summary

Combining the above discussions, we have confirmed ten literature candidates as new members of the  $\epsilon$  Cha Association ( $\epsilon$  Cha 1, 8, 10, 11, 13, 16, 17, RX J1147.7–7842, RX J1158.5–7754A and RX J1207.7–7953). We also confirmed 2MASS J1221–7116 from (Kiss et al. 2011). Nine stars ( $\epsilon$  Cha 9, 12, 14, 15, RX J1150.4–7704, RX J1150.9–7411, RX J1137.4–7648, RX J1202.8–7718, and RX J1243.1–7458) do not appear to be  $\epsilon$  Cha members or have uncertain memberships. Finally, we confirmed membership in  $\epsilon$  Cha of three of the four Torres et al. (2008) members also proposed by Mamajek et al. (2002) as members of Lower Centaurus Crux. The remaining candidate, CP–68 1388, is a likely member of LCC.

#### 5.4.4. Classical T Tauri Stars in $\epsilon$ Cha

Several of the candidates in Table 5.3 exhibited strong and variable H $\alpha$  emission during our multi-epoch *WiFeS/R7000* observations. In many cases the strength of this emission exceeded that expected from chromospheric activity (Barrado y Navascués & Martín 2003). These stars can therefore be considered candidate Classical T Tauri Stars (CTTSs), whose H $\alpha$  emission is driven primarily by accretion from a circumstellar disk (see Chapter 3).

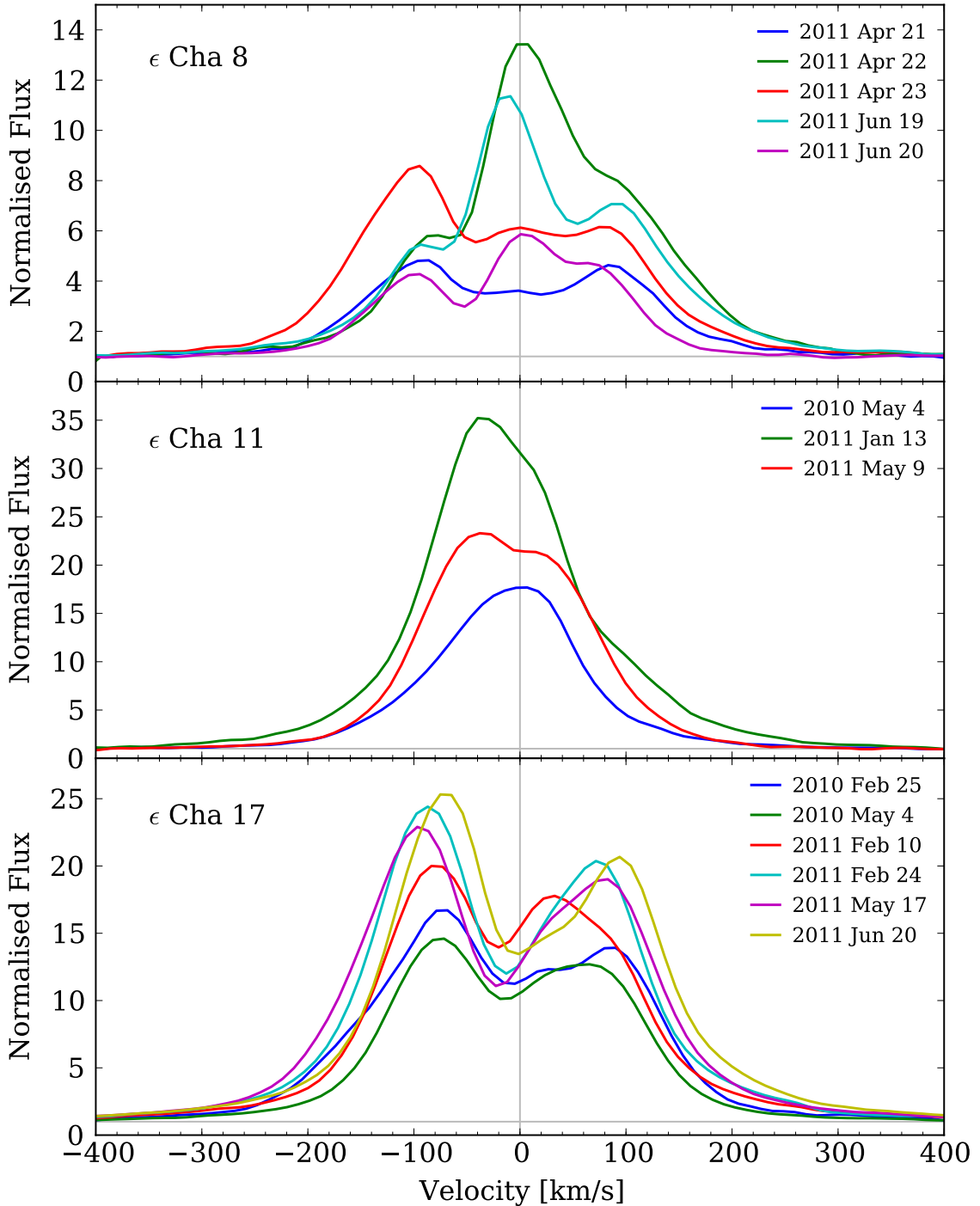


**Figure 5.9** Multi-epoch WiFeS/R7000 velocity profiles for three newly confirmed  $\epsilon$  Cha members with complex H $\alpha$  emission lines;  $\epsilon$  Cha 8,  $\epsilon$  Cha 11 and  $\epsilon$  Cha 17. All the profiles have been normalised over the region  $\pm 500\text{--}1000 \text{ km s}^{-1}$  and shifted to zero radial velocity.

Figure 5.9 presents the velocity profiles of the three new  $\epsilon$  Cha members with complex H $\alpha$  emission. All the profiles show  $v_{10}$  velocity widths well in excess of the 200–270 km  $\text{s}^{-1}$  criterion used in the literature to identify accretion (White & Basri 2003; Jayawardhana et al. 2003). Note the large *daily* variation in the triple-peaked profiles of  $\epsilon$  Cha 8. This is reminiscent of the variation seen in the spectra of the episodic accretor 2MASS J0820–8003 in Chapter 3. As well as H $\alpha$ , all three stars also showed He I  $\lambda 5876/6678$  emission and  $\epsilon$  Cha 11 displayed strong forbidden [O I]  $\lambda 6300/6363$  and [N II]  $\lambda 6584$  emission.

In addition to these extreme emitters,  $\epsilon$  Cha 10, 13 and 16 also produced variable H $\alpha$  emission of varying degrees (see Table 5.3).  $\epsilon$  Cha 10 would be a border-line accretor by the Barrado y Navascués & Martín (2003) EW criterion. The narrow ( $\lesssim 200$  km s $^{-1}$ ) line profile and lack of other emission lines commonly seen in accreting stars suggests the H $\alpha$  emission is chromospheric in origin.  $\epsilon$  Cha 16 flared to  $-35$  Å on 2011 June 19 from its quiescent level around  $-12$  Å. Again, the emission is likely chromospheric. The spectrum of  $\epsilon$  Cha 13 is unique among the new members, with H $\alpha$ , Na I D, He I and forbidden [O I], [O II] ( $\lambda 7320/7331$ ), [N II] ( $\lambda 6548/6583$ ), [S II] ( $\lambda 6716/6731$ ), [Ca II] ( $\lambda 7291/7324$ ) and [Fe II] ( $\lambda 7155$ ) emission lines all present (Figure 5.5). These are reminiscent of the  $\sim 10$  Myr CTTS binary TWA 30AB (Looper et al. 2010a,b). The emission is variable as only the H $\alpha$  line was present in the discovery spectrum of Luhman (2007). Forbidden emission usually arises in the outer regions of low-density, accretion-driven outflows from young stars (see reviews by Appenzeller & Mundt 1989; Hartigan 1997; Reipurth & Bally 2001). The presence of high-excitation forbidden [O II] lines in the R3000 spectrum requires higher densities than those typically found in protostellar winds. The emission may be induced by shocks in an ionised jet close to the star (Hartigan et al. 2004; Podio et al. 2009). The same shocks are also likely to be responsible for the weak [Ca II] and [Fe II] emission (and other refractory elements), via the reprocessing of dust grains (Nisini et al. 2005; Podio et al. 2006, 2009).

To confirm the presence of disks around these stars, we plot in Figure 5.10 near and mid-infrared photometry from 2MASS and the WISE Preliminary Data Release (Wright et al. 2010). *WiFeS/R7000* H $\alpha$  equivalent widths are also plotted versus the  $K_s$ –[W3] colour in the bottom-right panel. At 22 and 12  $\mu$ m, all but one of the candidates with strong H $\alpha$  emission also has a pronounced infrared excess. The exception is  $\epsilon$  Cha 16, which flared during our observations. At shorter wavelengths, only  $\epsilon$  Cha 13 lacks a strong excess at 3 and 5  $\mu$ m. This is usually interpreted as the signature of a transitional disk with a large inner opacity hole (Williams & Cieza 2011). The five stars with  $K_s$  – [W4]  $\approx 2.5$  have weak ( $< 10$  Å) H $\alpha$  emission and a small excess at 22  $\mu$ m. Their spectral energy distributions (SEDs) closely resemble the  $\eta$  Cha members RECX 3 and 4 (Gautier et al. 2008; Sicilia-Aguilar et al. 2009). The photospheric SEDs at wavelengths shorter than 22  $\mu$ m imply large inner holes in their disks. Alternatively, the weak 22  $\mu$ m excesses could result from second-generation dust in optically-thin debris disks (see review by Wyatt 2008).

To compare to the new members, we also obtained WISE photometry for the confirmed Torres et al. (2008) stars. In addition to the known CTTS MP Mus and Herbig Ae star DX Cha (=HD 104237A), we detected excesses in T Cha, which was a suspected CTTS from its highly variable H $\alpha$  emission (Schisano et al. 2009) and the *Spitzer* flat-spectrum source DZ Cha (=RX J1149.8–7850). Covino et al. (1997) reported a  $-32$  Å H $\alpha$  EW for DZ Cha, whereas our single *WiFeS* spectrum on 2011 February 25 showed only  $-2$  Å emission. Both stars may be binaries, based on the variation in their reported radial velocities (see §5.3.2). *Spitzer* observations of T Cha and DZ Cha were presented by Wahhaj et al. (2010).

Spectral energy distributions of the seven confirmed CTTSs (MP Mus, T Cha, DZ Cha,  $\epsilon$  Cha 8, 11, 13, 17) and the Herbig Ae star DX Cha are plotted in Figure 5.11.  $\epsilon$  Cha 11, 13 and DZ Cha all have rising mid-infrared SEDs. This is evidence of dust with a strong radial dependence, resulting in a sharp boundary to the inner opacity hole. This may be due to dynamical clearing by a companion (perhaps planetary, e.g. Bouwman et al. 2010)

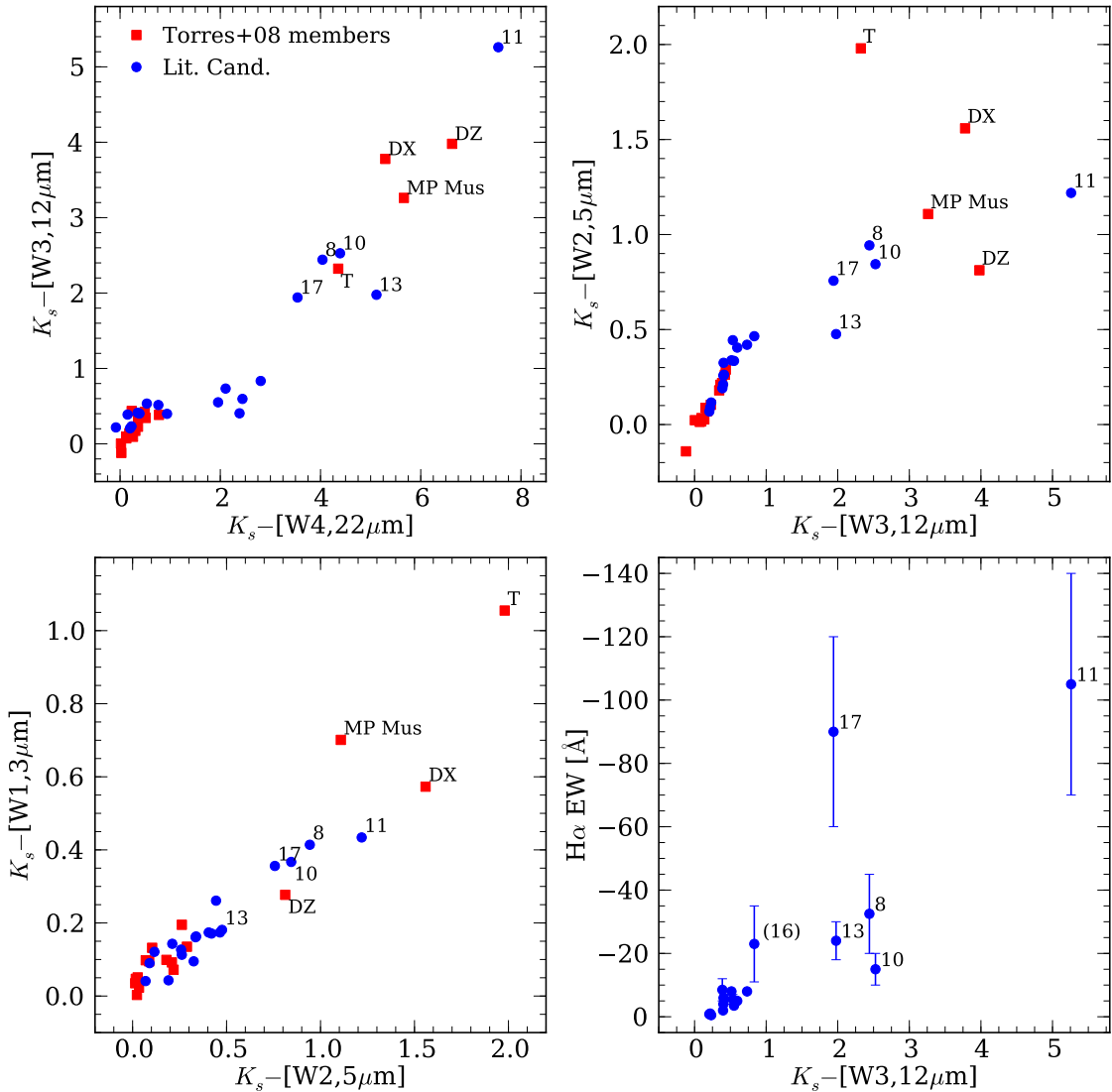


**Figure 5.10** WISE 3,5,12,22  $\mu\text{m}$  photometry relative to 2MASS  $K_s$  for  $\epsilon$  Cha members from Torres et al. (2008) (red squares) and literature candidates from Table 5.3 (blue circles). Stars mentioned in the text are labelled. The bottom-right panel shows the  $WiFeS/R7000$   $\text{H}\alpha$  equivalent widths of the literature candidates versus  $K_s - [\text{W}3]$ . Error bars give the range of widths observed in the multi-epoch spectra.  $\epsilon$  Cha 16 is normally quiescent at around  $-12 \text{ \AA}$  but flared to  $-35 \text{ \AA}$  on 2011 June 19. It has no appreciable excess in the WISE colours.

or photo-evaporation of the inner disk by the central star (Alexander et al. 2006). As seen in Figure 5.8, the under-luminosity of  $\epsilon$  Cha 11 is probably due to its dusty disk having an inclination close to edge-on. Two other stars with excess emission are also plotted in Figure 5.11. The SED of  $\epsilon$  Cha 1 is representative of the five sources with slight 22  $\mu\text{m}$  excesses in Figure 5.10 (see above).  $\epsilon$  Cha 10 has a strong infrared excess, but its weak  $\text{H}\alpha$  emission and lack of He I or forbidden emission imply it is a probably a Weak-lined T Tauri star (WTTS). Further monitoring of the star is necessary to see if it is an episodic accretor, like the  $\eta$  Cha halo member 2MASS J0820–8003 (Chapter 3).

With seven CTTSs and a Herbig Ae star,  $\epsilon$  Cha has more accreting members than  $\eta$  Cha (four, ECHA J0843.3–7905, ECHA J0844.2–7833, RECX 9, RECX 11; Jayawardhana et al. 2006; Song et al. 2004) and the  $\beta$  Pictoris Association (V4046 Sgr; Quast et al. 2000; Stempels & Gahm 2004). The TW Hydriæ Association has also been extensively studied down to

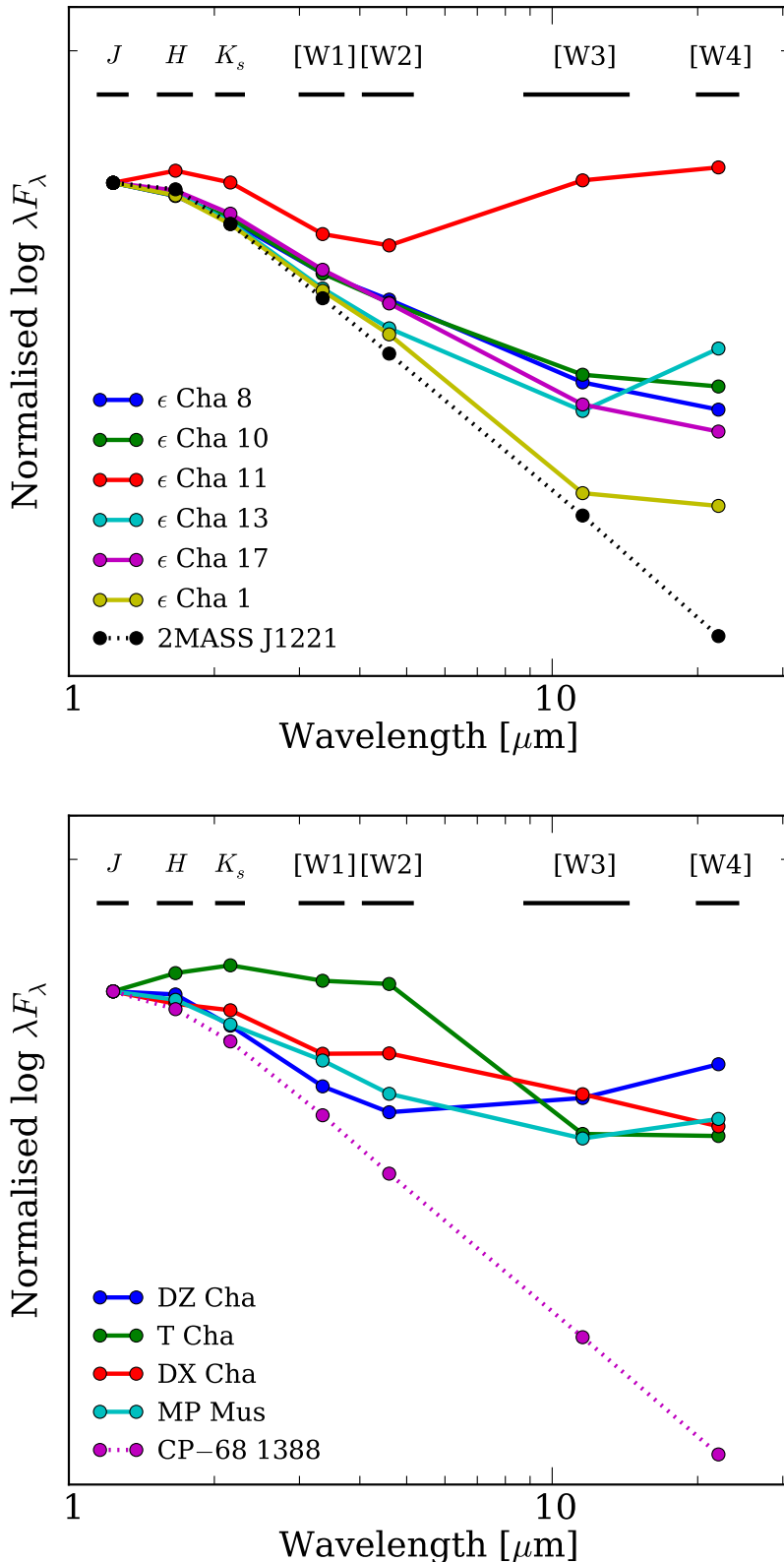


**Figure 5.11** 2MASS/WISE SEDs of disk-bearing  $\epsilon$  Cha members. Zero-magnitude fluxes and mean wavelengths are taken from Cohen et al. (2003) and Jarrett et al. (2011). Filter bandwidths are given by the black lines at the top of each plot. All the SEDs have been normalised to the  $J$ -band flux. *Top panel:* The four new CTTSs from the literature, the WTTS  $\epsilon$  Cha 10 and the weak-excess source  $\epsilon$  Cha 1. The latter is representative of the five sources in Figure 5.10 with  $K_s - [W4] \approx 2.5$ . *Bottom panel:* The three CTTS from the membership of Torres et al. (2008), plus the Herbig Ae star DX Cha (=HD 104237A). The non-excess sources 2MASS J1221–7116 and CP–68 1388 (dotted lines) represent the underlying photospheric continuum.

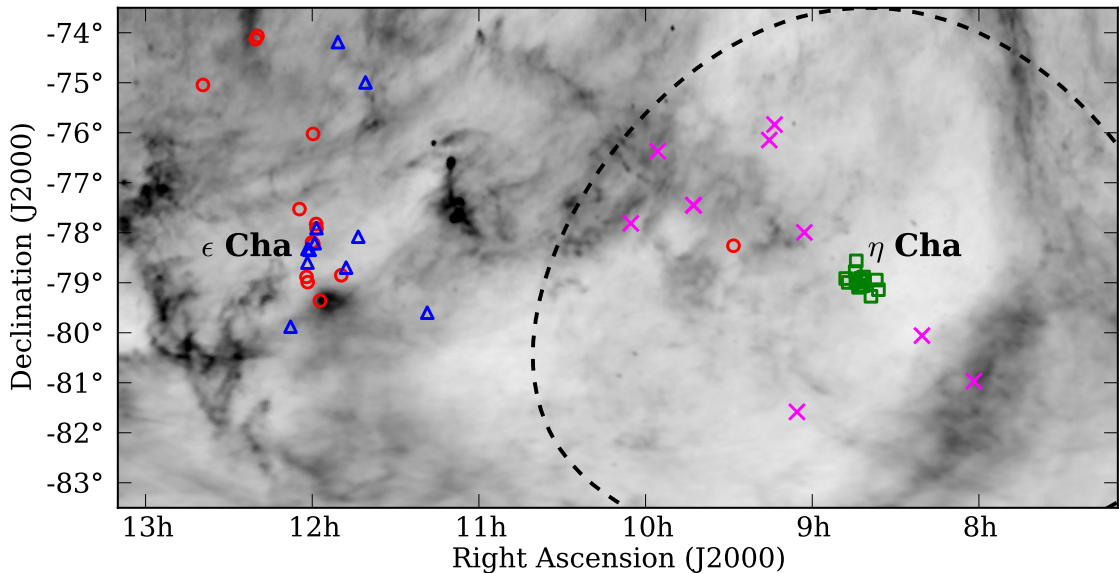


**Figure 5.12** IRAS 100  $\mu\text{m}$  map of Chamaeleon with  $\eta$  Cha members (green squares), halo members (magenta crosses, Chapter 2), previously confirmed  $\epsilon$  Cha members (red circles) and new  $\epsilon$  Cha members (blue triangles). The dashed line denotes the 5.5 deg radius around  $\eta$  Cha surveyed for new members (Chapter 2). The  $\epsilon$  Cha member within the search radius is HD 82879.

brown-dwarf masses. Seven of its members are actively accreting (TW Hya, TWA 3A, 27, 28, 30A, 30B, 31), including the brown dwarfs TWA 27 and TWA 28 (Jayawardhana et al. 2006;Looper et al. 2010a,b; Shkolnik et al. 2011). The large number of CTTSs in  $\epsilon$  Cha likely reflects a younger age than  $\beta$  Pic ( $\sim$ 12 Myr) or TWA ( $\sim$ 10 Myr). Future surveys for new members of  $\epsilon$  Cha will no doubt reveal more accreting objects at lower masses.

#### 5.4.5. Relationship to $\eta$ Chamaeleontis

The  $\epsilon$  Cha Association is almost certainly related in some way to the young open cluster  $\eta$  Chamaeleontis (Chapters 2 and 3; Mamajek et al. 1999), 10 degrees to the west. The groups share similar ages, distances and kinematics, which led Torres et al. (2008) to subsume four members of the cluster with good kinematics into their  $\epsilon$  Cha solution. We did not consider these stars  $\epsilon$  Cha members in this study. Figure 5.12 plots the distribution of  $\eta$  Cha members on the sky, with the newly-confirmed stars from this work. The central regions of each group are separated by  $\sim$ 25 pc in space. Although Torres et al. (2008) identified one member of  $\epsilon$  Cha that is closer to  $\eta$  Cha (HD 82879) and we have discovered several new halo members of  $\eta$  Cha in the region between the groups (Chapter 2), the low density of these stars and the wide separation of the dense central cores suggests the groups are separate entities (but note that the census of  $\epsilon$  Cha is likely far from complete, see §5.1.2).

After considering their gravity-sensitive spectral features, Lyo et al. (2008) were able to resolve the two groups in age, with  $\epsilon$  Cha appearing approximately 1–2 Myr *younger* than  $\eta$  Cha. However, only two stars in their late-type sample were confirmed kinematic members at the time (HD 104237D and E). We have confirmed as members an additional four stars ( $\epsilon$  Cha 1, 8, 10, 11), but rejected the other two ( $\epsilon$  Cha 9 has discrepant kinematics,  $\epsilon$  Cha 12 is a suspected  $\beta$  Pic member). Given the results of the Lyo et al. (2008) study, it is likely that the two groups are distinct, with subtly different space motions, ages and distances. However, their proximity and physical similarities suggest a common formation scenario.

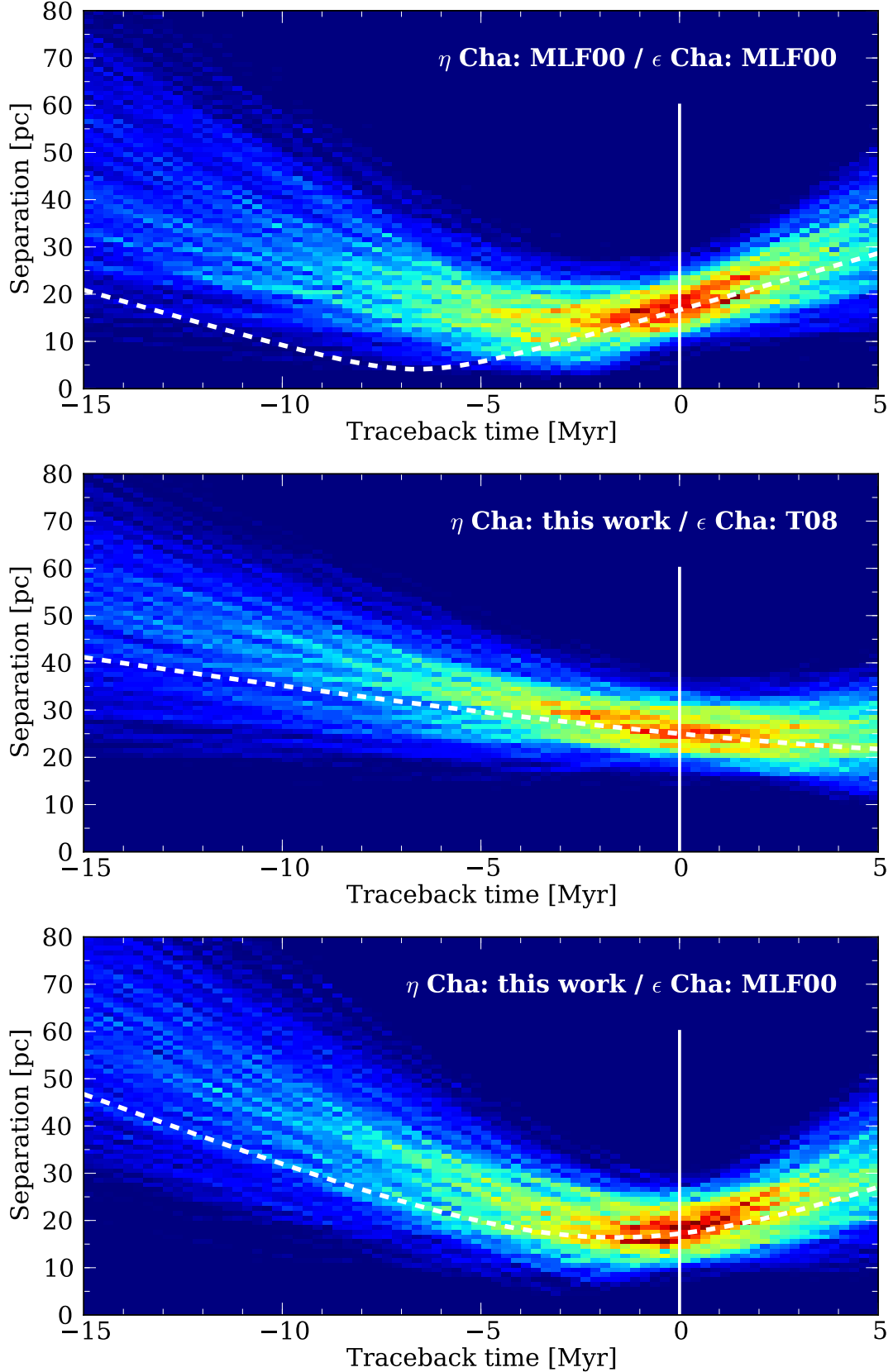


**Figure 5.13** Simulations of the  $\eta$  and  $\epsilon$  Cha separation with time. Each pixel shows the number of tracks passing through that point (blue=low, brown=high). The  $N = 1000$  realisations sample the  $\epsilon$  Cha space velocity and its uncertainty. Errors on  $\eta$  Cha are assumed negligible. Uncertainty in the present-day centre of  $\epsilon$  Cha is assumed normally distributed in  $(X, Y, Z)$  with  $\sigma = 5$  pc. The dashed lines assume zero errors on all quantities. *Top:* Positions and velocities from Mamajek et al. (2000). *Middle:*  $\eta$  Cha from Table 2.4,  $\epsilon$  Cha values from Torres et al. (2008) (position excludes their  $\eta$  Cha members). *Bottom:*  $\epsilon$  Cha values from Mamajek et al. (2000).

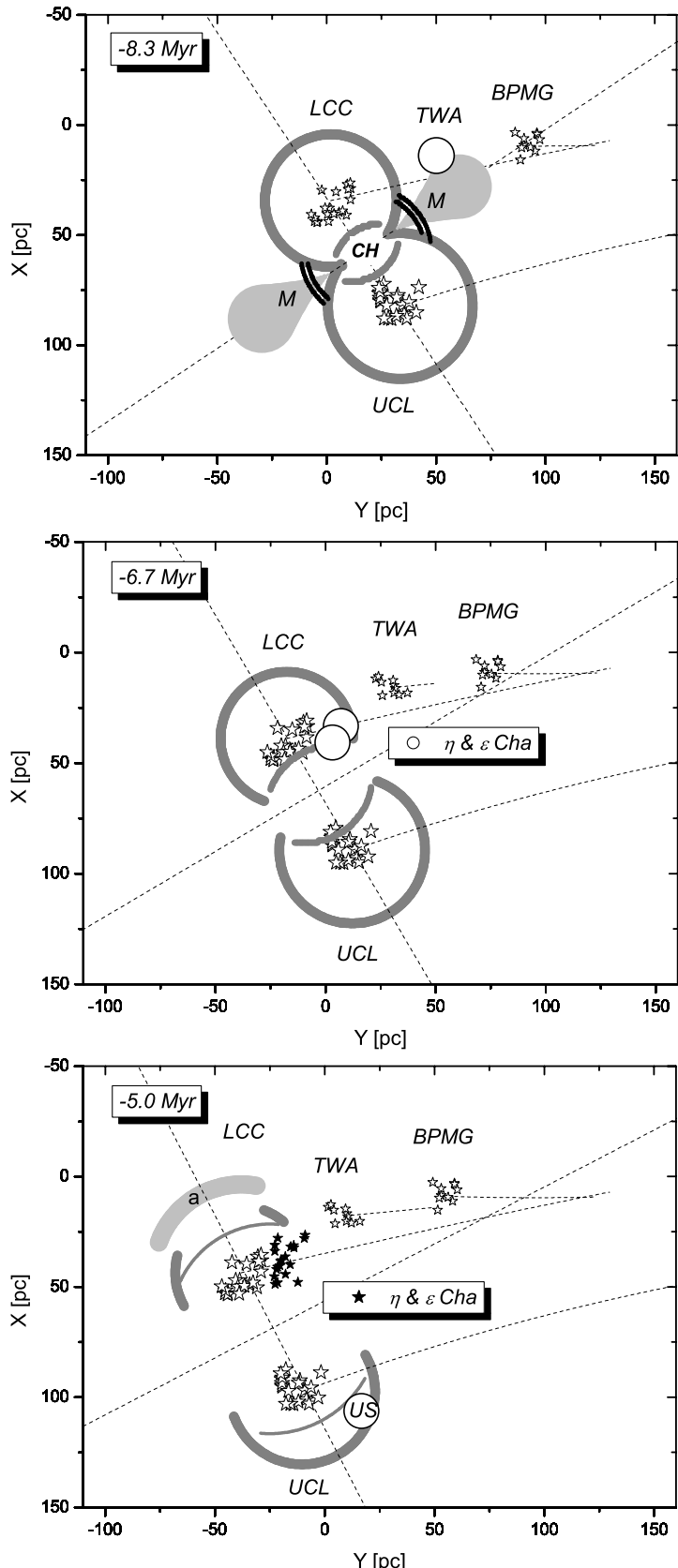


**Figure 5.14** Formation of the young groups near Sco-Cen, as simulated by Ortega et al. (2009, reproduced by permission of the AAS). *Top panel:* The formation of TWA 8 Myr ago in the Mach shock (M) formed by colliding supernovae and wind-driven bubbles from LCC and UCL. *Middle:* The “champagne flows” (CH) formed by the reverse shocks quickly propagate into the evacuated bubbles.  $\epsilon$  and  $\eta$  Cha were formed 6.7 Myr ago when the flow caught up with the expanding shell in the outskirts of LCC. *Bottom:* The reverse shock continues into the UCL bubble, leading to the formation of the Upper Scorpius subgroup ~5 Myr ago.

Using space motions and positions from Mamajek et al. (2000), Jilinski et al. (2005) showed that the centres of  $\eta$  and  $\epsilon$  Cha reached a minimum separation of  $\sim 3$  pc some 6–7 Myr ago. This agrees with their estimated evolutionary age and implies they were born together in the outskirts of Sco-Cen. However, these simulations did not take into account the large errors in the  $\epsilon$  Cha space motion, nor the uncertainty in the central position of the group. Our linear traceback analysis (Figure 5.13, top panel) demonstrates that such a small separation is unlikely at any epoch, given the quoted uncertainties in the  $\epsilon$  Cha velocity. Moreover, using the best-available kinematics for  $\eta$  Cha<sup>11</sup> from Table 2.4, it is clear that the two groups were unlikely to have ever been much closer than their current separation and were probably 20–40 pc apart at the time of their birth (Figure 5.13, bottom panels).

Ortega et al. (2009) posited that the two groups were born together in the “champagne flow” (Tenorio-Tagle 1979) created when reflected shocks of colliding supernovae-driven shells around LCC and UCL moved into the previously evacuated bubbles (Figure 5.14). According to this picture,  $\beta$  Pic and TWA were born in the flow generated by the approaching shells and the Mach shock formed after the shells collided, respectively.

Combining the results of the above studies with our new kinematics, it appears very likely that  $\eta$  and  $\epsilon$  Cha were born in two nearby—but distinct—regions in the periphery of LCC. The cloud that would later become  $\eta$  Cha was first to collapse, 5–8 Myr ago. Around 30 pc away, the gas that would form  $\epsilon$  Cha followed a few Myr later. The new traceback analysis places  $\epsilon$  Cha closer to the reverse shock of Ortega et al. (2009) than  $\eta$  Cha at the latter’s birth, so the champagne flow cannot be responsible for forming  $\epsilon$  Cha. The location of  $\epsilon$  Cha near the initial collision of the LCC and UCL bubbles leads us to speculate that it was in this turbulent environment that the material from which it would ultimately form began to collapse. Large turbulent velocity dispersions may hinder star formation (Herrera et al. 2011) and the decay of this turbulence over several Myr provides a natural explanation for the age difference between  $\eta$  and  $\epsilon$  Cha. Large-scale turbulent flows also explain why  $\epsilon$  Cha is more extended than  $\eta$  Cha. The core of  $\eta$  Cha was incredibly compact (see discussion in Moraux et al. 2007), presumably due to the violent compression of material between the reverse shock and the shell wall. Over time, dynamical evolution then dispersed many  $\eta$  Cha members into a low-density halo surrounding the cluster (Chapter 2).

## 5.5. Summary

The  $\epsilon$  Cha Association is the youngest kinematic group of stars in the solar neighbourhood. To investigate the low-mass membership of  $\epsilon$  Cha, we obtained medium-resolution, multi-epoch spectra of 19 candidates proposed in the literature. After considering their proper motions, radial velocities and Li I  $\lambda 6708$  equivalent widths, we confirmed 11 stars as new members, with estimated kinematic distances of 95–135 pc. The remaining candidates are likely to be members of the Cha I and II background cloud populations, as well as the Lower Centaurus Crux subgroup of Sco-Cen.

Several of the new members have strong and variable H $\alpha$  emission that is indicative of accretion from a circumstellar disk. Using newly available WISE photometry we confirmed

<sup>11</sup>The new and improved space motion for  $\eta$  Cha differs from the canonical value by  $2.4 \text{ km s}^{-1}$ , primarily due to an improved average radial velocity from 10 non-binary members,  $\langle \text{RV} \rangle = 18.3 \pm 0.1 \text{ km s}^{-1}$  (see §2.6.2).

the presence of significant infrared excesses in these stars (CTTSs) and several non-accreting members (WTTSs). As expected of a ‘transitional’ intermediate-age pre–main sequence population, the spectral energy distributions of disks in  $\epsilon$  Cha show a variety of morphologies, from optically-thick accretion disks, to weak-excess debris disks. Because of their age and proximity to the Sun, these new members will make ideal targets for future studies of disk properties and the formation of planetary systems around low-mass stars.

Finally, we have discussed the relationship between  $\epsilon$  Cha and the nearby open cluster  $\eta$  Cha. Combining recent results from the literature with improved kinematics for  $\eta$  Cha, we conclude the two groups were born within a few Myr of each other on the periphery of LCC. The  $\epsilon$  Cha Association may in fact be the end-result of a wave of star formation throughout Sco-Cen, as implied by subtle age, distance and velocity trends southward through LCC and into  $\epsilon$  Cha. Contrary to previous studies, we propose  $\eta$  Cha and  $\epsilon$  Cha were *not* born together, but were separated by  $\sim$ 30 pc at the time  $\eta$  Cha formed. Improved radial velocities, proper motions and distances for more  $\epsilon$  Cha members are vital for confirming this hypothesis.



# CHAPTER 6

---

## Conclusions

Although the Universe is under no obligation to make sense,  
students in pursuit of the Ph.D. are.

– Robert P. Kirshner<sup>1</sup>

Due to their youth (5–10 Myr) and proximity (90–120 pc), the open cluster  $\eta$  Chamaeleontis and nearby  $\epsilon$  Chamaeleontis Association are ideal laboratories to study the formation and evolution of planetary systems. To better understand their potential as planet hosts and identify promising targets for future studies, this thesis has explored the formation, dynamical evolution, accretion and disk properties of both groups' low-mass members.

The paucity of low-mass stars ( $0.025 < M/M_{\odot} < 0.15$ ) in  $\eta$  Cha has long been a puzzle. Previous efforts to find these 'missing' members through deep photometry of the cluster core or wide-field surveys have been singularly unsuccessful. Two possible explanations for their absence have been suggested; a top-heavy initial mass function (IMF) or dynamical evolution, which would have preferentially ejected low-mass stars to radii beyond that currently surveyed. Motivated by the apparent universality of the IMF and dynamical simulations by Moraux et al. (2007), who predicted the presence of such a halo of cluster ejectees, we undertook the widest ever (5.5 deg radius) survey for new members of  $\eta$  Cha.

Using existing photometry (DENIS, 2MASS) and proper motions (NOMAD, PPMXL), combined with extensive multi-epoch spectroscopy, we identified six new pre-main sequence stars surrounding  $\eta$  Cha at radii of 1.5–5 deg. To these we added four X-ray-bright stars from the ROSAT survey of young stars in the region. After considering each candidate's kinematics and modelling their ejection from  $\eta$  Cha as a function of time and distance, we subsequently confirmed four as dispersed cluster members. Another four candidates require better kinematics to confirm membership. Assuming our survey was complete over the  $0.08 < M/M_{\odot} < 0.3$  mass range of the X-ray-faint 2MASS/DENIS stars, the discovery of

---

<sup>1</sup>*Quarterly Journal of the Royal Astronomical Society*. 1991, Vol. 32, No. 3, p233

three new members in this range is in excellent agreement with the simulations of Moraux et al. (2007), who predicted 2–3 stars over the same mass range and search radius.

Despite small number statistics and uncertainties in the simulations—especially in modelling primordial binaries in such a rapidly evolving dynamical environment—the overall agreement between the models and our results is reassuring. We can therefore conclude that dynamical evolution alone is likely to be responsible for the current configuration of  $\eta$  Cha and it is not necessary to invoke an IMF deficient in low-mass objects. Improved modelling and new surveys to lower-mass limits and at larger radii are needed to fully confirm this conclusion. Current simulations imply there are at least several dozen members down to substellar masses awaiting discovery. Because most of the stars were ejected very early on at large velocities ( $>5 \text{ km s}^{-1}$ ), they will now be at radii of several tens of degrees from the cluster core. One such survey for these missing members is described in §6.1.

Of the four probable halo members, only 2MASS J0820–8003 had an appreciable excess in WISE 3–22  $\mu\text{m}$  photometry. We attribute this to a ‘transitional’ circumstellar disk. The star joins ten other  $\eta$  Cha members known to possess disks, most of which are also transitional. Since none of the four possible members show evidence of disks either, it appears that the dynamical processes responsible for their ejection are not conducive to long-term disk survival. The disk around 2MASS J0820–8003 may not have been so adversely affected by dynamics. The star is the closest new member to the cluster (1.5 deg) and would only need to have been ejected at  $\lesssim 1 \text{ km s}^{-1}$  to move to its current position. A large number of dispersed members lacking disks is also a natural explanation for the artificially high disk-fraction observed in the core of the cluster. However, the core members would presumably also have undergone significant dynamical interactions over time in the dense proto-cluster, which could easily destroy or warp their outer disks. How so many  $\eta$  Cha members retained disks in such an environment is a mystery. Observations and simulations of the outer regions of their disks will help resolve this discrepancy.

Two of the new halo stars, including 2MASS J0820–8003, were notable for their strong, variable H $\alpha$  emission during the multi-epoch observations. Based on the shape and strength of the emission, it is probably driven primarily by chromospheric activity, which can generate broad H $\alpha$  profiles during short flares. However, with a velocity width in excess of 400  $\text{km s}^{-1}$ , we also have evidence for at least one accretion event in 2MASS J0820–8003. The implied accretion rate of  $\sim 10^{-9} M_{\odot} \text{ yr}^{-1}$  is similar to those seen in other  $\eta$  Cha accretors. Such discrete, episodic accretion is presumably due to an inner disk cleared of dust but not completely free of gaseous material. This conclusion is supported by WISE photometry of the disk. Similar events have been observed in the  $\eta$  Cha member RECX 5, which may be a sign of episodic accretion in that star. Assuming the duty-cycle of accretion events is low (we estimate the event lasted less than 2 days), single-epoch surveys for accreting objects—especially in the critical 5–10 Myr age range when inner disks are cleared and giant planets form—are likely missing a large fraction of accreting objects. This may have important consequences for the gas-dissipation timescales derived from such surveys.

The only two pre-main sequence stars in our survey unlikely to be members of  $\eta$  Cha, RX J0942.7–7726 and 2MASS J0942–7727, were serendipitously found only 42'' apart, 3.5 deg to the northeast of the cluster. To the limits of the available observations, we have shown that they are coeval ( $\sim 10$  Myr), co-distant (100–150 pc) and almost certainly form a true

wide binary with a separation of 4000–6000 AU. Both stars have proper motions that agree within the errors and similar radial velocities. A traceback analysis argues for their birth in or near the Lower Centaurus Crux (LCC) or Upper Centaurus Lupus (UCL) subgroups of the Scorpius-Centaurus OB Association. Conversely, their small radial velocity difference ( $1\text{--}3 \text{ km s}^{-1}$ ) could mean the system is weakly bound or unbound, possibly as a result of the coincidental ejection of two single stars with similar velocity vectors from the subgroups.

Obtaining improved radial velocities for RX J0942.7–7726 and 2MASS J0942–7727 is a high priority. If these agree at the  $\lesssim 1 \text{ km s}^{-1}$  level expected of orbital motion, it is likely the two stars form a physical wide binary. If not, they must be considered unbound or the coincidental alignment of two unrelated young stars at similar distances. Further monitoring of RX J0942.7–7726 would then be warranted to determine if it too is a binary, as hinted by long-term radial velocity variations and similar hierarchical systems. Many of the suspected binaries in Chapters 2 and 5 would also benefit from radial velocity and imaging studies to ascertain their true status. Systemic velocities are vital to improving space motions, kinematic distances and membership in the young groups discussed in this work.

The very existence of RX J0942.7–7726AB and other wide binaries in the TW Hydriæ and  $\beta$  Pictoris associations suggests they underwent a different star formation process to denser groups like  $\eta$  Cha. The fragility of systems like RX J0942.7–7726AB explicitly forbids any strong dynamical interactions in the past 10 Myr, whereas the well-documented lack of wide ( $a > 20 \text{ AU}$ ) binaries in  $\eta$  Cha is clearly dynamical in origin. As discussed in Chapters 4 and 5,  $\eta$  Cha likely formed from the violent collapse of a small, dense cloud of perhaps a few tens of solar masses. The stars that comprise the unbound  $\beta$  Pictoris and TW Hydriæ associations were born in more distended turbulent flows, which would impart a larger spread of natal velocities while keeping wide binaries intact. RX J0942.7–7726AB presumably formed in a similar manner, from a smaller clouplet in the region. All of the groups kinematically linked to Sco-Cen, including  $\eta$  Cha, probably formed in close proximity to one another, brought into collapse by a passing spiral density wave or supernovae-driven bubbles around LCC and UCL (Sartori et al. 2003; Fernández et al. 2008; Ortega et al. 2009).

The key to understanding the formation of  $\eta$  Cha almost certainly lies with the nearby  $\epsilon$  Chamaeleontis Association, whose main body is 10 deg to the east of the cluster. Both groups have similar distances and kinematics but  $\epsilon$  Cha is 1–2 Myr younger. However, its membership is mired in uncertainty. To investigate the low-mass population of  $\epsilon$  Cha, we obtained medium-resolution, multi-epoch spectra of 19 candidates proposed in the literature. After considering their proper motions, radial velocities and Li I  $\lambda 6708$  equivalent widths, we confirmed 11 stars as members, with estimated kinematic distances of 95–135 pc. The remaining stars are members of the Cha I and II cloud populations, and nearby LCC.

Four new members ( $\epsilon$  Cha 8, 11, 13, 17) showed strong and/or variable H $\alpha$  emission indicative of accretion from a circumstellar disk. We confirmed the presence of significant infrared excesses in these stars and several WTTS members. With the exception of  $\epsilon$  Cha 13 and 17, which were observed by *Spitzer* (Manoj et al. 2011), these disks are new detections. As expected of a ‘transitional’ intermediate-age population, the spectral energy distributions of disks in  $\epsilon$  Cha show a variety of morphologies; from optically-thick accretion disks, to weak 22  $\mu\text{m}$  excess debris disks. Several stars have WISE photometry suggestive of large inner holes in their disks, possibly as a result of dynamically clearing by a planet.

Because of their age, proximity and minimal extinction, all of these new disks (and that around 2MASS J0820–8003) are ideal targets for future studies of disk and planetary system evolution around low-mass stars. The structure and mineralogy of circumstellar disks can be elucidated from mid-infrared photometry and spectroscopy (e.g. Sicilia-Aguilar et al. 2009; Bouwman et al. 2010). With *Spitzer* now on its warm mission, this work must be completed by ground-based facilities like T-ReCS on Gemini-South (De Buizer & Fisher 2005; Apai et al. 2004), VLT/VISIR (Rio et al. 1998; Geers et al. 2007), or—if it ever flies in the southern hemisphere—the FORCAST imager and spectrograph onboard SOFIA (Keller et al. 2010). Resolved, sub-millimetre imaging of inner disk holes is also finally available (Brown et al. 2008; Andrews et al. 2011) and will be a key contribution of the *Atacama Large Millimetre Array* (ALMA; van Dishoeck & Jørgensen 2008). The very recent discovery of the first directly-imaged young ( $\sim 2$  Myr) planet in the hole of such a disk (LkCa 15b; Kraus & Ireland 2012) aptly demonstrates the potential of these nearby, young, disk-bearing stars.

Motivated by their similar physical characteristics and juxtaposition on the sky, we have also investigated the relationship between—and origin of— $\eta$  and  $\epsilon$  Cha. Combining recent relative age determinations by Lyo et al. (2008) with the improved kinematics for  $\eta$  Cha derived in Chapter 2, we conclude that the two groups were born within a few Myr of each other in the outskirts of LCC. Contrary to previous studies, we propose  $\eta$  and  $\epsilon$  Cha were *not* born in close proximity to one another, but were separated by  $\sim 30$  pc at the time  $\eta$  Cha formed. According to this picture,  $\epsilon$  Cha formed a few Myr later, in the vicinity of colliding supernovae and stellar wind-driven bubbles from LCC and UCL (see Ortega et al. 2009). The groups’ almost-identical space motions mean they have never been much closer than their current 25 pc (10 deg) separation and as such, are unlikely to be causally related. Improved radial velocities, proper motions and distances for more  $\epsilon$  Cha members are vital for confirming this hypothesis. A holistic approach, combining the best-available stellar motions, an accurate galactic model and the evolution of the various structures in the interstellar medium surrounding Sco-Cen and Chamaeleon (de Geus 1992; Corradi et al. 1997; Mamajek et al. 2000) will be required to disentangle the two groups and their formation mechanisms. This work is ongoing.

To conclude, as predicted at the time of their discovery and confirmed through this work,  $\eta$  and  $\epsilon$  Cha are ideal laboratories to investigate the dynamical evolution and circumstellar disk properties of 5–10 Myr-old stars. With further study, these groups—and in particular the new members presented herein—promise to reveal much more about the formation and evolution of low-mass stars and their attendant planetary systems.

## 6.1. Future prospects

We finish this chapter and the thesis with a brief discussion of two further avenues for future work; a survey of existing photometry and proper motions for new members of  $\eta$  and  $\epsilon$  Cha across Chamaeleon, and the forthcoming SkyMapper Southern Sky Survey, which was one of the original motivations for this thesis. A short afterword is given in §6.2.

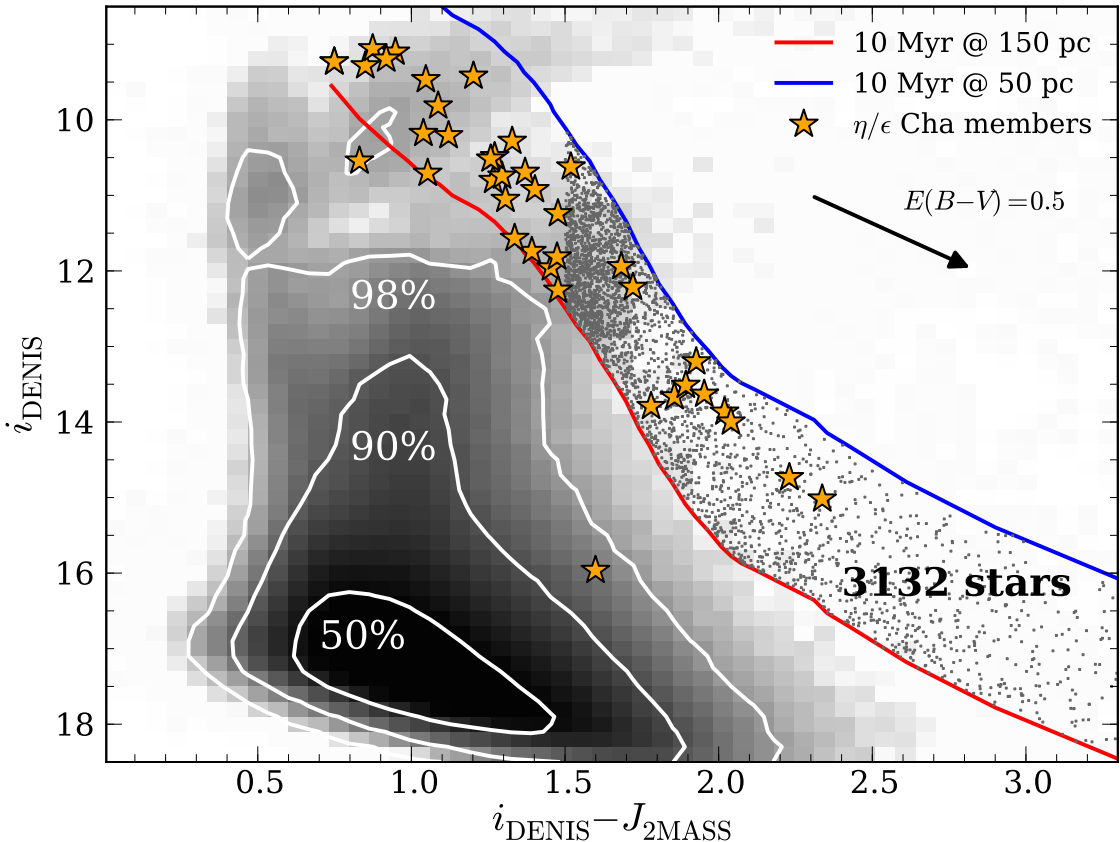


**Figure 6.1** Top: Colour-magnitude diagram for the new Chamaeleon survey. The grayscale is the logarithm of stars per cell, from  $N = 10$  to  $N = 10000$ . Contours give the enclosed fraction of objects. Stars redder than  $(i - J) = 1.5$  that lie between the 50–150 pc limits of a 10 Myr Baraffe et al. (1998) isochrone are plotted as points. The  $\epsilon$  Cha member at  $i \approx 16$  is  $\epsilon$  Cha 11, whose edge-on disk is responsible for its under-luminosity.

### 6.1.1. An ongoing survey for new members of $\eta$ and $\epsilon$ Cha

As noted by Torres et al. (2008) and underscored by the previous chapter, the identification of new members of  $\eta$  and  $\epsilon$  Cha in the region between the two groups is key to understanding their origins and any relationship between them. In Chapter 2 we discovered a handful of ejected  $\eta$  Cha members with masses  $0.08 < M/M_{\odot} < 0.3$  at radii up to 5 deg from the cluster. This is half the distance to the core of  $\epsilon$  Cha (Figure 5.12). Without doubt there are many more members of both groups awaiting discovery at radii and masses outside this range.

To this end, we are currently undertaking an extended DENIS/2MASS/PPMXL survey for new members of  $\eta$  and  $\epsilon$  Cha throughout Chamaeleon. By cross-matching these catalogues over the  $300 \text{ deg}^2$  region bounded by  $120^\circ < \alpha < 210^\circ$ ,  $-85^\circ < \delta < -70^\circ$  we have compiled a catalogue of  $\sim 4 \times 10^6$  stars with full  $i_{\text{DENIS}} + (JHK)_{\text{2MASS}}$  photometry and PPMXL proper motions. To illustrate the scale of the survey, Figure 6.1 shows the colour-magnitude diagram of the region. In contrast to the 81 photometric  $\eta$  Cha candidates from Chapter 2, there are now over 3000 stars redder than  $(i_{\text{DENIS}} - J_{\text{2MASS}}) = 1.5$  that lie between the 50–150 pc distance limits of a 10 Myr Baraffe et al. (1998) isochrone.

Kinematic information is *essential* to assessing membership and estimating distances to these stars. Although the vast majority ( $\gtrsim 95$  percent) will have proper motions inconsistent with  $\eta$  or  $\epsilon$  Cha, the combination of a wide field, variable levels of extinction, depth effects and non-

negligible proper motion errors demand a more nuanced candidate selection than that used in Chapter 2. Inspired by the recent Bayesian analyses of Rizzuto et al. (2011) and Gennaro et al. (2012), we are currently developing a new probabilistic method that simultaneously uses the available photometry and proper motions, combined with model isochrones and group space motions to select the best candidates for follow-up spectroscopy. It is similar to the convergence technique used by Torres et al. (2006, 2008) to identify members of young associations, without the need for observed radial velocities (which are predicted by the method). As well as  $\eta$  and  $\epsilon$  Cha, such an algorithm will be directly applicable to other young groups and forthcoming data from SkyMapper, which we describe below.

### 6.1.2. The SkyMapper Southern Sky Survey

In 2007 when this work started, the thesis was optimistically titled “*Towards a complete census of young stars in the solar neighbourhood with SkyMapper*”. Due to delays in commissioning the telescope and imager over the past four years, the project evolved into that presented in these chapters. With the facility finally on the verge of regular operation, is it timely (and perhaps slightly ironic) to finish this thesis by describing the features of the SkyMapper survey salient for young star work. Future studies will leverage these techniques to investigate low-mass pre-main sequence stars across the whole southern sky.

SkyMapper is a fully automated, 1.3-m survey telescope in operation at Siding Spring Observatory. With a  $5.7 \text{ deg}^2$  field-of-view and a 268-Megapixel Cassegrain imager, the telescope’s primary science goal is the SkyMapper Southern Sky Survey (4S); a six-band ( $uvgriz$ ), six-epoch digital survey of the entire  $2\pi \text{ sr}$  of southern sky to a limiting magnitude of  $g \approx 22.9$ . The study of the youngest stars in the solar neighbourhood has been identified as a key component of the 4S science case and survey design (Keller et al. 2007a,b).

#### Multi-colour photometry

The 4S actually consists of two surveys; a main survey with six 110-second exposures per filter over five years, and a shallow (5–30 second) three-epoch survey taken in photometric conditions for calibration. The main survey will reach a limiting magnitude of  $r \approx 19.5$  ( $\sigma_r < 0.1 \text{ mag}$ ), with the final co-added images reaching approximately a magnitude deeper. For an intermediate-age pre-main sequence population, the single-image limit corresponds to a spectral type of early-M (300 pc), late-M (100 pc) and mid-L (20 pc). Across Chamaeleon the photometry will be sensitive to the younger, more distant cloud population at  $\sim 150 \text{ pc}$ ,  $\eta$  and  $\epsilon$  Cha at  $\sim 100 \text{ pc}$  and any brown dwarfs in the solar vicinity. These nearby stars are particularly promising. The recent discovery of the  $\sim 40 \text{ Myr}$ -old Argus Association member AP Col at a distance of only 8.4 pc (Riedel et al. 2011) demonstrates that there are still many objects of “extraordinary value” left to discover in the solar neighbourhood.

The SkyMapper filter set has been optimised for stellar astrophysics and the accurate determination of stellar parameters (Keller et al. 2007b). The  $(r - i)$  colour is an excellent temperature discriminant for late-K to mid-M spectral types. By M8 however,  $(r - i)$  turns over and later spectral types are bluer in this colour. Similar to the  $(i_{\text{DENIS}} - J_{\text{2MASS}})$  colour used in Chapter 2,  $(i - z)$  is also suitable for stars cooler than M8, through to the L and early-T spectral types (Hawley et al. 2002). Photometric parallax relations exist for these colours

from the *Sloan Digital Sky Survey* (SDSS; West et al. 2005; Davenport et al. 2006). Assuming the uncertainties in these relations remain similar after adapting them to the SkyMapper bandpasses, the expected global 0.03 mag mean errors on 4S photometry should allow photometric distances to  $\pm 15$  percent for an M5 main sequence star at 100 pc.

Young stars are known to display an excess in blue and UV photometry up to ages of  $\sim 200$  Myr. This is likely to be a manifestation of the enhanced magnetic activity common in such stars (e.g. Lyo et al. 2008; Stauffer et al. 2003). Accretion-driven emission must also play a role in the youngest ( $< 10$  Myr) objects. The availability of all-sky  $u$ -band photometry from the 4S will provide another resource from which to identify young stars, complementing recent work with GALEX UV data (Rodriguez et al. 2011; Shkolnik et al. 2011).

Near and mid-infrared photometry from the WISE satellite (Wright et al. 2010) has been very efficient in identifying infrared excesses due to disks over its 3–22  $\mu\text{m}$  wavelength range (Chapters 3 and 5). The AKARI satellite (Murakami et al. 2007) has also recently released a mid and far-infrared all-sky survey in six bands covering 9–160  $\mu\text{m}$  (Ishihara et al. 2010; Yamamura et al. 2010). Both surveys are already proving bountiful resources for finding and characterising disk-bearing stars (Rebull et al. 2011; Liu et al. 2011; Takita et al. 2010). By combining 2MASS, WISE, AKARI and 4S photometry it will be possible to construct spectral energy distributions covering 0.3–160  $\mu\text{m}$  for several  $10^5$  sources. In addition to identifying disks and estimating reddening, such an ensemble would also allow the accurate derivation of stellar parameters, in particular effective temperature and luminosity, via the *Infrared Flux Method* (IRFM; Casagrande et al. 2008, 2010).

## Astrometry

As demonstrated in the previous chapters, accurate proper motions are vital to confirming membership of stars in pre-main sequence groups and understanding their internal dynamics. SkyMapper will provide relative astrometry to an accuracy of 50 mas per epoch for bright stars ( $r < 18$ ). Using only the 36 epochs of multi-colour main survey imaging, it should be possible to derive proper motions to  $\sim 5$  mas  $\text{yr}^{-1}$  over the 5 year survey baseline.

Adding further epochs over a wider baseline will improve the proper motion precision. Roeser et al. (2010) combined the USNO-B1.0 catalogue with 2MASS to create the PPMXL catalogue used throughout this work. Its quoted errors are typically 4–10 mas  $\text{yr}^{-1}$  depending on the observational history. By combining SkyMapper astrometry with PPMXL we can achieve an even better precision. As noted by Roeser et al. (2010), this is especially true in the deep southern sky, where most first-epoch astrometry is derived from images taken much later than at northern declinations (e.g. SERC plates taken at SSO from 1975–88, compared to Palomar POSS-I plates from 1950–58). In combination with the older epochs, the 10–15 year difference between 2MASS and SkyMapper imaging should enable proper motions to a precision of 2–3 mas  $\text{yr}^{-1}$  for most stars. This is a similar precision to space-based surveys like *Hipparcos* and Tycho-2 and well-matched to radial velocity measurements from high-resolution spectrographs (for reference, 1 km  $\text{s}^{-1}$  translates to 2 mas  $\text{yr}^{-1}$  at a distance of 100 pc). SkyMapper imaging will also be useful to projects like DANCE (*Dynamical Analysis of Nearby ClustErs*; Bouy 2011), who are using multi-wavelength archival observations of nearby star-forming regions to derive high-precision ( $< 1$  mas  $\text{yr}^{-1}$ ) proper motions.

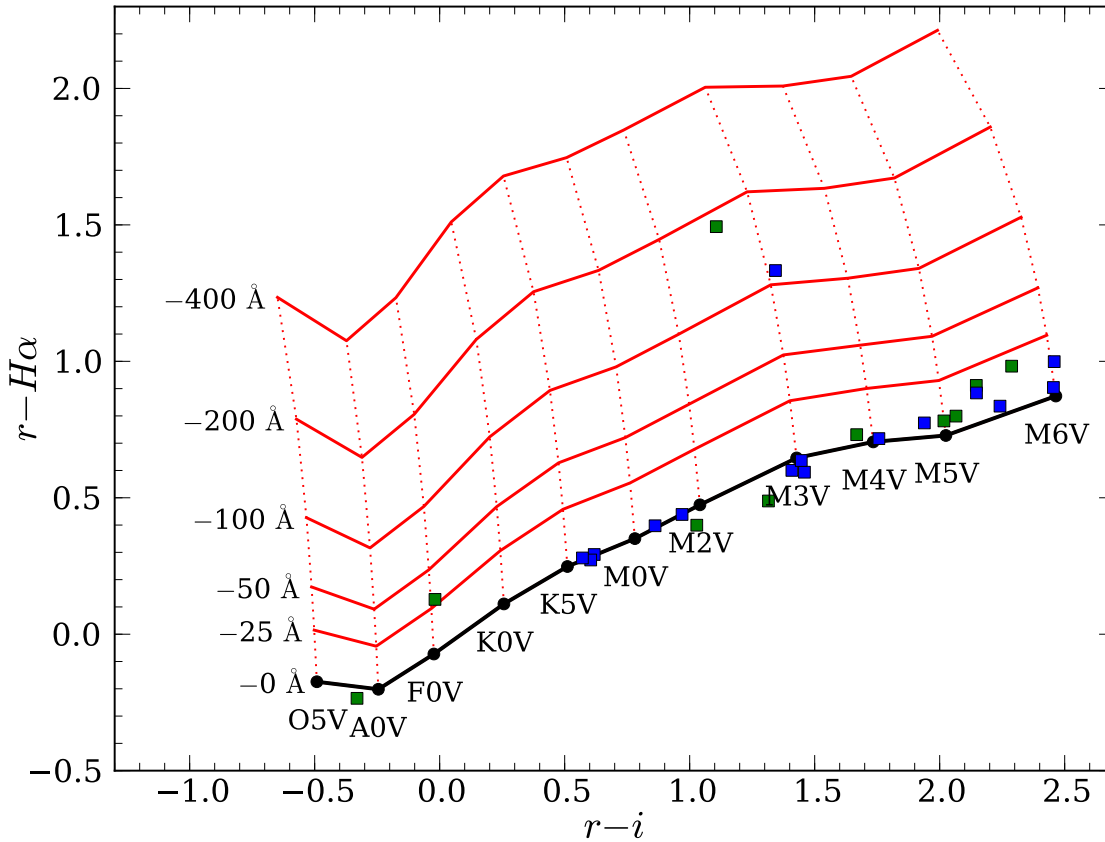


**Figure 6.2** Simulated SkyMapper  $(r-i)$ ,  $(r-H\alpha)$  colour plane, illustrating the effects of adding  $H\alpha$  emission of increasing equivalent width to Pickles (1998) empirical spectra. The shape of the as-yet unconstructed  $H\alpha$  filter is approximated by a Gaussian centred on 6563 Å with a FWHM of 100 Å. Blue and green squares show the result of synthetic photometry on  $\eta$  and  $\epsilon$  Cha spectra from Lyo et al. (2004a, 2008), respectively. The two stars with photometric equivalent widths  $>100$  Å are the  $\eta$  Cha CTTS ECHA J0843.3–7905 and  $\epsilon$  Cha 11.

## Variability

Young stars are well-known for their variability. The variation can be irregular (due to flares, accretion) or periodic (rotational modulation of star-spots), with amplitudes up to a few magnitudes and on timescales of hours to weeks. Although variability is neither a sufficient nor necessary indicator of youth, the utility of selecting candidates by variability in conjunction with broad-band colours has proved effective in large surveys (Briceño et al. 2001, 2005; Lamm et al. 2004). With a maximum of nine epochs per filter at staggered intervals (hours, days, weeks, months, years), SkyMapper light curves will not be densely sampled so no periodicity information will be available. However, in their survey for young stars in Orion, Briceño et al. (2005) showed that  $\sim 5$  observations are enough to obtain a reliable detection of variability, even at low signal-to-noise. Furthermore, we can examine variability in all six bands, which should aid in reducing contamination from noisy sources.

## $H\alpha$ photometry

$H\alpha$  emission is endemic in pre-main sequence stars. Strong ( $\gg 5$ – $10$  Å) emission is usually indicative of an accretion flow from a circumstellar disk (Chapter 3) and can be detected photometrically with narrow-band  $H\alpha$  filters (e.g. Sung et al. 2008; Barentsen et al. 2011).

In addition to *uvgriz* photometry, Skymapper will undertake a separate single-epoch H $\alpha$  survey around full moon when *u*-band observations are impractical. The Chamaeleon region lies at Galactic latitudes  $-25^\circ < b < -10^\circ$ , outside the bounds of existing Galactic plane H $\alpha$  surveys (e.g. Parker et al. 2005; Drew et al. 2005). SkyMapper photometry will provide a exciting niche to look for young, accreting stars across the entire region, as well as a multitude of other H $\alpha$  emitting objects (Wolf-Rayet stars, Be stars, symbiotic systems, cataclysmic variables, unresolved planetary nebulae; see Corradi et al. 2008).

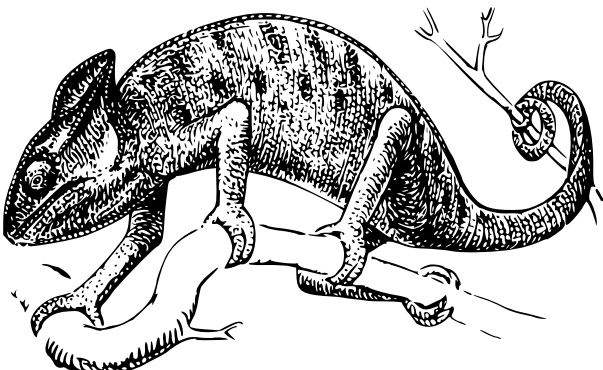
To demonstrate the utility of narrow-band H $\alpha$  photometry, Figure 6.2 depicts the simulated main sequence in SkyMapper ( $r - i, r - H\alpha$ ) colours, with H $\alpha$  emission of various strengths added to Pickles (1998) empirical spectra. By comparing observed photometry to these synthetic grids, objects with significant H $\alpha$  excess can be efficiently identified over wide fields. Equivalent widths and mass accretion rates can then be initially estimated without the need for spectroscopy (Barentsen et al. 2011; De Marchi et al. 2010).

## 6.2. Afterword

Like many Ph.D. projects, circumstances and serendipity have changed the course of this research many times over the past four and a half years. Despite my original thesis proposal on the low-mass population of the Scorpius-Centaurus OB Association bearing little resemblance to the work presented here, the questions it sought to answer—*where are young, low-mass stars found?, how did they get there?, do they still have circumstellar disks?*—are of arguably greater relevance to  $\eta$  and  $\epsilon$  Cha than they are to Sco-Cen.

It was the timely publication of the Moraux et al. (2007) paper on  $\eta$  Cha that prompted this work, and the serendipitous discoveries of Chapters 3 and 4 that sustained it. Interminable delays to SkyMapper notwithstanding, the project has since grown into a comprehensive investigation of two of the most revealing young groups in the southern sky. The results we have presented will hopefully ensure that, like their zygodactylous<sup>2</sup> cousins,  $\eta$  and  $\epsilon$  Chamaeleontis continue to be a source of fascination well into the future.

SJM (16 Feb. 2012)



*Chamaeleo chamaeleon*  
Common Chamaeleon (Linnaeus 1758)<sup>3</sup>

<sup>2</sup>zy-go-dac-tyl (ornithology) Having two toes pointing forward and two backward. A Chamaeleon's five toes are similarly fused into two groups that oppose one another. This bird-like arrangement makes them unique amongst reptiles and well-suited to their tree-dwelling lifestyle.

<sup>3</sup>Image credit: Pearson Scott Foresman/WikiMedia Foundation (from <http://openclipart.org>).



---

## Bibliography

- Alcala, J. M., Krautter, J., Covino, E., Neuhaeuser, R., Schmitt, J. H. M. M., & Wichmann, R. 1997, A&A, 319, 184 (ADS entry)
- Alcala, J. M., Krautter, J., Schmitt, J. H. M. M., Covino, E., Wichmann, R., & Mundt, R. 1995, A&AS, 114, 109 (ADS entry)
- Alexander, R. D., Clarke, C. J., & Pringle, J. E. 2006, MNRAS, 369, 229 (ADS entry)
- Allen, L. E., & Strom, K. M. 1995, AJ, 109, 1379 (ADS entry)
- Amado, P. J., & Byrne, P. B. 1997, A&A, 319, 967 (ADS entry)
- Andrews, S. M., Wilner, D. J., Espaillat, C., Hughes, A. M., Dullemond, C. P., McClure, M. K., Qi, C., & Brown, J. M. 2011, ApJ, 732, 42 (ADS entry)
- Apai, D., Pascucci, I., Sterzik, M. F., van der Bliek, N., Bouwman, J., Dullemond, C. P., & Henning, T. 2004, A&A, 426, L53 (ADS entry)
- Appenzeller, I., & Mundt, R. 1989, A&A Rev., 1, 291 (ADS entry)
- Armitage, P. J., & Clarke, C. J. 1997, MNRAS, 285, 540 (ADS entry)
- Augereau, J. C., Nelson, R. P., Lagrange, A. M., Papaloizou, J. C. B., & Mouillet, D. 2001, A&A, 370, 447 (ADS entry)
- Bagnulo, S., Jehin, E., Ledoux, C., Cabanac, R., Melo, C., Gilmozzi, R., & The ESO Paranal Science Operations Team. 2003, The Messenger, 114, 10 (ADS entry)
- Baraffe, I., & Chabrier, G. 2010, A&A, 521, A44 (ADS entry)
- Baraffe, I., Chabrier, G., Allard, F., & Hauschildt, P. H. 1998, A&A, 337, 403 (ADS entry)
- Baraffe, I., Chabrier, G., Barman, T. S., Allard, F., & Hauschildt, P. H. 2003, A&A, 402, 701 (ADS entry)
- Barentsen, G., et al. 2011, MNRAS, 415, 103 (ADS entry)
- Barman, T. S., Macintosh, B., Konopacky, Q. M., & Marois, C. 2011, ApJ, 735, L39 (ADS entry)

- Barnes, J. R., Jeffers, S. V., & Jones, H. R. A. 2011, MNRAS, 412, 1599 (ADS entry)
- Barrado y Navascues, D. 1998, A&A, 339, 831 (ADS entry)
- Barrado y Navascués, D. 2006, A&A, 459, 511 (ADS entry)
- Barrado y Navascués, D., & Martín, E. L. 2003, AJ, 126, 2997 (ADS entry)
- Barrado y Navascués, D., Stauffer, J. R., & Jayawardhana, R. 2004, ApJ, 614, 386 (ADS entry)
- Barrado y Navascués, D., Stauffer, J. R., Song, I., & Caillault, J.-P. 1999, ApJ, 520, L123 (ADS entry)
- Basri, G., & Batalha, C. 1990, ApJ, 363, 654 (ADS entry)
- Bastian, N., Covey, K. R., & Meyer, M. R. 2010, ARA&A, 48, 339 (ADS entry)
- Belloche, A., Parise, B., Schuller, F., André, P., Bontemps, S., & Menten, K. M. 2011, A&A, 535, A2 (ADS entry)
- Bertout, C. 1989, ARA&A, 27, 351 (ADS entry)
- Bertout, C., Robichon, N., & Arenou, F. 1999, A&A, 352, 574 (ADS entry)
- Bessell, M. S. 1990, A&AS, 83, 357 (ADS entry)
- . 1991, AJ, 101, 662 (ADS entry)
- . 1999, PASP, 111, 1426 (ADS entry)
- . 2005, ARA&A, 43, 293 (ADS entry)
- Bessell, M. S., & Brett, J. M. 1988, PASP, 100, 1134 (ADS entry)
- Bessell, M. S., Castelli, F., & Plez, B. 1998, A&A, 333, 231 (ADS entry)
- Beuzit, J.-L., et al. 2010, in Astronomical Society of the Pacific Conference Series, Vol. 430, Pathways Towards Habitable Planets, ed. V. Coudé Du Foresto, D. M. Gelino, & I. Ribas, 231 (ADS entry)
- Binney, J., & Tremaine, S. 2008, Galactic Dynamics: Second Edition (Princeton University Press) (ADS entry)
- Blaauw, A. 1964, ARA&A, 2, 213 (ADS entry)
- Bochanski, J. J., West, A. A., Hawley, S. L., & Covey, K. R. 2007, AJ, 133, 531 (ADS entry)
- Böhm, T., Catala, C., Balona, L., & Carter, B. 2004, A&A, 427, 907 (ADS entry)
- Boss, A. P. 1997, Science, 276, 1836 (ADS entry)
- . 2003, ApJ, 599, 577 (ADS entry)
- Bouwman, J., Lawson, W. A., Dominik, C., Feigelson, E. D., Henning, T., Tielens, A. G. G. M., & Waters, L. B. F. M. 2006, ApJ, 653, L57 (ADS entry)

- Bouwman, J., Lawson, W. A., Juhász, A., Dominik, C., Feigelson, E. D., Henning, T., Tielens, A. G. G. M., & Waters, L. B. F. M. 2010, *ApJ*, 723, L243 (ADS entry)
- Bouy, H. 2011, in Stellar Clusters & Associations: a RIA Workshop on Gaia (oral contribution). May 23–27 2011, Granada, Spain.
- Brandeker, A., Jayawardhana, R., Khavari, P., Haisch, Jr., K. E., & Mardones, D. 2006, *ApJ*, 652, 1572 (ADS entry)
- Briceño, C., Calvet, N., Hernández, J., Vivas, A. K., Hartmann, L., Downes, J. J., & Berlind, P. 2005, *AJ*, 129, 907 (ADS entry)
- Briceño, C., et al. 2001, *Science*, 291, 93 (ADS entry)
- Brown, J. M., Blake, G. A., Qi, C., Dullemond, C. P., & Wilner, D. J. 2008, *ApJ*, 675, L109 (ADS entry)
- Browning, M. K., Basri, G., Marcy, G. W., West, A. A., & Zhang, J. 2010, *AJ*, 139, 504 (ADS entry)
- Buccino, A. P., Díaz, R. F., Luoni, M. L., Abrevaya, X. C., & Mauas, P. J. D. 2011, *AJ*, 141, 34 (ADS entry)
- Burrows, A., et al. 1997, *ApJ*, 491, 856 (ADS entry)
- Caballero, J. A. 2009, *A&A*, 507, 251 (ADS entry)
- Calvet, N., Hartmann, L., & Strom, S. E. 2000, in Protostars and Planets IV, ed. Mannings, V., Boss, A.P., Russell, S. S. (Tuscon: University of Arizona Press), 377 (ADS entry)
- Cardelli, J. A., Clayton, G. C., & Mathis, J. S. 1989, *ApJ*, 345, 245 (ADS entry)
- Carpenter, J. M. 2001, *AJ*, 121, 2851 (ADS entry)
- Carpenter, J. M., Mamajek, E. E., Hillenbrand, L. A., & Meyer, M. R. 2006, *ApJ*, 651, L49 (ADS entry)
- Casagrande, L., Flynn, C., & Bessell, M. 2008, *MNRAS*, 389, 585 (ADS entry)
- Casagrande, L., Ramírez, I., Meléndez, J., Bessell, M., & Asplund, M. 2010, *A&A*, 512, A54 (ADS entry)
- Chabrier, G. 2003, *PASP*, 115, 763 (ADS entry)
- Chabrier, G., Baraffe, I., Allard, F., & Hauschildt, P. 2000, *ApJ*, 542, 464 (ADS entry)
- Chauvin, G., Lagrange, A.-M., Dumas, C., Zuckerman, B., Mouillet, D., Song, I., Beuzit, J.-L., & Lowrance, P. 2004, *A&A*, 425, L29 (ADS entry)
- . 2005a, *A&A*, 438, L25 (ADS entry)
- Chauvin, G., et al. 2005b, *A&A*, 438, L29 (ADS entry)
- Chen, C. H., Mamajek, E. E., Bitner, M. A., Pecaut, M., Su, K. Y. L., & Weinberger, A. J. 2011, *ApJ*, 738, 122 (ADS entry)

- Cleary, M. N., Haslam, C. G. T., & Heiles, C. 1979, A&AS, 36, 95 (ADS entry)
- Cohen, M., Wheaton, W. A., & Megeath, S. T. 2003, AJ, 126, 1090 (ADS entry)
- Corradi, R. L. M., et al. 2008, A&A, 480, 409 (ADS entry)
- Corradi, W. J. B., Franco, G. A. P., & Knude, J. 1997, A&A, 326, 1215 (ADS entry)
- Covino, E., Alcalá, J. M., Allain, S., Bouvier, J., Terranegra, L., & Krautter, J. 1997, A&A, 328, 187 (ADS entry)
- Currie, T., et al. 2011, ApJ, 729, 128 (ADS entry)
- da Silva, L., Torres, C. A. O., de La Reza, R., Quast, G. R., Melo, C. H. F., & Sterzik, M. F. 2009, A&A, 508, 833 (ADS entry)
- Davenport, J. R. A., West, A. A., Matthiesen, C. K., Schmieding, M., & Kobelski, A. 2006, PASP, 118, 1679 (ADS entry)
- Dawson, P. C., & De Robertis, M. M. 2005, PASP, 117, 1 (ADS entry)
- de Bruijne, J. H. J. 1999, MNRAS, 310, 585 (ADS entry)
- De Buizer, J., & Fisher, R. 2005, in ESO Astrophysics Symposia: High Resolution Infrared Spectroscopy in Astronomy, ed. H. U. Käufl, R. Siebenmorgen, & A. Moorwood, 84 (ADS entry)
- de Geus, E. J. 1992, A&A, 262, 258 (ADS entry)
- de la Reza, R., Jilinski, E., & Ortega, V. G. 2006, AJ, 131, 2609 (ADS entry)
- de la Reza, R., Torres, C. A. O., Quast, G., Castilho, B. V., & Vieira, G. L. 1989, ApJ, 343, L61 (ADS entry)
- De Marchi, G., Panagia, N., & Romaniello, M. 2010, ApJ, 715, 1 (ADS entry)
- de Winter, D., Grady, C. A., van den Ancker, M. E., Pérez, M. R., & Eiroa, C. 1999, A&A, 343, 137 (ADS entry)
- de Zeeuw, P. T., Hoogerwerf, R., de Bruijne, J. H. J., Brown, A. G. A., & Blaauw, A. 1999, AJ, 117, 354 (ADS entry)
- Dehnen, W., & Binney, J. J. 1998, MNRAS, 298, 387 (ADS entry)
- Desidera, S., et al. 2011, A&A, 529, A54 (ADS entry)
- Dhital, S., West, A. A., Stassun, K. G., & Bochanski, J. J. 2010, AJ, 139, 2566 (ADS entry)
- Dopita, M., Hart, J., McGregor, P., Oates, P., Bloxham, G., & Jones, D. 2007, Ap&SS, 310, 255 (ADS entry)
- Dopita, M., et al. 2010, Ap&SS, 327, 245 (ADS entry)
- Doppmann, G. W., White, R. J., Charbonneau, D., & Torres, G. 2007, in Proceedings of the Second Conference of Gemini Science Results, ed. A. Brunch & I. Fernandes

- Doyon, R., Lafrenière, D., Artigau, E., Malo, L., & Marois, C. 2010, in Proceedings of In the Spirit of Lyot 2010: Direct Detection of Exoplanets and Circumstellar Disks, ed. A. Boccaletti (ADS entry)
- Drew, J. E., et al. 2005, MNRAS, 362, 753 (ADS entry)
- Ducourant, C., Teixeira, R., Chauvin, G., Daigne, G., Le Campion, J.-F., Song, I., & Zuckerman, B. 2008, A&A, 477, L1 (ADS entry)
- Ducourant, C., Teixeira, R., Périé, J. P., Lecampion, J. F., Guibert, J., & Sartori, M. J. 2005, A&A, 438, 769 (ADS entry)
- Duquennoy, A., & Mayor, M. 1991, A&A, 248, 485 (ADS entry)
- Eggen, O. J. 1958, MNRAS, 118, 65 (ADS entry)
- Eggen, O. J. 1965, in Galactic Structure, ed. A. Blaauw & M. Schmidt (Chicago, IL USA: University of Chicago Press), 111 (ADS entry)
- . 1998, AJ, 116, 1314 (ADS entry)
- Eisner, J. A., Doppmann, G. W., Najita, J. R., McCarthy, D., Kulesa, C., Swift, B. J., & Teske, J. 2010, ApJ, 722, L28 (ADS entry)
- Elias, J. H., Frogel, J. A., Matthews, K., & Neugebauer, G. 1982, AJ, 87, 1029 (ADS entry)
- Epcstein, N., et al. 1999, A&A, 349, 236 (ADS entry)
- Evans, N., et al. 2009, ArXiv e-prints: astro-ph/0901.1691 (ADS entry)
- Faherty, J. K., Burgasser, A. J., West, A. A., Bochanski, J. J., Cruz, K. L., Shara, M. M., & Walter, F. M. 2010, AJ, 139, 176 (ADS entry)
- Fedele, D., van den Ancker, M. E., Henning, T., Jayawardhana, R., & Oliveira, J. M. 2010, A&A, 510, A72 (ADS entry)
- Feigelson, E. D. 1996, ApJ, 468, 306 (ADS entry)
- Feigelson, E. D., Lawson, W. A., & Garmire, G. P. 2003, ApJ, 599, 1207 (ADS entry)
- Feigelson, E. D., Lawson, W. A., Stark, M., Townsley, L., & Garmire, G. P. 2006, AJ, 131, 1730 (ADS entry)
- Feigelson, E. D., & Montmerle, T. 1999, ARA&A, 37, 363 (ADS entry)
- Fernández, D., Figueras, F., & Torra, J. 2008, A&A, 480, 735 (ADS entry)
- Fischer, D. A., & Marcy, G. W. 1992, ApJ, 396, 178 (ADS entry)
- Fleming, T. A., Giampapa, M. S., Schmitt, J. H. M. M., & Bookbinder, J. A. 1993, ApJ, 410, 387 (ADS entry)
- Fleming, T. A., Schmitt, J. H. M. M., & Giampapa, M. S. 1995, ApJ, 450, 401 (ADS entry)
- Fouqué, P., et al. 2000, A&AS, 141, 313 (ADS entry)

- Frink, S., Roeser, S., Alcalá, J. M., Covino, E., & Brandner, W. 1998, A&A, 338, 442 (ADS entry)
- Gardner, J. P., et al. 2006, Space Sci. Rev., 123, 485 (ADS entry)
- Gautier, III, T. N., Rebull, L. M., Stapelfeldt, K. R., & Mainzer, A. 2008, ApJ, 683, 813 (ADS entry)
- Geers, V. C., Pontoppidan, K. M., van Dishoeck, E. F., Dullemond, C. P., Augereau, J.-C., Merín, B., Oliveira, I., & Pel, J. W. 2007, A&A, 469, L35 (ADS entry)
- Gennaro, M., Prada Moroni, P. G., & Tognelli, E. 2012, MNRAS, 2180 (ADS entry)
- Gizis, J. E. 2002, ApJ, 575, 484 (ADS entry)
- Gizis, J. E., Reid, I. N., & Hawley, S. L. 2002, AJ, 123, 3356 (ADS entry)
- Grady, C. A., et al. 2004, ApJ, 608, 809 (ADS entry)
- Graham, J. R., et al. 2007, ArXiv e-prints: astro-ph/0704.1454 (ADS entry)
- Gregorio-Hetem, J., Lepine, J. R. D., Quast, G. R., Torres, C. A. O., & de La Reza, R. 1992, AJ, 103, 549 (ADS entry)
- Guenther, E. W., Esposito, M., Mundt, R., Covino, E., Alcalá, J. M., Cusano, F., & Stecklum, B. 2007, A&A, 467, 1147 (ADS entry)
- Haisch, Jr., K. E., Jayawardhana, R., & Alves, J. 2005, ApJ, 627, L57 (ADS entry)
- Haisch, Jr., K. E., Lada, E. A., & Lada, C. J. 2001, ApJ, 553, L153 (ADS entry)
- Hambly, N. C., Davenhall, A. C., Irwin, M. J., & MacGillivray, H. T. 2001, MNRAS, 326, 1315 (ADS entry)
- Hartigan, P. 1997, in American Institute of Physics Conference Series, Vol. 393, The seventh astrophysical conference: Star formation, near and far, ed. S. S. Holt & L. G. Mundy, 153–159 (ADS entry)
- Hartigan, P., Edwards, S., & Pierson, R. 2004, ApJ, 609, 261 (ADS entry)
- Hawarden, T. G., Leggett, S. K., Letawsky, M. B., Ballantyne, D. R., & Casali, M. M. 2001, MNRAS, 325, 563 (ADS entry)
- Hawley, S. L., Gizis, J. E., & Reid, I. N. 1996, AJ, 112, 2799 (ADS entry)
- Hawley, S. L., et al. 2002, AJ, 123, 3409 (ADS entry)
- Herbig, G. H. 1973, ApJ, 182, 129 (ADS entry)
- . 1978, in Problems of Physics and Evolution of the Universe, ed. Mirzoyan, L. V. (Yerevan, Armenia: Armenian Academy of Science), 171 (ADS entry)
- Hernández, J., Hartmann, L., Calvet, N., Jeffries, R. D., Gutermuth, R., Muzerolle, J., & Stauffer, J. 2008, ApJ, 686, 1195 (ADS entry)
- Hernández, J., et al. 2007, ApJ, 662, 1067 (ADS entry)

- Herrera, C. N., Boulanger, F., & Nesvadba, N. P. H. 2011, A&A, 534, A138 (ADS entry)
- Hessman, F. V., & Guenther, E. W. 1997, A&A, 321, 497 (ADS entry)
- Hillenbrand, L. A. 2005, in Space Telescope Science Institute Symposium Series, Vol. 19, A Decade of Extrasolar Planets around Normal Stars, ed. M. Livio, K. Sahu, & J. Valenti, 84–105 (ADS entry)
- Høg, E., et al. 2000, A&A, 355, L27 (ADS entry)
- Hogerheijde, M. 1998, PhD thesis, Department of Astronomy, University of California (ADS entry)
- Hoogerwerf, R., de Bruijne, J. H. J., & de Zeeuw, P. T. 2001, A&A, 365, 49 (ADS entry)
- Houk, N., & Cowley, A. P. 1975, University of Michigan Catalogue of two-dimensional spectral types for the HD stars. Volume I. Declinations  $-90^{\circ}$  to  $-53^{\circ}$  (Ann Arbor, USA: Department of Astronomy, University of Michigan) (ADS entry)
- Huélamo, N., Lacour, S., Tuthill, P., Ireland, M., Kraus, A., & Chauvin, G. 2011, A&A, 528, L7 (ADS entry)
- Irwin, J., Hodgkin, S., Aigrain, S., Bouvier, J., Hebb, L., & Moraux, E. 2008, MNRAS, 383, 1588 (ADS entry)
- Irwin, J., Hodgkin, S., Aigrain, S., Hebb, L., Bouvier, J., Clarke, C., Moraux, E., & Bramich, D. M. 2007, MNRAS, 377, 741 (ADS entry)
- Ishihara, D., et al. 2010, A&A, 514, A1 (ADS entry)
- James, D. J., Melo, C., Santos, N. C., & Bouvier, J. 2006, A&A, 446, 971 (ADS entry)
- Jarrett, T. H., et al. 2011, ApJ, 735, 112 (ADS entry)
- Jayawardhana, R., Coffey, J., Scholz, A., Brandeker, A., & van Kerkwijk, M. H. 2006, ApJ, 648, 1206 (ADS entry)
- Jayawardhana, R., & Greene, T., eds. 2001, Astronomical Society of the Pacific Conference Series, Vol. 244, Young Stars Near Earth: Progress and Prospects (ADS entry)
- Jayawardhana, R., Mohanty, S., & Basri, G. 2003, ApJ, 592, 282 (ADS entry)
- Jeffries, R. D. 2000, in Astronomical Society of the Pacific Conference Series, Vol. 198, Stellar Clusters and Associations: Convection, Rotation, and Dynamos, ed. Pallavicini, R. and Micela, G. and Sciortino, S., 245 (ADS entry)
- Jeffries, R. D., & Oliveira, J. M. 2005, MNRAS, 358, 13 (ADS entry)
- Jenkins, J. S., Ramsey, L. W., Jones, H. R. A., Pavlenko, Y., Gallardo, J., Barnes, J. R., & Pinfield, D. J. 2009, ApJ, 704, 975 (ADS entry)
- Jensen, E. L. N., Cohen, D. H., & Neuhäuser, R. 1998, AJ, 116, 414 (ADS entry)
- Jilinski, E., Ortega, V. G., & de la Reza, R. 2005, ApJ, 619, 945 (ADS entry)

- Johnson, D. R. H., & Soderblom, D. R. 1987, AJ, 93, 864 (ADS entry)
- Kaisler, D., Zuckerman, B., Song, I., Macintosh, B. A., Weinberger, A. J., Becklin, E. E., Konopacky, Q. M., & Patience, J. 2004, A&A, 414, 175 (ADS entry)
- Kasper, M., et al. 2010, in SPIE Conference Series, Vol. 7735, Ground-based and Airborne Instrumentation for Astronomy III, ed. I. McLean, S. Ramsay and H. Takami, 77352E (ADS entry)
- Kastner, J. H., Hily-Blant, P., Sacco, G. G., Forveille, T., & Zuckerman, B. 2010, ApJ, 723, L248 (ADS entry)
- Kastner, J. H., Zuckerman, B., & Bessell, M. 2008, A&A, 491, 829 (ADS entry)
- Kastner, J. H., Zuckerman, B., Weintraub, D. A., & Forveille, T. 1997, Science, 277, 67 (ADS entry)
- Kastner, J. H., et al. 2011, ApJ, 740, L17 (ADS entry)
- Kataria, T., & Simon, M. 2010, AJ, 140, 206 (ADS entry)
- Keller, L., Deen, C. P., Jaffe, D. T., Ennico, K. A., Greene, T. P., Adams, J. D., Herter, T., & Sloan, G. C. 2010, in SPIE Conference Series, Vol. 7735, Ground-based and Airborne Instrumentation for Astronomy III, ed. I. McLean, S. Ramsay and H. Takami, 77356N (ADS entry)
- Keller, S., Bessell, M., Schmidt, B., & Francis, P. 2007a, in Astronomical Society of the Pacific Conference Series, Vol. 364, The Future of Photometric, Spectrophotometric and Polarimetric Standardization, ed. C. Sterken, 177 (ADS entry)
- Keller, S. C., et al. 2007b, PASA, 24, 1 (ADS entry)
- Kenyon, S. J., & Hartmann, L. 1995, ApJS, 101, 117 (ADS entry)
- King, I., Gilmore, G., & van der Kruit, P. C. 1990, The Milky Way as a Galaxy (University Science Books) (ADS entry)
- King, J. R., Schuler, S. C., Hobbs, L. M., & Pinsonneault, M. H. 2010, ApJ, 710, 1610 (ADS entry)
- Kirkpatrick, J. D., Henry, T. J., & McCarthy, Jr., D. W. 1991, ApJS, 77, 417 (ADS entry)
- Kiss, L. L., et al. 2011, MNRAS, 411, 117 (ADS entry)
- Knude, J. 2010, ArXiv e-prints: astro-ph/1006.3676 (ADS entry)
- Knude, J., & Hog, E. 1998, A&A, 338, 897 (ADS entry)
- Koen, C., Kilkenny, D., van Wyk, F., & Marang, F. 2010, MNRAS, 403, 1949 (ADS entry)
- Köhler, R. 2001, AJ, 122, 3325 (ADS entry)
- Köhler, R., & Petr-Gotzens, M. G. 2002, AJ, 124, 2899 (ADS entry)

- Kouwenhoven, M. B. N., Goodwin, S. P., Parker, R. J., Davies, M. B., Malmberg, D., & Kroupa, P. 2010, MNRAS, 404, 1835 (ADS entry)
- Kovács, G., Zucker, S., & Mazeh, T. 2002, A&A, 391, 369 (ADS entry)
- Kraus, A. L., & Hillenbrand, L. A. 2007a, ApJ, 662, 413 (ADS entry)
- . 2007b, ApJ, 664, 1167 (ADS entry)
- . 2009, ApJ, 703, 1511 (ADS entry)
- Kraus, A. L., & Ireland, M. J. 2012, ApJ, 745, 5 (ADS entry)
- Kroupa, P. 1998, MNRAS, 298, 231 (ADS entry)
- Kroupa, P., & Boily, C. M. 2002, MNRAS, 336, 1188 (ADS entry)
- Lada, C. J. 1987, in IAU Symposium, Vol. 115, Star Forming Regions, ed. M. Peimbert & J. Jugaku, 1–17 (ADS entry)
- Lagrange, A.-M., et al. 2010, Science, 329, 57 (ADS entry)
- Lamm, M. H., Bailer-Jones, C. A. L., Mundt, R., Herbst, W., & Scholz, A. 2004, A&A, 417, 557 (ADS entry)
- Larson, R. B. 1981, MNRAS, 194, 809 (ADS entry)
- Law, N. M., Dhital, S., Kraus, A., Stassun, K. G., & West, A. A. 2010, ApJ, 720, 1727 (ADS entry)
- Lawson, W., & Feigelson, E. D. 2001, in Astronomical Society of the Pacific Conference Series, Vol. 243, From Darkness to Light: Origin and Evolution of Young Stellar Clusters, ed. T. Montmerle & P. André, 591 (ADS entry)
- Lawson, W. A., & Crause, L. A. 2005, MNRAS, 357, 1399 (ADS entry)
- Lawson, W. A., Crause, L. A., Mamajek, E. E., & Feigelson, E. D. 2001, MNRAS, 321, 57 (ADS entry)
- . 2002, MNRAS, 329, L29 (ADS entry)
- Lawson, W. A., Lyo, A., & Bessell, M. S. 2009, MNRAS, 400, L29 (ADS entry)
- Lawson, W. A., Lyo, A.-R., & Muzerolle, J. 2004, MNRAS, 351, L39 (ADS entry)
- Lépine, S., & Bongiorno, B. 2007, AJ, 133, 889 (ADS entry)
- Lépine, S., & Shara, M. M. 2005, AJ, 129, 1483 (ADS entry)
- Linnaeus, C. 1758, *Systema Naturae*, 10th edn. (Stockholm: Laurentius Salvius)
- Lissauer, J. J. 1993, ARA&A, 31, 129 (ADS entry)
- Liu, W. M., Padgett, D. L., Leisawitz, D., Fajardo-Acosta, S., & Koenig, X. P. 2011, ApJ, 733, L2 (ADS entry)

- Lomb, N. R. 1976, *Ap&SS*, 39, 447 (ADS entry)
- Looper, D. L., Bochanski, J. J., Burgasser, A. J., Mohanty, S., Mamajek, E. E., Faherty, J. K., West, A. A., & Pitts, M. A. 2010a, *AJ*, 140, 1486 (ADS entry)
- Looper, D. L., Burgasser, A. J., Kirkpatrick, J. D., & Swift, B. J. 2007, *ApJ*, 669, L97 (ADS entry)
- Looper, D. L., et al. 2010b, *ApJ*, 714, 45 (ADS entry)
- López-Santiago, J., Albacete Colombo, J. F., & López-García, M. A. 2010, *A&A*, 524, A97 (ADS entry)
- Low, F. J., Smith, P. S., Werner, M., Chen, C., Krause, V., Jura, M., & Hines, D. C. 2005, *ApJ*, 631, 1170 (ADS entry)
- Lowrance, P. J., et al. 1999, *ApJ*, 512, L69 (ADS entry)
- Luhman, K. L. 2004a, *ApJ*, 602, 816 (ADS entry)
- . 2004b, *ApJ*, 616, 1033 (ADS entry)
- . 2007, *ApJS*, 173, 104 (ADS entry)
- . 2008, *Handbook of Star Forming Regions*, Vol. II: The Southern Sky, ed. B. Reipurth (ASP Press), 169 (ADS entry)
- Luhman, K. L., Mamajek, E. E., Allen, P. R., & Cruz, K. L. 2009a, *ApJ*, 703, 399 (ADS entry)
- Luhman, K. L., Mamajek, E. E., Allen, P. R., Muench, A. A., & Finkbeiner, D. P. 2009b, *ApJ*, 691, 1265 (ADS entry)
- Luhman, K. L., Stauffer, J. R., & Mamajek, E. E. 2005, *ApJ*, 628, L69 (ADS entry)
- Luhman, K. L., Stauffer, J. R., Muench, A. A., Rieke, G. H., Lada, E. A., Bouvier, J., & Lada, C. J. 2003, *ApJ*, 593, 1093 (ADS entry)
- Luhman, K. L., & Steeghs, D. 2004, *ApJ*, 609, 917 (ADS entry)
- Luhman, K. L., et al. 2008, *ApJ*, 675, 1375 (ADS entry)
- Lyo, A.-R., Lawson, W. A., & Bessell, M. S. 2004a, *MNRAS*, 355, 363 (ADS entry)
- . 2008, *MNRAS*, 389, 1461 (ADS entry)
- Lyo, A.-R., Lawson, W. A., Feigelson, E. D., & Crause, L. A. 2004b, *MNRAS*, 347, 246 (ADS entry)
- Lyo, A.-R., Lawson, W. A., Mamajek, E. E., Feigelson, E. D., Sung, E.-C., & Crause, L. A. 2003, *MNRAS*, 338, 616 (ADS entry)
- Lyo, A.-R., Song, I., Lawson, W. A., Bessell, M. S., & Zuckerman, B. 2006, *MNRAS*, 368, 1451 (ADS entry)
- Madsen, S., Dravins, D., & Lindegren, L. 2002, *A&A*, 381, 446 (ADS entry)

- Mahmud, N. I., Crockett, C. J., Johns-Krull, C. M., Prato, L., Hartigan, P. M., Jaffe, D. T., & Beichman, C. A. 2011, *ApJ*, 736, 123 (ADS entry)
- Makarov, V. V. 2007, *ApJS*, 169, 105 (ADS entry)
- Makarov, V. V., Olling, R. P., & Teuben, P. J. 2004, *MNRAS*, 352, 1199 (ADS entry)
- Makarov, V. V., Zacharias, N., & Hennessy, G. S. 2008, *ApJ*, 687, 566 (ADS entry)
- Mamajek, E. E. 2003, in *Astrophysics and Space Science Library*, Vol. 299, Open Issues in Local Star Formation, ed. J. Lépine & J. Gregorio-Hetem, 39 (ADS entry)
- Mamajek, E. E. 2005a, *ApJ*, 634, 1385 (ADS entry)
- Mamajek, E. E. 2005b, in *Astronomical Society of the Pacific Conference Series*, Vol. 338, Astrometry in the Age of the Next Generation of Large Telescopes, ed. Seidelmann, P. K. and Monet, A. K. B., 280 (ADS entry)
- Mamajek, E. E. 2009, in *American Institute of Physics Conference Series*, Vol. 1158, Exoplanets and Disks: their formation and diversity: Proceedings of the International Conference, ed. T. Usuda, M. Tamura, & M. Ishii, 3–10 (ADS entry)
- Mamajek, E. E., & Feigelson, E. D. 2001, in *Astronomical Society of the Pacific Conference Series*, Vol. 244, Young Stars Near Earth: Progress and Prospects, ed. R. Jayawardhana & T. Greene, 104–115 (ADS entry)
- Mamajek, E. E., & Hillenbrand, L. A. 2008, *ApJ*, 687, 1264 (ADS entry)
- Mamajek, E. E., Lawson, W. A., & Feigelson, E. D. 1999, *ApJ*, 516, L77 (ADS entry)
- . 2000, *ApJ*, 544, 356 (ADS entry)
- Mamajek, E. E., & Meyer, M. R. 2007, *ApJ*, 668, L175 (ADS entry)
- Mamajek, E. E., Meyer, M. R., & Liebert, J. 2002, *AJ*, 124, 1670 (ADS entry)
- Manoj, P., et al. 2011, *ApJS*, 193, 11 (ADS entry)
- Marois, C., Macintosh, B., Barman, T., Zuckerman, B., Song, I., Patience, J., Lafrenière, D., & Doyon, R. 2008, *Science*, 322, 1348 (ADS entry)
- Marois, C., Zuckerman, B., Konopacky, Q. M., Macintosh, B., & Barman, T. 2010, *Nature*, 468, 1080 (ADS entry)
- Martín, E. L., & Ardila, D. R. 2001, *AJ*, 121, 2758 (ADS entry)
- Martín, E. L., Delfosse, X., Basri, G., Goldman, B., Forveille, T., & Zapatero Osorio, M. R. 1999, *AJ*, 118, 2466 (ADS entry)
- Martín, E. L., Guenther, E., Zapatero Osorio, M. R., Bouy, H., & Wainscoat, R. 2006, *ApJ*, 644, L75 (ADS entry)
- Martin, E. L., Rebolo, R., & Zapatero-Osorio, M. R. 1996, *ApJ*, 469, 706 (ADS entry)
- McKee, C. F., & Ostriker, E. C. 2007, *ARA&A*, 45, 565 (ADS entry)

- Megeath, S. T., Hartmann, L., Luhman, K. L., & Fazio, G. G. 2005, *ApJ*, 634, L113 (ADS entry)
- Mentuch, E., Brandeker, A., van Kerckwijk, M. H., Jayawardhana, R., & Hauschildt, P. H. 2008, *ApJ*, 689, 1127 (ADS entry)
- Messina, S., Desidera, S., Turatto, M., Lanzafame, A. C., & Guinan, E. F. 2010, *A&A*, 520, A15 (ADS entry)
- Mizuno, A., Yamaguchi, R., Tachihara, K., Toyoda, S., Aoyama, H., Yamamoto, H., Onishi, T., & Fukui, Y. 2001, *PASJ*, 53, 1071 (ADS entry)
- Mo, H., van den Bosch, F. C., & White, S. 2010, *Galaxy Formation and Evolution* (Cambridge University Press) (ADS entry)
- Moeckel, N., & Bate, M. R. 2010, *MNRAS*, 404, 721 (ADS entry)
- Moeckel, N., & Clarke, C. J. 2011, *MNRAS*, 415, 1179 (ADS entry)
- Mohanty, S., Jayawardhana, R., & Basri, G. 2005, *ApJ*, 626, 498 (ADS entry)
- Mohanty, S., Jayawardhana, R., Huélamo, N., & Mamajek, E. 2007, *ApJ*, 657, 1064 (ADS entry)
- Monet, D. G., et al. 2003, *AJ*, 125, 984 (ADS entry)
- Montes, D., Fernandez-Figueroa, M. J., de Castro, E., Cornide, M., Poncet, A., & Sanz-Forcada, J. 1998, in *Astronomical Society of the Pacific Conference Series*, Vol. 154, Cool Stars, Stellar Systems, and the Sun, ed. R. A. Donahue & J. A. Bookbinder, 1516 (ADS entry)
- Moraux, E., Lawson, W. A., & Clarke, C. 2007, *A&A*, 473, 163 (ADS entry)
- Moro, D., & Munari, U. 2000, *A&AS*, 147, 361 (ADS entry)
- Mouillet, D., Larwood, J. D., Papaloizou, J. C. B., & Lagrange, A. M. 1997, *MNRAS*, 292, 896 (ADS entry)
- Murakami, H., et al. 2007, *PASJ*, 59, 369 (ADS entry)
- Murphy, S. J., Lawson, W. A., & Bessell, M. S. 2010, *MNRAS*, 406, L50 (ADS entry)
- Murphy, S. J., Lawson, W. A., Bessell, M. S., & Bayliss, D. D. R. 2011, *MNRAS*, 411, L51 (ADS entry)
- Muzerolle, J., Calvet, N., Briceño, C., Hartmann, L., & Hillenbrand, L. 2000, *ApJ*, 535, L47 (ADS entry)
- Muzerolle, J., Hillenbrand, L., Calvet, N., Briceño, C., & Hartmann, L. 2003, *ApJ*, 592, 266 (ADS entry)
- Nakajima, T., Morino, J., & Fukagawa, M. 2010, *AJ*, 140, 713 (ADS entry)
- Nakajima, T., & Morino, J.-I. 2012, *AJ*, 143, 2 (ADS entry)
- Natta, A., Testi, L., Muzerolle, J., Randich, S., Comerón, F., & Persi, P. 2004, *A&A*, 424, 603 (ADS entry)

- Nehmé, C., Gry, C., Boulanger, F., Le Bourlot, J., Pineau Des Forets, G., & Falgarone, E. 2008, *A&A*, 483, 471 (ADS entry)
- Neuhäuser, R. 1997, *Science*, 276, 1363 (ADS entry)
- Nguyen, D. C., Scholz, A., van Kerkwijk, M. H., Jayawardhana, R., & Brandeker, A. 2009, *ApJ*, 694, L153 (ADS entry)
- Nidever, D. L., Marcy, G. W., Butler, R. P., Fischer, D. A., & Vogt, S. S. 2002, *ApJS*, 141, 503 (ADS entry)
- Nisini, B., Bacciotti, F., Giannini, T., Massi, F., Eisloffel, J., Podio, L., & Ray, T. P. 2005, *A&A*, 441, 159 (ADS entry)
- Olsen, E. H. 1994, *A&AS*, 104, 429 (ADS entry)
- Ortega, V. G., de la Reza, R., Jilinski, E., & Bazzanella, B. 2002, *ApJ*, 575, L75 (ADS entry)
- . 2004, *ApJ*, 609, 243 (ADS entry)
- Ortega, V. G., Jilinski, E., de La Reza, R., & Bazzanella, B. 2007, *MNRAS*, 377, 441 (ADS entry)
- Ortega, V. G., Jilinski, E., de la Reza, R., & Bazzanella, B. 2009, *AJ*, 137, 3922 (ADS entry)
- Osterbrock, D. E., Fulbright, J. P., Martel, A. R., Keane, M. J., Trager, S. C., & Basri, G. 1996, *PASP*, 108, 277 (ADS entry)
- Padgett, D. L., et al. 2006, *ApJ*, 645, 1283 (ADS entry)
- Parker, Q. A., et al. 2005, *MNRAS*, 362, 689 (ADS entry)
- Patience, J., King, R. R., de Rosa, R. J., & Marois, C. 2010, *A&A*, 517, A76 (ADS entry)
- Perryman, M. A. C., & ESA. 1997, *ESA Special Publication*, Vol. 1200, *The HIPPARCOS and TYCHO catalogues: Astrometric and photometric star catalogues derived from the ESA HIPPARCOS Space Astrometry Mission* (ESA Publications Division) (ADS entry)
- Persi, P., Marenzi, A. R., & Goméz, M. 2003, in *ESA Special Publication*, Vol. 511, *Exploiting the ISO Data Archive. Infrared Astronomy in the Internet Age*, ed. C. Gry, S. Peschke, J. Matagne, P. Garcia-Lario, R. Lorente, & A. Salama, 221 (ADS entry)
- Phan-Bao, N., et al. 2008, *MNRAS*, 383, 831 (ADS entry)
- Pickles, A. J. 1998, *PASP*, 110, 863 (ADS entry)
- Pinsonneault, M. H. 2010, in *IAU Symposium*, Vol. 268, *Light elements in the Universe*, ed. C. Charbonnel, M. Tosi, F. Primas, & C. Chiappini, 375–380 (ADS entry)
- Platais, I., Melo, C., Mermilliod, J., Kozhurina-Platais, V., Fulbright, J. P., Méndez, R. A., Altmann, M., & Sperauskas, J. 2007, *A&A*, 461, 509 (ADS entry)
- Podio, L., Bacciotti, F., Nisini, B., Eisloffel, J., Massi, F., Giannini, T., & Ray, T. P. 2006, *A&A*, 456, 189 (ADS entry)
- Podio, L., Medves, S., Bacciotti, F., Eisloffel, J., & Ray, T. 2009, *A&A*, 506, 779 (ADS entry)

- Pojmanski, G. 2002, *Acta Astronomica*, 52, 397 (ADS entry)
- Pollack, J. B., Hubickyj, O., Bodenheimer, P., Lissauer, J. J., Podolak, M., & Greenzweig, Y. 1996, *Icarus*, 124, 62 (ADS entry)
- Poncet, A., Montes, D., Fernandez-Figueroa, M. J., & Miranda, L. F. 1998, in *Astronomical Society of the Pacific Conference Series*, Vol. 154, Cool Stars, Stellar Systems, and the Sun, ed. R. A. Donahue & J. A. Bookbinder, 1772 (ADS entry)
- Preibisch, T., Guenther, E., Zinnecker, H., Sterzik, M., Frink, S., & Roeser, S. 1998, *A&A*, 333, 619 (ADS entry)
- Preibisch, T., & Mamajek, E. E. 2008, *Handbook of Star Forming Regions*, Vol. II. The Southern Sky, ed. B. Reipurth (ASP Press), 235
- Prugniel, P., & Soubiran, C. 2004, ArXiv e-prints: astro-ph/0409.214 (ADS entry)
- Quast, G. R., Torres, C. A. O., de La Reza, R., da Silva, L., & Mayor, M. 2000, in *IAU Symposium*, Vol. 200, Birth and Evolution of Binary Stars, ed. B. Reipurth & H. Zinnecker, 28P (ADS entry)
- Ramsay Howat, S. K., & Greaves, J. S. 2007, *MNRAS*, 379, 1658 (ADS entry)
- Raymond, S. N., Quinn, T., & Lunine, J. I. 2005, *ApJ*, 632, 670 (ADS entry)
- Rebull, L. M., et al. 2011, *ApJS*, 196, 4 (ADS entry)
- Reid, I. N., Gizis, J. E., Kirkpatrick, J. D., & Koerner, D. W. 2001, *AJ*, 121, 489 (ADS entry)
- Reid, I. N., Hawley, S. L., & Gizis, J. E. 1995, *AJ*, 110, 1838 (ADS entry)
- Reid, N. 2003, *MNRAS*, 342, 837 (ADS entry)
- Reiners, A., Bean, J. L., Huber, K. F., Dreizler, S., Seifahrt, A., & Czesla, S. 2010, *ApJ*, 710, 432 (ADS entry)
- Reipurth, B., & Bally, J. 2001, *ARA&A*, 39, 403 (ADS entry)
- Riaz, B., Gizis, J. E., & Harvin, J. 2006, *AJ*, 132, 866 (ADS entry)
- Riddick, F. C., Roche, P. F., & Lucas, P. W. 2007, *MNRAS*, 381, 1067 (ADS entry)
- Riedel, A. R., Murphy, S. J., Henry, T. J., Melis, C., Jao, W.-C., & Subasavage, J. P. 2011, *AJ*, 142, 104 (ADS entry)
- Rio, Y., et al. 1998, in *SPIE Conference Series*, Vol. 3354, Infrared Astronomical Instrumentation, ed. A. M. Fowler, 615–626 (ADS entry)
- Rizzuto, A. C., Ireland, M. J., & Robertson, J. G. 2011, *MNRAS*, 416, 3108 (ADS entry)
- Rodriguez, D. R., Bessell, M. S., Zuckerman, B., & Kastner, J. H. 2011, *ApJ*, 727, 62 (ADS entry)
- Roeser, S., Demleitner, M., & Schilbach, E. 2010, *AJ*, 139, 2440 (ADS entry)

- Rucinski, S. M., & Krautter, J. 1983, A&A, 121, 217 (ADS entry)
- Saar, S. H., & Donahue, R. A. 1997, ApJ, 485, 319 (ADS entry)
- Sartori, M. J., Lépine, J. R. D., & Dias, W. S. 2003, A&A, 404, 913 (ADS entry)
- Scargle, J. D. 1982, ApJ, 263, 835 (ADS entry)
- Schisano, E., Covino, E., Alcalá, J. M., Esposito, M., Gandolfi, D., & Guenther, E. W. 2009, A&A, 501, 1013 (ADS entry)
- Schlegel, D. J., Finkbeiner, D. P., & Davis, M. 1998, ApJ, 500, 525 (ADS entry)
- Schmidt-Kaler, T. 1982, New Series, Vol. 2, Landolt-Börnstein, ed. K. H. Hellwege (Berlin: Springer-Verlag), 453
- Schmitt, J. H. M. M., Fleming, T. A., & Giampapa, M. S. 1995, ApJ, 450, 392 (ADS entry)
- Scholz, A., Coffey, J., Brandeker, A., & Jayawardhana, R. 2007, ApJ, 662, 1254 (ADS entry)
- Scholz, A., & Eisloffel, J. 2005, A&A, 429, 1007 (ADS entry)
- Scholz, A., & Jayawardhana, R. 2006, ApJ, 638, 1056 (ADS entry)
- Scholz, R.-D., McCaughrean, M. J., Zinnecker, H., & Lodieu, N. 2005, A&A, 430, L49 (ADS entry)
- Schwartz, R. D. 1992, Low Mass Star Formation in Southern Molecular Clouds: The Chamaeleon Dark Clouds and T-Associations, ed. Reipurth, B. (Garching: European Southern Observatory), 93 (ADS entry)
- Sherry, W. H., Walter, F. M., & Wolk, S. J. 2004, AJ, 128, 2316 (ADS entry)
- Shkolnik, E., Liu, M. C., & Reid, I. N. 2009, ApJ, 699, 649 (ADS entry)
- Shkolnik, E. L., Liu, M. C., Reid, I. N., Dupuy, T., & Weinberger, A. J. 2011, ApJ, 727, 6 (ADS entry)
- Shu, F. H., Adams, F. C., & Lizano, S. 1987, ARA&A, 25, 23 (ADS entry)
- Sicilia-Aguilar, A., Hartmann, L. W., Fürész, G., Henning, T., Dullemond, C., & Brandner, W. 2006, AJ, 132, 2135 (ADS entry)
- Sicilia-Aguilar, A., Henning, T., & Hartmann, L. W. 2010, ApJ, 710, 597 (ADS entry)
- Sicilia-Aguilar, A., Henning, T., Juhász, A., Bouwman, J., Garmire, G., & Garmire, A. 2008, ApJ, 687, 1145 (ADS entry)
- Sicilia-Aguilar, A., et al. 2009, ApJ, 701, 1188 (ADS entry)
- Siess, L., Dufour, E., & Forestini, M. 2000, A&A, 358, 593 (ADS entry)
- Silverstone, M. D., et al. 2006, ApJ, 639, 1138 (ADS entry)
- Skemer, A. J., Close, L. M., Szűcs, L., Apai, D., Pascucci, I., & Biller, B. A. 2011, ApJ, 732, 107 (ADS entry)

- Skrutskie, M. F., et al. 2006, AJ, 131, 1163 (ADS entry)
- Slesnick, C. L., Carpenter, J. M., & Hillenbrand, L. A. 2006a, AJ, 131, 3016 (ADS entry)
- Slesnick, C. L., Carpenter, J. M., Hillenbrand, L. A., & Mamajek, E. E. 2006b, AJ, 132, 2665 (ADS entry)
- Smith, B. A., & Terrile, R. J. 1984, Science, 226, 1421 (ADS entry)
- Song, I., Bessell, M. S., & Zuckerman, B. 2002, ApJ, 581, L43 (ADS entry)
- Song, I., Zuckerman, B., & Bessell, M. S. 2003, ApJ, 599, 342 (ADS entry)
- . 2004, ApJ, 600, 1016 (ADS entry)
- Spezzi, L., et al. 2008, ApJ, 680, 1295 (ADS entry)
- Stahler, S., & Palla, F. 2004, *The Formation of Stars* (Weinheim: Wiley-VCH)
- Stauffer, J. R., Hartmann, L. W., Prosser, C. F., Randich, S., Balachandran, S., Patten, B. M., Simon, T., & Giampapa, M. 1997, ApJ, 479, 776 (ADS entry)
- Stauffer, J. R., Jones, B. F., Backman, D., Hartmann, L. W., Barrado y Navascués, D., Pinsonneault, M. H., Terndrup, D. M., & Muench, A. A. 2003, AJ, 126, 833 (ADS entry)
- Steinmetz, M., et al. 2006, AJ, 132, 1645 (ADS entry)
- Stellingwerf, R. F. 1978, ApJ, 224, 953 (ADS entry)
- Stelzer, B., Scholz, A., & Jayawardhana, R. 2007, ApJ, 671, 842 (ADS entry)
- Stempels, H. C., & Gahm, G. F. 2004, A&A, 421, 1159 (ADS entry)
- Stempels, H. C., & Piskunov, N. 2003, A&A, 408, 693 (ADS entry)
- Sterzik, M. F., Alcalá, J. M., Covino, E., & Petr, M. G. 1999, A&A, 346, L41 (ADS entry)
- Sterzik, M. F., & Durisen, R. H. 1995, A&A, 304, L9 (ADS entry)
- Straižys, V. 1992, *Multicolor stellar photometry* (Tuscon: Pachart Publishing House) (ADS entry)
- Sung, H., Bessell, M. S., Chun, M.-Y., Karimov, R., & Ibrahimov, M. 2008, AJ, 135, 441 (ADS entry)
- Takita, S., Kataza, H., Kitamura, Y., Ishihara, D., Ita, Y., Oyabu, S., & Ueno, M. 2010, A&A, 519, A83 (ADS entry)
- Teixeira, R., Ducourant, C., Chauvin, G., Krone-Martins, A., Song, I., & Zuckerman, B. 2008, A&A, 489, 825 (ADS entry)
- Tenorio-Tagle, G. 1979, A&A, 71, 59 (ADS entry)
- Terranegra, L., Morale, F., Spagna, A., Massone, G., & Lattanzi, M. G. 1999, A&A, 341, L79 (ADS entry)

- Testa, P., Huenemoerder, D. P., Schulz, N. S., & Ishibashi, K. 2008, *ApJ*, 687, 579 (ADS entry)
- Testi, L., Palla, F., & Natta, A. 1999, *A&A*, 342, 515 (ADS entry)
- Torres, C. A. O., da Silva, L., Quast, G. R., de la Reza, R., & Jilinski, E. 2000, *AJ*, 120, 1410 (ADS entry)
- Torres, C. A. O., Quast, G. R., da Silva, L., de La Reza, R., Melo, C. H. F., & Sterzik, M. 2006, *A&A*, 460, 695 (ADS entry)
- Torres, C. A. O., Quast, G. R., de La Reza, R., da Silva, L., & Melo, C. H. F. 2001, in Astronomical Society of the Pacific Conference Series, Vol. 244, Young Stars Near Earth: Progress and Prospects, ed. R. Jayawardhana & T. Greene, 43 (ADS entry)
- Torres, C. A. O., Quast, G. R., de La Reza, R., da Silva, L., & Melo, C. H. F. 2003a, in Astronomical Society of the Pacific Conference Series, Vol. 287, Galactic Star Formation Across the Stellar Mass Spectrum, ed. J. M. De Buizer & N. S. van der Blieck, 439–444 (ADS entry)
- Torres, C. A. O., Quast, G. R., de La Reza, R., da Silva, L., Melo, C. H. F., & Sterzik, M. 2003b, in Astrophysics and Space Science Library, Vol. 299, Open Issues in Local Star Formation, ed. J. Lépine & J. Gregorio-Hetem, 83 (ADS entry)
- Torres, C. A. O., Quast, G. R., Melo, C. H. F., & Sterzik, M. F. 2008, Handbook of Star Forming Regions, Vol. II: The Southern Sky, ed. Reipurth, B. (ASP Press), 757 (ADS entry)
- Udry, S. 2010, in Proceedings of the conference In the Spirit of Lyot 2010: Direct Detection of Exoplanets and Circumstellar Disks, ed. A. Boccaletti (ADS entry)
- van Dishoeck, E. F., & Jørgensen, J. K. 2008, *Ap&SS*, 313, 15 (ADS entry)
- van Leeuwen, F. 2007, *A&A*, 474, 653 (ADS entry)
- van Leeuwen, F., Evans, D. W., Grenon, M., Grossmann, V., Mignard, F., & Perryman, M. A. C. 1997, *A&A*, 323, L61 (ADS entry)
- Voges, W., et al. 1999, *A&A*, 349, 389 (ADS entry)
- . 2000, IAU Circ., 7432, 3 (ADS entry)
- Vogt, S. S., Penrod, G. D., & Hatzes, A. P. 1987, *ApJ*, 321, 496 (ADS entry)
- Wahhaj, Z., et al. 2010, *ApJ*, 724, 835 (ADS entry)
- Webb, R. A., Zuckerman, B., Platais, I., Patience, J., White, R. J., Schwartz, M. J., & McCarthy, C. 1999, *ApJ*, 512, L63 (ADS entry)
- Weidner, C., Bonnell, I. A., & Moeckel, N. 2011, *MNRAS*, 410, 1861 (ADS entry)
- Weidner, C., & Kroupa, P. 2006, *MNRAS*, 365, 1333 (ADS entry)
- Weidner, C., Kroupa, P., Nürnberger, D. E. A., & Sterzik, M. F. 2007, *MNRAS*, 376, 1879 (ADS entry)

- Weise, P., Launhardt, R., Setiawan, J., & Henning, T. 2010, A&A, 517, A88 (ADS entry)
- West, A. A., Walkowicz, L. M., & Hawley, S. L. 2005, PASP, 117, 706 (ADS entry)
- Westin, T. N. G. 1985, A&AS, 60, 99 (ADS entry)
- White, R. J., & Basri, G. 2003, ApJ, 582, 1109 (ADS entry)
- White, R. J., Gabor, J. M., & Hillenbrand, L. A. 2007, AJ, 133, 2524 (ADS entry)
- Whittet, D. C. B., Prusti, T., Franco, G. A. P., Gerakines, P. A., Kilkenny, D., Larson, K. A., & Wesselius, P. R. 1997, A&A, 327, 1194 (ADS entry)
- Wichmann, R., Schmitt, J. H. M. M., & Hubrig, S. 2003, A&A, 399, 983 (ADS entry)
- Wilking, B. A. 1989, PASP, 101, 229 (ADS entry)
- Williams, J. P., & Cieza, L. A. 2011, ARA&A, 49, 67
- Wilson, R. E. 1953, General Catalogue of Stellar Radial Velocities. (Washington DC: Carnegie Institute) (ADS entry)
- Wright, E. L., et al. 2010, AJ, 140, 1868 (ADS entry)
- Wyatt, M. C. 2008, ARA&A, 46, 339 (ADS entry)
- Yamamura, I., Makiuti, S., Ikeda, N., Fukuda, Y., Oyabu, S., Koga, T., & White, G. J. 2010, VizieR Online Data Catalog, 2298, 0 (ADS entry)
- Yee, J. C., & Jensen, E. L. N. 2010, ApJ, 711, 303 (ADS entry)
- Zacharias, N., et al. 2010, AJ, 139, 2184 (ADS entry)
- Zboril, M., Byrne, P. B., & Rolleston, W. R. J. R. 1997, MNRAS, 284, 685 (ADS entry)
- Zinnecker, H., & Yorke, H. W. 2007, ARA&A, 45, 481 (ADS entry)
- Zuckerman, B., Rhee, J. H., Song, I., & Bessell, M. S. 2011, ApJ, 732, 61 (ADS entry)
- Zuckerman, B., & Song, I. 2004, ARA&A, 42, 685 (ADS entry)
- Zuckerman, B., Song, I., & Bessell, M. S. 2004, ApJ, 613, L65 (ADS entry)
- Zuckerman, B., Song, I., Bessell, M. S., & Webb, R. A. 2001a, ApJ, 562, L87 (ADS entry)
- Zuckerman, B., Song, I., & Webb, R. A. 2001b, ApJ, 559, 388 (ADS entry)
- Zuckerman, B., & Webb, R. A. 2000, ApJ, 535, 959 (ADS entry)
- Zuckerman, B., Webb, R. A., Schwartz, M., & Becklin, E. E. 2001c, ApJ, 549, L233 (ADS entry)

## APPENDIX A

---

# Isochrone colour transformations

In this appendix we describe the transformations from the Baraffe et al. (1998) and Siess et al. (2000) model isochrones to our observed  $i_{\text{DENIS}}$  and  $J_{\text{2MASS}}$  colours, as well as the effects of interstellar extinction and reddening.

### $J_{\text{2MASS}}$ transformation

These transformations were determined by Carpenter (2001) and subsequently updated on the 2MASS website<sup>1</sup>. The Baraffe et al. (1998) model  $J$  magnitudes are on the CIT system (Elias et al. 1982). The linear transformation between  $J_{\text{2MASS}}$  and  $J_{\text{CIT}}$  is:

$$J_{\text{2MASS}} = K_{\text{2MASS}} + 1.068 \times (J - K)_{\text{CIT}} - 0.020 \quad (\text{A.1})$$

where  $K_{\text{2MASS}} = K_{\text{CIT}} - 0.019 + 0.001 \times (J - K)_{\text{CIT}}$

The Siess et al. (2000) model  $J$  magnitudes are derived from the conversion table of Kenyon & Hartmann (1995), who used Bessell & Brett (1988) as the source of their near-infrared photometry. The transformation to  $J_{\text{2MASS}}$  is given by:

$$J_{\text{2MASS}} = K_{\text{2MASS}} + 0.983 \times (J - K)_{\text{B\&B}} - 0.018 \quad (\text{A.2})$$

where  $K_{\text{2MASS}} = K_{\text{B\&B}} - 0.039 + 0.001 \times (J - K)_{\text{B\&B}}$

### $I_C$ to $i_{\text{DENIS}}$ transformation

Both sets of isochrones use Cousins  $I_C$  magnitudes. Unfortunately there exist no published transformations between  $I_C$  and  $i_{\text{DENIS}}$ . Agreement between DENIS photometry and the Cousins-CIT system is quoted as better than 0.05 mag (e.g. Phan-Bao et al. 2008). To test this requires a large sample of stars with Cousins and DENIS photometry. Most bright, red *Hipparcos* stars are saturated in DENIS and suffer from poor photometric quality. We therefore formed a (heterogeneous) sample of late-type stars from various southern clusters with  $I_C$  and DENIS photometry. The sample consisted of K and M-type stars from the

<sup>1</sup><http://www.astro.caltech.edu/jmc/2mass/v3/transformations/>

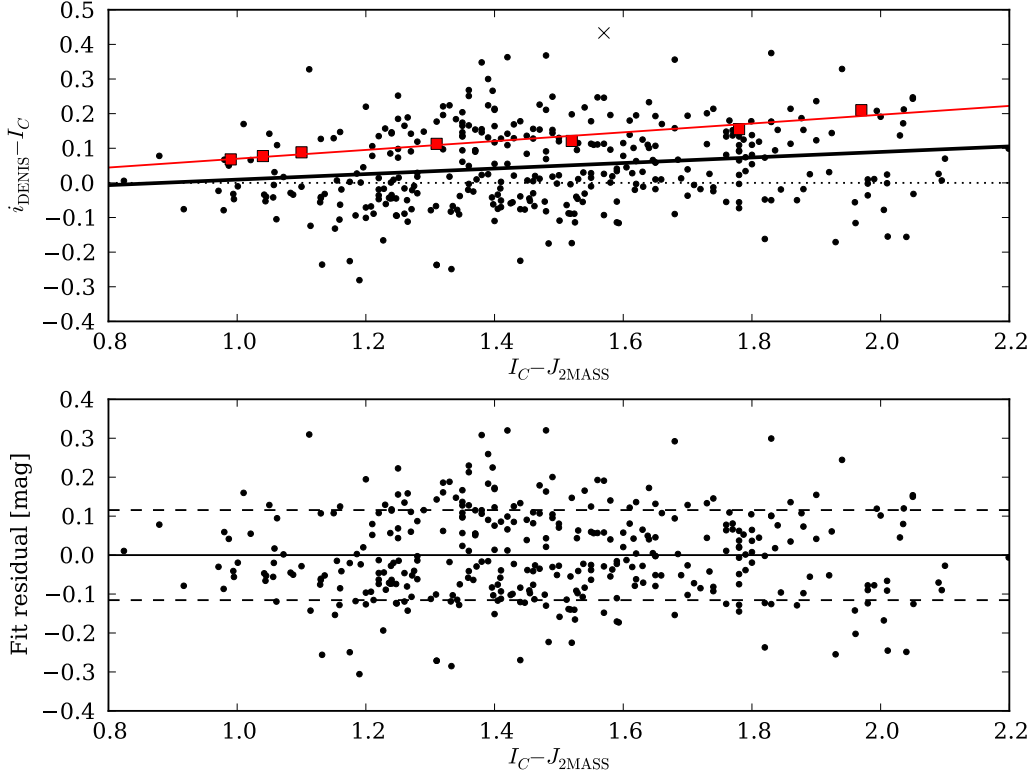


**Figure A.1** Linear transformation between  $i_{\text{DENIS}}$  and Cousins  $I_C$  for 352 southern cluster stars. Red squares are empirical M-dwarfs from the Pickles (1998) library (see text).

clusters  $\eta$  Cha (14 stars, Lawson et al. 2001, 2002; Lyo et al. 2004b), NGC 2547 (72 stars, Irwin et al. 2008), NGC 2516 (23 stars, Irwin et al. 2007),  $\epsilon$  Ori (46 stars, Scholz & Eislöffel 2005), IC 2391 (35 stars, Barrado y Navascués et al. 2004) and  $\sigma$  Ori (175 stars, Sherry et al. 2004). We derived the following linear transformation from 352 stars (see Figure A.1):

$$i_{\text{DENIS}} = I_C + 0.080 \times (I_C - J_{\text{2MASS}}) - 0.070 \quad (\text{A.3})$$

with an RMS residual of 0.12 mag in  $(i_{\text{DENIS}} - I_C)$ . The fit is valid over the colour range  $0.8 < (I_C - J_{\text{2MASS}}) < 2.2$  (K to mid-M spectral types) and was determined iteratively with a  $3\sigma$  clipping that rejected 13 obviously discrepant stars. Despite the scatter, Figure A.1 confirms the good agreement between the two systems, with only a small colour term ( $m < \sigma_{\text{fit}}$ ). The scatter in the relation is most likely the result of observational errors. Our chosen clusters have a small range of reddening ( $0 \lesssim E(B - V) \lesssim 0.1$ ), so it is unlikely the transformation is affected by this. Furthermore, each of the clusters shows a similar trend, regardless of their individual reddening.

As a cross-check we performed synthetic photometry on M0–M6 dwarfs from the empirical library of Pickles (1998), with filter response curves from the Asiago Database of Photometric Systems<sup>2</sup> (Moro & Munari 2000) and absolute calibrations from Bessell et al. (1998) and Fouqué et al. (2000). The results are shown overlaid in Figure A.1. As the Pickles spectra do not extend beyond 1  $\mu\text{m}$  we adopted main sequence ( $I_C - J$ ) colours from the compilation of Kenyon & Hartmann (1995). A fit to these points yields a similar linear transformation:

$$i_{\text{DENIS}} = I_C + 0.127 \times (I_C - J_{\text{2MASS}}) - 0.057 \quad (\text{A.4})$$

<sup>2</sup><http://ulisse.pd.astro.it/Astro/ADPS/>

Prior to comparison to the observations, the model isochrones were transformed into the observational space using Equations A.1, A.2 and A.3. In transforming  $I_C$  to  $i_{\text{DENIS}}$  we chose to use the observed photometry over the synthetic relation to avoid possible biases from incorrect filter responses or absolute flux calibrations. The choice of transformation has negligible effect on the resultant isochrone (see Figure A.2).

## 2MASS two-colour diagrams

Bessell & Brett (1988) tabulated dwarf and giant loci in standardised  $(JHK)_{\text{B\&B}}$  colours. The following transformations to 2MASS colours were adopted from the 2MASS website (after Carpenter 2001):

$$\begin{aligned}(J - H)_{\text{2MASS}} &= 0.990 \times (J - H)_{\text{B\&B}} - 0.049 \\ (H - K)_{\text{2MASS}} &= 0.971 \times (H - K)_{\text{B\&B}} + 0.034\end{aligned}\quad (\text{A.5})$$

## Extinction and reddening

We adopt the relative extinctions calculated by Schlegel et al. (1998, their Table 6). In our colour-magnitude diagrams we assume:

$$\begin{aligned}A_{J_{\text{2MASS}}} &\approx A_{J_{\text{UKIRT}}} = 0.902 \times E(B - V) \\ A_{i_{\text{DENIS}}} &\approx A_{I_{\text{CTIO}}} = 1.962 \times E(B - V)\end{aligned}\quad (\text{A.6})$$

The component of the reddening vector along the  $(i_{\text{DENIS}} - J_{\text{2MASS}})$  axis is therefore:

$$A_{i_{\text{DENIS}}} - A_{J_{\text{2MASS}}} = E(i_{\text{DENIS}} - J_{\text{2MASS}}) = 1.06 \times E(B - V) \quad (\text{A.7})$$

In the near-infrared we adopt the following relations from Schlegel et al. (1998):

$$\begin{aligned}A_J - A_H &= E(J - H) = 0.326 \times E(B - V) \\ A_H - A_K &= E(H - K) = 0.209 \times E(B - V)\end{aligned}\quad (\text{A.8})$$

where the colour-excesses are in the UKIRT system (Hawarden et al. 2001). We assume this approximates the 2MASS system to first order. All of the above conversions assume an  $R_V = 3.1$  extinction law from Cardelli et al. (1989).

Figure A.2 illustrates the effects of transforming and reddening the model isochrones. Given the inherent uncertainty in the isochrones themselves, transforming to the observed  $(i_{\text{DENIS}}, J_{\text{2MASS}})$  colours has minimal effect on the isochrone shape and position. Reddening has the overall effect of shifting the best-fitting isochrone to larger distances for a given age.

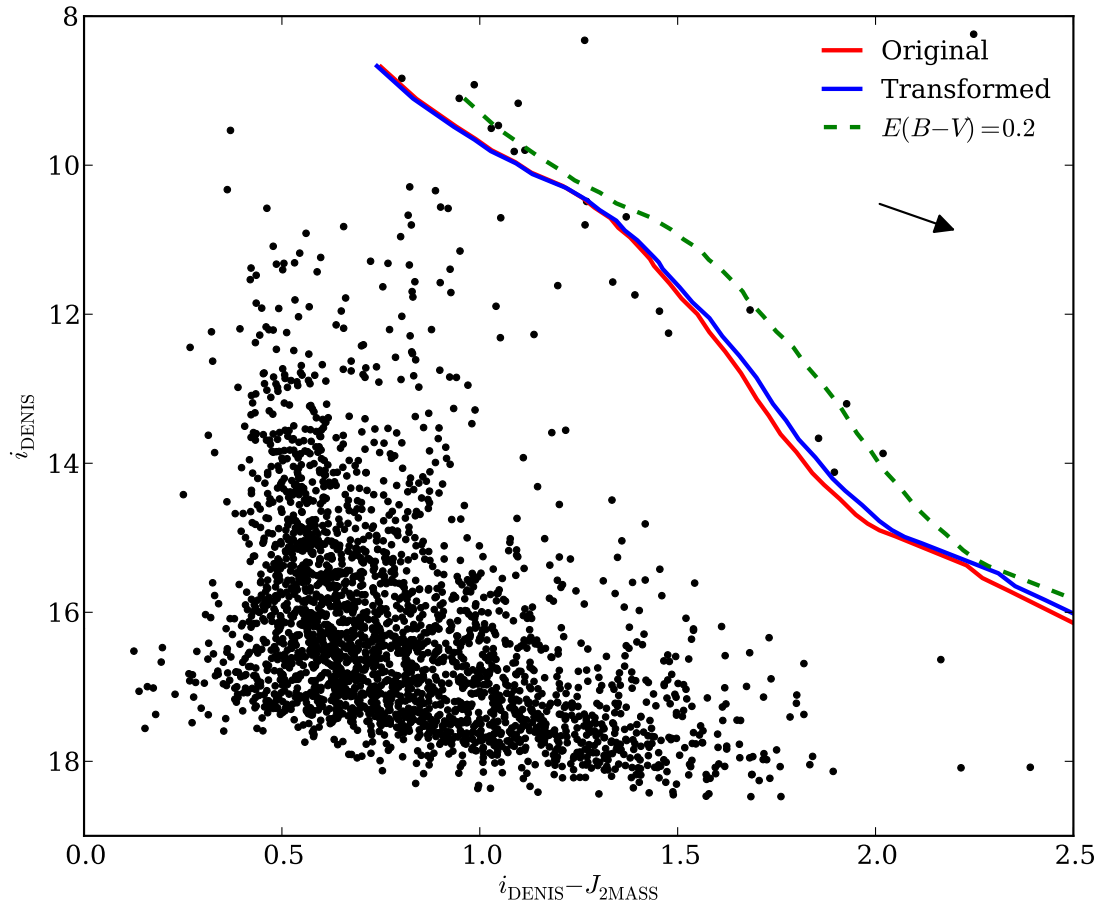


**Figure A.2** Colour-magnitude diagram of stars within 20' of the centre of  $\eta$  Cha. The red line shows a Baraffe et al. (1998) 10 Myr isochrone at a distance of 100 pc. The blue line has been transformed into the  $(i_{\text{DENIS}}, J_{\text{2MASS}})$  observational space, while the green dashed line shows the effects of reddening by  $E(B - V) = 0.2$  (arrow).

## APPENDIX B

---

# Derivation of the epicyclic approximation

We follow the standard derivation of Binney & Tremaine (2008) and Mo et al. (2010). This differs from that used by Makarov et al. (2004), who follow King et al. (1990) in using Lindblad's original approach. Makarov et al. (2004) derive the approximation in heliocentric coordinates in terms of the initial XYZ position and UVW velocity of the test particle. The two derivations are equivalent, as are the standard angular frequencies  $\Omega$ ,  $\kappa$  and  $v$ .

We first assume a gravitational potential for the Galactic disk  $\Phi$  that is axisymmetric around the normal to the disk. We also assume that such a potential is symmetric about the disk plane. In cylindrical  $(R, \phi, z)$  coordinates the equations of motion for such a potential are:

$$\begin{aligned}\ddot{R} - R\dot{\phi}^2 &= -\frac{\partial\Phi}{\partial R} \\ \frac{d}{dt}(R^2\dot{\phi}) &= 0 \\ \ddot{z} &= -\frac{\partial\Phi}{\partial z}\end{aligned}\tag{B.1}$$

Noting that the second equation implies the conservation of angular momentum about the  $z$  axis;  $R^2\dot{\phi} = \text{constant} = L_z$ , the equations of motion can also be written

$$\ddot{R} = -\frac{\partial\Phi_{\text{eff}}}{\partial R} \quad \text{and} \quad \ddot{z} = -\frac{\partial\Phi_{\text{eff}}}{\partial z}\tag{B.2}$$

where the effective potential  $\Phi_{\text{eff}}(R, z)$  is defined as

$$\Phi_{\text{eff}}(R, z) = \Phi(R, z) + \frac{L_z^2}{2R^2}\tag{B.3}$$

The effective potential has a minimum at  $z = 0$  (by symmetry) and at  $R = R_g$ :

$$\frac{\partial\Phi_{\text{eff}}}{\partial R} = \frac{\partial\Phi}{\partial R} - \frac{L_z^2}{R^3} = 0 \quad \text{which means} \quad \left.\frac{\partial\Phi}{\partial R}\right|_{(R_g, 0)} = \frac{L_z^2}{R_g^3} = R_g\dot{\phi}^2\tag{B.4}$$

The *guiding centre* radius  $R_g$  therefore corresponds to a circular orbit with constant angular speed  $\dot{\phi} = \Omega_g = \sqrt{(1/R)\partial\Phi/\partial R} = L_z/R_g^2$ . We can approximate the effective potential

around  $(R, z) = (R_g, 0)$  by the second-order Taylor expansion around this point. If we define  $x = (R - R_g)$  the expansion is:

$$\begin{aligned}\Phi_{\text{eff}} \simeq & \Phi_{\text{eff}}(R_g, 0) + x \frac{\partial \Phi_{\text{eff}}}{\partial R} \Big|_{(R_g, 0)} + z \frac{\partial \Phi_{\text{eff}}}{\partial z} \Big|_{(R_g, 0)} \\ & + \frac{1}{2} x^2 \frac{\partial^2 \Phi_{\text{eff}}}{\partial R^2} \Big|_{(R_g, 0)} + \frac{1}{2} z^2 \frac{\partial^2 \Phi_{\text{eff}}}{\partial z^2} \Big|_{(R_g, 0)} + xz \frac{\partial^2 \Phi_{\text{eff}}}{\partial R \partial z} \Big|_{(R_g, 0)}\end{aligned}\quad (\text{B.5})$$

The second and third terms are zero at the point  $(R_g, 0)$ . The cross-term is also zero as we assume the potential is symmetric about  $z = 0$ . The effective potential then becomes

$$\begin{aligned}\Phi_{\text{eff}} \simeq & \Phi_{\text{eff}}(R_g, 0) + \frac{1}{2} x^2 \frac{\partial^2 \Phi_{\text{eff}}}{\partial R^2} \Big|_{(R_g, 0)} + \frac{1}{2} z^2 \frac{\partial^2 \Phi_{\text{eff}}}{\partial z^2} \Big|_{(R_g, 0)} \\ = & \Phi_{\text{eff}}(R_g, 0) + \frac{1}{2} (\kappa x)^2 + \frac{1}{2} (\nu z)^2\end{aligned}\quad (\text{B.6})$$

where we define the constants:

$$\kappa^2 = \frac{\partial^2 \Phi_{\text{eff}}}{\partial R^2} \Big|_{(R_g, 0)} \quad \text{and} \quad \nu^2 = \frac{\partial^2 \Phi_{\text{eff}}}{\partial z^2} \Big|_{(R_g, 0)} \quad (\text{B.7})$$

In this second-order Taylor expansion of the effective potential the equations of motion (Eqn. B.2) simplify to those of harmonic oscillators:

$$\ddot{x} = -\kappa^2 x \quad \text{and} \quad \ddot{z} = -\nu^2 z \quad (\text{B.8})$$

which have the general solutions:

$$x(t) = X \cos(\kappa t + \alpha) \quad \text{and} \quad z(t) = Z \cos(\nu t + \beta) \quad (\text{B.9})$$

for constants  $X, Z, \alpha$  and  $\beta$ . What about the azimuthal coordinate  $\phi$ ? Realising that angular momentum is conserved and  $\dot{\phi} = L_z/R^2$  and  $\Omega_g = L_z/R_g^2$ , we have

$$\dot{\phi} = \frac{L_z}{R_g^2} \frac{1}{(x/R_g + 1)^2} \simeq \Omega_g \left(1 - 2 \frac{x}{R_g}\right) \quad (\text{B.10})$$

Substituting for  $x(t)$  and integrating we arrive at

$$\phi = \Omega_g t - 2 \frac{\Omega_g}{R_g \kappa} X \sin(\kappa t + \alpha) + \phi_0 \quad (\text{B.11})$$

If we convert the cylindrical  $(R, \phi, z)$  coordinate system to a Cartesian system  $(x, y, z)$ , co-moving with the guiding centre  $(R_g, \phi)$ ; for  $X \ll R_g$  this simplifies to:

$$\begin{aligned}y(t) &= -2 \frac{\Omega_g}{\kappa} X \sin(\kappa t + \alpha) \\ &= -Y \sin(\kappa t + \alpha)\end{aligned}\quad (\text{B.12})$$

In the new coordinate system  $x$  and  $z$  are the same as above and  $y$  points in the direction of Galactic rotation. In this frame the star can be thought of as simultaneously oscillating around the guiding centre vertically and in an ellipse in the  $xy$  plane (the epicycle). The motion can be described by three angular frequencies; the epicyclic frequency  $\kappa$ , the vertical frequency  $\nu$  and the angular velocity of the guiding centre,  $\Omega_g$ . The vertical motion is independent of the epicyclic motion. The size of the epicycle is dictated by the ratio of  $\kappa$  to  $\Omega_g$ :  $X/Y = \kappa/2\Omega_g$ .

A schematic of epicyclic motion is shown in Figure B.1. The resultant orbital motion following Equations B.9 and B.12 in a Galactocentric inertial frame is traced in Figure B.2. Like in the general case, although close to circular, the orbit is not closed in such a frame.

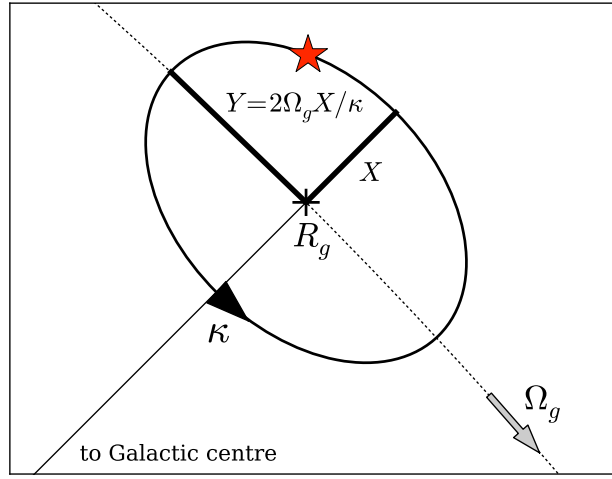


**Figure B.1** Schematic of epicyclic motion. The star (red) moves around the epicycle with angular velocity  $\kappa$ , while its centre  $R_g$  orbits the Galactic centre in the opposite sense in a circular orbit with velocity  $\Omega_g$ . Throughout its epicyclic motion the star also moves sinusoidally in the Z-direction with velocity  $v$  and amplitude  $Z$ .

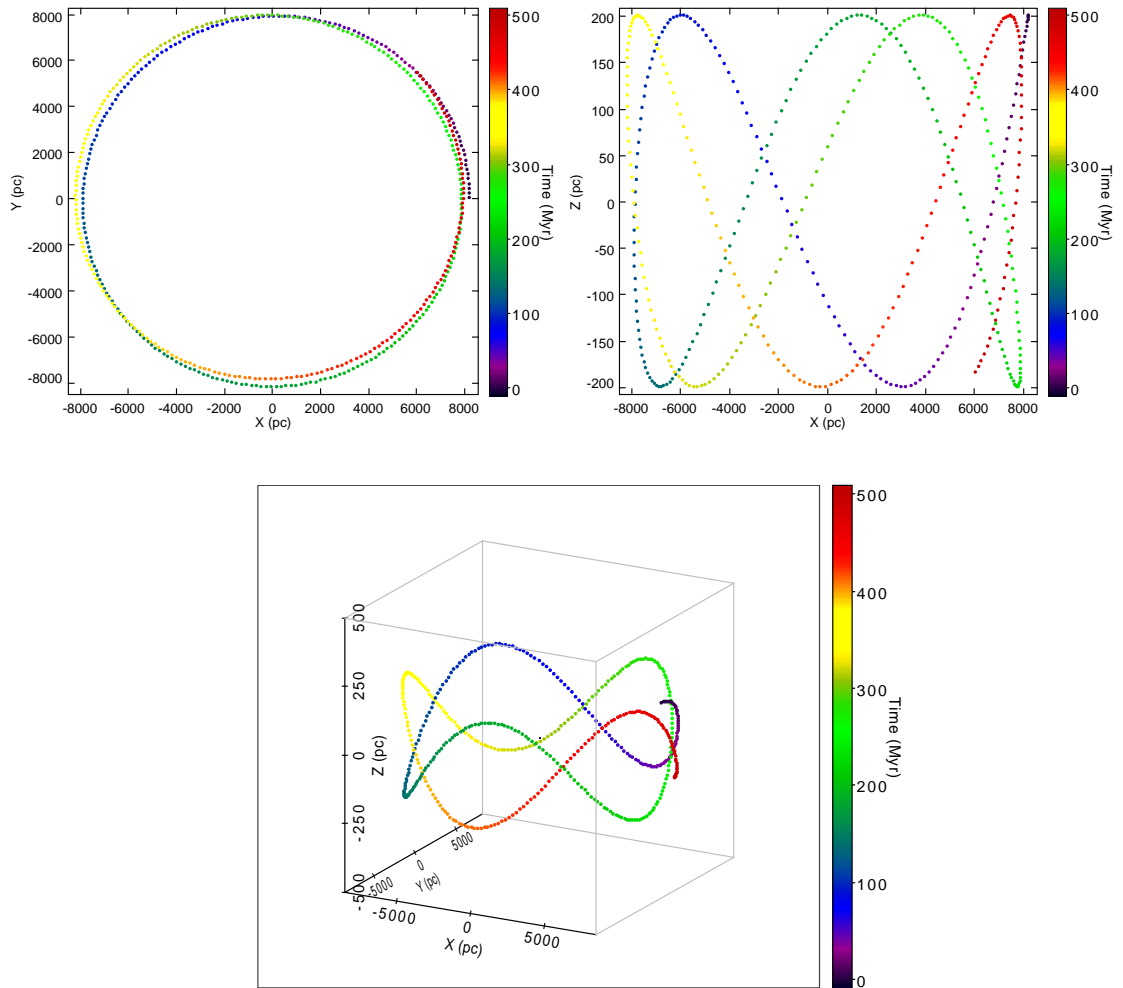


**Figure B.2** Orbital motion for the epicycle in Fig. B.1 with  $\kappa_0 = 0.0367 \text{ km s}^{-1} \text{ pc}^{-1}$ ,  $\Omega_0 = 0.0272 \text{ km s}^{-1} \text{ pc}^{-1}$  (Binney & Tremaine 2008, Table 1.2),  $R_g = R_\odot = 8000 \text{ pc}$  and  $X = Z = 200 \text{ pc}$ . The coordinate system has its origin at the Galactic centre.



## APPENDIX C

---

### WiFeS radial velocity precision

Our nightly radial velocity standard observations provide a large sample of cross-correlations to assess the velocity precision of the *WiFeS* instrument at a resolution of  $R \approx 7000$ .

Each night we typically observed 4–7 bright M-type radial velocity standards from the list of Nidever et al. (2002). These stars have velocities stable to  $\sim 100$  m s $^{-1}$  from multiple high resolution spectra over several years of observations. As a nightly quality check each standard was cross-correlated using the IRAF task *fxcor* against all the other standards from that night over the region 6000–6500 Å. Prior to cross-correlation the spectra were continuum normalised by subtracting a boxcar smoothed spectrum, following the method of Dawson & De Robertis (2005). The Nidever et al. (2002) velocity of the template spectrum was used to derive the radial velocity after correction to a heliocentric frame.

Figure C.1 shows the difference between the *WiFeS* and Nidever et al. radial velocities for the 637 nightly cross-correlations of standards made during the thesis. The absolute value is given as the sign of the difference is arbitrary and depends only on which star was the template. The RMS deviation of the velocities,  $\sqrt{\sum \Delta RV^2/N}$ , is 2.04 km s $^{-1}$ , while the median is 1.40 km s $^{-1}$ . All measurements are shown in Figure C.1—when deriving the velocities of candidates any standards showing unusually large deviations relative to the other stars (typically  $>2$ –4 km s $^{-1}$ ) were rejected from the night’s analysis.

The distribution of velocities appears normally distributed. To quantify the degree of normality we performed two-sample Kolmogorov-Smirnov tests against various *absolute* normal distributions, each with  $N = 637$  samples, changing the mean and standard deviation. The result of these tests is shown in Figure C.2 where we plot the KS confidence  $P_{KS}$  as a function of  $\mu_{|\Delta RV|}$  and  $\sigma_{|\Delta RV|}$ . The sign of  $\mu_{|\Delta RV|}$  is unimportant as the distribution is symmetric about  $\mu = 0$ . If  $P_{KS}$  is high then we cannot reject the hypothesis that the distribution from which the two samples are drawn is the same. Figure C.2 shows the observed velocity differences are consistent with a normal distribution of  $(\mu_{|\Delta RV|}, \sigma_{|\Delta RV|}) \approx (0, 2)$  km s $^{-1}$ , with a degeneracy towards smaller  $\sigma$  and larger  $\mu$  values. For comparison, two different  $N = 637$  normal distributions are plotted with the observed data in Figure C.1.

We err on the side of simplicity and conclude that in the instrumental limit of high signal-to-noise ( $S/N \gtrsim 30$  pixel $^{-1}$  over 6000–6500 Å) the distribution of velocities is best described by

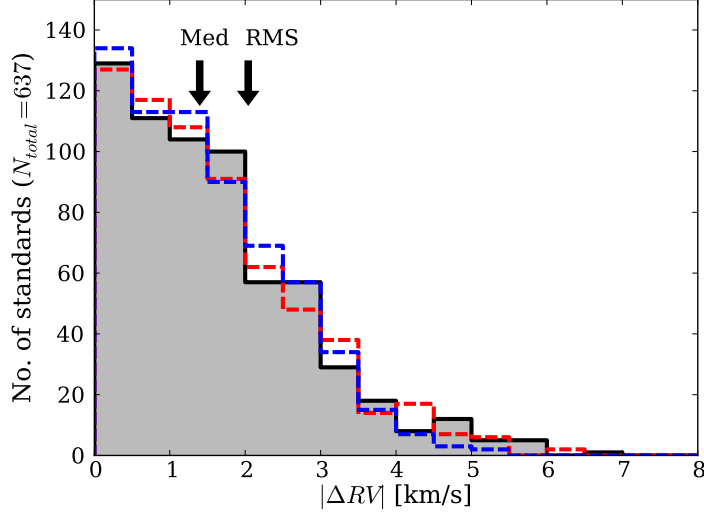


**Figure C.1** *WiFeS* absolute velocity differences for 637 cross-correlations of M-type standards from Nidever et al. (2002). The median ( $1.40 \text{ km s}^{-1}$ ) and RMS ( $2.04 \text{ km s}^{-1}$ ) velocity differences are marked. Also shown are typical  $N = 637$  normal distributions with  $(\mu_{|\Delta RV|}, \sigma_{|\Delta RV|}) = (0, 2) \text{ km s}^{-1}$  (red) and  $(1.2, 1.5) \text{ km s}^{-1}$  (blue).

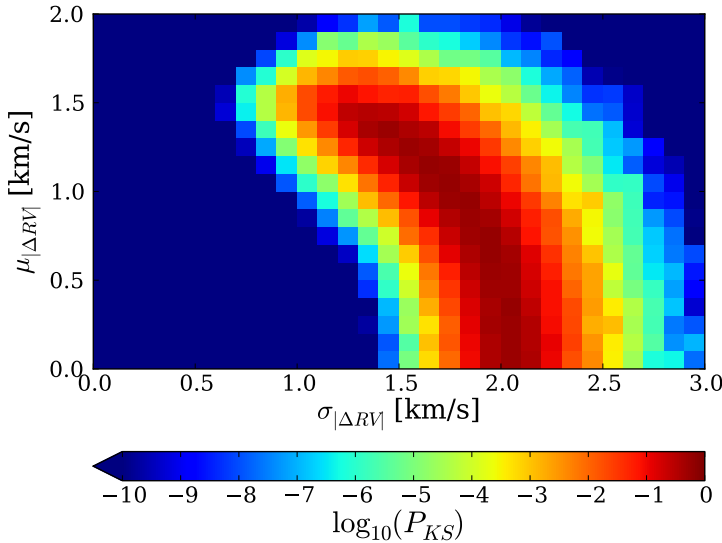


**Figure C.2** Two-sample KS tests for the *WiFeS* velocities against various absolute normal distributions. Each pixel shows the logarithm of the mean of the confidence  $P_{KS}$  after 100 realisations. If  $P_{KS}$  is high then we cannot reject the hypothesis that the distributions from which the two samples are drawn is the same.

a normal distribution with zero mean velocity shift and a standard deviation of  $\sim 2 \text{ km s}^{-1}$ . Even with a smaller  $\sigma$  value the shift in mean velocity is small (of order  $\sigma$ ). At the fainter magnitudes of our candidates ( $14 < V < 17$ ) the radial velocity precision falls. From multiple observations of several candidates (which are assumed constant in RV) we estimate our derived velocities are accurate to  $2\text{--}3 \text{ km s}^{-1}$ .

To cross-check these results we cross-correlated several sky spectra extracted from candidate observations and the Osterbrock et al. (1996) high-resolution sky spectrum (smoothed to  $R = 7000$  and sampled to the *WiFeS* wavelength scale). In all cases they agreed to  $< 2.5 \text{ km s}^{-1}$ , with a typical difference of  $\lesssim 1 \text{ km s}^{-1}$ .

We also briefly compare our results to those of the HAT-South project (G. Zhou & D. Bayliss,

private communication). The HAT-South team are confirming planet transit candidates with *WiFeS*  $R7000$  velocities to filter eclipsing binaries from true transiting planets, which would not be expected to show measurable velocity variations. One such binary velocity curve is shown in Figure C.3. From telluric absorption features they also derived single-epoch velocity precisions of  $\sim 2 \text{ km s}^{-1}$ , with an RMS residual for the six measurements of  $\sim 3 \text{ km s}^{-1}$ , when compared to a best-fitting zero-eccentricity orbit. Such RMS values are typical (Figure C.4) and reflect the small number of observations of each star.

A final useful check on our velocities would be to measure the radial velocity curves for several *known* low-amplitude  $\delta$  Scuti or eclipsing binary variable stars and test our ability to recover the variation as a function of signal-to-noise. This is left as future work.

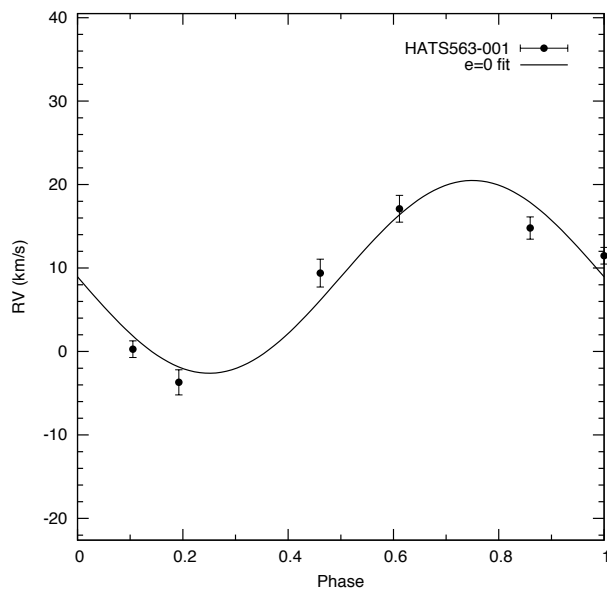


**Figure C.3** *WiFeS* radial velocity curve for the  $V = 12.1$  eclipsing binary HATS563-001. The solid line is a zero eccentricity least-squares fit to the data with an RMS residual of  $2.9 \text{ km s}^{-1}$  (image courtesy G. Zhou, RSAA).

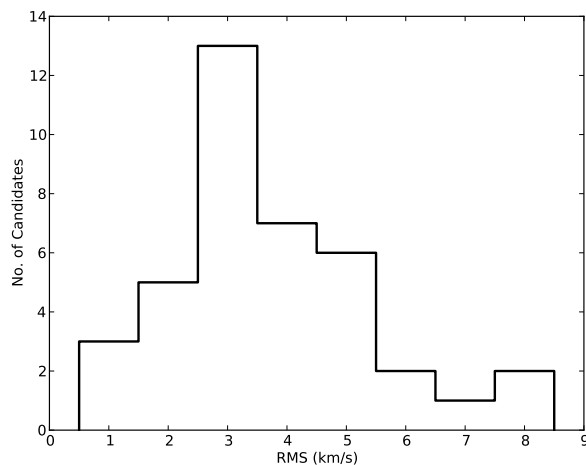


**Figure C.4** Histogram of RMS velocity-fit residuals for 44 new eclipsing binary systems observed as part of HAT-South follow-up. The distribution has a mean of  $3.9 \text{ km s}^{-1}$  and a standard deviation of  $2.0 \text{ km s}^{-1}$  (image courtesy G. Zhou, RSAA).